Potential of Chromium Isotopes as a Tracer of Past Ocean Oxygenation

Thesis

Potential of Chromium Isotopes as a Tracer of Past Ocean Oxygenation

A thesis presented for the degree of

Doctor of Philosophy

Pierre Bonnand

MSc (Clermont-Ferrand), 2007

May 2011

Centre for Earth, Planetary, Space and Astronomical Research (CEPSAR)

Department of Earth and Environmental Sciences

The Open University, Milton Keynes, UK

Abstract

Levels of atmospheric oxygen (O_2) have increased from <2% of the present atmospheric level (PAL) to values similar to the PAL during the Neoproterozoic. This is likely to have resulted in significant changes in redox conditions in the oceans. The aim of this study is to provide new constraints on redox conditions in shallow seawater during the Neoproterozoic by analysis of the rare earth element (REE) concentration and chromium (Cr) isotopic composition of marine carbonates. To this end, a new method for δ^{53}Cr analysis in low concentration samples has been developed. In addition, the Cr isotopic composition of modern and Phanerozoic carbonates, and seawater, have been determined to provide new constraints of the environmental behaviour of Cr isotopes.

Modern seawater is characterised by heavy δ^{53}Cr values (+0.55-1.55‰) relative to the continental crust (-0.12‰), which indicates that Cr isotopes are fractionated during oxidative weathering. Importantly, the Cr isotopic composition of modern carbonates, precipitated in shallow water, is within the range of seawater. This suggests that fractionation of Cr isotopes during carbonate precipitation is minimal, and carbonates should provide a record of seawater δ^{53}Cr. Carbonate samples of Phanerozoic age also have high δ^{53}Cr values (0.737-1.994‰), consistent with oxidative weathering on the continents at this time.

Most of the Neoproterozoic carbonates have significantly lower δ^{53}Cr values than the modern and Phanerozoic carbonates. However, oolitic limestones deposited just prior to the first Cryogenian glaciations, have higher δ^{53}Cr (+0.571-1.004‰). Together, the δ^{53}Cr and REE data suggest that the operation of the Cr cycle was significantly different in the Neoproterozoic. Changes in δ^{53}Cr reflect either a shift in the relative importance of riverine and hydrothermal sources, and/or changes in levels of atmospheric O_2. Modelling indicates that shallow waters were either dysoxic or suboxic during the Cryogenian, and levels of atmospheric O_2 must have been less than 30-40% PAL.

Acknowledgements

Firstly, I would like to thank my supervisors: Ian Parkinson, Rachael James, Ian Fairchild and Nick Rogers. The work presented in this study would not have been possible without their help and their guidance. Thanks must go to Bruce Schaefer for his help during the fieldtrip in Australia. Thanks also go to Mark Rehkamper and Anthony Cohen for their constructive criticism.

Thank you to Sam Hammond for running the labs so efficiently and for her help with the ICP-MS measurements, to Manuela Fehr for her help with the Neptune and for sharing the lab with me and to Anne-Mari for her help with the Cr chemistry.

A large number of people need to be thanked for making my time in Milton Keynes such a great experience. First of all, Alison and Ian for sharing an office with me; it was a pleasure to go to work over the last three years and it is partly because I had a good time in the office with you two. More generally, I would like to thank the other PhD students and staff members at the OU for sharing numerous coffee breaks and "Friday Beers" (and Wednesday pub as well). I would also like to thank my housemates: Joe, Josh, Gaz and Lottie. I hope that living with a Frenchman was not too difficult. I really enjoyed the barbecues that we have done during the "long" and "hot" English summers.

I would like to express my gratitude to Emilie's friends and colleagues in Graz that made my stays in Austria such great and fantastic time. Thanks must go to Kurt Stuewe and the University of Graz for letting me write most of my thesis in Graz.

Thank must go to our friends that came on the other side of the English Channel to visit us: Damien, Sandrine and Tibo, to Matt and Aline for sharing the great experience of Alaska wilderness and to Tibo for inviting us to the Reunion Island.

I would like to thank my family for always being there for me and supporting me. Special thanks go to Maman, Papa, Clement, Isaline and Aloys and Jean-Baptiste. Thanks must go to Emilie's family (Jean, Pascale, Arnaud and Carline and Matthieu) for their support over the last three years.

Finally, I couldn't have done this without the love and support of Emilie. Thank you for your help, your affection and for everything that we have done together. I promise, I will not work on weekends now that my thesis is finished.

Pierre

Remerciements

Je voudrais tout d'abord remercier mes directeurs de thèse : Ian Parkinson, Rachael James, Ian Fairchild et Nick Rogers. Le travail présenté dans cette thèse a grandement bénéficié de votre aide et de nos discussions. Je voudrais aussi remercier Bruce Schaefer pour son aide sur le terrain en Australie ainsi que Mark Rehkamper et Anthony Cohen pour leur remarques constructives durant ma soutenance de Thèse.

Merci à Sam Hammond pour s'être occupée des laboratoires de manière si efficace et pour son aide durant les analyses ICP-MS ; à Manuela Fehr pour son aide avec le Neptune et pour avoir partagé le lab avec moi ; enfin, merci à Anne-Mari pour son aide avec la chimie Cr.

Je voudrais profiter de ces quelques lignes pour remercier grandement les personnes qui ont fait de mon séjour à Milton Keynes une très belle expérience. Tout d' abord, je remercie Alison et Ian d'avoir partagé le bureau avec moi. C'était un plaisir d'aller au travail pendant ces trois dernières années et cela est en partie grâce à vous! Plus généralement, j'aimerais remercier les autres thésards et les membres du staff de Open pour avoir partagé avec moi de nombreuses pauses café et " Fridays beers " (et " Wednesday pub " aussi). J'aimerais remercier mes colocataires : Joe, Josh, Gaz et Lottie. J'espère que vivre avec un français n'était pas trop difficile. J'ai vraiment apprécié les nombreux barbecues que nous avons fait pendant les " long " et " chaud " été anglais.

J'aimerais aussi remercier les collègues et amis d'Emilie à Graz qui ont fait de mes séjours en Autriche de fantastiques moments. Merci a Kurt Stuewe et l'Université

de Graz pour m'avoir laissé écrire la plus grande partie de ma thèse a Graz.

Un grand merci aussi à nos amis qui sont venus de l'autre côté de la manche pour nous rendre visite : Damien et Sandrine ainsi que Tibo. Merci à Matt et Aline pour avoir partagé notre expérience en Alaska et à Tibo pour nous avoir accueillit à la Réunion.

J'aimerais remercier ma famille pour avoir été continuellement là pour moi et pour m'avoir toujours encouragé à suivre ma voie. Un grand merci à maman, papa, Clément, Isaline, Aloys et Jean-Baptiste. Merci aussi a la famille d'Emilie (Jean, Pascale, Arnaud, Carline et Matthieu) pour leur soutien pendant les trois dernières années.

Finalement, Je n'aurais pas pu faire ce travail sans l'amour et l'aide d'Emilie. Merci beaucoup pour ton aide, ton affection et pour tout ce que nous avons fait tous les deux. Je te promets que je ne travaillerai plus le weekend maintenant que ma thèse est finie.

Pierre

Contents

List of Figures

List of Tables

Chapter 1

Introduction

1.1 Rationale

The variation in the level of oxygenation in the past oceans and atmosphere has been widely studied over the last 30 years (e.g. Rouxel et al., 2005; Holland, 2006). These studies have revealed that the Earth system is characterised by large variations in the level of oxygenation, and these changes are associated with dramatic extinctions on the Earth's surface. The study of the chemical composition of marine sediments, such as carbonates, provides crucial information about how the chemistry of the oceans responds to changes in the Earth's environmental conditions. For example, analysis of traditional stable isotope systems, such as oxygen and carbon, in marine carbonates have been used to assess changes in ocean temperature, ice volume, productivity and ventilation. Information on levels of seawater oxygenation, on the other hand, tends to come from the analysis of non-traditional stable isotopes, such as molybdenum (Mo) and iron (Fe) (e.g. Siebert et al., 2003; Rouxel et al., 2005). However, the behaviour of Mo and Fe in seawater is strongly regulated by the presence of free hydrogen sulphide (H_2S), so these two isotope systems are most sensitive to euxinic conditions. As euxinic conditions are rare in shallow waters (which are in contact with the atmosphere), Mo and Fe isotopes rarely provide information about levels of oxygenation in shallow water environments. In contrast to Mo and Fe, chromium (Cr) is not regulated by H_2S; Cr speciation only responds to changes in levels of seawater oxygenation. Moreover, Cr has a simple solution

chemistry relative to Mo and Fe. For these reasons, chromium stable isotopes have the potential to record past changes in ocean redox conditions. In addition, the study of Cr isotopes in shallow water carbonates should help to constrain redox conditions in shallow waters that, crucially, will be in equilibrium with the level of O_2 in the atmosphere.

Although using isotopic systems as a proxy for past redox conditions is a growing research field, their ability to produce quantitative information about dissolved oxygen concentrations in the shallow oceans and, by inference, oxygen concentrations in the atmosphere, is not yet fully developed. This thesis aims to redress this, by analysis of Cr isotopes in marine carbonates from the Neoproterozoic, a time for which there is strong evidence for increases in atmospheric oxygen and the oxygen content of the shallow oceans. The data are interpreted in the context of Cr isotope data obtained from modern marine carbonates and, for the first time, seawater. In this way, the aim of this thesis is to test the applicability of Cr isotopes as a redox proxy.

1.2 The oxygenation history of the Earth

The oxygenation history of the atmosphere and oceans has attracted significant interest over the last 30 years (e.g. Holland, 2006). On the basis of geochemical studies, the evolution of atmospheric oxygen is divided into five stages (Holland, 2006; Fig. 1.1).

Stage 1, the Archaean (prior to 2.4 Ga), is characterised by exceptionally low atmospheric O_2 concentrations (<2 ppm), coupled with anoxic conditions in both the shallow and deep ocean.

Stage 2 is characterised by a marked increase in atmospheric O_2, reaching ~10% present atmospheric level (PAL). This is the so-called 'Great Oxidation Event' (GOE), which occurred between 2.4 and 2.0 Ga. During the GOE, the oxygen concentration of the surface waters is thought to be in equilibrium with the atmosphere (Holland, 2006), whereas the deep ocean remained anoxic.

Stage 3, between 1.85 and 0.85 Ga, is characterised by relatively constant levels of

atmospheric O_2 (Holland, 2006), and the oceans are thought to be strongly stratified (Planavsky et al., 2010).

Stage 4 is the Neoproterozoic Era (0.85 to 0.54 Ga) during which there appears to be a large increase in atmospheric O_2, with concentrations increasing from about 5-10% PAL to close to PAL (90% PAL) (Fig. 1.1, Holland, 2006). The Neoproterozoic is characterised by a series of major climate perturbations (Fairchild and Kennedy, 2007), so it seems unlikely that the O_2 concentration increased gradually during this period. Rather, the Neoproterozoic is likely to be characterised by large

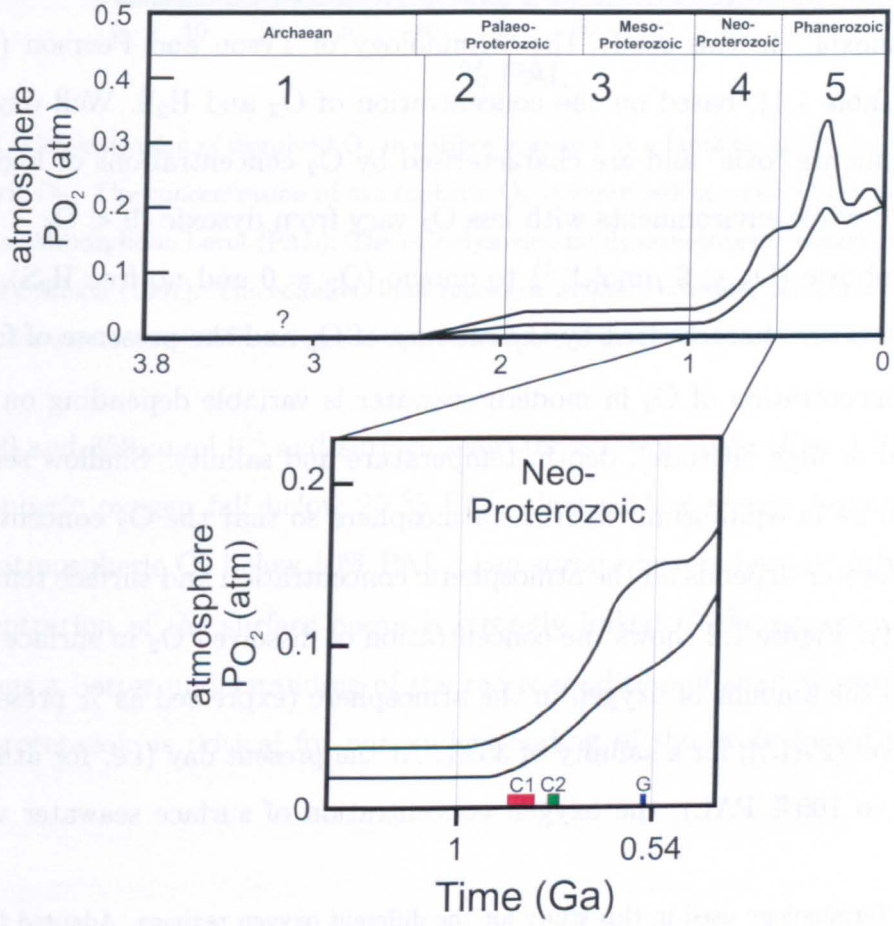

Figure 1.1: Variation of the oxygen concentration in the atmosphere from the Archaean to the present with emphasis on the Neoproterozoic Era. Modified after Holland (2006). The three Neoproterozoic glaciations are labelled C1 (first Cryogenian glaciation), C2 (second Cryogenian glaciation) and G (the Gaskiers glaciation). Numbers represent the different stages in the evolution of atmospheric O_2 (see text for details). Each curve presents a model for the oxygenation of the atmosphere.

variations in atmospheric O_2. These large variations in atmospheric O_2 are likely to be accompanied by major changes in the redox condition of the ocean. Importantly, the Neoproterozoic is a key period in the evolution of the atmospheric O_2 because, at this time, the high level of O_2 became stabilised and probably enhanced the development of life on Earth (Knoll, 2003).
Stage 5 (0.54 Ga to present) is characterised by relatively high O_2 concentration in the atmosphere, although there is strong evidence that there have been large variations in the atmospheric O_2 concentration during the Phanerozoic (Holland, 2006).

There is no consensus on the definition of the terminology used in studies of seawater anoxia. In this study, the terminology of Tyson and Pearson (1991) is adopted (Table 1.1), based on the concentration of O_2 and H_2S. Well oxygenated environments are "oxic" and are characterised by O_2 concentrations of higher than 90 μmol l^{-1} while environments with less O_2 vary from dysoxic ($9 < O_2 < 90$ μmol l^{-1}), to suboxic ($O_2 < 9$ μmol l^{-1}) to anoxic ($O_2 = 0$ and no free H_2S). Euxinic environments are characterised by the absence of O_2 and the presence of free H_2S.

The concentration of O_2 in modern seawater is variable depending on location (equatorial or high latitude), depth, temperature and salinity. Shallow seawater is thought to be in equilibrium with the atmosphere so that the O_2 concentration in surface seawater depends on the atmospheric concentration and surface temperature and salinity. Figure 1.2 shows the concentration of dissolved O_2 in surface seawater relative to the amount of oxygen in the atmosphere (expressed as % present atmospheric level (PAL)), for a salinity of 35‰. At the present day (i.e. for atmospheric O_2 equal to 100% PAL), the oxygen concentration of surface seawater varies be-

Table 1.1: Terminology used in this study for the different oxygen regimes. Adapted from Tyson and Pearson (1991).

	O_2 (μmol l^{-1})	free H_2S
Oxic	> 90	no
Dysoxic	90-9	no
Suboxic	< 9	no
Anoxic	0	no
Euxinic	0	yes

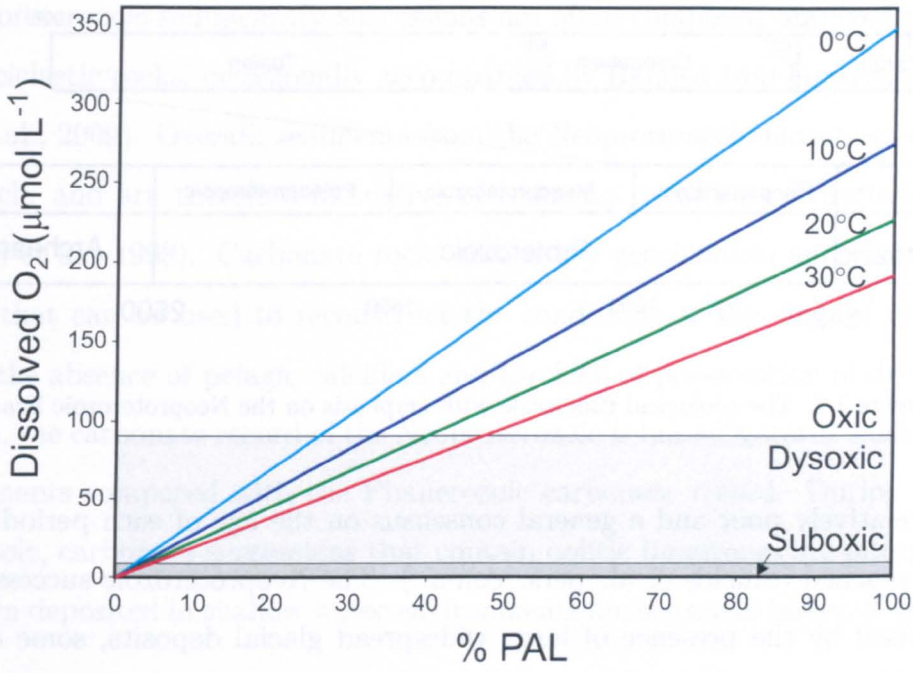

Figure 1.2: Concentration of dissolved O_2 in surface seawater as a function of the concentration of atmospheric O_2. The concentration of atmospheric O_2 is expressed in terms of the percentage of the Present Atmospheric Level (PAL). The oxic-dysoxic and dysoxic-suboxic boundaries are from Tyson and Pearson (1991). The coloured lines represent different seawater temperatures, and are calculated for a salinity of 35‰ using the equation reported by Benson and Krause (1984).

tween 200 and 350 μmol l^{-1} and surface seawater is always oxic (Fig. 1.2). If levels of atmospheric oxygen fall below 25 % PAL, then surface waters become dysoxic while at atmospheric O_2 below 10% PAL, then surface waters become suboxic. The O_2 concentration of the surface ocean is strongly linked to the presence of life on Earth, thus a better understanding of the redox condition of shallow waters during the Neoproterozoic is critical for our understanding of the evolution of the Earth system.

1.3 The Neoproterozoic Era

The Neoproterozoic Era began 1000 Ma (Fig. 1.3) and ended at the Proterozoic-Phanerozoic transition, some 542 Ma (Amthor et al., 2003). The Neoproterozoic Era is sub-divided into the Tonian (1000 - ? Ma), the Cryogenian (? - 635Ma) and the Ediacaran (635-542 Ma) (Fig. 1.3). The age constraints on the Neoproterozoic

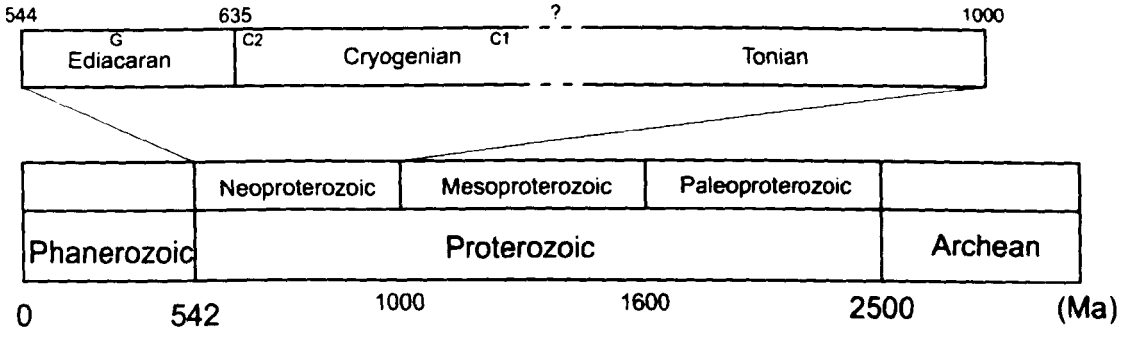

Figure 1.3: The geological time scale with emphasis on the Neoproterozoic Era.

Era are relatively poor and a general consensus on the age of each period has not yet been reached (Shields et al. pers. comm.). The Neoproterozoic successions are characterised by the presence of large widespread glacial deposits, some of which have been interpreted to be of global extent (Knoll, 2000; Fairchild and Kennedy, 2007). There are no glacial deposits described before 750 Ma; all glaciations are confined to the Cryogenian and Ediacaran periods (Fig. 1.3). Three main glacial periods have been described. The oldest has been dated at about 716 Ma (Macdonald et al., 2010) and is called the first Cryogenian glaciation (C1, Sturtian). The second major glacial event is the end-Cryogenian glaciation (C2, Marinoan), and the end of this glaciation has been dated at about 635 Ma (Condon et al., 2005; Hoffmann et al., 2004; Kendall et al., 2006). The last major glaciation episode is called the Gaskiers (G) glaciation (Fig. 1.3). This occurred at about 580 Ma, in the Ediacaran period, and has been described in Newfoundland (Halverson et al., 2007). However, the chronology of the first Cryogenian glaciation is still strongly debated because of potential overlapping ages between glacial events (Condon et al., 2005, Rooney et al., 2011). These uncertainties mean that the terminology used above is likely to change in the future. The glacial units are often overlain by cap carbonates (Fairchild and Kennedy, 2007). These cap carbonates, which are unique to the Neoproterozoic Era, are usually thin, but laterally extensive dolomite horizons which make a sharp contact with the overlying glacial deposits. Although these cap carbonates have been widely studied, their origin and the mechanisms responsible for their chemical characteristics (such as large negative carbon isotopes excursions) are still under debate (Fairchild and Kennedy, 2007).

Neoproterozoic sedimentary successions are often composed of mixed carbonate and siliciclastic rocks, occasionally accompanied by Banded Iron Formations (BIFs) (Frei et al., 2009). Overall, sediments from the Neoproterozoic have been described as Fe-rich, and are therefore indicative of reducing conditions (Kirschvink, 1992; Hoffman et al., 1998). Carbonate rocks record key geochemical and climate information that can be used to reconstruct the conditions at the time of deposition. Due to the absence of pelagic calcifiers and the lack of preservation of deep-marine deposits, the carbonate record of the Neoproterozoic is biased towards shallow-water environments compared with the Phanerozoic carbonate record. During the Neoproterozoic, carbonate successions that contain oolitic limestones are interpreted to have been deposited in shallow water environments during warm intervals (Fairchild, 1993).

In order to understand the climate and chemical evolution of the Neoproterozoic the sedimentary record has been widely studied (Halverson et al., 2010). Several geochemical tools have been employed to study the Neoproterozoic successions, including C and Sr isotopes. A brief description of these geochemical tools is given in the following paragraphs.

1.4 Neoproterozoic chemostratigraphy

The chemical composition of sedimentary successions, or "chemostratigraphy" can be used to derive (i) the seawater composition at the time of deposition, (ii) the provenance of water masses, and (iii) changes in environmental variables that control the chemical signal studied. The lack of good biostratigraphical and/or radiochronological constraints for the Neoproterozoic inhibits correlation of the different successions worldwide, and in order to make such correlations chemostratigraphy has been widely used. However, the chemical variables must be sensitive to variations in seawater chemistry, and must not be affected (to any significant extent) by secondary processes that degrade the primary chemical signal. The chemical variations can also be interpreted in terms of environmental and tectonic changes. However, in re-

cent years these interpretations have been strongly debated (Knauth and Kennedy, 2009). During the Neoproterozoic time period, chemostratigraphy has only been applied using specific tools, of which C isotopes have been most widely discussed.

1.4.1 Carbon isotopes

The carbon isotope composition of carbonate minerals ($\delta^{13}C_{carb}$) is widely used for chemostratigraphy during the Neoproterozoic (Kaufman et al., 1997; Kennedy et al., 2001; Schrag et al., 2002; Higgins and Schrag, 2003; Halverson et al., 2005; Jiang et al., 2007). The carbon isotopic compositions of unaltered carbonates can be used to reconstruct the carbon isotope composition of dissolved inorganic carbon (DIC) of seawater in equilibrium with the carbonates. The C isotope composition is reported relative to "Vienna Pee Dee Belemnite" using the standard notation $\delta^{13}C$. The Neoproterozoic Era is characterised by high $\delta^{13}C_{carb}$ relative to modern day seawater, and also by large negative excursions (Fig. 1.4, Halverson et al., 2010). These two features are characteristic of the Neoproterozoic and are interpreted to reflect the true behaviour of carbon isotopes in Neoproterozoic seawater. The large $\delta^{13}C_{carb}$ suggest that the carbon cycle could not have been at steady state for all of the Neoproterozoic. The large variations in the C isotopic composition of seawater have been used to model climate changes that occurred during this period (Kaufman et al., 1997; Halverson et al., 2002; Schrag et al., 2002; Halverson et al., 2010). Several hypotheses have been proposed to explain the significant periods of high $\delta^{13}C_{carb}$ such as a strongly stratified ocean, a high evaporation rate, or high fractional burial of organic carbon (Hayes et al., 1999). These overall high $\delta^{13}C_{carb}$ values are interrupted by large negative carbon isotopes excursions, which remain poorly understood.

In recent years the use of C isotopes for chemostratigraphic purposes has been strongly debated. Indeed, several studies have interpreted the variation in C isotopes recorded as not reflecting the seawater signal (e.g. Knauth and Kennedy, 2009). Rather, it has been proposed that some of the C isotope excursions could be explained by marine, meteoric or burial diagenesis (Fairchild and Kennedy, 2007;

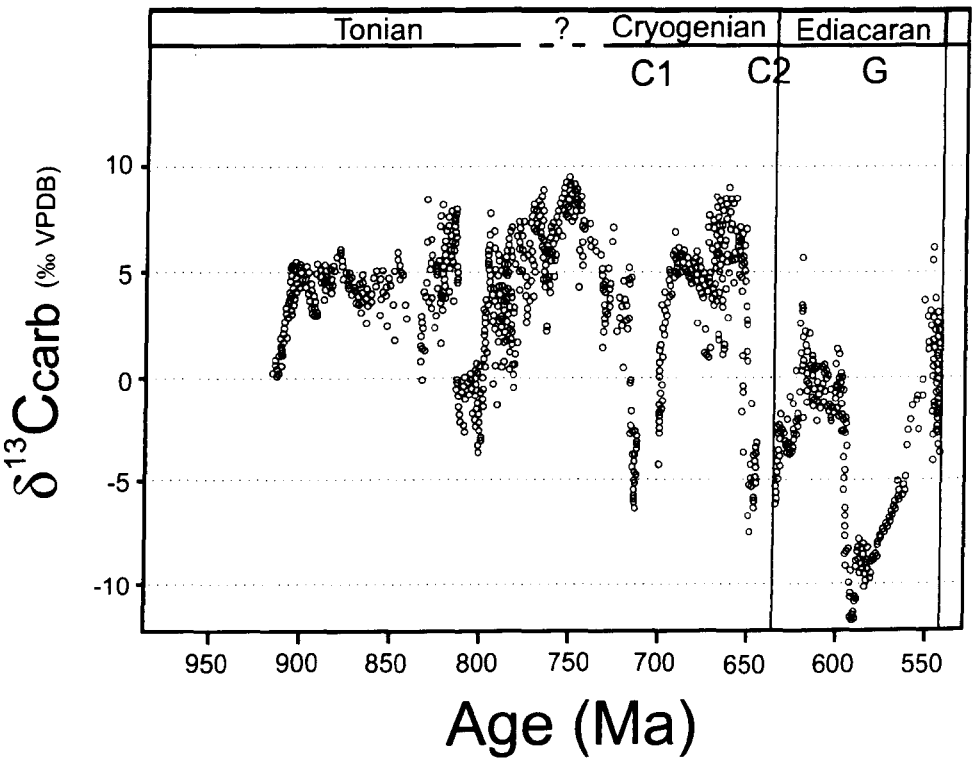

Figure 1.4: Carbon isotope curve for Neoproterozoic seawater. The shaded areas represent glacial events. Modified after Halverson et al. (2010).

Knauth and Kennedy, 2009). The use of C isotopes for chemostratigraphy has also been discussed by Frimmel (2009) who suggested that the low residence time of C relative to the seawater mixing time implies that C isotopes could record a local signal rather than a global signal. Frimmel (2009) demonstrated that proximal and distal carbonates from the same time period do not record the same C isotope data and therefore suggested that the use of C isotopes for chemostratigraphy should be only applied to distal sections. It is also important to test if the signal recorded by the carbonate samples is primary or if it was affected by post-depositional processes. In order to determine the least affected samples, empirical screening criteria have been used and $\delta^{13}C_{carb}$ isotope data is interpreted to be reflecting a primary signal if, for example, Mn/Sr < 0.2, $\delta^{18}O$ > -10‰ and Fe/Mn < 0.5 (e.g. Derry et al., 1992).

1.4.2 Oxygen isotopes

The utility of oxygen isotopes for chemostratigraphy in the Proterozoic is highly debated (Jaffres et al., 2007). Overall, the $\delta^{18}O$ value of Neoproterozoic rocks is lower than it is in Cenozoic carbonates (Veizer et al., 1999). However, the interpretation of this general observation has not yet reached a consensus. A number of studies have suggested that the O isotopic composition in seawater has remained constant through Earth's history (e.g. Muehlenbachs, 1998), whilst others suggest that seawater $\delta^{18}O$ has varied (Shields et al., 2003). This subject is still strongly debated and, in this study, the $\delta^{18}O$ value of Neoproterozoic carbonates is used as an indicator of diagenetic effects: O isotopes are strongly affected by diagenetic fluids and increased post-depositional temperatures (Jacobsen and Kaufman, 1999).
Mass-independent oxygen isotope fractionation in sulphate have also been applied to Neoproterozoic sediments (Bao et al., 2008, Bao et al., 2009) and the variations observed have been interpreted in terms of high atmospheric pCO_2 and low O_2 production (Bao et al., 2008).

1.4.3 Sulphur isotopes

Sulphur isotopes ($\delta^{34}S$) can be measured from minerals containing either sulphates or sulphides. In the Neoproterozoic successions, $\delta^{34}S$ has been measured in evaporites, barite and carbonates (e.g. Halverson et al., 2010). In the latter, $\delta^{34}S$ is measured in carbonate-associated sulphate-bearing minerals and can be interpreted as reflecting the seawater sulphate composition. The $\delta^{34}S$ measured in sulphide-bearing minerals such as pyrite records the net fractionation effects during bacterial sulphate reduction and by oxidative recycling of sulphide (Canfield and Teske, 1996; Detmers et al., 2001; Hurtgen et al., 2005). The Neoproterozoic is characterised by a sharp increase in $\delta^{34}S$ after the end-Cryogenian glaciations (Halverson et al., 2010). The sulphur isotope record for the early Neoproterozoic is not yet resolved. However, Johnston et al. (2010) used $\delta^{34}S$ in the Chuar Group to demonstrate that shallow seawater was ferruginous during the Tonian period.

1.4.4 Radiogenic isotopes

Radiogenic isotopes can be used for two purposes in the Neoproterozoic successions. The first is radiometric dating. For example, Rb-Sr and Re-Os have been used to date different Neoproterozoic formations and help to correlate the different glaciation events (e.g. Kendall et al., 2006). Secondly, radiogenic isotopes can be used as a source tracer. The two main radiogenic isotope proxies used for Neoproterozoic successions are Sr and Nd isotopes.

1.4.4.1 Sr isotopes

Sr isotopes are used in chemostratigraphy to characterise the source of Sr in seawater. The seawater Sr budget is determined by (i) the riverine input (characterised today by radiogenic $^{87}Sr/^{86}Sr$ of $\sim$0.712) and (ii) the hydrothermal flux (characterised by unradiogenic $^{87}Sr/^{86}Sr$ of $\sim$0.703). Although strongly dependent on the hydrothermal flux, the Sr residence time in modern day oceans ranges from 2.5 to 3.2 Ma (Palmer and Edmond, 1992; Jones and Jenkyns, 2001; Vance et al., 2009) and therefore only global changes will be recorded by the Sr isotopes in carbonates. Thus, $^{87}Sr/^{86}Sr$ is a useful monitor of global changes in tectonic and climate regimes over long periods of time ($>$ $\sim$1 Ma). The Sr isotopic composition of past seawater can be reconstructed from analysis of pristine calcite, barite and other Sr-bearing chemical precipitates. For the Neoproterozoic, calcite is the main material used to reconstruct the Sr isotope composition of seawater (Fig. 1.5). Nevertheless, it has been shown that the Sr concentration and Sr isotopic composition of carbonates can be affected by diagenesis (Azmy et al., 1999; Halverson et al., 2007). This alteration results in a decrease in Sr concentration and in an increase of the $^{87}Sr/^{86}Sr$ isotope ratio (Jacobsen and Kaufman, 1999). In order to be interpreted as reflecting a primary signal, carbonates used for chemostratigraphy must be characterised by a high Sr concentration (>1000 ppm), and low Mn/Sr (<0.2) and Rb/Sr (<0.001) ratios (Jacobsen and Kaufman, 1999).

The Neoproterozoic seawater Sr curve has been presented in numerous publications (e.g. Thomas et al., 2004; Halverson et al., 2010). Overall, the Sr isotopic composi-

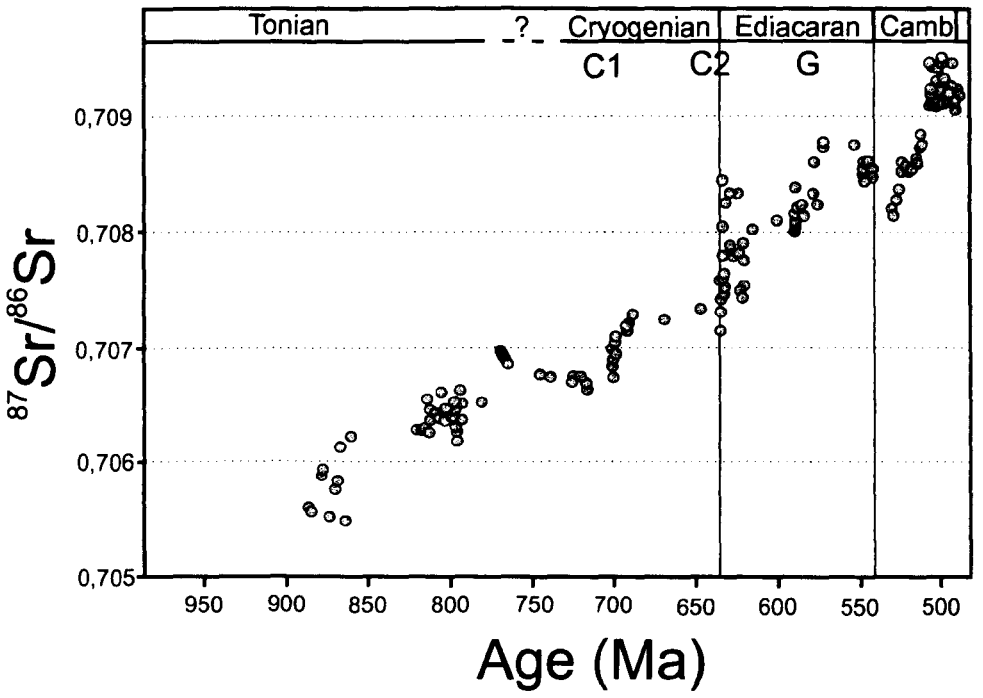

Figure 1.5: Composite plot of high quality Sr isotope data for Neoproterozoic seawater. The shaded areas represent glacial events. Modified after Halverson et al. (2010).

tion ($^{87}Sr/^{86}Sr$ ratio) of seawater is thought to increase from 0.7055 to 0.7085 during the Neoproterozoic. However, this general trend seems to be also strongly affected by the major glaciations occurring during this period and especially before the first and after the second glaciations. The Sr isotopic composition of seawater decreases from 0.7070 to 0.7063 before the first Cryogenian glaciation (Fairchild et al., 2000; Halverson et al., 2010; Shields et al. pers. comm.). This decrease has been interpreted to reflect weathering of a large volume of flood basalts (Halverson et al., 2007), although it could also be explained by a decrease in the riverine input and/or a relative increase in the hydrothermal input to seawater. The second shift in Sr isotopes is located after the second Cryogenian glaciation and has been interpreted in terms of an increase in weathering rate after the glaciations (Higgins and Schrag, 2003). The Sr isotopic composition of carbonates during the Neoproterozoic is also used to correlate successions worldwide (e.g. Halverson et al., 2010).

1.4.4.2 Nd isotopes

Nd isotopes in pristine carbonates can give reliable chemostratigraphic information. Indeed, carbonate samples record the initial $^{143}Nd/^{144}Nd$ ratio of seawater. The isotopic residence time of Nd in the seawater/rock interface is only a few hundred years (Tachikawa et al., 1999), and so is much shorter than the mixing time of the oceans. Nd isotopes can potentially be used to trace the source and flow of dissolved REEs in the Neoproterozoic oceans (Elderfield, 1988; Keto and Jacobsen, 1988). This tool has not been yet widely applied to Neoproterozoic carbonates and therefore a general trend cannot be discussed.

1.4.5 Elemental concentrations and ratios

In the chemostratigraphy literature and more generally, elemental concentrations and elemental ratios have been widely applied to characterise marine sedimentary environments and to assess the redox conditions at the time of deposition (Tribovillard et al., 2006; Algeo and Lyons, 2006; Lyons and Severmann, 2006; Scott et al., 2008). The concentration of redox-reactive elements (such as Mo) has been measured widely in shales (Schroder and Grotzinger, 2007; Scott et al., 2008) but cannot be easily applied to the carbonate record because of low concentrations of Mo and U in carbonates. Redox conditions in the water column strongly influence the redox state of Fe and it has been postulated that the ratio of highly reactive Fe (carbonate-associated Fe, Fe oxides and oxyhydroxides, and Fe sulphides) to total Fe in sediments reflects the paleo-redox condition (Canfield et al., 2007; Canfield et al., 2008). This proxy has been mainly applied to middle shelf sediments (Canfield et al., 2008; Nagy et al., 2009).

However the main proxy used for the carbonate record is REE concentration. The REEs are not significantly fractionated during precipitation and sedimentation (McLennan, 1989). Due to their short residence time in the ocean, REE concentration in carbonates can be used to determine their source and trace water mixing in seawater (Nothdurft et al., 2004; Frimmel, 2009). Furthermore, two of the REE elements can be used for direct information on seawater chemistry. Eu is often used to trace

hydrothermal input in the seawater (Derry and Jacobsen, 1990; Danielson et al., 1992). Moreover, Ce can be used to determine the redox condition of the ambient seawater (Wright et al., 1987) because differences in the behaviour of Ce(III) and Ce(IV) in natural waters results in a negative Ce anomaly in carbonates in oxic conditions (Wright et al., 1987).

The Y/Ho ratio of modern carbonates can be used to distinguish between marine carbonate and non-marine carbonate. This is because the Y/Ho concentration ratio of seawater, although variable, ranges from 35 to 60 (Nozaki et al., 1997; Lawrence et al., 2006) whereas the continental crust is characterised by a Y/Ho ratio of 26.2 (Kamber et al., 2005). This proxy has been used to distinguish between distal and proximal settings in Neoproterozoic carbonates from Namibia (Frimmel, 2009) and to reconstruct the degree of oxygenation of seawater in Late Ediacaran-Cambrian platform carbonates (e.g. Schroder and Grotzinger, 2007).

1.4.6 Non-traditional stable isotopes

Associated with these widely developed and applied proxies, a number of new systems are being applied to study chemical precipitation. These new proxies are mainly based on stable isotope systems such as Ca, B or Fe. Boron and Ca isotopes have been applied to Neoproterozoic sediments and have been interpreted to relate to variations in pCO_2 and weathering rates, respectively (Kasemann et al., 2005; Kasemann et al., 2010). Mg isotopes could also be used to determine the variation in the weathering fluxes during glacial periods. And finally, other non-traditional stable isotopes, not previously applied to Neoproterozoic successions, could be used such as Mo, Fe and Cr to determine redox conditions and Zn and Cu as proxies for biological activity (e.g. Pichat et al., 2003).

1.4.7 Climate and Redox Models for the Neoproterozoic

Several models have been proposed to explain the chemical variations recorded in the sedimentary record as well as the characteristics of Neoproterozoic sedi-

ments, notably low-latitude glacial deposits and the rapid change from glacial conditions to a warm environment. These models are: the Snowball Earth model (Kirschvink, 1992), the Slushball model (Schrag and Hoffman, 2001), the HOLIST model (Williams, 2000; Williams, 2008) and finally the zipper rift Earth model (Eyles and Januszczak, 2004). These models, described and discussed in Fairchild and Kennedy (2007), have been proposed to understand climate evolution during the Neoproterozoic and especially during the glaciations. However, none of these models emphasizes the redox condition in the ocean before, during or after the glacial periods except for the Snowball model where the occasional presence of BIFs has been used as evidence for an oxygen-depleted ice-covered ocean (Hoffman et al., 1998).

As described above, the Neoproterozoic seems to be the period in the Earth's history where the O_2 concentration in the atmosphere increased the most from about 10% to almost 80% PAL (Holland, 2006). This increase is probably linked with a strong change in redox conditions in the oceans. In Holland's model, the O_2 concentration in the atmosphere and in the ocean increased gradually during the Neoproterozoic (Holland, 2006). It has been argued that during the Neoproterozoic, the deep water changed from anoxic (maybe ferruginous) to oxic conditions (Canfield et al., 2008).

Several models have been proposed to explain the characteristics of the water column during this period (Canfield et al., 2008; Johnston et al., 2010; Li et al., 2010). Overall, they describe highly reduced redox conditions in the water column (anoxic, euxinic and ferruginous). Li et al. (2010) describe the water column in terms of four distinctive layers: (i) oxygenated shallow water, (ii) a ferruginous layer, (iii) a sulphidic layer and finally a second ferruginous layer (Fig. 1.6). Although this model is aimed at understanding the redox conditions in the deeper part of the water column, the shallow water is assumed to be oxygenated, although little is known on the level of oxygenation of the shallow water during the Neoproterozoic. Furthermore, it has been argued that at the beginning of the Tonian period, the shallow seawater was ferruginous (Johnston et al., 2010).

The model proposed by Li et al. (2010) is mainly based on the study of deep-sea

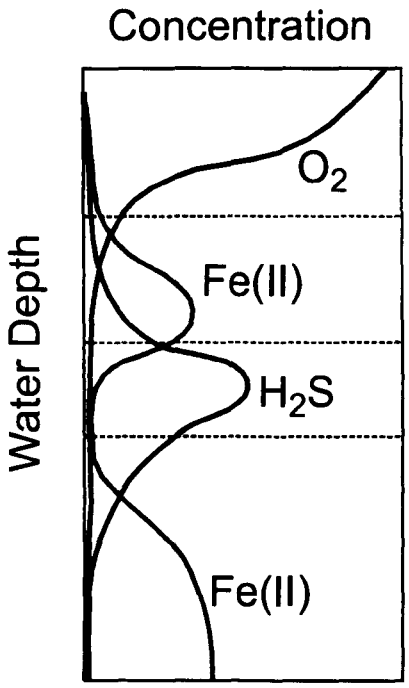

Figure 1.6: Schematic redox model of the Ediacaran Ocean. Modified from Li et al. (2010)

sediments and the redox of the shallow water and therefore the variation in atmospheric O_2 concentration has not been studied in any detail for the Neoproterozoic, especially during and after the glacial events.

1.5 Chromium Chemistry

Chromium is a transition metal occurring in group 6B of the periodic table. The ionic radius of Cr varies from 0.04 nm for Cr(VI) to 0.094 nm for Cr(III), and strongly depends on coordination type, chemical form and spin (Winter, 2001). Cr is also characterised by a wide range of oxidation states from 0 to +6. Only three of these oxidation states are found in nature: Cr(0), Cr(III) and Cr(VI). In some minerals (such as spinel) Cr can also be present as Cr(II), but this is a minor species. Cr has four stable isotopes, ^{50}Cr, ^{52}Cr, ^{53}Cr and ^{54}Cr and their natural abundances are 4.345%, 83.789%, 9.509% and 2.465% respectively (Winter, 2001). ^{53}Cr is produced by the radioactive decay of ^{53}Mn which has a short half-life (3.6 Ma) and is therefore considered to be extinct in the Earth (Birck and Allegre, 1985). However, this system has been applied widely to meteoritic material to constrain the timescale of the Solar

System formation (Birck and Allegre, 1985). ^{54}Cr has also been studied because it is a neutron-rich isotope that is enriched during nucleosynthetic processes (Trinquier et al., 2008b).

1.5.1 Cr concentration of terrestrial material

The Cr concentration in terrestrial materials is highly variable. In the Earth's mantle, Cr occurs almost exclusive as Cr(III) and Cr_2O_3 concentrations range from 0.41% to 0.55% (Henderson, 1982; McDonough and Sun, 1995), while in the continental crust, Cr concentrations range from 20 ppm in felsic igneous rocks (such as granites) to more than 2000 ppm in ultramafic igneous rocks but with an average around 100 ppm. The low abondance f Cr in the continetal crust relative to the mantle can be explained by the compatible behavior of Cr during partial melting. Black shales are enriched in transition metals (including Cr), with Cr concentrations ranging from 20 to 3000 ppm (average 100 ppm; Quinby-Hunt et al., 1997). The average Cr concentration in the continental crust is around 100 ppm (McLennan, 2001). In carbonates, the Cr concentration, although it has not been studied extensively, is thought to be about 10 ppm or less. The Cr concentration in other hydrogenous materials is relatively low and for example the Cr concentration ranges from 9 to 34 ppm in Fe-Mn crusts and ~26 ppm in Fe-Mn nodules (Hein et al., 1997). Moreover, Cr(III) is kinetically inert to reaction with sulphide and is not incorporated into pyrite (Morse and Luther, 1999).

1.5.2 Occurrence of Cr in aqueous systems

The Cr content of natural waters is highly variable from 2 nM to more than 100 nM (Ball and Izbicki, 2004), but for most natural waters it is below 40 nM and occurs in both the trivalent and hexavalent forms (Connelly et al., 2006). In seawater, the Cr concentration has been reported to be between 2 and 10 nM. Although thermodynamically, Cr(VI) should be the only Cr species present in seawater, a number of studies have reported the presence of non-negligible amounts of Cr(III) (e.g. Sander et al., 2003). The relative proportion of these species is strongly linked with the

Eh-pH conditions, as shown in the Eh-pH diagram for Cr in Figure 1.7 (Ball and Nordstrom, 1998). The Cr(VI) concentration in seawater has been determined to be between 2 and 4 nM (e.g. Jeandel and Minster, 1987).

Cr(VI) and Cr(III) behave differently in the natural environment (Pettine, 2000). Cr(VI) is thought to form stable oxy-anions and is therefore highly soluble in seawater. Cr(III) however, is believed to readily form hydroxide complexes and is removed from the system relatively quickly. It has been postulated in numerous publications that Cr(III) is insoluble under modern day seawater Eh-pH conditions (e.g. Elderfield, 1970; Murray et al., 1983).

At seawater Eh-pH conditions, the main Cr species should be Cr(VI) as either CrO_4^{2-} and $HCrO_4^-$ species (Elderfield, 1970). In low Eh environments, the main Cr species is Cr(III), although the form of the Cr(III) varies as a function of pH (Fig. 1.7). At low pH, Cr^{3+} is the dominant species and as the pH increase $Cr(OH)^{2+}$, $Cr(OH)_2^+$, $Cr(OH)_3$ and $Cr(OH)_4^-$ become stable (Zink et al., 2010). Trivalent Cr is believed to form complexes with a variety of ligands: hydroxyl, sulphate, fluoride, chloride and organic ligands (Rai et al., 1987). Under oxidising conditions (high Eh), dissolved Cr is thought to be present as Cr(VI), either in the form of $HCrO_4^-$ or CrO_4^{2-}, depending on pH (Fig. 1.7). However, Accornero et al. (2010) proposed that the main form of Cr in seawater is $NaCrO_4^-$. It is however important to note that little is known on the behavior of Cr with organics ligands.

A number of studies have determined the Cr concentration and Cr speciation in river waters (e.g. Pettine et al., 1997; Li and Xue, 2001). Relatively low concentrations have been reported in river water, typically ~10 nM and the main species is Cr(VI) (e.g. Li and Xue, 2001). A number of studies have also reported dominant Cr(III) in river waters (Pankow et al., 1977, Shuman and Dempsey, 1977).

Chromium is delivered to the oceans mainly by the riverine input with minor inputs from atmospheric and hydrothermal sources (Jeandel and Minster, 1984). There are no measurements of Cr in high temperature hydrothermal fluids, but low temperature fluids from the North Fiji Basin are reported to have dissolved Cr concentrations of up to 48 nM (Sander and Koschinsky, 2000) which extrapolates to an

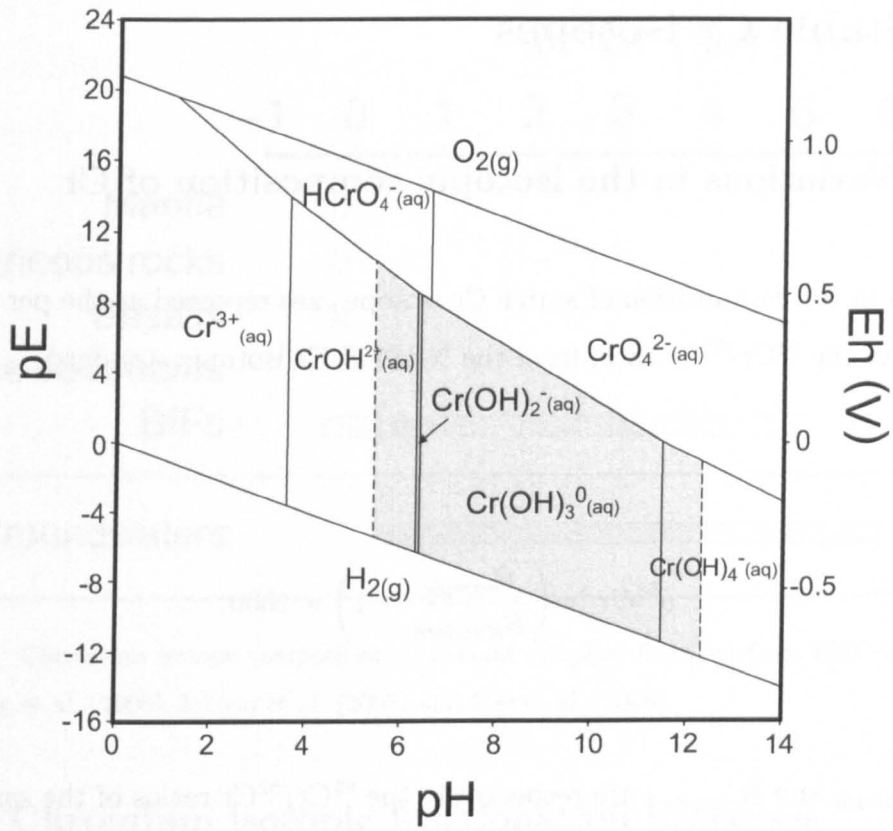

Figure 1.7: Eh-pH diagram for aqueous inorganic chromium hydrolysis species in groundwater at 25°C. The grey area indicates the stability zone of $Cr(OH)_3(s)$ for a total Cr concentration of 5 μM. Modified from Ball and Nordstrom (1998).

endmember value of ~1200 nM. The hydrothermal flux represents a small source of Cr (<10% of the riverine flux) but, because of scavenging of Cr by Fe-Mn oxides in the hydrothermal plume, hydrothermal activity most likely results in an overall loss of Cr from seawater (German et al., 1991b).

In summary, the Cr concentration of terrestrial materials is very variable. Cr is enriched in the mantle and the continental crust and is found in relatively low concentrations in secondary phases such as carbonates. Due to the large difference in concentration between the continental crust and hydrogenous precipitates, the detrital contribution must be carefully assessed for Cr isotopic studies in such precipitates.

1.6 Stable Cr isotopes

1.6.1 Variations in the isotopic composition of Cr

Variations in the composition of stable Cr isotopes are reported as the per mil (‰) deviation of the $^{53}Cr/^{52}Cr$ ratio from the NBS979 Cr isotopic standard:

$$\delta^{53}Cr = \left(\frac{R_{sample}}{R_{standard}} - 1 \right) \times 1000 \tag{1.1}$$

where R_{sample} and $R_{standard}$ are respectively the $^{53}Cr/^{52}Cr$ ratios of the sample and the NBS979 standard. There is a growing interest in stable Cr isotopes, and a recent study made the first attempts to apply the system to trace the increase of O_2 in the atmosphere (Frei et al., 2009). The Cr isotope inventory of terrestrial silicates has been presented by Schoenberg et al. (2008). The $\delta^{53}Cr$ value of the mantle and the continental crust is -0.15 ± 0.11‰ (Fig. 1.8; Schoenberg et al., 2008). Sediments from the Arabian Sea have been analysed and are characterised by slightly higher $\delta^{53}Cr$ values of around -0.032‰ (Schoenberg et al., 2008). Frei et al. (2009) have published Cr isotopic compositions of Proterozoic BIFs and the $\delta^{53}Cr$ value is between -0.2 and 4.9‰. This variation is attributed to Cr isotope fractionation during oxidative weathering.

Groundwater Cr isotopic compositions have been measured and range from 0.3 to 5.9‰ (Ellis et al., 2004; Izbicki et al., 2008). These Cr isotopic compositions are the heaviest measured to date in natural samples and are thought to reflect redox reactions occurring in the Cr cycle. It has been postulated that modern day seawater has a $\delta^{53}Cr > 0$‰ which reflects oxidising conditions (Izbicki et al., 2008; Frei et al., 2009). However, the Cr isotopic compositions of river waters and hydrothermal fluids have not yet been measured; this study presents the first data for seawater.

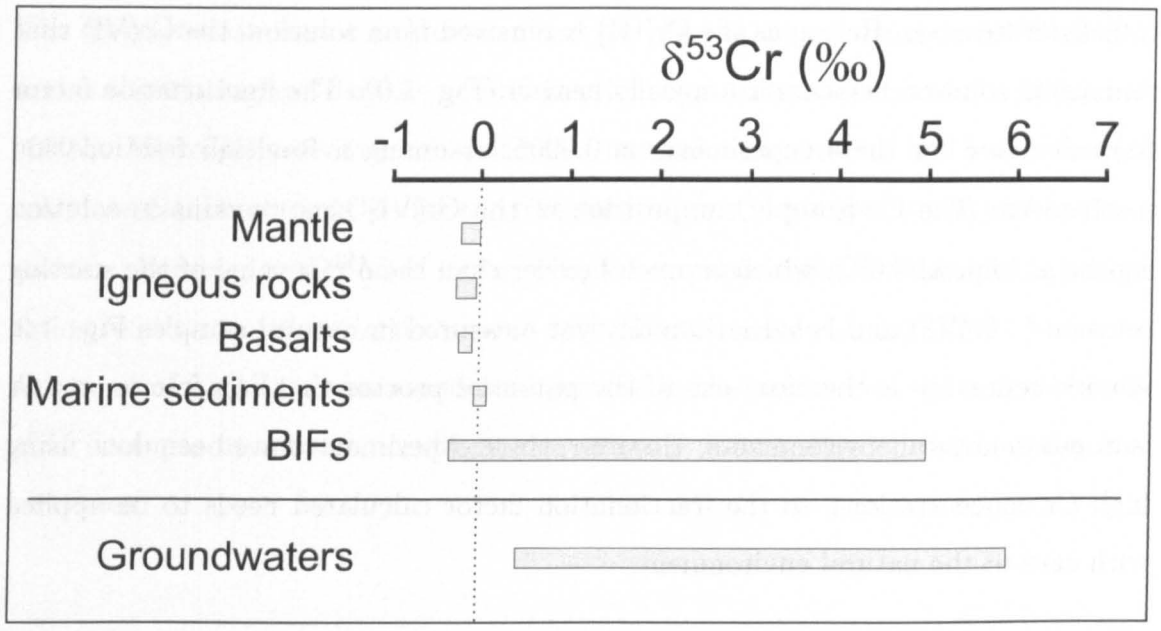

Figure 1.8: Chromium isotope composition of natural samples. Data are from Ellis et al. (2004), Schoenberg et al. (2008), Izbicki et al. (2008) and Frei et al. (2009)

1.6.2 Chromium isotopic fractionation processes

Isotopes of metal redox-sensitive elements have been used as palaeo-redox proxies. The two most widely used are Fe (e.g. Rouxel et al., 2005) and Mo (Siebert et al., 2003; Duan et al., 2010; Voegelin et al., 2010). However, others redox-sensitive elements such as Cr have the potential to provide constraints on the redox condition of seawater because Cr isotopes are fractionated during redox reactions. Cr isotopes have been used to assess the increase in atmospheric O_2 concentration in the atmosphere during the Proterozoic (Frei et al., 2009). However, several processes can fractionate Cr isotopes and in order to interpret Cr isotopes data it is important to understand which reactions are likely to fractionate the isotopes. Several redox reactions have been investigated.

1.6.2.1 Abiotic reduction

In the natural environment, abiotic reduction of Cr(VI) to Cr(III) occurs in the presence of electron donors such as Fe(II) and reduced sulphur (Puls et al., 1999). Ellis et al. (2002) demonstrated that Cr isotopes are fractionated during abiotic reduction. In their experiments, the lighter isotopes are preferentially reduced relative

to heavier isotopes. Hence, as the Cr(III) is removed from solution, the Cr(VI) that remains in solution becomes isotopically heavier (Fig. 1.9). The fractionation factor (α) calculated for these experiments is 0.9965, assuming a Rayleigh fractionation mechanism. The Cr isotopic composition of the Cr(VI) that remains in solution can be as high as 7.6‰, which is much heavier than the δ^{53}Cr value of the starting solution (+0.4‰) and heavier than any yet measured in natural samples Fig. 1.9. Abiotic reduction is therefore one of the potential process that can fractionate Cr isotopes in natural environments. However, these experiments have been done using high Cr concentrations, so the fractionation factor calculated needs to be applied with care to the natural environment.

1.6.2.2 Microbial reduction of Cr(VI)

It has been proposed that biological activity is primarily responsible for the reduction of Cr(VI) under both anaerobic and oxic conditions (Lovley, 1993). The impact of such reactions has been studied by Sikora et al. (2008), who found that the microbially mediated reduction of Cr(VI) fractionates the Cr isotopic composition, the residual Cr(VI) becoming heavier during the reduction process (Fig. 1.9).

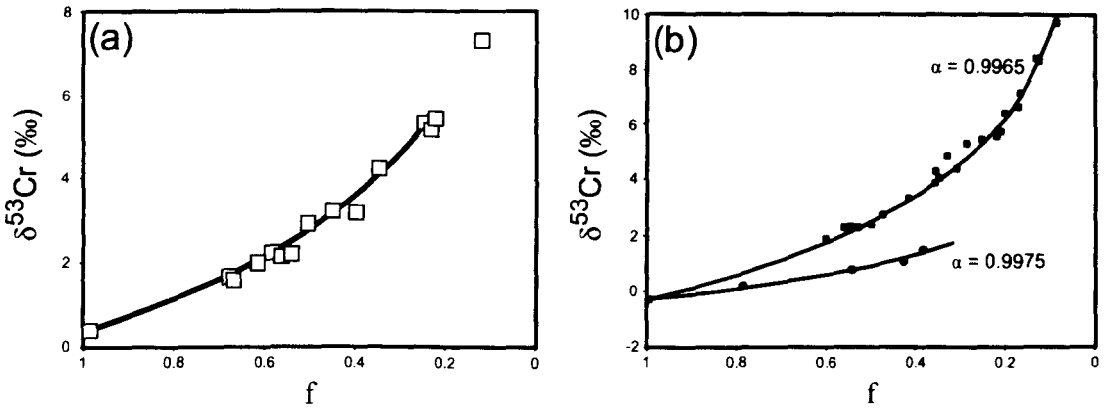

Figure 1.9: Cr isotopic composition of Cr(VI) in solution during reduction by (a) abiotic reduction reaction (modified from Ellis et al. (2002)) and (b) microbially mediated reduction (modified from Sikora et al. (2008)). f is the fraction of Cr(VI) that remains in solution following partial reduction to Cr(III). The solid lines correspond to a Rayleigh fractionation equation, where α is the fractionation factor. Red squares show experiment were done with $\leq$ 100 μM electron donor and green circles experiments were done with a 10 nM electron donor (Sikora et al., 2008).

The fractionation factor (α) determined during the experiments is 0.9965-0.9975 and is slightly higher than the abiotic fractionation factor determined by Ellis et al. (2002). Microbial activity is ubiquitous in natural environments and therefore such reactions can be responsible for the fractionation of Cr isotopes in natural environments. Microbial reduction of Cr in soils, for example could fractionate Cr isotope ratios relative to values in the source rock (Bartlett and James, 1979). Microbial reduction of Cr(VI) is also a potential process in the modern oceans and the study of Cr isotopes in seawater could give us valuable information on marine microbial processes.

1.6.2.3 Oxidation

Cr isotopes could also be fractionated during oxidation reactions. Zink et al. (2010) investigated the Cr isotopic fractionation during oxidation of Cr(III) to Cr(VI). In their experiments, the fractionation factor obtained is lower compare to the reduction fractionation factor ($\alpha = 1.00006$). Their experiments were carried out in closed systems and minimal isotope fractionation was observed during oxidation of Cr(III). However, it is important to note that oxidation during weathering is likely to occur in an open system. Further investigations are required to determine if Cr(III) oxidation during weathering could potentially fractionate Cr isotopes.

1.6.2.4 Sorption

Sorption effects have been described as a potential process for Cr isotope fractionation. Both Cr(VI) and Cr(III) are likely to absorb onto particles although Ellis et al. (2004) demonstrated that Cr(VI) absorption onto goethite was negligible at equilibrium under natural pH conditions. However they also demonstrated that sorption under non-equilibrium (i.e. kinetically-driven) conditions can lead to fractionation of Cr isotopes by up to 1‰. Therefore, adsorption could fractionate Cr isotopes in river systems.

1.6.2.5 Interaction between Cr(VI) species

Ellis et al. (2004) studied Cr isotope fractionation between $HCrO_4^-$ and CrO_4^{2-} under equilibrium conditions and concluded that there was no fractionation between these species. For this reason, all of the variation that they measured in Cr isotopes was attributed to reduction reactions.

1.6.2.6 Interaction between Cr(III) and Cr(VI)

More recently, the equilibrium process between Cr(III) and Cr(VI) in solution has been investigated by Zink et al. (2010), who demonstrated that after 8 weeks, equilibrium between Cr(III) and Cr(VI) in solution was not obtained. This result led to the conclusion that Cr(III) and Cr(VI) in natural waters will not reach equilibrium and therefore Cr isotopes studies of Cr(III) and Cr(VI) isotopic composition could give valuable information on the natural Cr cycle.

In summary Cr isotopes can be fractionated by several processes in the natural environment. The sparse data on Cr isotopes and the different processes that could affect the Cr isotopes have been summarized in Figure 1.10. It is important to note the Cr cycle is not well understood in the natural system, but this thesis will go some way to providing answers to these gaps in our knowledge.

1.7 Thesis Aims

As described above, the Cr isotopic composition of marine sedimentary rocks has the potential to record past redox conditions in the oceans. This is because Cr isotopes are fractionated during redox reactions and therefore a estimation of Cr reduction can be made. The main aim of this study is to investigate the use of Cr isotope analyses of carbonate rocks to determine the redox condition and the O_2 atmospheric concentration during the Neoproterozoic. The project focuses on the oxygenation of shallow waters during the Neoproterozoic, from before the first glaciations to the Proterozoic-Phanerozoic transition, using carbonates as a chemical indicator of seawater chemistry. In order to understand the relationship between the Neoproterozoic rocks that we have collected and the seawater from which they

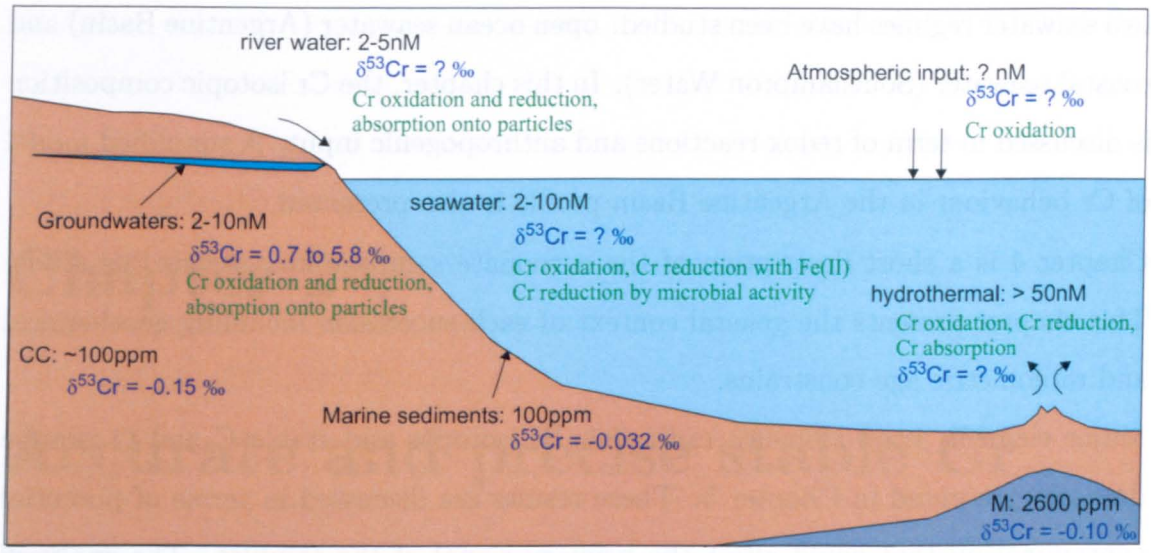

Figure 1.10: Chromium concentration and chromium isotopic composition inputs in to the modern oceans illustrating the composition of various inputs to the system. CC is the continental crust, M is the mantle. Data are from Cranston and Murray (1978), Sander and Koschinsky (2000), Sander et al. (2003), Ellis et al. (2004), Schoenberg et al. (2008) and Izbicki et al. (2008)

formed, I have also analysed modern and Phanerozoic carbonates, and focused on inorganic carbonates such as ooids or oolitic limestones.

It is also clearly important to better understand the behaviour of Cr in the modern ocean and in the modern environment (Fig. 1.10). In order to do this, I have analysed a suite of seawater samples from the Argentine Basin and from Southampton Water. In order to measure Cr isotopes in carbonates, which typically have less than 10 ppm Cr, and seawater with even lower Cr concentrations, I have developed a new analytical method both in terms of a low blank Cr separation technique and high-precision measurements of isotope ratios by multicollector inductively coupled plasma mass spectrometry (MC-ICP-MS).

1.8 Thesis structure

Chapter 2 outlines the methodology developed and used in this study to measure Cr isotopes in low concentration samples. This chapter has been published in the Journal of Analytical Atomic Spectrometry (Bonnand et al., 2011).

Chapter 3 presents the Cr isotopic composition of seawater samples. In this chapter,

two seawater regimes have been studied: open ocean seawater (Argentine Basin) and coastal seawater (Southampton Water). In this chapter, the Cr isotopic composition is discussed in term of redox reactions and anthropogenic input. A simplified model of Cr behaviour in the Argentine Basin profile is also presented.

Chapter 4 is a short description of the carbonate samples analysed in this study. This chapter presents the general context of each succession including geochemical and radiometric age constrains.

Major element, trace element, radiogenic Sr isotopes and stable C and O isotope data are presented in Chapter 5. These results are discussed in terms of potential contamination that could affect the primary signal of the samples. The analysed samples are then discussed in terms of interpreting the composition of the water from which the carbonates were deposited.

Chapter 6 presents the Cr isotopic composition of all carbonates analysed in this study. This chapter also presents a model of the redox conditions in the ocean during the Neoproterozoic.

Chapter 7 presents the conclusions of the thesis.

Chapter 2

Accurate and precise stable Cr isotopes

2.1 Introduction

Chromium has four stable isotopes, ^{50}Cr, ^{52}Cr, ^{53}Cr and ^{54}Cr, with abundances of 4.31%, 83.789%, 9.501% and 2.365%, respectively (De Laeter et al., 2003). Most Cr isotope studies of natural samples have focused on the investigation of ^{53}Cr enrichments in meteoritic materials due to the decay of the now extinct short-lived radionuclide ^{53}Mn, which can be used to provide a chronology for the earliest history of the solar system (Birck and Allegre, 1984; Birck and Allegre, 1988; Gotz and Heumann, 1988; Lugmair and Shukolyukov, 1998; Birck, 2004). Additionally, it has been determined that some meteorites have nucleosynthetic ^{54}Cr anomalies (Birck and Allegre, 1988; Gotz and Heumann, 1988; Lugmair and Shukolyukov, 1998; Birck, 2004; Trinquier et al., 2007).

Studies performed more recently have reported that small natural variations in the stable Cr isotope ratios can occur in terrestrial samples as a result of mass dependent fractionation processes (Schoenberg et al., 2008; Frei et al., 2009). In addition, it has been demonstrated that the ratio of ^{53}Cr to ^{52}Cr can be used to identify Cr from anthropogenic sources, and/or to identify chemical reactions involving Cr (Ellis et al., 2002; Johnson and Bullen, 2004; Izbicki et al., 2008). For example, it has been shown that Cr isotopes fractionate during the reduction of Cr(VI) to Cr(III):

the lighter isotopes are preferentially reduced, enriching the remaining Cr(VI) in the heavier isotopes by up to 7.6‰ on the $^{53}Cr/^{52}Cr$ ratio (Ellis et al., 2002). Cr isotopic fractionation may also occur during the oxidation of Cr(III) to Cr(VI) (Zink et al., 2010). Critically, the behaviour of Cr(VI) and Cr(III) is different in aquatic systems, where Cr(VI) is soluble and Cr(III) is highly particle reactive and insoluble (Cranston and Murray, 1978). Thus, Cr isotopes may be used to track the reduction of Cr(VI) and contaminant remediation (Johnson and Bullen, 2004; Izbicki et al., 2008), which is important because Cr(VI) is a carcinogen, whereas Cr(III) is much less toxic (Kimbrough et al., 1999). Furthermore, Cr isotopes can potentially be utilised to reconstruct past redox conditions in the ocean (Frei et al., 2009; Bonnand et al., 2009).

Consequently, there is a growing interest in the measurement of Cr isotopic variations in low temperature terrestrial materials. However, although Cr is relatively abundant in the solid Earth with concentrations of 2630 $\mu g\ g^{-1}$ in the mantle (McDonough and Sun, 1995) and 56-185 $\mu g\ g^{-1}$ in the continental crust (Taylor and McLennan, 1995; Rudnick et al., 2003; Kemp et al., 2003; Palme et al., 2007), the Cr concentration in natural waters (groundwaters, rivers and seawater) and their chemical precipitates is considerably lower ($\sim$2 $\mu g\ g^{-1}$ in carbonates)(Jeandel and Minster, 1987; Connelly et al., 2006; Bonnand et al., 2009). To study such systems requires improvements in our ability to measure Cr isotopes in low-level samples.

The first measurements of stable Cr isotope ratios were made by thermal ionisation mass spectrometry (TIMS) using a double spike technique (Ellis et al., 2002; Johnson and Bullen, 2004; Ball and Bassett, 2000). These measurements required 0.5-1 μg of Cr and the external precision on the $^{53}Cr/^{52}Cr$ ratio was $\pm$0.2‰. However, the advent of high-resolution Multiple Collector Inductively Coupled Plasma Mass Spectrometry (MC-ICP-MS) instrumentation has led to a significant improvement in the precision of stable Cr isotope measurements. Recent studies report an external precision for the $^{53}Cr/^{52}Cr$ ratio of $\pm$0.024‰ using double spike (Schoenberg et al., 2008) and $\pm$0.06‰ using standard-sample bracketing (Halicz et al., 2008) methods, respectively. Nevertheless, all high-precision Cr isotope studies published to date require samples that contain at least 1μg of Cr.

This study reports new methods for the chemical purification and high-precision analysis of stable Cr isotopes in carbonates with low levels of Cr, by MC-ICP-MS.

2.2 Analytical procedures

2.2.1 Sample preparation

Samples were prepared in a metal free clean room in Class 100 laminar flow hoods at the Open University. All mineral acids were quartz distilled and then sub-boiled in a perfluoroalkoxy (PFA) still. PFA Centrifuge tubes were cleaned with 10% HNO_3 and then rinsed with 18.2 MΩ grade H_2O from a Millipore system (MQ H_2O). PFA Savillex® beakers were cleaned with concentrated HNO_3 for 48h on a hotplate at 130 °C, followed by cleaning with concentrated HCl and were finally rinsed with MQ H_2O.

Carbonate samples were milled to a fine powder using either an agate bowl Tema® or a ceramic mortar. Special care was taken to avoid any metal contamination during the crushing procedure. In order to optimise the double spike procedure (Section 2.2.3), the Cr concentration of each sample was first determined by ICP-MS (Agilent 7500) at the Open University. The requisite amount of spike was then added to the sample powders (70-150 mg) in a centrifuge tube. The samples were leached in 6 ml of 0.5 M HCl. The acid strength was kept as low as possible in order to avoid the dissolution of any detrital components. The leaching procedure takes about 24 h at room temperature. During this period, the samples were agitated at least twice by placing them in an ultrasonic bath for 20 min. After leaching, the samples were centrifuged for 20 min at 4000 rpm and the supernatant was transferred to a cleaned PFA Savillex® beaker. The residue was rinsed with 4 ml of MQ H_2O, centrifuged and the supernatant H_2O was added to the acid. The samples were dried down slowly at 110 °C on a hotplate. In order to reduce all Cr species to Cr(III) and to equilibrate the spike Cr and sample Cr, the residue was then re-dissolved in 6 M HCl and left on the hotplate overnight (Trinquier et al., 2008a). After dry-down, the samples were re-dissolved once more in 0.5 ml of 6 M HCl. This solution was heated

overnight in a closed vial. Prior (<1 h) to starting the Cr separation procedure, the samples were diluted with MQ H_2O to give a 0.5 M HCl solution.

2.2.2 Separation of Cr from the sample matrix

High precision measurements of Cr isotope ratios by MC-ICP-MS require separation of Cr from the sample matrix in order to avoid potential matrix effects and to minimize isobaric interferences. Two different methods for the separation of Cr have been reported. The first method utilises a cation exchange resin, which allows isolation of Cr(III) from the matrix (Birck and Allegre, 1984; Trinquier et al., 2008a). The second technique uses an anion exchange resin to separate Cr(VI) (which forms an oxy-anion) from the matrix (Ball and Bassett, 2000). Although both methods allow effective separation of Cr, they can not be easily applied to the study of low concentration samples because the blank contribution from the separation procedure is too high (2-20 ng).

For this reason, we have established a new method for the separation of Cr. This is based on a technique used at the Institut de Physique du Globe de Paris (IPGP) (Birck and Allegre, 1984; Trinquier et al., 2008a), but the Cr is eluted from the column using 0.5 M HCl rather than 1 M HCl, as this allows better separation of Cr from the sample matrix. Briefly, 2.9 ml of BioRad AG 50W-X8 (200-400 mesh) cation exchange resin is loaded in a 30 ml PFA Savillex column (that has an internal diameter of 6.4 mm). The resin is cleaned with 10 ml of 8 M HNO_3, 40 ml of 6 M HCl, and 40 ml of MQ water. The column is then pre-conditioned with 12 ml of 0.5 M HCl. The sample is loaded onto the column in 6 ml of 0.5 M HCl and a further 1-4 ml of 0.5 M HCl is then added to the column, depending on the Fe content of the sample. The purified Cr is collected in these 7-10 ml of 0.5 M HCl. The remaining cations are then eluted with 10 ml of 6 M HCl in order to clean the resin, which can be reused for multiple separations. The Cr fraction is evaporated to dryness and re-dissolved in 0.6 M HNO_3 for MC-ICP-MS analysis.

It is important to note that the Cr elution curve presented in Figure 2.1 is characterised by the presence of two peaks for Cr. Indeed, a feature of the column chemistry is that a second (smaller) Cr elution peak occurs after ~20 ml of 0.5 M

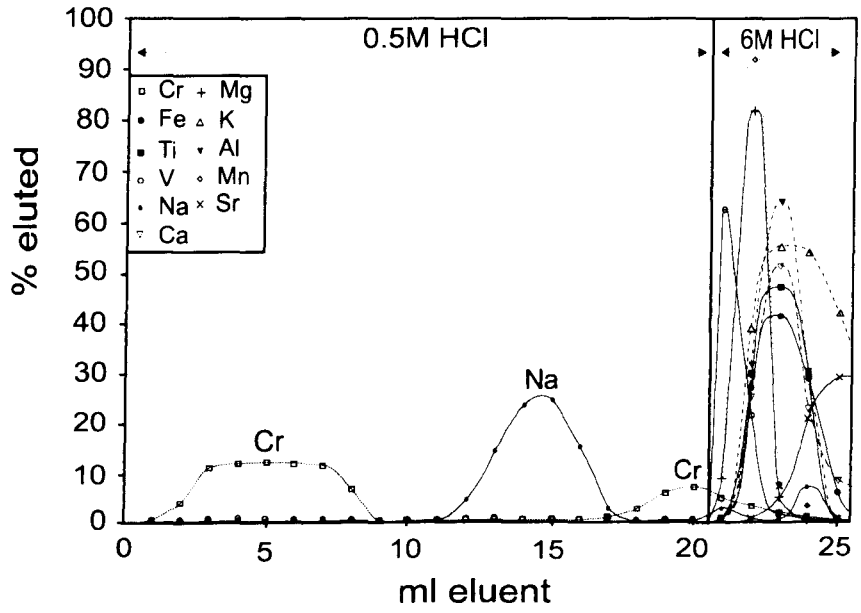

Figure 2.1: Elution curves for key elements from the cation exchange resin (see text for details).

HCl (Fig. 2.1); this feature was also observed by Trinquier et al. (2008a). As other elements, in addition to Cr, are eluted in the second peak, only the first Cr peak is collected. Importantly, Trinquier et al. (2008a) noted that the isotopic composition of the Cr eluted in the first peak was heavier than that of the Cr eluted in the second peak (Trinquier et al., 2008a). Given that 70-80% of the total Cr is eluted in the first peak (Fig. 2.1), this could result in 1-2‰ fractionation in the $^{53}Cr/^{52}Cr$ ratio (Schoenberg et al., 2008). In order to counteract this effect, we therefore add the isotope spike to the sample before the column chemistry.

2.2.3 Analysis of Cr isotopes

2.2.3.1 Double spike technique

The use of an isotopically enriched double-spike to correct for fractionation of stable isotopes during sample processing and for instrumental mass bias effects was first proposed by Dodson (1963) and has been applied to numerous isotope systems, which have $\geq$4 isotopes. This technique is ideal for analysis of Cr isotopes in terrestrial samples, which are only affected by mass dependent fractionation, as only a spiked sample needs to be analysed once the composition of the reference standard

(i.e. NBS 979) has been determined (Albarede and Beard, 2004). Moreover, this technique enables precise determination of the Cr concentration in the sample via the isotope dilution equation. The $^{53}Cr/^{52}Cr$ isotope ratios are reported as the per mil variation from the Cr isotope reference material NBS 979:

$$\delta^{53}Cr(‰) = \left(\frac{(^{53}Cr/^{52}Cr)_{sample}}{(^{53}Cr/^{52}Cr)_{NBS979}} - 1 \right) \times 1000 \quad (2.1)$$

In this study we purposefully chose a ^{50}Cr-^{54}Cr spike for two practical reasons. ^{50}Cr and ^{54}Cr are the two least abundant Cr isotopes, but are sensitive to isobaric interferences from Ti, V and Fe. Therefore measuring a spiked solution containing ^{50}Cr and ^{54}Cr reduces the uncertainties on the measured $^{50}Cr/^{52}Cr$ and $^{54}Cr/^{52}Cr$ ratios required for the double-spike calculation, and reduces the influence of any isobaric interferences. However, in order to produce accurate and precise data, the double-spike technique must be carefully optimised (Galer, 1999). This requires: 1) establishing the most appropriate spike composition; 2) solving the double-spike equations in the correct isotopic space (i.e., the denominator isotope for each of the isotope ratios); and 3) adding an appropriate amount of spike. Optimisation is best described by the error magnification term, where:

$$\gamma = \frac{\sigma^{ds}}{\sigma^{nat}} \quad (2.2)$$

σ^{ds} is the uncertainty for a given ratio derived from the double-spike measurements, and σ^{nat} is the uncertainty of the natural un-spiked run. Our calculations are similar to those described in Galer (1999), except we solve for the exponential mass fractionation law. Rudge et al. (2009) suggest that other Cr double-spike combinations provide slightly better error magnification behaviour than the ^{50}Cr-^{54}Cr combination, but our calculations indicate that a ^{50}Cr-^{54}Cr double-spike produces low γ values for all three Cr isotope ratios. In addition, the double-spike equation that we use in this study (see next section, Eq. 2.3) is best solved in ^{52}Cr isotope space. Other approaches can be used for calculating spike optimisation, such as those described in Rudge et al. (2009), but the absolute error magnification values depend

specifically on how the double-spike equations are solved (Galer, 1999), which explains why our ^{50}Cr-^{54}Cr double-spike is different in composition from that of Rudge et al. (2009). In order to calculate the optimal spike/sample ratio, Equation 2.3 is solved using different proportions of spike and sample. We use an ion model based on the one described by Ludwig (1986) to calculate the uncertainty on signal intensity of each isotope which is then propagated to calculate the uncertainty on each of the isotope ratios; note that this model assumes that both the spiked and unspiked samples contain the same quantity of Cr. The error magnification is calculated using a Monte Carlo simulation in which the uncertainties of the three Cr isotope ratios for each spike/sample mixture are used to generate 500 data points for each analysis. These data points have a Gaussian distribution around the mean value. Each of the 500 data points is then run through the deconvolution program and the mean uncertainty of the deconvolved data is calculated. Results of these calculations are presented in Figure 2.2. The error magnification terms (γ) for the deconvolved ^{53}Cr/^{52}Cr and ^{54}Cr/^{52}Cr ratios are less than 2, and the error magnification for the deconvolved ^{50}Cr/^{52}Cr ratio is less than 3, for a wide range of spike/sample mixtures. A spike/sample mixture that generates a ^{50}Cr/^{52}Cr ratio of 0.386 provides the smallest error. Routinely, our spike/sample mixtures have ^{50}Cr/^{52}Cr ratios of 0.3-0.5, although the error magnification term for δ^{53}Cr is less than 2 for ^{50}Cr/^{52}Cr ratios of between 0.14 and 1.26, making optimal spiking straightforward.

An in-house ^{50}Cr-^{54}Cr double-spike was prepared from ^{50}Cr (96.1% pure) and ^{54}Cr (96.8% pure) chromium metal spikes purchased from Oak Ridge National Laboratory. Two single spikes were made by dissolving the Cr-metal in 6 M HCl. The Cr concentration in the single spike solutions was determined by isotope dilution versus a gravimetric standard, and the double-spike was then prepared by mixing the single spikes in the appropriate proportions. The double-spike was calibrated by TIMS (ThermoFisher Scientific Triton) at The Open University using standard filament loading techniques (Ellis et al., 2002), because the total mass fractionation on the TIMS is small and adheres closely to exponential mass fractionation behaviour. Pure NBS 979, the pure ^{50}Cr-^{54}Cr double-spike and spike/standard mixtures were analysed. The isotopic composition of the double-spike is then calculated using

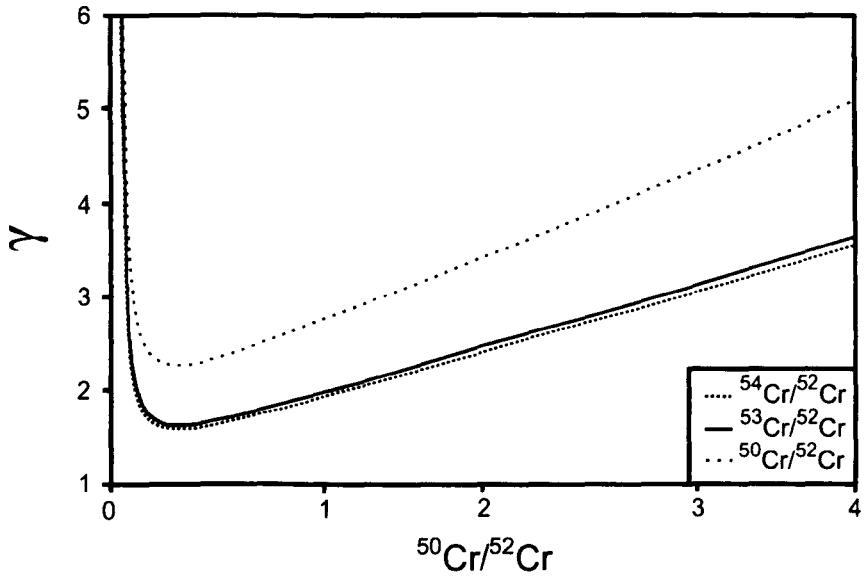

Figure 2.2: Error magnification term (γ) for the deconvolved $^{50}Cr/^{52}Cr$, $^{53}Cr/^{52}Cr$ and $^{54}Cr/^{52}Cr$ as a function of the $^{50}Cr/^{52}Cr$ in the spike/sample mixture (see text for details).

Equation 2.3, by treating the pure double-spike as an unknown. The isotopic composition of the double-spike was derived from twenty separate analyses of standards, spikes and spike/standard mixture and it is reported in Table 2.1.

2.2.3.2 MC-ICP-MS procedure

Cr isotope ratios were determined by MC-ICP-MS (ThermoFisher Scientific Neptune) at the Open University. This instrument is equipped with 9 faraday cups that allow the simultaneous collection of all four Cr isotopes (^{50}Cr, ^{52}Cr, ^{53}Cr, and ^{54}Cr), as well as ^{56}Fe, ^{49}Ti and ^{51}V. In this study each of the cups was connected to a 10^{11} Ω resistor. Measurements of ^{56}Fe, ^{49}Ti and ^{51}V allow us to correct for the isobaric interferences from ^{54}Fe on ^{54}Cr, and ^{50}V and ^{50}Ti on ^{50}Cr. Cr isotope measurements are also sensitive to interferences from polyatomic species such as $^{40}Ar^{13}N$, $^{40}Ar^{14}N$ and $^{40}Ar^{16}O$ on ^{53}Cr, ^{54}Cr and ^{56}Fe, respectively. However, we are able to fully resolve these interferences from the Cr and Fe isotope masses by operating the MC-ICP-MS at increased mass resolution ("medium" or "high" mass resolution) (Weyer and Schwieters, 2003).

Over the course of this study, different measurement protocols were tested. Ini-

Table 2.1: Isotopic composition of the Open University ^{50}Cr-^{54}Cr double-spike.

	$^{50}Cr/^{52}Cr$	$^{53}Cr/^{52}Cr$	$^{54}Cr/^{52}Cr$
Average ratio (n=20)	19.74494	0.1442076	9.882788
2 s.d.	0.00203	0.0000123	0.000939
2 s.d. (‰)	0.103	0.0851	0.095

tially, the samples were nebulized by a Teflon micro-nebulizer in free aspiration mode with an uptake rate of 50 μl min^{-1} and the aerosol was sprayed into the plasma via the ThermoFisher stable introduction system (SIS) that consists of a dual cyclonic/double pass spraychamber. The MC-ICP-MS was equipped with ThermoFisher X-cones, and operated in high-resolution ($8000<\Delta M/M<10000$) mode. Under these conditions, a 200 ng ml^{-1} Cr solution yielded an ion beam intensity of 2 V for ^{52}Cr. In an effort to reduce the concentration of Cr in the solution (and hence the sample size), samples were introduced with an Aridus 2 desolvating sample introduction system with the MC-ICP-MS in medium resolution ($5000<\Delta M/M<6500$) mode. In order to minimize the interference of ArN on Cr, the Aridus was carefully tuned to produce a stable signal, with good mass resolution, without the addition of N_2. This analytical set-up (Table 2.2) allows measurement of a 50 ng ml^{-1} Cr solution and gives an ion beam intensity of 9-12 V for ^{52}Cr. The higher ion-beams compared to the SIS are necessary since the background is larger with the Aridus 2 ($\sim$10-15 mV for ^{52}Cr) compared to the SIS ($\sim$0.5 mV for ^{52}Cr). Nevertheless, each Cr isotope analysis requires only 100 ng of Cr - an improvement on existing techniques by a factor of 4.

The following measurement protocol is utilized. The amplifier gain of each faraday cup is measured daily. Each isotopic analysis of a sample and or standard consists of measurement of 100 ratios (8.4 s integrations) in blocks of 10, which takes $\sim$20 min. A baseline of 30 s is measured every 2 blocks of data acquisition. On-peak backgrounds (50 ratios of 8.4 s integrations) are measured before every sample and standard analysis. The system is washed with 0.9 M HNO_3 for 5-10 min before every background measurement until the background drops to $\sim$10-15 mV of ^{52}Cr. Each analytical session starts with two or three analyses of a spiked NBS 979 solution,

Table 2.2: Instrumental operating parameters.

Cup configuration	^{49}Ti (L3), ^{50}Cr (L2), ^{51}V (L1), ^{52}Cr (C), ^{53}Cr (H1), ^{54}Cr (H2), ^{56}Fe (H3)
Scan type	Static mode
Mass resolution	$\sim$ 6500
Aridus uptake rate	50 μl.min^{-1}
Sensitivity	$\sim$ 180 V.ppm^{-1}
Integration time	8.389 s
Number of blocks	10
Number of cycles (per block)	10

Note that the Aridus 2 is operated without N_2 gas to minimise interferences from ArN^+

and this solution is analysed every two samples in order to monitor the drift of the machine.

2.2.4 Data processing

The Cr isotopic composition of the samples and standards was determined offline, although baseline and gain corrections are made on-line using the ThermoFisher software. The on-mass background is subtracted from the raw intensity for all Cr isotope masses, and ^{50}Cr/^{52}Cr, ^{53}Cr/^{52}Cr, and ^{54}Cr/^{52}Cr ratios are calculated for each of the 100 cycles. The double-spike calculations assume an exponential mass fractionation law (Albarede and Beard, 2004) and the isotopic composition of the sample is solved using Equation 2.3:

$$F^i(X_{sp}^{ref}, f_{nat}, f_{mix}) = X_{sp}^{ref} R_{sp}^i + (1 - X_{sp}^{ref}) r_{nat}^i \left(\frac{M^i}{M^{ref}}\right)^{f_{nat}} - r_{mix}^i \left(\frac{M^i}{M^{ref}}\right)^{f_{mix}} = 0 \quad (2.3)$$

where R_{sp}^i , is the isotope ratio of i in the spike, r_{nat}^i and r_{mix}^i are the measured isotope ratios of i in the sample and mixture, and M^i and M^{ref} are the true masses of the isotope i and the reference isotope. F^i is a closure function for the spike-sample mixture, which must be equal to zero. The equation is solved using an iterative Newton-Raphson procedure (Albarede and Beard, 2004) that recovers the proportion of spike in the mixture (X_{sp}^{ref}), the fractionation factor for the spiked

sample (f_{mix}) and the fractionation factor for the sample (f_{nat}), which allows us to calculate the isotopic composition of the original sample. The isotope ratios for NBS979 used for referencing our isotope data (e.g. to calculate δ^{53}Cr) in this study, were obtained by TIMS and MC-ICP-MS by internal normalisation to a $^{50}Cr/^{52}Cr$ ratio of 0.051859 (Birck and Allegre, 1984). This yielded $^{53}Cr/^{52}Cr$ = 0.1134561 and $^{54}Cr/^{52}Cr$ = 0.0282112 and these values are all within the uncertainty of those reported in previous studies (Birck and Allegre, 1984; Trinquier et al., 2008a).

2.3 Results and discussion

2.3.1 Separation of Cr from the sample matrix

The efficacy of our Cr separation technique was tested using both a multi-elemental solution and a certified dolomite reference material (JDo-1). Figure 2.1 shows that this technique effectively separates Cr from the carbonate matrix, even though Ca/Cr and Mg/Cr ratios are > 10000 in the original solution. Moreover, interfering elements such as Ti, V and Fe are primarily eluted only when 6 M HCl is added to the column, although a small proportion (~0.0008%) of the Fe is eluted with 0.5 M HCl. For this reason, the quantity of 0.5 M HCl added to the column after the sample is loaded in 6ml is reduced (from 4 ml to 1 ml) for samples that contain high Fe. This reduces the Cr yield slightly (by <5%), but the key effect of this strategy is that $^{56}Fe/^{54}Cr$ is always <0.3 (and usually <0.05), even for high-Fe samples.

The total blank of our Cr separation procedure is between 0.12 and 0.20 ng, which is negligible (<0.1%) compared to the amount of Cr processed through the columns (~250 ng).

2.3.2 Reproducibility and accuracy of Cr isotopic measurements

The long-term instrumental reproducibility was determined by measuring a spiked NBS 979 Cr standard (Fig. 2.3, Table 2.3). The δ^{53}Cr values recovered by the

double-spike technique are within error of 0‰, as expected, but the overall average value is slightly positive, with δ^{53}Cr = 0.035 ± 0.056‰ (2s.d., n = 147). Another MC-ICP-MS study reports average δ^{53}Cr values that are slightly negative (Schoenberg et al., 2008), although these authors point out that by internally normalizing the daily average of the δ^{53}Cr value of the standard to the nominal value of zero, the long-term instrumental reproducibility is improved. Applying this technique to our data produces average δ^{53}Cr values of 0.000 ± 0.031‰ (2s.d.) for all 147 standard measurements. The internal error (2s.e.) of measurements of δ^{53}Cr in both natural samples and standard-spike mixtures is usually ~0.010‰.

The external reproducibility of the entire technique (sample leaching, column chemistry and isotope analysis) is estimated by multiple analysis of the JDo-1 dolomite reference material. This standard was leached ten times over the course of this study, and each leachate was then processed through the column chemistry and analysed. JDo-1 is appreciably isotopically heavier than NBS 979 with δ^{53}Cr = +1.719 ± 0.057‰ (2s.d., n = 10; Fig. 2.4; Table 2.3). The reproducibility of the δ^{53}Cr values for this sample is worse than the external reproducibility of the synthetic NBS 979 solution; this might be caused by small amounts of matrix in the Cr fraction, or the heterogeneity of JDo-1. Nevertheless, the value of 0.057‰ that we obtain for the precision of $\delta^{53}Cr_{JDo-1}$ is an indication of external precision of a sample analysis. However, Schoenberg et al. (2008) note that there is an additional source of inaccuracy inherent in the double-spike measurements. We do not know whether natural samples are fractionated by kinetic or equilibrium fractionation, but we assume in Equation 2.3 that the natural fractionation is kinetic. The difference between the laws produces an inaccuracy of -0.009‰ per 1‰ difference in the true δ^{53}Cr value, using the double-spike technique. Therefore this uncertainty needs to be propagated into the external reproducibility as follows:

$$2SD = \sqrt{(-0.009‰ \times \delta^{53}Cr_{NBS979})^2 + (2\sigma_{external})^2} \qquad (2.4)$$

In the case of JDo-1, this increases the uncertainty from 0.057‰ to 0.059‰, which is negligible. However, for samples that have extreme δ^{53}Cr values (+7‰),

the overall uncertainty would increase to ~0.080‰.

In order to test the effect of the chemical purification technique on the accuracy of our isotope measurements, a synthetic carbonate sample was analysed. This sample consists of the NBS 979 standard doped with a carbonate matrix (Ca, Mg, Na, Fe, Ti and V) in the same proportions as found in natural carbonate samples. This solution was then spiked and treated as a sample. The Cr isotopic composition of this

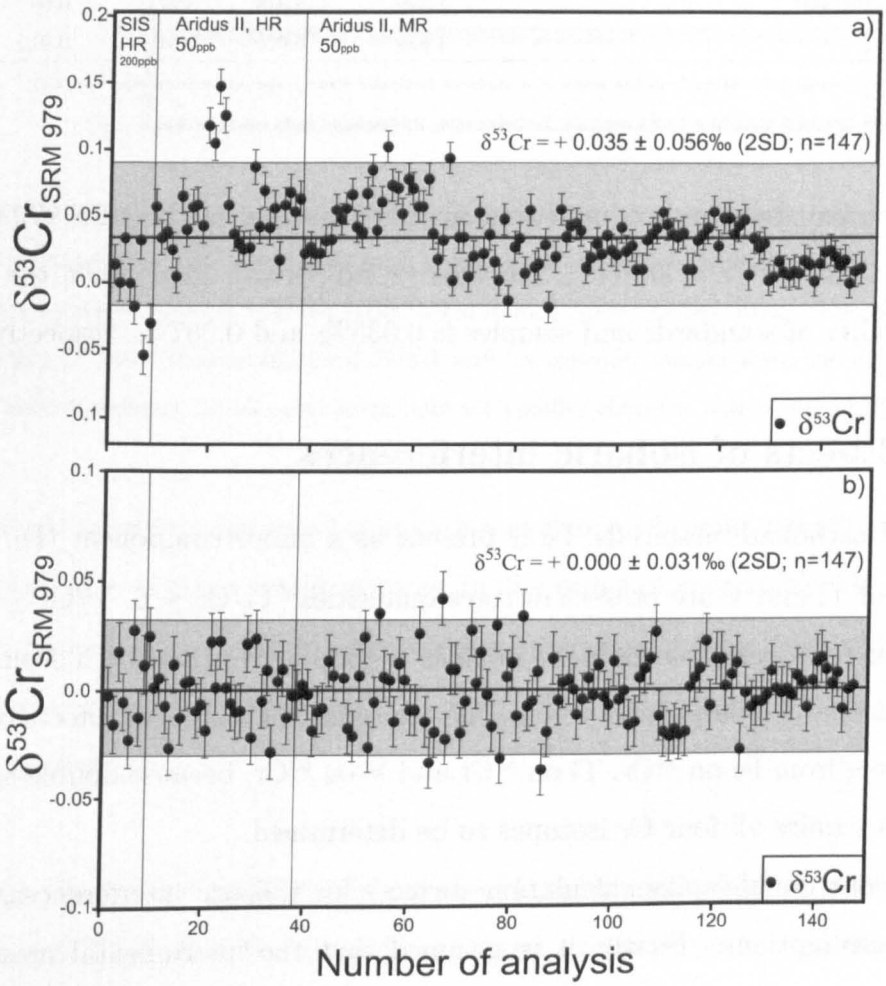

Figure 2.3: Long-term reproducibility of δ^{53}Cr for the NBS 979 Cr standard. Each data point represents analysis of a spiked NBS 979 sample deconvolved using our double-spike program. Error bars depict 2 standard errors of an individual analysis, which consists of measurement of 100 isotope ratios. (a) Uncorrected data, and (b) data normalised to the daily average δ^{53}Cr value of the standard, which is assumed to be zero. The grey area represents the 2 standard deviation envelope for the average δ^{53}Cr values for NBS 979. HR = high resolution mode; MR = medium resolution mode.

Table 2.3: Cr isotopic composition and Cr concentration of standards measured by double-spike MC-ICP-MS

	δ^{53}Cr (‰)	2σ (‰)	Cr (ppm)	2σ (ppm)
NBS979 (n = 147)[a] (uncorrected)	0.035	0.056		
NBS979 (n = 147)[a] (daynormalised)	0.000	0.031		
NBS979 (n = 4)[a] (Ca-doped + cation column)	0.011	0.008		
JDo-1 (n = 10)[a]	1.719	0.059	7.26	0.34
JLs-1[b]	1.994	0.020	1.05	0.01
BCS-CRM 512[b]	0.737	0.009	0.82	0.03
BCS-CRM 513[b]	1.329	0.018	3.97	0.06
Cal-S[b]	1.819	0.020	2.51	0.01

[a] σ is the standard deviation from the mean of n analyses (includes error propagation from equation 2.4)

[b] σ is the standard error of a single analysis (includes error propagation from equation 2.4)

synthetic carbonate sample is indistinguishable from that of the NBS 979 standard (Fig. 2.4) with δ^{53}Cr = 0.011 ± 0.008‰ (2 s.d., n=4), given that the external reproducibility of standards and samples is 0.035‰ and 0.057‰, respectively.

2.3.3 Effects of isobaric interferences

In natural carbonate materials, Fe is present as a minor component (Fe/Cr up to ~2000) and Ti and V are present in trace quantities (Ti/Cr ≤ 6, V/Cr ≤ 2). Even though our Cr separation method provides a good separation of Cr from the carbonate matrix, it is important to carefully consider the potential effects of isobaric interferences from Fe on ^{54}Cr, Ti on ^{50}Cr and V on ^{50}Cr, because double-spike measurements require all four Cr isotopes to be determined.

Although our double-spike calculation corrects for isobaric interferences, it makes two key assumptions. Firstly, it is assumed that the instrumental mass bias for Ti, V, and Fe is the same as it is for Cr. Other studies have indicated that this is unlikely to be true, as the mass bias can vary by as much as 400 ppm amu^{-1} on some MC-ICP-MS instruments (Thirlwall, 2002; Albarede et al., 2004). However, work done on our MC-ICP-MS (Parkinson et al., unpublished data) suggests that the variation in mass bias is <100 ppm amu^{-1}. Secondly, it is assumed that the interfering elements have natural isotopic compositions, mainly because it is difficult or, in the case of V, impossible, to determine their isotope compositions at the same

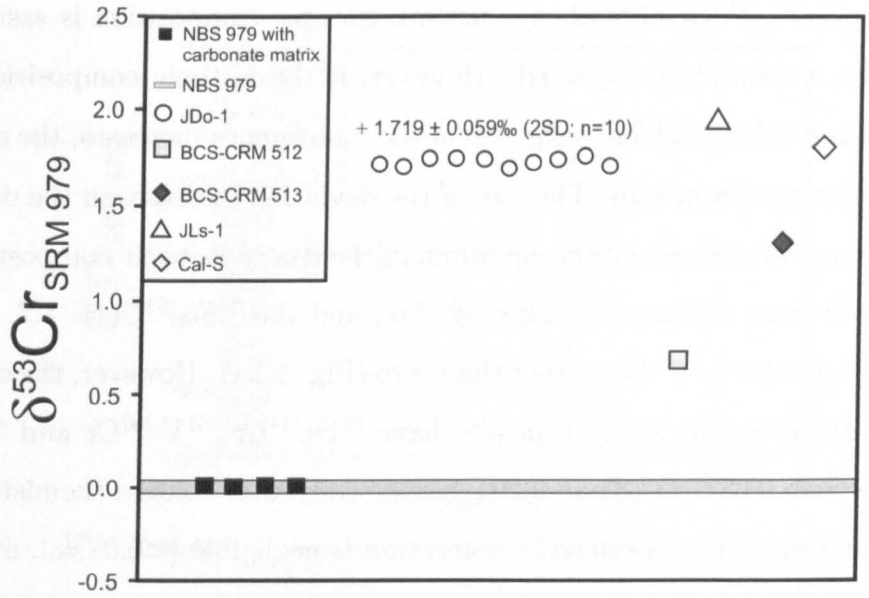

Figure 2.4: Cr isotopic composition of carbonates that have been processed through the ion exchange procedures. The NBS 979 doped with a carbonate matrix (see text for details) is compared to the long-term reproducibility of the NBS 979 standard (grey shaded area). Also plotted is the reproducibility of the dolomite standard JDo-1 and Cr isotopic compositions for four additional carbonate rock standards. In all cases error bars are smaller than the size of the symbol.

time as Cr. It is well documented that cation exchange chromatography can lead to fractionation of transition metal isotopes in the order of several ‰ (Anbar et al., 2000; Schoenberg et al., 2008). Since we aim to reduce the quantity of interfering elements, any Ti, V or Fe that is eluted along with the Cr is almost certainly isotopically fractionated.

In order to test the sensitivity of our double-spike method to variable amounts of non-natural Ti, V and Fe in our Cr analyses, we have performed some simple numerical calculations. A spiked NBS 979 solution is "contaminated" with variable amounts of Ti, V and Fe, that have $^{51}V/^{50}V$, $^{49}Ti/^{50}Ti$ and $^{56}Fe/^{54}Fe$ ratios that differ from the "natural" composition by -3‰ to +3‰. These mixtures are then fractionated (using the exponential mass fractionation law) by the amount usually produced by our MC-ICP-MS. The resulting composition is then put through our double-spike deconvolution program, which calculates the isotope composition of NBS 979. The results of our calculations (Fig. 2.5) show that the deconvolution

program recovers a δ^{53}Cr of 0 when a natural isotopic composition is assumed for Ti, V and Fe, as would be expected. However, if the isotopic composition varies from the natural value, and/or as the size of the interference increases, the recovered δ^{53}Cr value deviates from zero. The size of the deviation increases in the order V < Fe < Ti. By way of example, if the contaminant Fe has an isotopic composition that is fractionated from the natural value by 3‰, and the ^{56}Fe/^{54}Cr = 1.7, then the recovered δ^{53}Cr value is -0.1‰, rather than zero (Fig. 2.5a). However, the carbonate samples analysed in this study typically have ^{56}Fe/^{54}Cr, ^{51}V/^{50}Cr and ^{49}Ti/^{50}Cr ratios of less than 0.05, 0.0008 and 0.001, respectively after column chemistry. Thus, the error induced by the interference correction is negligible (<0.01‰), even if the "contaminant" has a non-natural isotopic composition.

2.3.4 Applicability of the exponential mass fractionation law

As discussed in Section 2.3.2, analyses of spiked NBS 979 solutions yield slightly positive δ^{53}Cr and additionally systematic positive and negative deviations of ^{54}Cr/^{52}Cr and ^{50}Cr/^{52}Cr respectively from the NBS 979 values, irrespective of whether the solution has been run through the column chemistry or not. Although the offset in ^{53}Cr is small and within the analytical uncertainties identical to zero, it is useful to explore their potential causes. The deviations in ^{54}Cr/^{52}Cr and ^{50}Cr/^{52}Cr from NBS 979 are double the value of δ^{53}Cr, which suggests that the slight offsets in the Cr isotope compositions from the nominal value of zero are mass dependent and related to the correction for instrumental mass fractionation. Similar effects have been noted for Nd and Hf isotopes (Nowell et al., 2003; Thirlwall and Anczkiewicz, 2004) indicating that instrumental mass fractionation does not always perfectly obey the exponential law (Nowell et al., 2003; Thirlwall and Anczkiewicz, 2004; Bermin et al., 2006) and a generalized power law is sometimes more appropriate (Thirlwall and Anczkiewicz, 2004).

Traditionally, the fractionation law can be derived from the slope of the natural logarithms of the measured isotope ratios (i.e. ^{53}Cr/^{52}Cr vs ^{54}Cr/^{52}Cr) (Bermin et al., 2006). However, the instrumental mass fractionation on our MC-ICP-MS is very stable from day to day, so the spread in the isotope ratios of the NBS 979

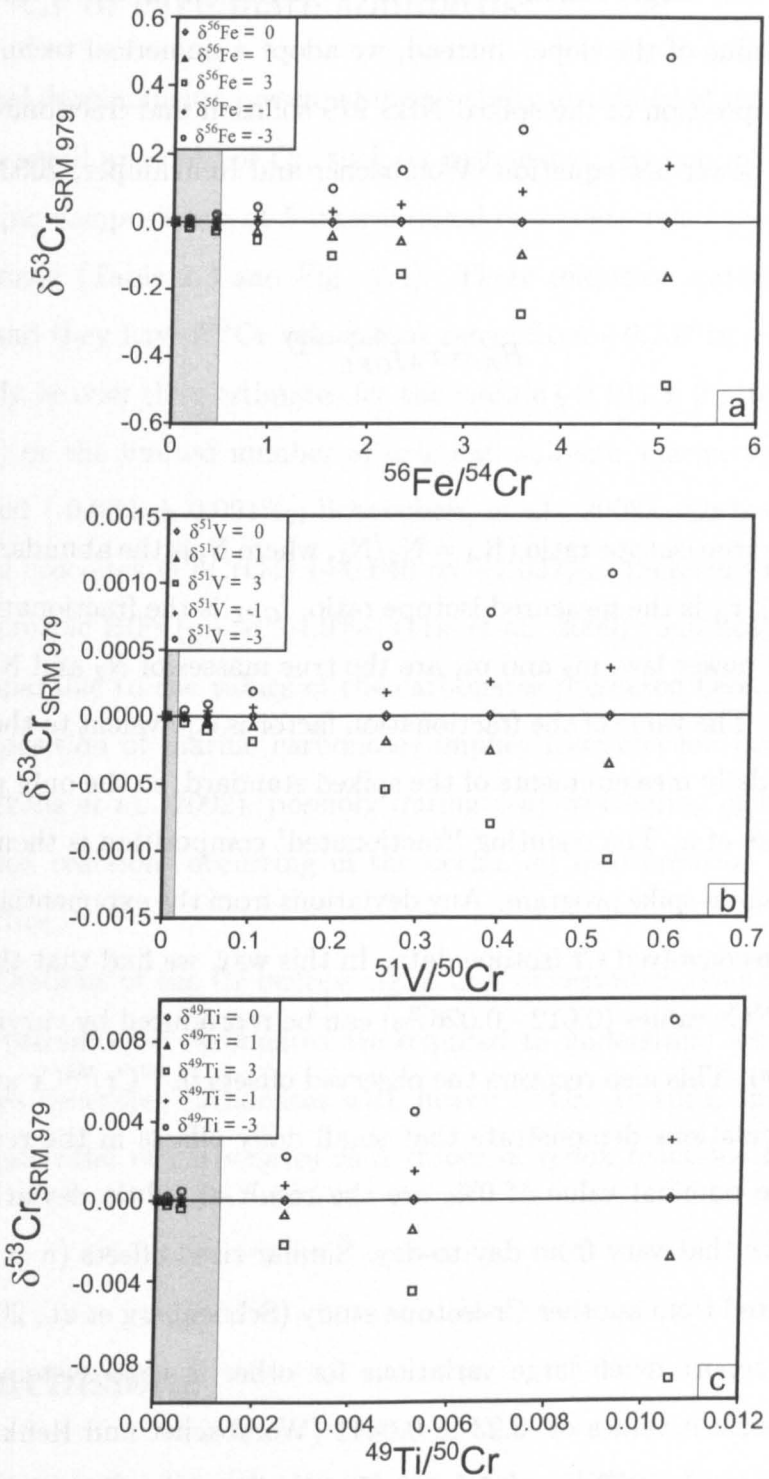

Figure 2.5: Effects of "non-natural" (fractionated) isobaric interferences from (a) iron, (b) vanadium, and (c) titanium on δ^{53}Cr, as a function of the element/Cr ratio. The 'true' δ^{53}Cr value of the NBS 979 reference material is 0. The effects of varying the isotopic composition of the interfering element are shown by the different symbols (see text for details). Grey shaded areas show the range of element/Cr ratios for carbonate materials determined in this study.

standard is not very large, making it difficult to derive any statistically valid information on the value of the slope. Instead, we adopt a numerical technique, taking the isotopic composition of the spiked NBS 979 solution and fractionating it using the generalized power law equation (Wombacher and Rehkamper, 2003):

$$R_A = r_A f_{GPL}^{(m_2^n - m_1^n)} \tag{2.5}$$

where R_A is the true isotope ratio ($R_A = N_2/N_1$, where N_i is the abundance of isotope i in the sample), r_A is the measured isotope ratio, f_{GPL} is the fractionation factor for the generalised power law, m_2 and m_1 are the true masses of N_2 and N_1 and n is an exponent term. The value of the fractionation factor is equivalent to the one that we observe in our daily measurements of the spiked standard, so the only parameter we vary is the value of n. The resulting 'fractionated' composition is then deconvolved through our double-spike program. Any deviations from the exponential law produce offsets in the deconvolved Cr isotope data. In this way, we find that the total range of measured δ^{53}Cr values (0.012 - 0.026‰) can be reproduced by varying n between 0.058 and 0.090. This also recovers the observed offsets in $^{50}Cr/^{52}Cr$ and $^{54}Cr/^{52}Cr$. Thus, our calculations demonstrate that small daily offsets in the recovered δ^{53}Cr value from the nominal value of 0‰ are the result of subtle deviations from the exponential law that vary from day-to-day. Similar sized offsets (n = -0.04 ± 0.02) can be calculated from another Cr-isotope study (Schoenberg et al., 2008), although some studies report much large variations for other isotope systems on different instruments, with n values of -0.23 ± 0.0441 (Wombacher and Rehkamper, 2003), -0.1937 (Anbar et al., 2000) and 0.5-1.039 (Thirlwall and Anczkiewicz, 2004). If such large deviations from the exponential law occur routinely, then a generalised power law equation may be required to solve the double spike equations. However, in this study, the deviation from the exponential law produces uncertainties similar to those produced by the counting statistics and it is not a major source of uncertainty in our measurements.

2.3.5 δ^{53}Cr of carbonate standards

The analytical developments presented in this study are aimed at measuring samples that contain small amounts of Cr, such as carbonates. By way of demonstration, the Cr isotopic compositions of 5 international carbonate reference materials have been determined (Table 2.3 and Fig. 2.4). These reference materials are natural carbonates and they have δ^{53}Cr values that range from +0.737 to +1.994‰, which is significantly heavier than estimates for the mantle (-0.104 ± 0.110‰; Schoenberg et al., 2008)) or the limited number of oxic and sub-oxic marine sediments previously analysed (-0.032 ± 0.091‰; Schoenberg et al., 2008). Only Cr(VI)-bearing hydrothermal crocoites (PbCrO4) (+0.640 to +1.037‰) (Schoenberg et al., 2008) and Neoproterozoic BIFs (up to ~4.9‰) (Frei et al., 2009) yield heavy δ^{53}Cr values that are comparable to the values of the carbonates presented here. The heavy Cr isotopic composition of marine carbonates implies fractionation involving Cr(III) and Cr(IV) (Ellis et al., 2002), possibly during: (a) weathering of the continental crust. b) redox reactions occurring in the ocean. c) incorporation of Cr into the carbonate lattice.

Future investigations of the Cr isotope signatures of seawater, river waters and experimentally precipitated carbonates are required to understand which (if any) of these processes generates carbonates with heavy δ^{53}Cr. In turn, this will help to validate the potential of carbonates as a tracer of redox reactions in the natural environment.

2.4 Conclusions

A low blank (0.12-0.20 ng) method has been developed that allows effective separation of small quantities of Cr (≥250 ng) from carbonate samples using a simple, one-step column chemistry procedure. We have been able to precisely measure the Cr isotopic composition of these samples, by careful optimisation of a desolvating sample introduction system (Aridus 2) coupled to a Neptune MC-ICP-MS (operated with X-cones in medium resolution mode), which produces a sensitivity of

$\sim$180 V ppm^{-1}. The addition of a ^{50}Cr-^{54}Cr double spike allows the determination of mass-dependent variations in δ^{53}Cr and correction of mass fractionation during Cr separation on the ion exchange column and during the mass spectrometer measurement. The long-term reproducibility of δ^{53}Cr for a spiked NBS 979 reference material is 0.031‰ (2s.d., n = 147), which is comparable to that reported in other studies that utilise significantly larger sample sizes. Numerical simulations indicate that small deviations in the δ^{53}Cr for the NBS 979 standard between analytical sessions are due to small variations in the mass fractionation behaviour of the MC-ICP-MS. Modelling the effects of potential isobaric interferences indicates that for carbonate samples, interferences from Ti, V and Fe are negligible.

The developed techniques have been applied to the measurement of Cr isotopes in low-level carbonate materials, for the first time. Our data indicate that carbonates have distinctly heavy δ^{53}Cr values compared to the continental crust and mantle. Although the origin of these heavy δ^{53}Cr values is not yet fully understood, natural carbonates have the potential to record redox reactions in modern and palaeo-oceans.

Chapter 3

Cr concentration and Cr isotopic composition of seawater

3.1 Introduction

Chromium is a trace element in seawater, present in concentrations of only a few nanomoles per litre (Table 3.1; Jeandel and Minster, 1987). Early work suggested that concentrations of chromium were depleted in surface seawater, and assigned chromium to the "recycled" group of elements whose distribution in the oceans is similar to that of the nutrient elements nitrate, phosphate and silicate (Whitfield and Turner, 1987). However, more recent work indicates that the surface depletion is modest, and there is no substantial difference between Atlantic and Pacific deep water concentrations (e.g. Sirinawin et al., 2000). Moreover, there is no correlation between Cr and the nutrient elements at the global scale (Sirinawin et al., 2000). For this reason, Cr is probably best described as intermediate between a "conservative" and "recycled" element. The residence time of Cr in the ocean is believed to be betweeb 10,000 and 40,000 years (Campbell and Yeats, 1981; Whitfield and Turner, 1987). The typical Cr concentration water depth profile is presneted in Figure 3.1.

In oxic seawater, the dominant chromium oxidation state is usually Cr(VI), which is consistent with thermodynamic calculations (Elderfield, 1970). However, significant amounts of Cr(III) have also been measured; the percentage of Cr(III) is usually $\leq$5% (e.g. Mugo and Orians, 1993), although some authors have found much higher

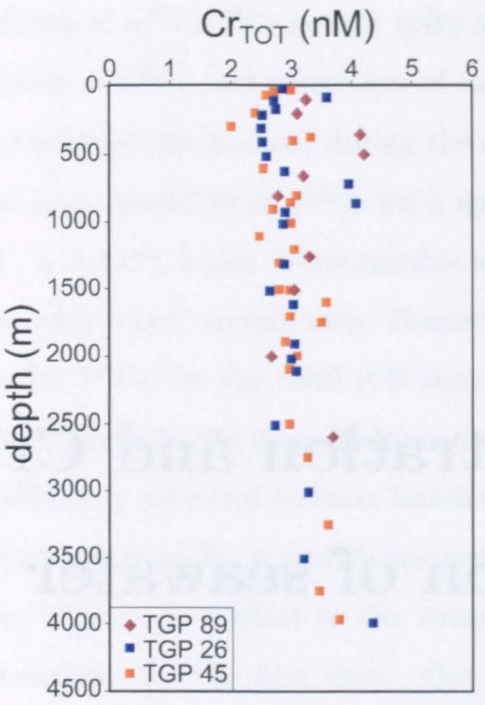

Figure 3.1: Vertical profile of total Cr in the North Atlantic Ocean for three stations. Modified after Jeandel and Minster (1987). The Three stations are TGP 26, TGP 45 and TGP 89 (Jeandel and Minster, 1987)

quantities, sometimes accounting for over 90% of the total dissolved Cr (Sander et al., 2003; Connelly et al., 2006).

Several mechanisms have been put forward to explain the unexpected presence of Cr(III). Cr(III) can be produced by reduction of Cr(VI) by photochemically produced Fe(II) (Gaberell et al., 2003), and by the reduction of Cr(VI) by organic matter (Kaczynski and Kieber, 1994). Moreover, it has recently been shown that marine phytoplankton (diatoms, red and green algae) directly catalyse the photoreduction of Cr(VI) to Cr(III), even without the presence of iron (Li et al., 2009). This is consistent with field observations that levels of Cr(III) are highest during periods of high biological activity (Connelly et al., 2006). Release of Cr(III) from decomposing sinking particulate matter has also been suggested as a mechanism for the production of this oxidation state in deeper waters (Achterberg and Van Den Berg, 1997).

It is also important to note that the oxidation of Cr(III) to Cr(VI) is slow relative

Table 3.1: Chromium concentrations in oceanic waters

Ocean area	Authors	Cr(VI) nM	CrTOT nM
NE Pacific Ocean	Cranston and Murray (1978)	1.6-3.5	
NW Atlantic Ocean	Campbell and Yeats (1981)		3.2-5.2
Japan sea and Pacific Ocean	Nakayama et al. (1981)	1.7-4.5	7.1-11.7
NE Pacific Ocean	Cranston (1983)		1.7-4.0
East Pacific Ocean	Murray et al. (1983)	1.1-6.0	
East Pacific Rise	Jeandel and Minster (1984)		1.9-15.8
South Pacific Ocean	Golimowski et al. (1985)		2.4
South and North Pacific Ocean	Jeandel and Minster (1987)		2.3-6.5
North Atlantic Ocean	Jeandel and Minster (1987)		2.0-4.6
Mediterranean	Jeandel and Minster (1987)		2.8-3.7
Mediterranean and Alboran Sea	Sherrell and Boyle (1988)		2.5-5.9
Atlantic Ocean near Gibraltar	Sherrell and Boyle (1988)		2.9-3.5
Pacific Ocean	Isshiki et al. (1989)	2.1-4.2	2.9-4.6
Indian Ocean	Ghaddaf (1990)	0.3-2.4	0.9-2.8
NW Mediterranean	Boussemart et al. (1992)	4.5-5.8	
North Pacific Ocean	Mugo and Orians (1993)	2.3-4.3	2.3-4.3
North Atlantic Ocean	Mugo and Orians (1993)		2.5-4.5
Mediterranean and Gibraltar	Achterberg and Van Den Berg (1997)	1.7-3.5	1.7-4.7
South and North Atlantic Ocean	Sirinawin et al. (2000)	3.1-7.3	
Arctic Ocean	Sirinawin et al. (2000)	3.0-6.1	
Caribbean Sea	Sander et al. (2003)	1.5-2.5	
Pacific Ocean	Sander et al. (2003)	0.7-6.8	6.3-19.4
Sargasso Sea	Connelly et al. (2006)		2.5-6.5

to the kinetics of the Cr reduction mechanisms discussed above. In this connection, Cutter (1992) suggests that the presence of Cr(III) may reflect the build-up of this oxidation state caused by differences between reduction and oxidation rates.

Analysis of the Cr isotopic composition of seawater has the potential to provide new insight as to the mechanisms that regulate the behaviour of Cr in seawater. In particular, Cr isotope measurements could help to constrain the sources of Cr to the ocean, provide mechanistic explanations for the distribution of Cr(VI) and Cr(III), and assess the controls on the availability of toxic Cr(VI). This is because Cr isotopes are fractionated during both oxidation and reduction reactions (Ellis et al., 2002; Zink et al., 2010), and by biotic reduction (Sikora et al., 2008). Moreover, different Cr reservoirs have different Cr isotope signatures (Izbicki et al., 2008; Schoenberg et al., 2008).

To date, however, there are no reports of the Cr isotope composition of seawater. Izbicki et al. (2008) speculate that the Cr isotopic composition of seawater is heavy relative to the continental crust and mantle, and measurements of the δ^{53}Cr composition of seawater precipitates (marine carbonates and Proterozoic banded iron formations; respectively, Bonnand et al., 2011 and Frei et al., 2009) support this idea. In order to measure the Cr isotope composition of seawater directly, a number of challenges need to be overcome. First, the low concentration of Cr in seawater (2-10 nM) requires a large sample volume. Moreover, the likely presence of significant Cr(III) means that the isotopic composition of both Cr(VI) and Cr(III) must be determined. Finally, low-blank methodologies for the separation of Cr from the sample matrix, and analysis of Cr isotopes with high accuracy and precision must be developed.

Here, I present the first ever measurements of Cr isotopes in (i) open ocean and (ii) coastal seawater samples. First, Cr(III) and total Cr (Cr(VI) + Cr(III)) are preconcentrated using a Fe co-precipitation technique. Then, in order to aid separation of Cr from Fe, the sample is first processed through an anion exchange resin, before processing through the cation exchange resin as described in Chapter 2. Chromium isotopes are measured by MC-ICP-MS using a double spike technique, as described in Bonnand et al. (2011) and Chapter 2. The data reveal that there is significant variation in the Cr isotope composition of seawater (δ^{53}Cr = -0.116 to +1.748‰). I then go on to provide a preliminary interpretation of these isotope data.

3.2 Sample location

Seawater samples were collected from the Argentine Basin in the South Atlantic (Fig. 3.2), and from Southampton Water in the UK (Fig. 3.3).

3.2.1 Argentine Basin

The sampling site in the Argentine Basin is located within the subtropical gyre at a depth of 5349 m. Samples were collected in February 2010 from RRV James Cook (cruise JC42) from five sampling depths in the uppermost (low nutrient) part of

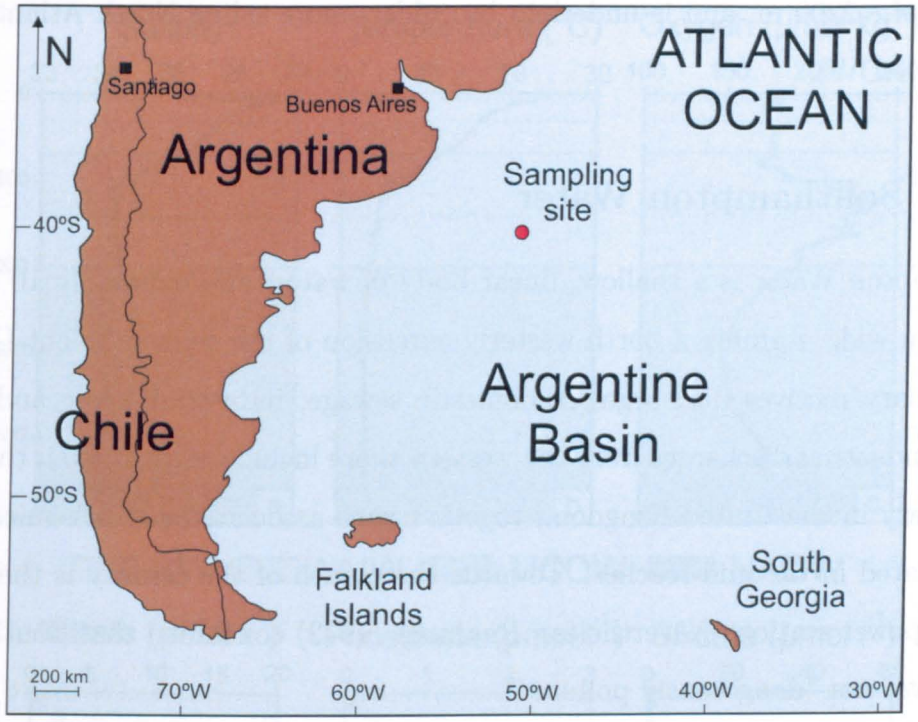

Figure 3.2: Map showing sampling location in the Argentine Basin.

the water column (30, 150, 700, 1500 and 2289 m water depth). Measurements of conductivity, temperature, depth, and dissolved oxygen were made at the time of water sampling; the data are shown in Figure 3.4. Water samples were collected using acid-clean 10-L Go-Flo bottles mounted on a CTD frame deployed from a Kevlar wire. In addition to Cr and Cr isotopes, the water samples were also analysed for their nutrient (nitrate, silicate and phosphate) content (Fig. 3.4). No nitrite was detectable in any of the water samples.

The hydrographic data presented in Figure 3.4 can be described in terms of four different water masses. The uppermost part of the water column (0 to ~300 m) is relatively warm and saline, with intermediate levels of dissolved oxygen. This is not a true water mass, and is commonly known as "surface water" (Heywood and King, 2002). This water is underlain by fresher, highly oxygenated Antarctic Intermediate Water (AAIW), which reaches to depths of ~1000 m. Beneath the AAIW, which has recently descended from the surface, lies the low oxygen signature of Upper Circumpolar Deep Water (UCDW), which is also clearly identified by its high phosphate signature (Fig. 3.4; Heywood and King, 2002). UCDW extends to

a depth of ~2200 m, and is underlain by colder, more saline North Atlantic Deep Water (NADW).

3.2.2 Southampton Water

Southampton Water is a shallow, linear body of water, approximately 10 km long and 2 km wide, forming a north-westerly extension of the central Solent (Fig 3.3). The estuary receives discharges of domestic sewage, industrial waste and cooling water. Industrial discharges from the western shore include effluent from the largest oil refinery in the United Kingdom, together with associated petrochemical industries located in the mid-reaches. Towards the mouth of the estuary is the oil-fired Fawley power station. Nevertheless, Raymont (1972) concluded that Southampton Water was not "dangerously polluted".

The water samples collected in this study were from Southampton water at Stanmore Point, at a water depth of 11 m in the outermost part of the estuary. Samples were collected from RV Callista in July 2010, using 5-L acid-cleaned Niskin

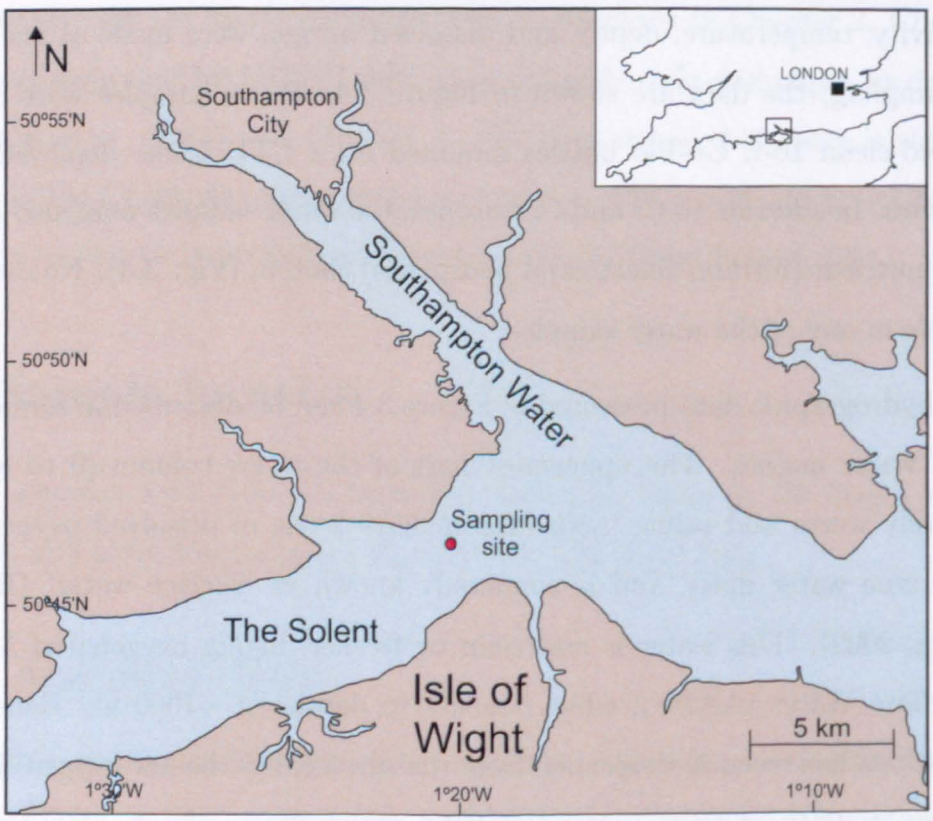

Figure 3.3: Map showing sampling location in Southampton Water.

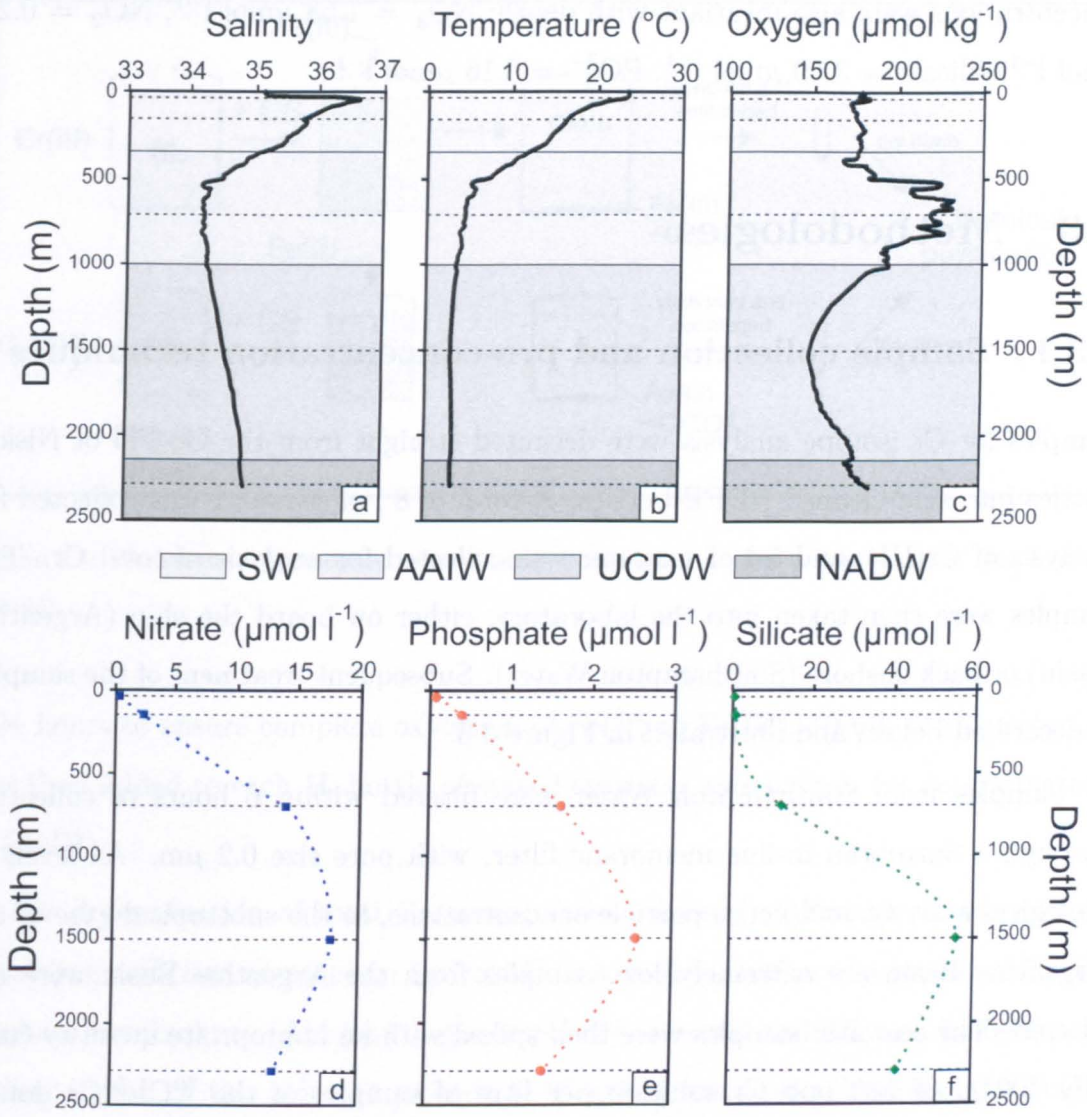

Figure 3.4: Vertical distribution of (a) salinity, (b) temperature, (c) dissolved oxygen, (d) nitrate, (e) phosphate and (f) silicate in the Argentine Basin. The dashed horizontal lines show the depths from which the samples were collected. The solid horizontal lines show the position of the different water masses: SW = surface water, AAIW = Antarctic Intermediate Water; UCDW = Upper Circumpolar Deep Water; NADW = North Atlantic Deep Water.

bottles mounted on a mini-CTD frame that was deployed on a Kevlar wire from the rear deck of the boat. In addition to Cr and Cr isotopes, the water samples were also analysed for their nutrient (nitrate, silicate and phosphate) content.

At the time of sampling, the water column was well-mixed and essentially marine in character. Neither temperature nor salinity show any variation with depth; the temperature of the seawater was 19°C and the salinity was 34 per mil. Nutrient

concentrations were also invariant with depth; NO_3^- = 1.58 μmol l^{-1}, NO_2^- = 0.21 μmol l^{-1}, silicate = 3.59 μmol l^{-1}, PO_4^{3-} = 0.16 μmol l^{-1}.

3.3 Methodologies

3.3.1 Sample collection and pre-concentration techniques

Samples for Cr isotope analysis were decanted straight from the Go-Flo or Niskin bottles into acid-cleaned HDPE bottles. A total of 8 l of seawater was collected for analysis of Cr(III), and 5 l of seawater was collected for analysis of total Cr. The samples were then taken into the laboratory, either on board the ship (Argentine Basin) or back onshore (Southampton Water). Subsequent treatment of the samples is described below, and illustrated in Figure 3.5.

Samples from Southampton Water were filtered within 6 hours of collection through a Sartobran in-line membrane filter, with pore size 0.2 μm. As levels of biological activity, and hence particle concentrations, in the subtropical gyre of the Argentine Basin are extremely low, samples from the Argentine Basin were not filtered. The seawater samples were then spiked with an appropriate quantity (usually 100 μl of 580 ppb Cr solution per litre of sample) of the ^{50}Cr-^{54}Cr double spike. The samples were left to equilibrate for at least an hour, before starting the co-precipitation procedure.

The Cr in the seawater samples was pre-concentrated using an Fe co-precipitation technique (Fig. 3.5) described in Connelly et al. (2006) and modified from Cranston and Murray (1978). Briefly, Cr(III) is scavenged from seawater by adding a solution of Fe(III) hydroxide at pH 8 - 8.5 and shaking. Total Cr (Cr(III) + Cr(VI)) is co-precipitated by Fe(II) hydroxide. During shaking, the Fe(II) hydroxide is oxidised and the Cr(VI) is reduced to Cr(III). The Fe(III) hydroxide then scavenges the Cr(III), resulting in quantitative removal of all dissolved Cr.

To this end, a suspension of Fe(III) hydroxide was produced by adding sufficient ammonium hydroxide to a 2 mM solution of ammonium Fe(II) sulphate hexahydrate (Aldrich) to give a pH of between 8 and 8.5. This solution was shaken, and left for

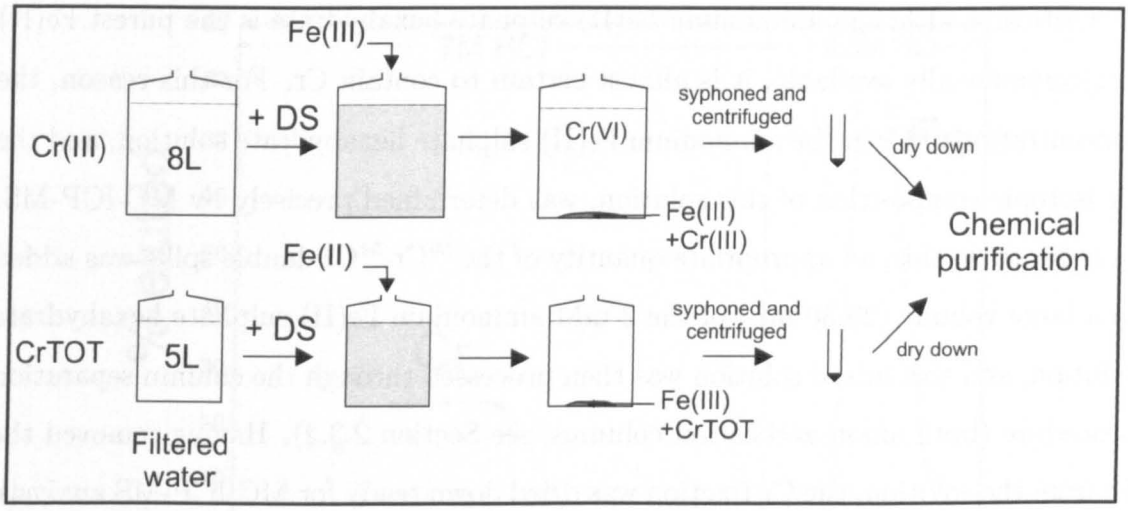

Figure 3.5: Procedure for pre-concentration of Cr from seawater. DS = double spike. (see text for details).

~24 hours to ensure complete oxidation of Fe(II) to Fe(III). 10 mL of this solution was then added to each 1L bottle of spiked seawater and shaken, for determination of Cr(III).

For determination of total Cr, a suspension of Fe(II) hydroxide was produced by adding sufficient ammonium hydroxide to a 2 mM solution of ammonium Fe(II) sulphate hexahydrate (Aldrich) to give a pH of between 8 and 8.5, and immediately adding 10 mL of this solution to each 1l of spiked seawater. Crucially, the Fe(II) hydroxide solution must be added to the seawater sample within 10 minutes, or the Fe(II) will start to oxidise. The samples were then shaken and left to equilibrate.

Within ~24 hours, the Fe (and Cr) precipitates out of solution and falls to the bottom of the bottles. In order to collect the precipitate, the supernatant water was carefully siphoned out of the bottle, until ~0.5 L remained. The precipitate and the remainder of the water were then decanted into clean 50 mL centrifuge tubes, and centrifuged at 4000 rpm for 15 minutes. After removing the supernatant fluid, the precipitates were then re-combined and dried down on a hotplate to remove any remaining fluid. The Fe residue was then re-dissolved in 4 ml of 7M HCl, and left overnight on a hotplate. The sample was then dried down and re-dissolved in 4 ml of 7M HCl; prior to loading onto the anion exchange resin (see Section 2.3.2), an additional 2 mL of 7M HCl was added to the sample, giving a total volume of 6 mL.

Critically, although ammonium Fe(II) sulphate hexahydrate is the purest Fe(II) salt commercially available, it is almost certain to contain Cr. For this reason, the concentration of Cr in the ammonium Fe(II) sulphate hexahydrate solution, and the Cr isotopic composition of this solution, was determined precisely by MC-ICP-MS. In order to do this, an appropriate quantity of the ^{50}Cr-^{54}Cr double spike was added to a large volume (20-30 mL) of the 2 mM ammonium Fe(II) sulphate hexahydrate solution, and this mixed solution was then processed through the column separation procedure (both anion and cation columns, see Section 2.3.2). Having removed the Fe from the solution, the Cr fraction was dried down ready for MC-ICP-MS analysis.

3.3.2 Separation of Cr from the Fe-matrix

The technique used to separate Cr from the sample matrix is given in Chapter 2 and Bonnand et al. (2011). However, because the pre-concentrated seawater samples contain significant Fe (up to 9 mg), an additional separation step was developed, modified from that reported by Grimaud and Michard (1974), in order to ensure that this Fe is completely separated from the Cr.

To this end, a cleaned Bio Rad Poly-Prep column is loaded with 2mL of Bio Rad AG1-X8 anion exchange resin, 200-400 mesh in Cl- form. The resin is cleaned first with 10 mL of 15M HNO_3, then with MQ water, followed by 10 mL of 0.5M HCl, more MQ water, 10 mL of 12M HCl, MQ water, and finally with 10mL of 7M HCl. Although this cleaning step is long, it ensures that the blank contribution from the columns is very low. The sample (in 6 mL of 7M HCl) is loaded on to the resin. As Cr(III) is not retained by the anion exchange resin, it passes straight through the column, whereas Fe(III) is strongly absorbed. A further 4 mL of 7M HCl is added to the column, and the Fe(III) is eluted in ~4 mL of 0.5M HCl. The elution curve for this procedure is shown in Figure 3.6. The Cr yield from this column procedure is ~95%.

The Cr fraction is evaporated to dryness, and re-dissolved in 0.5 mL of 6M HCl before being processed through the second stage of the column chemistry procedure. Briefly, (for full details see Bonnand et al., 2011 and Chapter 2), Cr is separated on a cation exchange resin (Bio Rad AG50 X8, 200-400 mesh). The Cr fraction is

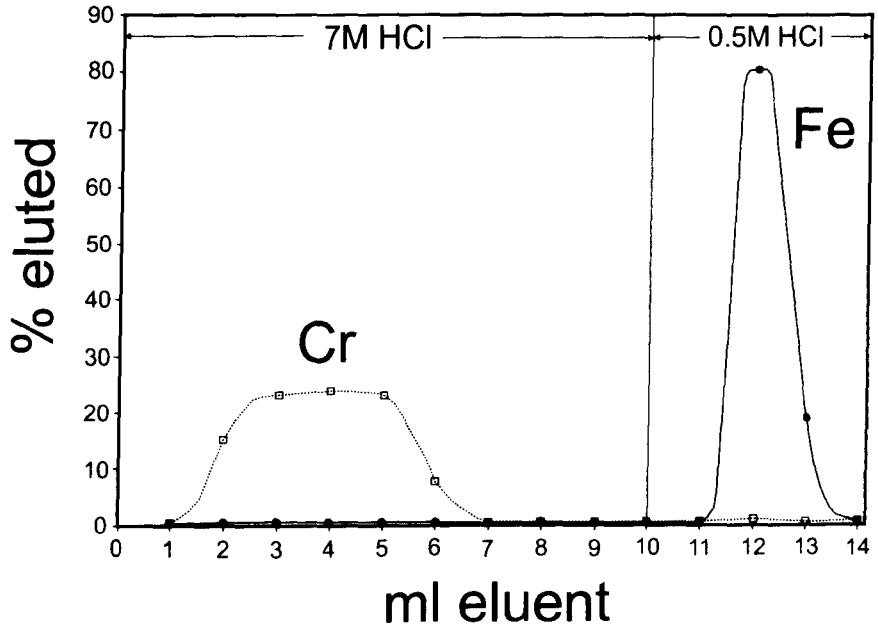

Figure 3.6: Elution curve for Cr and Fe from the anion exchange resin (see text for details).

eluted in 10 mL of 0.5M HCl, and is completely separated from cations that could potentially interfere with Cr during the mass spectrometry measurements (Ca, Na, K, Ti, V and Fe).

After this second stage, the Cr fraction is dried down and ready for MC-ICP-MS analysis. The total blank of the chemistry procedure (both stages) is ~0.5 ng, which is negligible compared to the amount of Cr processed through the column (~ 500 ng).

3.3.3 Mass spectrometry

All isotopic measurements were carried out with a ThermoFisher Scientific Neptune at the Open University. A full description of the measurement method is provided in Bonnand et al. (2011) and Chapter 2 and only a brief description is given here. The ThermoFisher Scientific Neptune was equipped with a CETAC Aridus II desolvating sample introduction system which was fitted with a 50 μL min^{-1} nebuliser. The mass spectrometer is equipped with 9 Faraday cups (each associated with an amplifier of $10^{11}\Omega$), which allows the four Cr isotopes (^{50}Cr, ^{52}Cr, ^{53}Cr and ^{54}Cr) and three potential interfering elements (^{49}Ti, ^{51}V and ^{56}Fe) to be measured simulta-

neously. The ion beams of ^{49}Ti, ^{51}V and ^{56}Fe were monitored to correct for isobaric interferences from ^{50}Ti, ^{50}V and ^{54}Fe respectively. Each isotopic analysis consisted of 50 measurements of the on-peak background followed by 100 measurements of the sample.

The Cr separated from the seawater samples was re-dissolved in 3% HNO_3 to give a Cr concentration in solution of 50 ppb for mass spectrometry. 50 ppb of Cr typically gives an ion beam of 10-12 V of ^{52}Cr, and ~70 ng of Cr was required to make a Cr isotope measurement. After each analysis, the Aridus was washed with 0.9 M HNO_3 solution for at least 10 minutes, in order to reduce the background on ^{52}Cr to less than 10 mV. The $\delta^{53}Cr$ value of each sample was obtained by normalising to mean value of measurements of the standard NBS 979 solution on that day. In this way, the effects of small differences in the mass fractionation of the MC-ICP-MS over long time periods are minimised (e.g. Schoenberg et al., 2008; Bonnand et al., 2011).

The long term reproducibility of the isotope ratio measurements was assessed by multiple measurements of a spiked NBS 979 standard solution containing 50 ppb of Cr; for $\delta^{53}Cr$, the external precision is ± 0.031‰ (n = 147; Table 3.2 and Bonnand et al., 2011). However, the external reproducibility of a sample (the carbonate standard reference material JDo-1) that has been processed through column chemistry is slightly worse (± 0.059‰; n = 10).

3.3.4 Cr isotope notation and data processing

The Cr isotope data are reported relative to the NBS979 standard Cr isotope reference material, as follows:

$$\delta^{53}Cr = \left(\frac{R_{sample}}{R_{standard}} - 1 \right) \times 1000 \qquad (3.1)$$

where R_{sample} and $R_{standard}$ are respectively the $^{53}Cr/^{52}Cr$ ratios of the sample and the NBS979 standard. The deconvolution procedure for the ^{50}Cr-^{54}Cr double spike is described in Bonnand et al. (2011) and Chapter 2. The Cr concentration in the

seawater samples was determined by isotopic dilution, as follows:

$$C_{sample} = M_{Natural} \times \left(\frac{m_{spike}}{m_{sample}}\right) \times \left(\frac{C_{spike}}{M_{spike}}\right) \times \left(\frac{P^{54}Cr_{spike} - P^{52}Cr_{spike} \times R_{mix}}{R_{mix} \times P^{52}Cr_{Natural} - P^{52}Cr_{Natural}}\right) \quad (3.2)$$

where C_{sample} and C_{spike} are respectively the Cr concentration in the sample and the spike, $M_{Natural}$ and M_{Spike} are the atomic mass of Cr in the sample and in the spike, m_{sample} and m_{spike} are the masses of sample powder and spike, and P^xCr_{spike} and $P^xCr_{Natural}$ are the proportion of ^{54}Cr or ^{52}Cr , respectively, in the spike or the natural composition. The error on this isotope dilution (ID) calculation is determined from the standard deviation (2σ) of the isotope ratio measurement. This error is small (~0.1%) and negligible relative to other sources of uncertainty. These include the weighing errors on both the spike and the sample, and the blank correction. The total uncertainty on the Cr concentration in the seawater samples is ~3%.

3.3.5 Speciation of Cr in natural waters

The speciation of Cr in natural waters and the behaviour of Cr(VI) and Cr(III) in solution have been widely studied in the past (e.g. Ball and Nordstrom, 1998). However, these calculations were made at concentration much higher than in natural waters and modelling at appropriate concentrations for seawater were required. The first modelling done in this study was an Eh-pH diagram for Cr concentration close to the seawater concentration of ~5 nM. This modelling was done with Geochemist's Workbench® software. The Cr concentration was fixed at 5 nM and the modelling was done for a temperature of 25°C. The main Cr species described in the literature were used in the calculation ($HCrO_4^-$, CrO_4^{2-}, Cr_2O_7, Cr^{3+}, $Cr(OH)^{2+}$, $Cr(OH)_2^+$, $Cr(OH)_3^0$ and $Cr(OH)_4^-$). The second critical information required to understand and interpret Cr isotopes data in seawater is the variation of the Cr fraction with Eh. It has been postulated that Cr in oxic seawater is mainly Cr(VI) either as CrO_4^{2-} or $HCrO_4^-$ species (Elderfield, 1970) and for a standard seawater pH the

Cr(III) compounds should be $Cr(OH)_2^+$ and $Cr(OH)_3^0$ (Zink et al., 2010). The aim of this modelling is to determine the dominant Cr compounds under different redox conditions (from reduced to oxic). For this modelling, the pH was fixed at 8.2 and the Cr concentration was set to 5 nM. This modelling was done using an average seawater composition in term of major and minor cations and anions (Appendix D). The calculation were accomplished using PHREECQ software and the equilibrium constants used were from Rai et al. (1987).

3.4 Results

3.4.1 Evaluation of the co-precipitation and chemical purification procedures

In order to evaluate the veracity of the column separation procedures for Cr isotope ratios, a mixed solution of the ^{50}Cr-^{54}Cr double spike and the NBS979 Cr isotope reference material was processed through both anion and cation column chemistry procedures. The Cr isotopic composition measured for this solution is $\delta^{53}Cr$ = -0.056 ± 0.012‰ (Table 3.2 and Fig. 3.7).

To test for any potential effects of the Fe co-precipitation procedure, four aliquots of the same mixed standard-spike solution were co-precipitated with Fe(III) hydroxide, and then passed through both steps of the chemical purification procedure. The Cr isotopic composition of the standard is -0.042 ± 0.029‰ (2SD, n = 4) (Table 3.2), which is close to that of the mixed standard-spike solution that had only passed through column chemistry.

3.4.2 Cr concentration and Cr isotope composition of the ammonium Fe(II) sulphate hexahydrate solution

The concentration of Cr in the 2 mM ammonium Fe(II) sulphate hexahydrate solution is 0.97 ± 0.03 ng ml^{-1} (2σ, where σ is the standard deviation, n = 3). The average $\delta^{53}Cr$ value of this Cr is -0.34 ± 0.11‰ (2σ, where σ is the standard deviation, n = 3). Given that up to 80 ml of this solution were added to each sample, the

Table 3.2: Cr isotopic composition of the standard-spike solution, with and without chemical purification and co-precipitation. Ch. = chemical purification (2 steps), cop. + Ch. = co-precipitation and chemical purification (2 steps). NBS979 and JD0-1 data are fron Bonnand et al. (2011)

	chemical treatment	$\delta^{53}Cr_{TOT}$ (‰)	2σ	n
NBS979	None	0.000	0.031†	147
JDo-1	Ch.	1.719	0.059†	10
NBS979	Ch.	-0.056	0.012*	1
NBS979	cop. + Ch.	-0.049	0.010*	1
NBS979	cop. + Ch.	-0.047	0.010*	1
NBS979	cop. + Ch.	-0.052	0.011*	1
NBS979	cop. + Ch.	-0.021	0.013*	1
average(NBS979)	cop. + Ch.	-0.042	0.029†	4

† σ is the standard deviation from the mean of n analyses.

* σ is the standard error of one analysis.

contribution of Cr from the Fe solution is non-negligible, consisting of up to ~10 % of the total Cr. For this reason, the Cr concentration and Cr isotopic composition of the samples reported in Table 3.3 are corrected for this blank contribution.

3.4.3 Cr concentration and Cr isotope composition of samples from Southampton Water

The Cr concentration and Cr isotopic composition of the seawater samples from Southampton Water are presented in Table 3.3 and Figure 3.7. As the water column was well mixed at the time of sampling, unsurprisingly the Cr concentration and Cr isotope composition of each of the samples are within error of each other at the level of the external precision; the average concentration of Cr(III) is 1.68 nM, and the average δ^{53}Cr value of the Cr(III) is +1.722 ± 0.036‰ (2σ, where σ is the standard deviation). The average concentration of total Cr (Cr(III) + Cr(VI)) is 1.82 nM, with a δ^{53}Cr value of +1.549 ± 0.014‰ (2σ, where σ is the standard deviation). Thus, Cr(III) seems to be the dominant form of Cr in Southampton Water, consisting of about 90% of the total Cr. Moreover, the δ^{53}Cr value of the Cr(III) is higher than the δ^{53}Cr value of the total Cr in all samples.

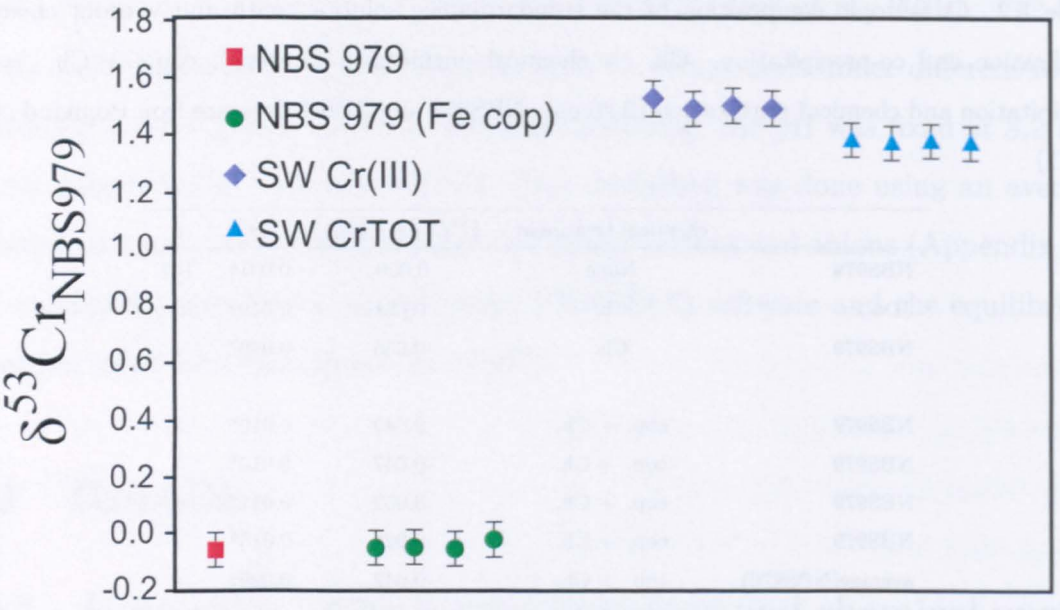

Figure 3.7: Cr isotopic composition of the chromium isotope standard reference material NBS 979, that has passed through both stages of the column chemistry (red square), or has been co-precipitated with Fe and then passed through column chemistry (green circles), shown together with the Cr isotopic composition of the seawater samples from Southampton Water (SW).

3.4.4 Cr concentration and Cr isotope composition of samples from the Argentine Basin

The Cr concentration and the Cr isotopic composition of seawater collected from different depths in the Argentine Basin are presented in Table 3.3 and Figure 3.8. The concentration of Cr(III) varies from 3.92 nM in the sample recovered from closest to the sea surface (30 m water depth), to 5.72 nM in the sample recovered from 1500m water depth. The concentration of total Cr shows less variation, ranging from 5.80 to 6.50 nM. As for Southampton Water, the dominant species of Cr in the Argentine Basin also appears to be Cr(III); Cr(III) comprises between 62 and 99% of the total Cr.

Table 3.3: Cr concentration and Cr isotopic composition of seawater samples from the Argentine Basin and Southampton Water.

		Uncorrected data						Blank corrected data					
Sampling site	depth (m)	CrTOT (nM)	Cr(III) (nM)	$\delta^{53}Cr_{(III)}$ (‰)	2s.e. (‰)	$\delta^{53}Cr_{TOT}$ (‰)	2s.e. (‰)	CrTOT (nM)	Cr(III) (nM)	$\delta^{53}Cr_{(III)}$ (‰)	2s.e. (‰)	$\delta^{53}Cr_{TOT}$ (‰)	2s.e. (‰)
Argentine	30	6.55	4.11	-0.127	0.009	0.431	0.008	6.36	3.92	-0.116	0.023	0.454	0.022
Basin	150	6.43	5.40	0.154	0.015	0.675	0.011	6.24	5.21	0.173	0.022	0.706	0.022
	700	6.69	4.99	0.448	0.015	0.571	0.011	6.50	4.80	0.480	0.024	0.598	0.021
	1500	5.99	5.91	0.755	0.013	0.531	0.009	5.80	5.72	0.793	0.023	0.560	0.021
	2289	6.27	5.39	0.158	0.009	0.507	0.010	6.08	5.19	0.177	0.026	0.534	0.021
Southampton	surf.	2.05	1.89	1.534	0.010	1.374	0.008	1.86	1.70	1.748	0.036	1.554	0.035
Water	2	2.04	1.90	1.500	0.014	1.363	0.009	1.85	1.71	1.709	0.036	1.543	0.035
	5	2.02	1.87	1.511	0.010	1.373	0.008	1.83	1.67	1.722	0.036	1.557	0.035
	11.5	2.04	1.93	1.499	0.010	1.363	0.008	1.85	1.74	1.709	0.036	1.543	0.035
	Average	2.04	1.90	1.511	0.032*	1.368	0.012*	1.85	1.68	1.722	0.036*	1.549	0.014*

* In this case, s.e. is the standard deviation from the mean of 4 analyses

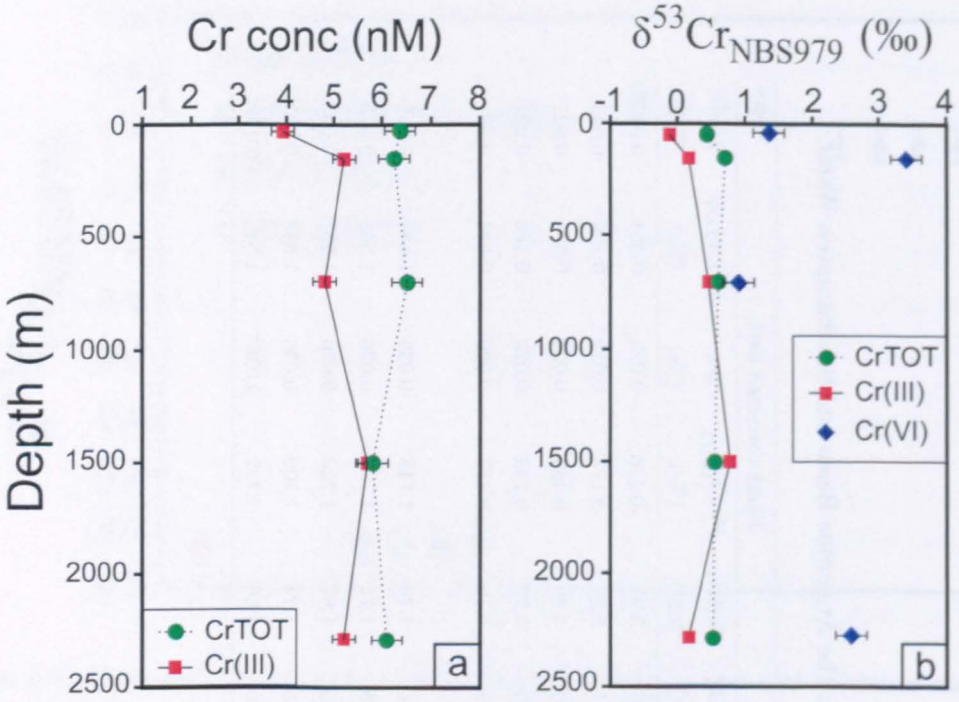

Figure 3.8: Profiles of (a) Cr concentration and (b) Cr isotopic composition in seawater samples from the Argentine basin. The Cr(VI) isotopic composition is inferred by mass balance. The Cr(VI) isotopic composition for the sample at 1500 m is not shown because of large uncertainties in the concentration measurements.

The Cr isotopic composition (δ^{53}Cr) of the Cr(III) varies from -0.116 to +0.793‰. The lowest δ^{53}Cr value is in the sample collected from closest to the sea surface (30 m water depth). The Cr isotopic composition of the total Cr shows less variation, with δ^{53}Cr values ranging from +0.454 to +0.706‰. Again, the sample collected from closest to the sea surface has the lowest δ^{53}Cr value. Samples from the middle part of the profile (700 and 1500 m water depth) have similar δ^{53}Cr values for Cr(III) and total Cr; for all other samples, the Cr isotopic composition of Cr(III) is lighter compared to the Cr isotopic composition of total Cr.

3.4.5 Speciation of Cr in natural waters

The speciation of Cr in natural waters has been studied and Cr(VI) and Cr(III) are believed to behave differently (Pettine, 2000). Cr(VI) is soluble whereas Cr(III) is considered to be strongly insoluble (Rai et al., 1987). However, Eh-pH diagrams

used to make such interpretations are for relatively high Cr concentrations (5 μM) (Ball and Nordstrom, 1998; Fig. 3.9). Indeed, the Cr concentration of modern day seawater is much lower, in the order of a few nM (e.g. Jeandel and Minster, 1987; see Table 3.1). Therefore, the Eh-pH diagrams presented in Figure 3.9 are calculated for different Cr concentrations. Figure 3.9a assumes a total Cr concentration of 5 μM. At this concentration and between a pH of 5.5 and 12.3 Cr(III) is insoluble and precipitates in the form $Cr(OH)_{3(s)}$. Figure 3.9b, however, was calculated with a total Cr concentration of 5 nM which is typical of modern seawater. In this case the Cr concentration is below the saturation limit of $Cr(OH)_3$ and therefore Cr(III) can be present in its dissolved form.

In oxic seawater, the main Cr species should be Cr(VI) in the form CrO_4^{2-} or $HCrO_4^-$ (Elderfield, 1970). However, new modelling, conducted as part of this thesis work using PHREECQ software, indicates that in seawater, the main Cr(VI) species is $NaCrO_4^-$ (Fig. 3.10). This finding can be explained by the relatively high concentration of Na in seawater; previous studies have only calculated Cr species for ground waters or pure water (Ball and Nordstrom, 1998; Zink et al., 2010). These

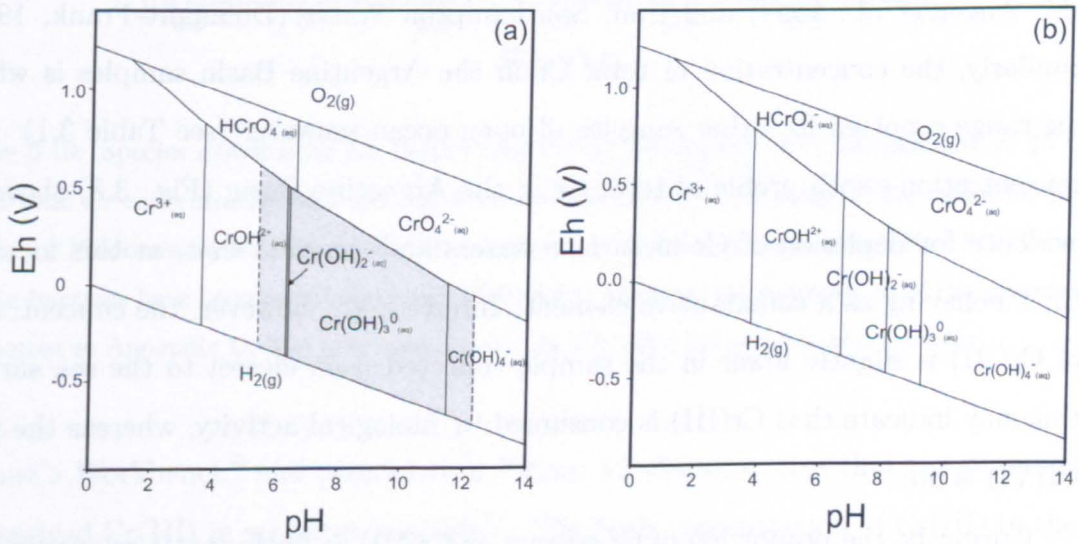

Figure 3.9: Eh-pH diagrams for aqueous inorganic chromium hydrolysis species in groundwater at 25°C. (a) The grey area indicates the stability zone of $Cr(OH)_{3(s)}$ for a total Cr concentration of 5 μM. Modified from Ball and Nordstrom (1998). (b) Eh-pH calculated with Geochemistry Workbench® software for a total Cr concentration of 5 nM.

results are in agreement with another study on Cr speciation in seawater (Accornero et al., 2010). It is however important to note that our calculation did not incorporate $MgCrO_4^0$ and $CaCrO_4^0$ and these two compounds may also play an important role on the Cr(VI) behavior in seawater, but more probably in high Mg concentration waters (Accornero et al., 2010).

3.5 Discussion

As this study reports for the first time the Cr isotopic composition of modern seawater, this section firstly presents a careful, critical evaluation of the data and then goes on to provide a preliminary interpretation of the data, in terms of their potential implications for the effects of biogeochemical and redox processes on the Cr and Cr isotopic composition of seawater.

3.5.1 Concentrations of Cr(III) and total Cr

The concentration of total Cr in the Southampton Water samples (1.82 nM) is within the range reported for other samples collected from the Solent (3.39 ± 2.42 nM; Auger et al., 1999) and from Southampton Water (Dolamore-Frank, 1984). Similarly, the concentration of total Cr in the Argentine Basin samples is within the range reported for other samples of open ocean seawater (see Table 3.1). The concentration-depth profile of total Cr in the Argentine Basin (Fig. 3.8) shows no evidence for depletion of Cr in surface waters and suggests that, at this location, Cr is behaving as a conservative element. Interestingly, however, the concentration of Cr(III) is slightly lower in the sample collected from closest to the sea surface; this may indicate that Cr(III) is consumed by biological activity, whereas the toxic Cr(VI) is not.

Curiously, the proportion of Cr present as Cr(III) at both sites is relatively high; ≥62%. This contrasts with most other previous studies, which typically report that Cr(VI) is the dominant oxidation state in oceanic water (e.g. Mugo and Orians, 1993; Achterberg and Van Den Berg, 1997; Connelly et al., 2006). There are several potential explanations for this finding. Firstly, the modelling done with Geo-

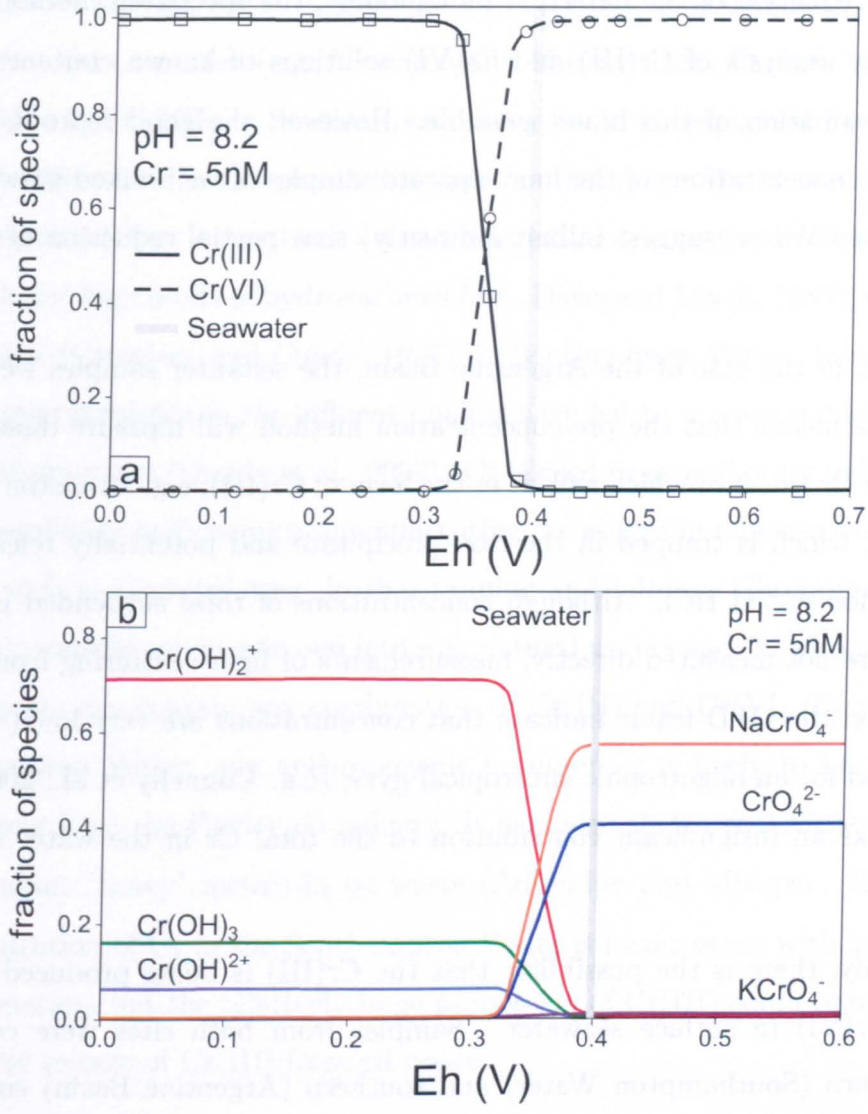

Figure 3.10: Species distribution for Cr(III) and Cr(VI) in seawater for a temperature of 25°C and a total Cr concentration of 5 nM. (a) Predominant Cr species at different Eh values for pH = 8.2. (b) Predominant Cr(III) and Cr(VI) complexes at different Eh values for pH = 8.2. These species fractions have been calculated using PHREEQC software; the composition of the seawater is reported in Appendix D. The grey area reports the Eh value for modern oxic seawater.

chemist's Workbench® and presented in Figure 3.9 demonstrates that the presence of dissolved Cr(III) in seawater is possible. The high concentration of Cr(III) in the Argentine Basin could be explained by the difference in kinetics of oxidation and reduction reactions.

Secondly, there is the possibility that some of the Fe in the Fe(III) hydroxide solution used to pre-concentrate the Cr was actually in the form of Fe(II), caus-

ing partial reduction of the Cr(VI). Unfortunately, the speciation method was not validated by analysis of Cr(III) and Cr(VI) solutions of known concentration, so a proper evaluation of this is not possible. However, the good reproducibility of the Cr(III) concentrations of the four separate samples of well-mixed seawater from Southampton Water, suggest (albeit indirectly) that partial reduction of Cr(VI) is unlikely.

Thirdly, in the case of the Argentine Basin, the seawater samples were not filtered. This means that the pre-concentration method will measure dissolved plus particulate Cr (most of which will be in the form of Cr(III); e.g. Cranston and Murray, 1980), which is trapped in the iron precipitate and potentially released upon re-dissolution in 7M HCl. Although concentrations of total suspended particulate matter were not measured directly, measurements of light scattering from a sensor mounted on the CTD frame indicate that concentrations are very low ($\sim$10 μg/L, as expected for an oligotrophic subtropical gyre; (e.g. Connelly et al., 2006), which would make an insignificant contribution to the total Cr in the water sample ($\leq$ 2%).

Fourthly, there is the possibility that the Cr(III) is being produced by reduction of Cr(VI) in surface seawater. Samples from both sites were collected in the northern (Southampton Water) and southern (Argentine Basin) summers, so photochemically-induced reduction of Cr(VI), in the presence of either Fe(II) (Richard and Bourg, 1991), organic matter (Kleber and Helz, 1992) or marine phytoplankton (Li et al., 2009), is possible. This could explain high concentrations of Cr(III) in the well-mixed surface layer (all samples from Southampton Water, and the uppermost samples collected from the Argentine Basin), as well as in water masses that have recently been at the surface (i.e. AAIW, which was sampled at 700 m water depth in the Argentine Basin).

High levels of Cr(III) in deeper waters could be explained by release of Cr(III) from decomposing sinking particulate matter in deeper waters (Achterberg and Van Den Berg, 1997). However, as discussed above, levels of particulate material are low in the Argentine Basin, and are unlikely to contribute significant Cr to the dissolved Cr pool.

The Cr species in river water is still highly debated as both dominant Cr(VI) and Cr(III) have been reported (e.g. Cranston and Murray, 1980, Pankow et al., 1977). The high level of Cr(III) in Southampton water could be explained by input from rivers. Finally, there is the possibility that Southampton Water receives anthropogenic inputs of Cr. It has been argued that effluent from the Fawley refinery is responsible for high levels of hydrocarbons (e.g. Dicks and Levell, 1989), copper and possibly lead (Croudace and Cundy, 1995), in Southampton Water. In recent years however, improvements in the effluent quality have led to a mark reduction in the level of contaminants (Cundy et al., 2003). Cr is used in several other industries, including metallurgy and chemical manufacturing, as well as in numerous commercial processes such as electroplating, leather tanning and mining. Chromium from anthropogenic sources can be released into soil, natural waters and the atmosphere and waste effluents can contain any combination of Cr(III) and Cr(VI) (Stanin, 2005). In Southampton Water, any anthropogenic input of Cr is likely to be associated with effluents from the Fawley oil refinery. It has been shown that Cr is one of the most abundant "heavy" metals in oil waste (Adesodun and Mbagwu, 2008). The low concentration of Cr in the Southampton Water is inconsistent with a high level of contamination, but the relatively large proportion of Cr(III) could potentially be explained by release of Cr(III) from oil waste.

3.5.2 Veracity of Cr isotope measurements

Critically, the double-spike method used to make the Cr isotope measurements relies on equilibrium being achieved between the Cr in the spike and the Cr in the sample. For this to occur, the speciation of the Cr in the spike should be the same as the speciation of the Cr in the sample. The spike used in this study is a Cr(III) spike; this means that the spike will equilibrate instantenously with the Cr(III) in the seawater. If Cr isotopes are fractionated during the co-precipitation procedure, then the double spike will properly correct for that fractionation. However, the same Cr(III) spike was also used for analyses of Cr isotopes in the total Cr (Cr(III) + Cr(VI)) fraction. Importantly, in this case the co-precipitation technique is based on the reduction of the Cr(VI) in the sample to Cr(III). Grimaud and Michard (1974)

have shown that the total reduction of Cr(VI) to Cr(III) is achieved immediately after the addition of Fe(II) to the solution. This means that the Cr(III) in the spike should instantaneously equilibrate with the Cr(III) derived from the reduction of Cr(VI), prior to the precipitation of the Fe(II) hydroxide. Thus, if the Cr isotopes are fractionated during the precipitation the double spike will properly correct for that fractionation. If the reduction of Cr(VI) with Fe(II) is not complete, then the Cr isotope composition of the total Cr will be incorrect. Although this has not been tested directly, the fact that δ^{53}Cr value of total Cr in the four replicate samples from Southampton Water is reproducible (well within the external precision of the isotope measurements), strongly suggests that all of the Cr(VI) is reduced to Cr(III), and equilibrium with the Cr(III) spike is achieved.

The double spike technique also needs to accurately correct for any isotope fractionation during the two-step chemical separation procedure. Although the Cr isotopic compositions obtained for the standard-spike mixture that has been through chemistry are comparable to the expected value (δ^{53}Cr = 0‰), they are very slightly lighter (-0.056‰; Table 3.2). One possibility is that this is because the Cr forms a complex with the 7M HCl before it is passed through the anion exchange column, but the double spike calculation assumes that mass fractionation is due to the fractionation of metallic Cr metal, not Cr complexes (see Chapter 2). However, as discussed in Chapter 2 and Bonnand et al. (2011), the difference in the Cr isotopic composition of NBS979 that has, and has not, been through the columns is small, and within the external precision of the isotope measurements (±0.059‰, Bonnand et al., 2011).

For all of these reasons, the pre-concentration procedure, the chemical separation technique, and the mass spectrometry procedures adopted for this study, give reliable data for the Cr concentration and Cr isotopic composition of seawater. Crucially, the reproducibility of replicate analysis of the samples from Southampton Water, for both Cr concentrations and Cr isotopes, for both Cr species, is excellent (Table 3.3).

3.5.3 Cr isotopic composition of seawater

With the exception of one sample (from 30 m water depth, in the Argentine Basin), the δ^{53}Cr value of Cr(III) and total Cr is higher than the average δ^{53}Cr value of silicate rocks from the Earth's crust and mantle (-0.124 ± 0.101‰; Schoenberg et al., 2008). Moreover, the δ^{53}Cr values of seawater samples from Southampton Water are significantly higher (by around 1‰) than the δ^{53}Cr values of seawater samples from the Argentine Basin. To date, there are no measurements of the Cr isotope composition of river waters, which are the most important source of Cr to the ocean (≥90%, or 3.7×10^{10} g Cr yr^{-1}; Chester and Murphy, 1988). If rivers are the most significant source of Cr in Southampton Water (i.e. anthropogenic sources are small), then the data from Southampton Water strongly suggest that the Cr isotopic composition of the continental flux is significantly higher than that of the crust itself, indicating that Cr isotopes are fractionated during the weathering process and/or during the riverine cycle. In this connection, Izbicki et al. (2008) report positive δ^{53}Cr values of +1.2 and +2.3‰ in groundwater recharge areas having low Cr concentrations. Furthermore, our own Cr isotope analyses of carbonate minerals that have precipitated from seawater (see Chapter 5) reveal positive Cr isotope values (0.65 - 0.76‰). As oxidation of Cr(III) (the dominant Cr species in silicate rocks; Rai et al., 1989) does not appear to result in significant isotope fractionation (Zink et al., 2010), it seems likely that Cr(VI) is fractionated on mineral surfaces, prior to entering solution (Izbicki et al., 2008).

Samples from the Argentine Basin are more likely to be influenced by atmospheric sources; however, on a global scale, the atmospheric flux of Cr is ≤10% of the fluvial flux (Chester and Murphy, 1988). The lower δ^{53}Cr values of total Cr in seawater samples from the Argentine Basin may indicate that addition of Cr from the dissolution of atmospheric dust is accompanied by significantly less isotope fractionation than terrestrial weathering processes. Interestingly, the δ^{53}Cr value of Cr(III) in the sample recovered from closest to the sea surface (from 30 m water depth), is indistinguishable from the average value for the crust (-0.116‰, compared to the average crustal value of -0.124‰; Schoenberg et al., 2008). However, it is im-

portant to note that levels of Cr in surface seawater at this site are not significantly enriched.

The Cr isotopic composition of Cr(III) versus total Cr may reveal important information about the processes that regulate the speciation of Cr in seawater. In the Argentine Basin, the two samples closest to the surface have significantly lower δ^{53}Cr values for Cr(III) than for CrTOT (by 0.53 - 0.57‰). As discussed above, the δ^{53}Cr value of Cr(III) in the sample from 30 m water depth is the same as the average value for silicate rocks but, because Cr isotopes are fractionated by the reduction of Cr(VI), with the light isotopes enriched in the reduced Cr(III) species, there is also the possibility that the lighter Cr(III) δ^{53}Cr values are the result of reduction of Cr(VI) to Cr(III) in surface waters.

As discussed in Section 3.1, reduction of Cr(VI) can occur in the presence of photochemically produced Fe(II) (Gaberell et al., 2003) or organic matter (Kaczynski and Kieber, 1994), and can occur directly in the presence of marine phytoplankton (Li et al., 2009). Assuming that Cr is not lost (or added) to seawater during the reduction process, then it is possible to estimate the δ^{53}Cr value of both the Cr(III) and Cr(VI) by means of the Rayleigh distillation equation:

$$\delta^{53}Cr_{(VI)} = \delta^{53}Cr_{ini} + 10^3 \times (\alpha - 1) * lnf \tag{3.3}$$

where f is the proportion of Cr(VI), α is the isotope fractionation factor (0.9965; Ellis et al., 2002), $\delta^{53}Cr_{(VI)}$ is the Cr isotopic composition of the Cr(VI) remaining in solution and $\delta^{53}Cr_{ini}$ the Cr isotopic composition of the initial Cr(VI) (i.e. before reduction). According to mass balance:

$$\delta^{53}Cr_{TOT} = \delta^{53}Cr_{(VI)} \times x + \delta^{53}Cr_{(III)} \times (1 - x) \tag{3.4}$$

where $\delta^{53}Cr_{TOT}$ is the Cr isotopic composition of total Cr, $\delta^{53}Cr_{(VI)}$ and $\delta^{53}Cr_{(III)}$ are the Cr isotopic compositions of, respectively, Cr(VI) and Cr(III), and x is the fraction of Cr(VI) in the system.

The results of this modelling are shown in Figure 3.11. The first model (Fig. 3.11a), assumes that all of the Cr is initially present as Cr(VI), and the initial δ^{53}Cr value is assumed to be +0.454‰, i.e. the $\delta^{53}Cr_{TOT}$ value of seawater in the uppermost sample from the Argentine Basin. As the Cr(VI) is reduced to Cr(III), the Cr(VI) that remains becomes isotopically heavier as the light isotopes are preferentially reduced. The δ^{53}Cr value of the Cr(III) that is produced also becomes isotopically heavier, although the difference in isotopic composition between the Cr(VI) and Cr(III) is less if the system is fully open (i.e. the Cr(III) produced is removed from solution as it is produced; blue line). Figure 3.11a demonstrates that neither the δ^{53}Cr value of the Cr(III) nor the δ^{53}Cr value of the Cr(VI) in the sample recovered from 30 m water depth in the Argentine Basin can be accounted for using either the Rayleigh model or the fully-open model; the isotope fractionation between the two species is much smaller than either of the models predict.

However, the results of these models are strongly dependent on the starting conditions. For example, Kieber et al. (2002) report that the speciation of Cr in rainwater is highly variable, with Cr(III)/CrTOT ranging from 0.25 to 0.75. The

Figure 3.11 *(facing page)*: Modelling of the variation in δ^{53}Cr due to reduction of Cr(VI) to Cr(III). f is the fraction of the initial Cr(VI) that remains in solution. (a) Initial solution containing only Cr(VI); variation in $\delta^{53}Cr_{(III)}$ is shown for an open system, where the Cr(III) is not removed from the system (blue line) and when Cr(III) is removed from the system (red line). The dashed and dotted lines correspond to an equilibrium isotope fractionation with a constant difference of $\Delta^{53/52}Cr_{(Cr(III)-Cr(VI))}$ of -1.5‰. Black square shows the measured δ^{53}Cr value for Cr(III) in seawater from the Argentine Basin at 30 m depth; black circle shows the calculated δ^{53}Cr value for Cr(VI). Both black square and black circle are located at a f value of 0.38 that has been measured for the 30 m sample. (b) Initial solution contains variable proportion of Cr(III) to total Cr (see key). Solid red and blue lines assume that all Cr is initially present as Cr(VI) (as for (a)). The black square and circle show the Cr isotopic composition of Cr(III) and Cr(VI) in the 30 m sample (Table 3.3). (c) Initial solution contains variable proportion of Cr(III) to total Cr (see key), as the Cr(III) forms it is removed from the system. Black diamond shows the measured δ^{53}Cr value for Cr(III) in seawater from the Argentine Basin at 30 m depth; black circle shows the calculated δ^{53}Cr value for Cr(VI). Open diamond and open circle show the δ^{53}Cr value for Cr(III) and Cr(VI) respectively from the Argentine Basin at 150 m depth.

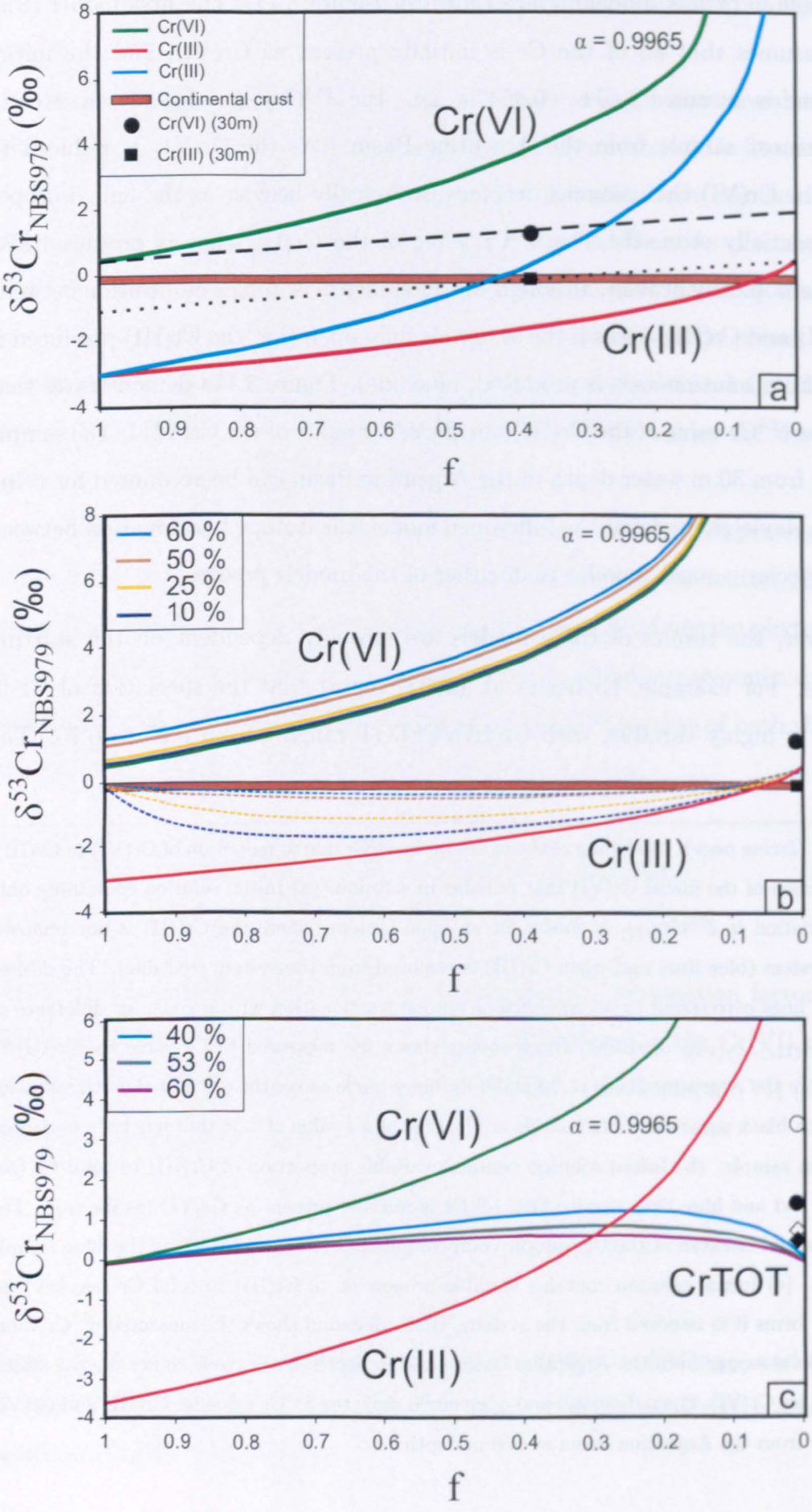
Cr(VI)
Cr(III)
Cr(III)
Continental crust
Cr(VI) (30m)
Cr(III) (30m)
α = 0.9965
Cr(VI)
Cr(III)
a
δ53CrNBS979 (‰)
f
60 %
50 %
25 %
10 %
α = 0.9965
Cr(VI)
Cr(III)
b
δ53CrNBS979 (‰)
f
40 %
53 %
60 %
Cr(VI)
α = 0.9965
CrTOT
Cr(III)
c
δ53CrNBS979 (‰)
f

effect of varying the proportion of Cr(VI) to Cr(III) in the initial solution is described by Equation 3.5 and is shown in Figure 3.11b.

$$\delta^{53}Cr_{(III)} = \delta^{53}Cr_{(III)initial} \times PCr_{(III)dust} + \delta^{53}Cr_{(III)reduction} \times PCr_{(III)reduction} \quad (3.5)$$

In Equation 3.5, $\delta^{53}Cr_{(III)}$ is the Cr isotopic composition of the Cr(III) pool, $\delta^{53}Cr_{(III)initial}$ is the Cr isotopic composition of rainwater, which is assumed to be equal to the continental crust value (-0.124 ± 0.101‰), $\delta^{53}Cr_{(III)reduction}$ is the Cr isotopic composition of the Cr(III) produced by reduction of the Cr(VI) pool, and $PCr_{(III)dust}$ and $PCr_{(III)reduction}$ are the proportions of Cr(III) from the dust and from the reduction of Cr(VI), respectively.

Figure 3.11b demonstrates that it may just about be possible to model the measured values of $\delta^{53}Cr_{(III)}$ and $\delta^{53}Cr_{(VI)}$ in the sample from 30 m water depth if the proportion of Cr(III) is high (~90%). Nevertheless, this model cannot explain the relatively high $\delta^{53}Cr_{(III)}$ value of the sample from 150 m water depth (+0.173‰, Table 3.3), nor can it explain the relatively high proportion of Cr(III) that is measured in all samples from the Argentine Basin (≥60%). Finally, Figure 3.11c considers the effects of variable initial Cr(III)/CrTOT, together with the loss of Cr(III) from the system. In this case:

$$\delta^{53}Cr_{TOT} = \delta^{53}Cr_{initial} \times PCr_{(III)} + \delta^{53}Cr_{(VI)} \times (1 - PCr_{(III)}) \quad (3.6)$$

where $\delta^{53}Cr_{TOT}$ is the Cr isotopic composition of the total Cr, $\delta^{53}Cr_{initial}$ is the initial Cr isotopic composition of the solution, which is assumed to be equal to the continental crust value (-0.124 ± 0.101‰, Schoenberg et al., 2008), $\delta^{53}Cr_{(VI)}$ is the Cr isotopic composition of the Cr(VI) remaining into solution, and PCr(III) is the proportion of Cr(III) in the system, which is given by:

$$PCr_{(III)} = \frac{1 - PCr_{(VI)initial}}{1 - PCr_{(VI)initial} \times (1 - f)} \quad (3.7)$$

where $PCr_{(VI)initial}$ is the proportion of Cr(VI) in the initial solution and f is the fraction of Cr(VI) remaining in solution.

In this scenario, the δ^{53}Cr value of total Cr becomes heavier as reduction proceeds. The values of $\delta^{53}Cr_{TOT}$ and $\delta^{53}Cr_{(III)}$ measured in samples recovered from 30 m and 150 m water depth in the Argentine Basin can be predicted by this model. Thus, although more data are required, it seems likely that the Cr isotope signature of surface waters from the Argentine Basin are best explained in terms of input from atmospheric sources, combined with partial reduction of Cr(VI) to Cr(III).

In contrast to the seawater samples from the Argentine Basin, the seawater samples from Southampton Water have higher δ^{53}Cr values for Cr(III) than for total Cr (by 0.173‰). In this case, the Cr(III) could not have been produced by the reduction of Cr(VI), as the $\delta^{53}Cr_{(III)}$ should be lighter than $\delta^{53}Cr_{TOT}$ (Ellis et al., 2002). This raises the possibility that the continental flux of Cr to seawater is dominated by Cr(III), which has high δ^{53}Cr and is fractionated from its crustal source. Studies of groundwaters do indicate that oxic groundwaters have high δ^{53}Cr (Izbicki et al., 2008); however, the dominant Cr oxidation state appears to be Cr(VI), rather than Cr(III) (e.g. Ellis et al., 2002; Izbicki et al., 2008). The presence of Cr(III) in the Southampton water samples could also be explained by the reduction of Cr(VI) to Cr(III) in the estuarine environment, or adsorption of Cr onto particles under non-equilibrium conditions (Pettine et al., 1997). Pettine et al. (1997) have demonstrated that Cr(III) can be absorbed onto particles in the estuarine environment; however, this would remove Cr(III) from the system, which is not what is observed in this study.

This raises the possibility that the source of Cr(III) in Southampton Water is anthropogenic. As discussed in Section 3.5.1, Cr from anthropogenic sources could be in the form of both Cr(III) and Cr(VI); moreover, the Cr is likely to have been exposed to differing redox conditions. Thus, the relatively high δ^{53}Cr values measured in the Southampton seawater samples could potentially be explained by input of anthropogenic Cr. However, this is entirely speculative because, at this point in time, specific details on the chemical composition of waste effluent discharged

into Southampton Water are not known, and the Cr isotope compositions of the potential anthropogenic sources are unknown.

3.6 Conclusions

The chromium concentration and Cr isotopic composition of seawater has been determined for samples collected from (i) the Argentine Basin, and (ii) Southampton Water. Concentrations of total Cr are higher in the open ocean samples (Argentine Basin; 5.80 - 6.50 nM) than they are in coastal seawater (Southampton Water; 1.82 nM). Concentrations of Cr show little variation with depth at either site. However, concentrations of Cr(III) are slightly reduced in surface waters from the Argentine Basin, suggesting that Cr(III) may be consumed by biological activity. Surprisingly, the dominant oxidation state of Cr at both sites is Cr(III), which comprises 60 - 90 % of the total chromium, higher than has been typically reported in other studies. The reason for the high proportion of Cr(III) is not clear; there is a chance that it is an artefact of the Cr pre-concentration technique, although this is unlikely, but it may also be due to reduction of Cr(VI) by either photochemical or biochemical processes, release of Cr(III) from sinking particulate material or, in the case of Southampton Water, inputs of river water and/or anthropogenic Cr.

In the Argentine Basin, δ^{53}Cr values are between -0.116 and 0.793‰, whereas samples from Southampton Water have δ^{53}Cr values that range from 1.543 to 1.748‰. Thus, with the exception of one sample (that has δ^{53}Cr = -0.116‰), the Cr isotopic composition of seawater is heavier than the Cr isotopic composition of the continental crust value (-0.124‰). This indicates that Cr isotopes are fractionated during the weathering process and/or in the riverine system. In the Argentine Basin, the Cr isotopic composition of total Cr tends to be higher than the Cr isotopic composition of Cr(III), by up to 0.57‰. Two different processes can influence the Cr isotopic composition in seawater: (i) the source of Cr into the ocean and (ii) the redox reactions occurring in the water column. The Cr isotopic composition of Cr(III) in the shallow water indicates that in the Argentine Basin the main source of Cr in the ocean is probably dust input with $\delta^{53}Cr_{(III)}$ close to the continental

crust value. By contrast, the Cr isotopic composition of total Cr is lower than the Cr isotopic composition of Cr(III) in Southampton Water, by ~0.17‰. This is inconsistent with Cr(III) production by reduction of Cr(VI). We suggest that input of Cr(III) in the Southampton Water is from river water and/or anthropogenic sources.

These preliminary data suggest that Cr isotopes have the potential to reveal unique information about the sources of Cr to seawater, as well as biogeochemical and redox processes. However, they also reveal that the Cr isotopic composition of seawater may be highly variable, and additional data from a variety of different oceanic regimes are required in order to verify our results. Moreover, it is important to note that our interpretation of these seawater data at the present time is highly speculative in the absence of Cr isotope data for rivers, atmospheric particles and anthropogenic sources.

Chapter 4

Geological and regional setting

4.1 Introduction

The aim of this study is to assess redox conditions in the Neoproterozoic ocean utilizing rare earth element (REE) concentration data and Cr isotopes in carbonates. As previously discussed in Chapter 1, the Neoproterozoic Era is characterized by major episodes of glaciations that led to the deposition of glacial deposits globally, often with a characteristic cap carbonate (Fairchild and Kennedy, 2007). Carbonate rocks are present in many Neoproterozoic sequences, usually forming in shallow water environments, as pelagic calcifying organisms had not yet evolved. In order to assess the Cr isotopic composition of seawater on a global scale, several Neoproterozoic sequences have been selected for analysis. These are from South Australia (the Adelaide Geosyncline), Scotland (the Dalradian Supergroup), Central East Greenland, and Morocco. In this chapter, the geological background of these four locations is described and existing geochemical data (mainly C and Sr isotopes) are summarized. Geochronology and general correlations between these sequences and others from different parts of the world will also be discussed. Finally, this section includes a short description and discussion of the Phanerozoic and modern carbonates analysed during the course of this study.

4.2 The Adelaide rift complex (South Australia)

The Adelaide rift complex is a Neoproterozoic to middle Cambrian basin located in South Australia (Fig 4.1) and its formation is related to the breakup of the Rodinia supercontinent. The present distribution of rock units in the Adelaide geosynclines (Fig. 4.1) is controlled by the Delamerian Orogen (~500 Ma; Preiss, 2000). It has been shown that the Adelaide rift complex has experienced low grade metamorphism in the greenschist facies (Preiss, 2000). The Adelaide rift complex ("Adelaide Geosyncline") contains a thick, variably deformed Neoproterozoic succession of sediments (Preiss, 1987) that developed through several successive episodes of Neoproterozoic rifting. The basin consists of more than 15 km of sediments that formed during at least five rift cycles (Preiss, 2000; Walter et al., 2000). The strata are divided into three so-called "Supergroups", the Warrina, the Heysen and the Moralana (Fig. 4.2; Preiss, 1982). The Warrina Supergroup represents the early rift sequences, the Heysen Supergroup encompasses all the glacial, interglacial and post-glacial sediments, and the Moralana Supergroup consists entirely of Cambrian sediments (Preiss, 2000). The Supergroups have been subdivided into sub-groups and formations, as shown in Figure 4.2. The succession has been divided into 12 informal units (sequence sets) (Preiss et al., 1993). These units do not always correspond to the existing lithostratigraphic subdivisions.

4.2.1 Existing age constraints

In order to make comparisons with other Neoproterozoic sequences worldwide, a good understanding of the geochronology of the sedimentation in the basin is important. The geochronological control on sedimentation in the Adelaide rift complex is still a matter of debate. Historically, different techniques have been used to constrain the geochronology of the sedimentation: U-Pb on volcanic bodies (Wingate et al., 1998), whole rock Rb-Sr (Compston et al., 1966), and U-Pb on zircons (e.g. Calver et al., 2004). In this section, the more recent and most accurate chronological constraints are emphasized.

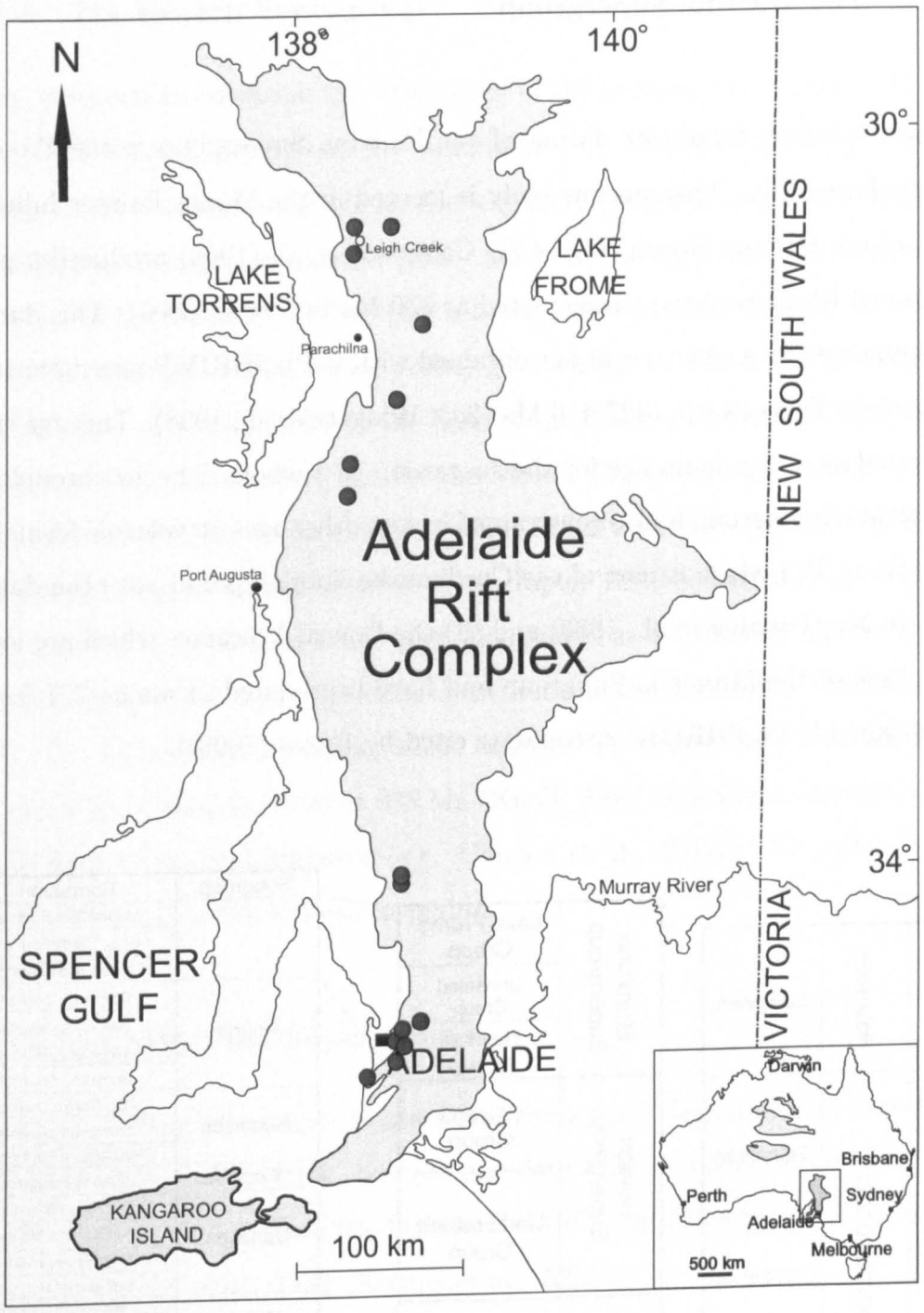

Figure 4.1: Simplified map showing the distribution of Neoproterozoic rocks in the Adelaiden Geosyncline (South Australia). The grey area represents the sediments of the three Supergroups; purple circles show sampling localities. The inset shows Neoproterozoic basins in Australia. Adapted from Williams (2008).

4.2.1.1 The Warrina Supergroup

The most obvious target for dating of the Warrina Supergroup is the Wooltana Volcanic Formation. This igneous body is located in the Mount Painter Inlier and is part of the Callana Group (Fig. 4.2). Compston et al. (1966) produced a poorly constrained Rb-Sr isochron (recalculated as 830 Ma by Preiss, 2000). This date has been supported by a more recent age obtained with U-Pb SHRIMP measurements of the Gairdner Dyke swarm (827 ± 6 Ma (2σ); Wingate et al., 1998). This age can be interpreted as a maximum age for the succession as a whole. The geochronology of the Warrina Supergroup is also constrained by two other ages on volcanic formations: (i) the Rook Tuff which is part of the Curdimurka Subgroup and has been dated at 802 ± 10 Ma (Fanning et al., 1986) and (ii) the Boucat Volcanics which are located at the base of the Mundalio Subgroup and have been dated at about 777 ± 7 Ma (unpublished U-Pb SHRIMP zircon date cited by Preiss (2000)).

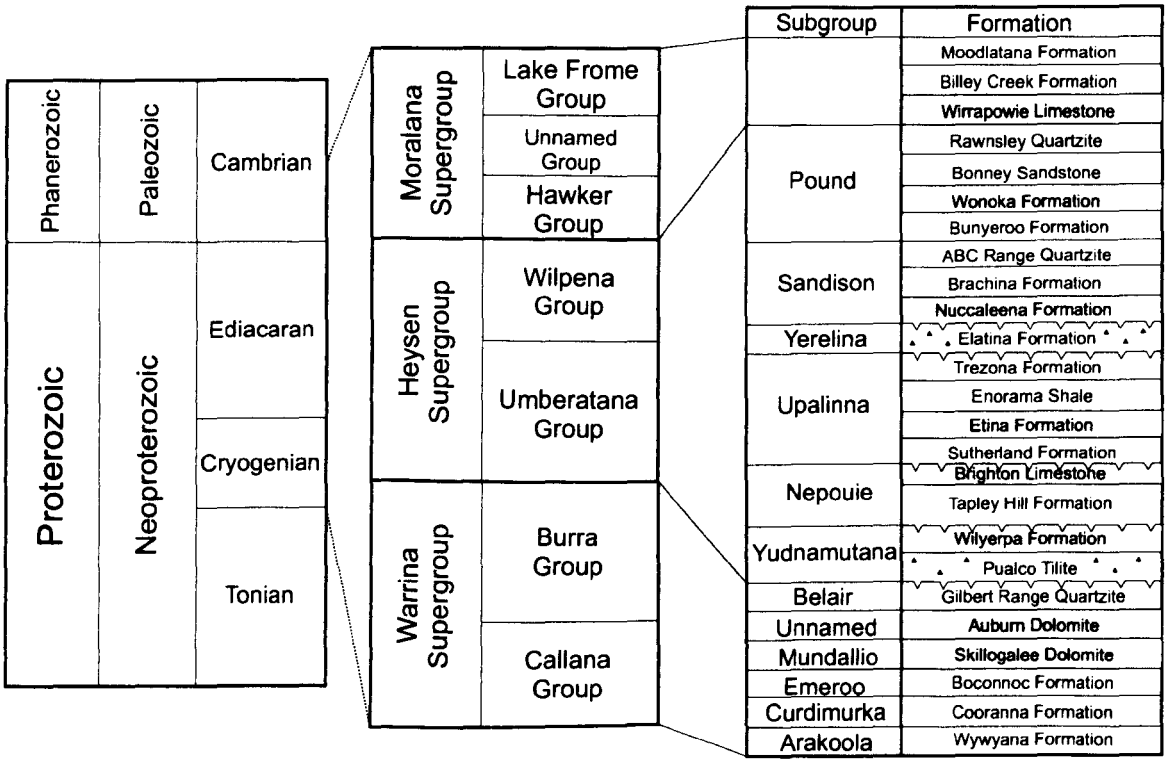

Figure 4.2: Schematic log of the sedimentation in the Adelaide Rift Complex. Modified from Preiss (2000). The formations sampled in this study are shown in grey.

4.2.1.2 The Heysen Supergroup

Several attempts to constrain the chronology of the sedimentation during the deposition of the Heysen Supergroup are summarized by Mahan et al. (2010). Despite the large number of ages available for the sequence, the geochronological constraints on the Heysen Supergroup remain poor. Many of the ages reported overlap, and only a few of them can be used to give a better constraint on the time of sedimentation. For example, Calver et al. (2004) gave an age of 582 ± 4 Ma using U-Pb SHRIMP data on a rhyodacite at the base of the Elatina formation. This age can be interpreted as a maximum age for the second Cryogenian glaciation. Another dating constraint on the sedimentation (about 643 ± 2.4 Ma) is reported by Kendall et al. (2006) using Re-Os for the base of the Tapley Hill Formation (Fig. 4.2). This age is particularly critical as it has been interpreted as a minimum age for the first Cryogenian glaciation. It also provides constraints on the duration of the interglacial period. The Nuccaleena formation, which consists of cap carbonate from the second Cryogenian glaciation, is dated at 635 Ma (Knoll, 2000) based on a correlation with sections from China and Namibia (e.g. Condon et al., 2005). This age is used to constrain the start of the Ediacaran period.

4.2.1.3 The Moralana Supergroup

The Moralana Supergroup encompasses sediments from the Cambrian. In addition to biostratigraphic information, there is one date (522 ± 2 Ma),obtained by U-Pb SHRIMP data on zircons from the Sellicks Hill tuff, that constrains the age of sedimentation (Cooper et al., 1992; Jenkins et al., 2002).

In summary, the Warrina Supergroup consists of the Callanna and the Burra groups (Fig. 4.2) and is believed to have been deposited between the end of the Tonian and the Cryogenian, from 850 to 735 Ma. The Heysen Supergroup consists of the Umberatana and the Wilpena Groups, and is believed to have been deposited between the end of the Neoproterzoic (the middle of the Cryogenian, 735 Ma) and the end of the Ediacaran (545 Ma). The Moralana Supergroup comprises the Hawker

and Lake Frome groups (Normanville and Kanmantoo groups in the Mount Lofty Ranges) and was deposited at the beginning of the Cambrian, between about 545 Ma and 505 Ma. Given the loose radiometric constraints, in order to compare the Adelaide Geosyncline to the rest of the Neoproterozoic sequences worldwide, better age constraints on the sequence are required.

4.2.2 Geochemical data

A number of geochemical studies have been conducted on the Adelaide Geosyncline (e.g. Kennedy, 1996, Hoffman and Schrag, 2002). These have focused on different parts of the succession and use a number of geochemical techniques (C, O, S and Sr isotopes) to assess and to understand the sedimentation processes and the geological setting (Calver and Walter, 2000; McKirdy et al., 2001). In this section, a brief summary of the data available and general trends will be described and discussed. Most of the data available for this sequence are based on the Heysen Supergroup. McKirdy et al. (2001) focused their study on the Umberatana group, which is the lower part of the Heysen Supergroup (Figs. 4.2 and 4.3), and represents a close to complete record of the interglacial period. The carbon isotopic record of this period has been described by McKirdy et al. (2001). The post-glacial carbonates have $\delta^{13}C$ values of around -5‰. The $\delta^{13}C$ values then increase to about +8‰ to +10‰ through the Wonoka Formation (Fig. 4.3). Close to the top of the Wonoka Formation, the carbonate $\delta^{13}C$ values plunge to -9‰, before increasing again to -3‰ just before the next glaciation. The Nuccaleena formation, which is the cap carbonate that marks the end of the second Cryogenian glaciation, is characterised by a decrease in $\delta^{13}C$ from -1‰ at the base to -3‰ at the top (McKirdy et al., 2001). Calver and Walter (2000) focused their study on organic carbon in the Wilpena Group (which is found in the upper part of the Heysen Supergroup, Fig. 4.2) and demonstrated that the C-isotopic composition of organic carbon after the second Cryogenian glaciation varied through time. These variations are interpreted to be related to the stratification of the oceans after the glaciation. Sr isotopes data obtained for some of their samples yield $^{87}Sr/^{86}Sr$ ratios of 0.70825 that are consistent with the seawater curve for the time period (Calver and Walter, 2000;

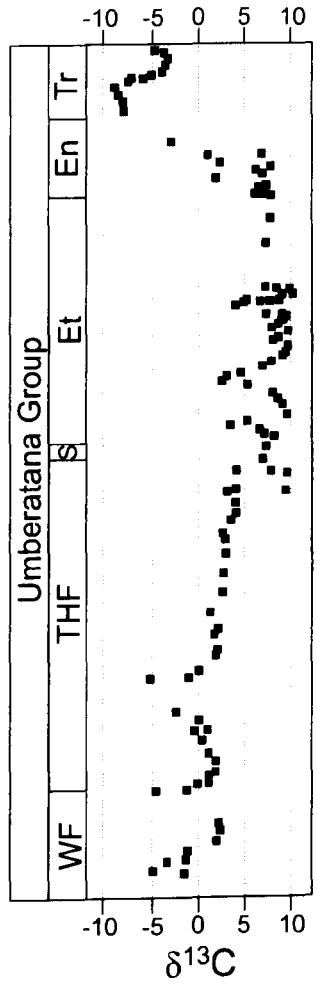

Figure 4.3: Carbon isotopic curve for the Umberatana Group. Modified after McKirdy et al. (2001). Abbreviations: WF, Wonoka Formation; THF, Tapley Hill Formation; S, Sutherland Formation; Et, Etina Formation; En, Enorama Formation; Tr, Trezona Formation. The grey area highlights the Trezona negative carbon isotopes excursion.

Halverson et al., 2007).

In summary, the geochemical studies on the Adelaide Rift Complex reveal that the record of carbonate $\delta^{13}C$ is characterised by several large excursions, one of which (the Trezona anomaly) is located just before the second Cryogenian glaciation (Fig. 4.3). Another important excursion is located in the Wonoka formation. These two excursions may have been caused by changes in the carbon cycle, and/or by changes in environmental conditions (Calver and Walter, 2000; McKirdy et al., 2001). The record of carbonate $\delta^{13}C$ has also been used to correlate the Australian sequence with other Neoproterozoic sequences worldwide. The Wonoka excursion has been

correlated to the Shuram excursion in China; however, it is not clear whether this excursion represents a primary signal, or is caused by diagenesis (e.g. Derry, 2010; Halverson et al., 2010).

4.2.3 Sample Locations

Samples spanning the entire succession in the Adelaide rift complex (Fig. 4.1) were collected during a fieldwork campaign in 2009. As this study focuses on analyses of Cr isotopes in carbonates, sampling was restricted to units where carbonate was present, but this covers all three Supergroups (Fig. 4.2). The sample locations are shown on Figure 4.1. The Burra group, which corresponds to the sedimentation before the first glaciation, was sampled in four different formations (Skillogalee Dolomite, Auburn Dolomite, Castambul Formation and MonteCute Dolomite). The Umberatana Group, which encompasses the glacial strata, was sampled in four formations (Warcowie Dolomite, Brighton Limestone, Balcanoona Formation (Fig. 4.4e), and Etina Formation). The Wilpena Group, which is end-Neoproterozoic, was sampled in two formations (Nuccaleena Formation (Fig. 4.4a-b) and Wonoka Formation (Fig. 4.4f)). Samples of the Wirrapowie Limestone were collected to representat the Marinna Supergroup of Cambrian age. Samples from the Nuccaleena formation were collected on several occasions, in order to assess the variation of Cr isotopes in the basin and to use this formation as a test for diagenetic effects on the Cr isotopes.

4.3 The Dalradian supergroup

The Dalradian Supergroup of Scotland and Ireland was one of the first localities where glacigenic deposits were related to the Neoproterozoic (Thomson, 1871). The Dalradian crops out along a linear belt from Shetland, through mainland Scotland, to northwest Ireland. It consists of siliciclastic and carbonate rocks deposited from the Neoproterozoic to the middle Cambrian (Anderton, 1985; Harris et al., 1994). Although palaeolatitudinal reconstructions are uncertain, Dalradian sedimentation is believed to have taken place on the eastern margin of Laurentia (Cawood et al.,

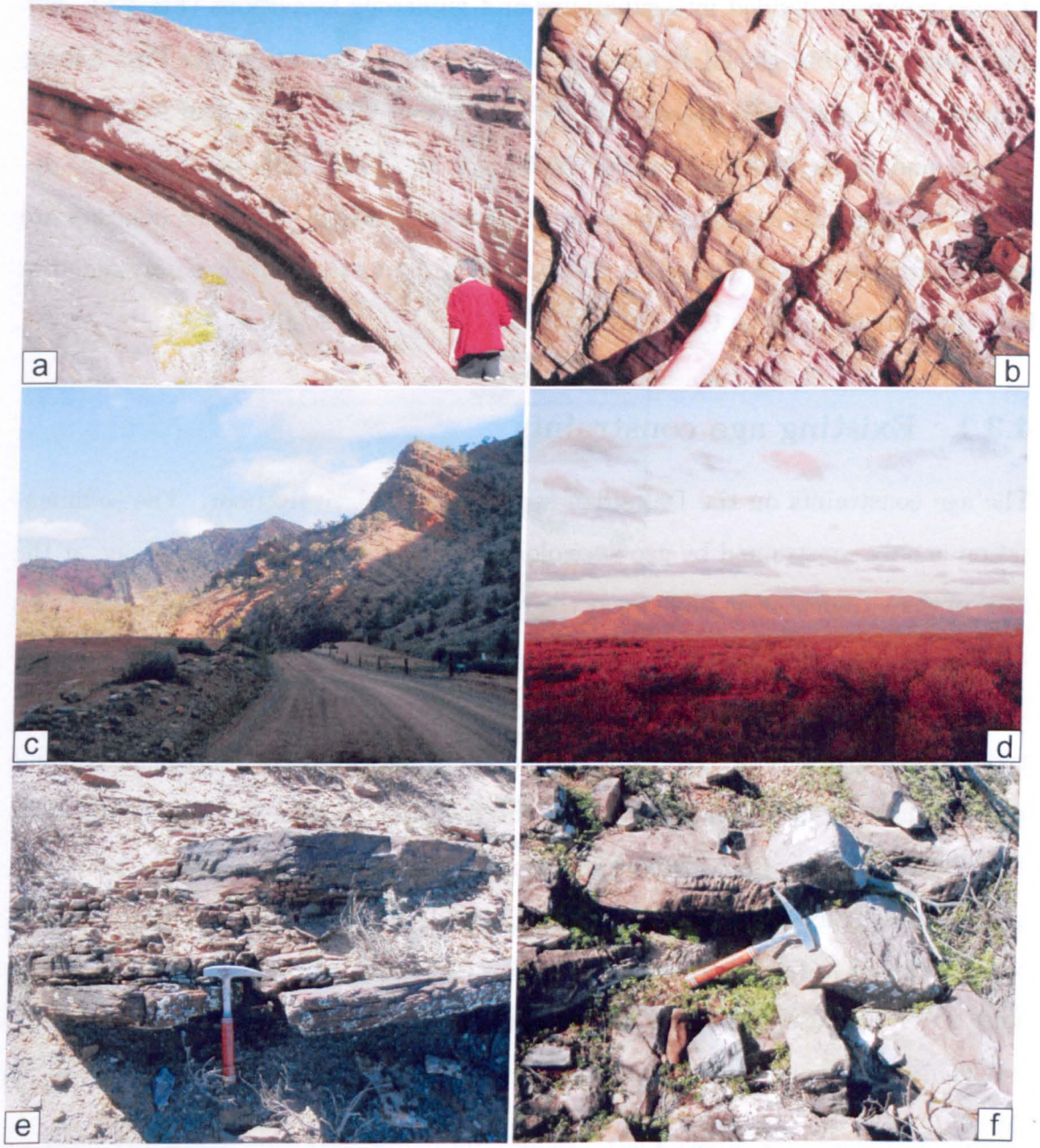

Figure 4.4: Field photos in the Adelaide rift complex. (a) photo showing the Nuccaleena Formation near Adelaide. (b) Outcrop of the Nuccaleena formation (sample A6). (c) View of the Neoproterozoic succession in the Brachina Gorge. (d) View of the Flinders ranges from Parachilna. (e) Outcrop photo of the Balcaloona Dolomite formation (sample A14) and (f) Outcrop photo of the Wonoka formation (sample A19).

2003). The Dalradian Supergroup is divided into four main groups that are, from the oldest to the youngest, Grampian, Appin, Argyll and Southern Highland. Each of these groups is divided into subgroups and numerous formations (Fig 4.5). For many years, only one glacial deposit was described in the literature: the Port Askaig formation, which is laterally very extensive (Spencer, 1971; Eyles and Eyles, 1983; Arnaud and Eyles, 2006). However, McCay et al. (2006) have more recently described three glacial deposits; these are illustrated in Figure 4.5. The deposits are termed the Port Askaig formation, the Stralinchy diamictite (which is only found in Ireland) and the Loch na Cille beds (Condon and Prave, 2000).

4.3.1 Existing age constraints

The age constraints on the Dalradian sequence are relatively poor. The sedimentation is only constrained by geochronological dating of two formations, one at the base of the sedimentation and one at the top. The first age was obtained from U-Pb isotope analyses of primary monazite in pegmatites (Noble et al., 1996). This age of 806 $\pm$ 4 Ma comes from the Grampian Shear Zone located at the base of the Dalradian Supergroup (Fig. 4.5). The second age comes from the Tayvallich volvanic rocks, which are located at the base of the Southern highland group. ^{207}Pb-^{206}Pb isotopic analyses of zircons from a keratophyre sampled on the Tayvallich peninsula give an age of 595 $\pm$ 4 Ma (Halliday et al., 1989). However, a more recent study on zircons from a felsic tuff collected at Port a' Bhuailteir on the Tayvallich peninsula give a ^{206}Pb/^{238}U age of 601.4 $\pm$ 3.7 Ma (Dempster et al., 2002). In summary, the sedimentation of the Dalradian sequence occurred from about 800 Ma to about 500 Ma (Fig. 4.5).

The main focus of this study is the Appin and Argyll groups. The Appin Group consists of a succession of siliciclastic rocks, quartzite and carbonates deposited in shallow to deep marine environments. The Group is divided into three Subgroups, the Lochaber Subgroup, the Ballachullish Subgroup and the Blair Atholl Subgroup. The 806 Ma age from the Grampian group (Noble et al., 1996) can be interpreted as a maximum age for the Appin Group. The Argyll group encompasses two glacial deposits (the Port Askaig Formation and the Stralinchy Daimictite) and is divided

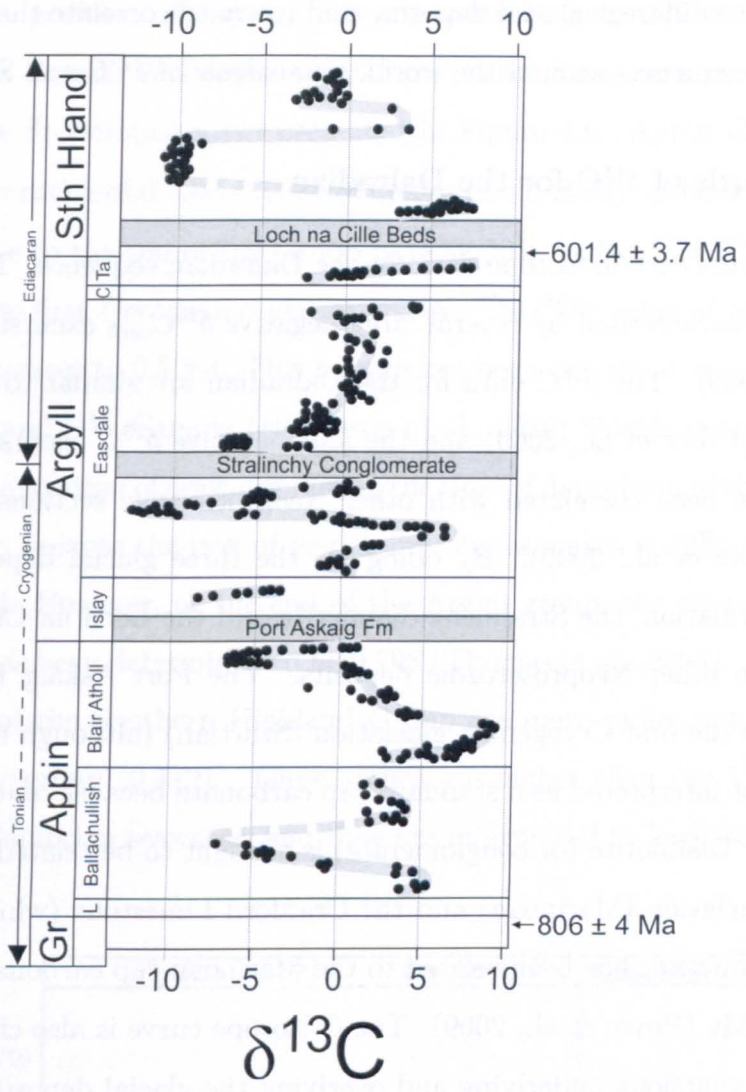

Figure 4.5: Carbon isotopic curve of the Dalradian Supergroup. Figure modified after Prave et al. (2009). Abbreviations: Gr, Grampian Group; Sth Hland, South Highlands Group; L, Lochaber Subgroup; C, Crinan Subgroup and Ta, Tayvallich Subgroup. The grey curve is the $\delta^{13}C$ of seawater.

into four Subgroups; the Islay Subgroup (oldest), the Easdale Subgroup, the Crinan Subgroup and the Tayvallich Subgroup (youngest).

4.3.2 Geochemical data

The chemostratigraphy of the Dalradian supergroup has been investigated in several studies (Brasier and Shields, 2000; Thomas et al., 2004; McCay et al., 2006; Prave et al., 2009, Sawaki et al., 2010). The main focus of these studies was to provide age

constraints on the different glacial deposits, and to try to correlate them with other Neoproterozoic sequences around the world, by analysis of $\delta^{13}C$ and Sr isotopes.

4.3.2.1 Records of $\delta^{13}C$ for the Dalradian

Figure 4.5 presents carbon isotope data for the Dalradian sequence. The Dalradian Supergroup is characterised by several large negative $\delta^{13}C_{carb}$ excursions (Fig. 4.5; Prave et al., 2009). The $\delta^{13}C$ data for the Dalradian are similar to the record of seawater $\delta^{13}C$ (Prave et al., 2009) and the four negative $\delta^{13}C$ excursions shown in Figure 4.5 have been correlated with other Neoproterozoic sections from around the world (Prave et al., 2009). By doing so, the three glacial deposits (i.e. the Port Askaig formation, the Stralinchy diamictite and the Loch na Cille beds) have been related to other Neoproterozoic deposits. The Port Askaig Formation has been related to the first Cryogenian glaciation (Sturtian) (although the Bonahaven formation is not interpreted as a standard cap carbonate because of its complexity). The Stralinchy Diamictite (or conglomerate) is thought to be related to the second Cryogenian glaciation (Marinoan) and the Cranford Limestone (which overlies the Stralinchy Diamictite) has been related to the Marinoan cap carbonates, which has an age of 635 Ma (Prave et al., 2009). The C isotope curve is also characterised by two negative excursions underlying and overlying the glacial deposit of the second Cryogenian glaciation (Fig. 4.4; Prave et al., 2009). Finally, the Loch na Cille beds have been related to the Gaskiers glaciation, with the C isotope excursion occurring after the Gaskiers glaciation correlated to the Wonoka-Shuram anomaly (Prave et al., 2009).

4.3.2.2 Records of $^{87}Sr/^{86}Sr$ for the Dalradian

The Sr isotope chemostratigraphy in the Dalradian has been studied in different publications (e.g. Brasier and Shields, 2000; Thomas et al., 2004; Sawaki et al., 2010). In Figure 4.6, the Seawater Sr isotopic composition variation during the Neoproterozoic is presented (Halverson et al., 2010) associated with a compilation of Sr isotopic composition measurements for the Dalradian sequence. In general, the Sr isotope signature of the Dalradian carbonates closely matches the seawater

Sr isotope composition. However, it is important to note that this argument can be circular as Sr rich carbonate around the world have been used to determine the composite Sr isotopes curve presented in Figure 4.6. Appin Group sediments have $^{87}Sr/^{86}Sr$ ratios of 0.7064-0.7065 (Thomas et al., 2004), although the sediments deposited close to the top of the Group have slightly higher $^{87}Sr/^{86}Sr$, up to 0.707. Just before the first Cryogenian glaciation, the $^{87}Sr/^{86}Sr$ value of the Appin group sediments decreases to 0.7063. This feature has been described in other successions in Greenland and NW Canada (Halverson et al., 2010; Shields pers. Comm.). The Sr isotopic composition of seawater during the time of deposition of the Argyll Group is still unclear, because the lack of Sr-rich limestones makes it difficult to detect the primary signal. However, at the end of the Argyll group, the seawater Sr isotopic composition has been determined to be 0.708 (Thomas et al., 2004). The Sr isotopic compositions of the Southern Highland Group are more radiogenic in comparison with the lower group (0.712). These values are higher than the $^{87}Sr/^{86}Sr$ values accepted for Cambrian seawater, and they are interpreted to have been overprinted

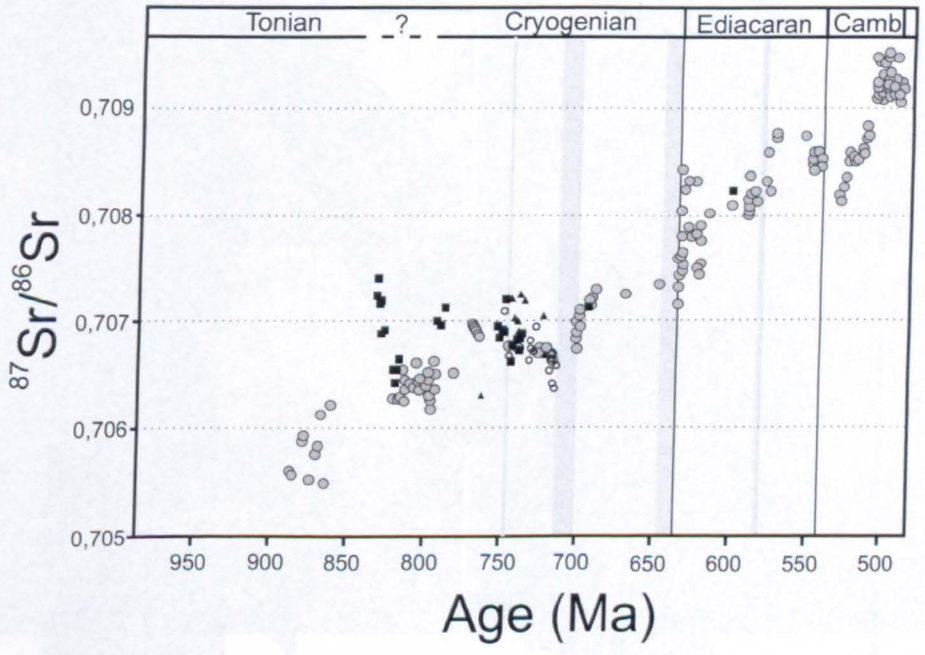

Figure 4.6: $^{87}Sr/^{86}Sr$ ratio from the Dalradian Supergroup placed on the composite seawater Sr isotopic curve for the Neoproterozoic modified from Halverson et al. (2010). The black and white points are data from the Dalradian (Sawaki et al., 2010, Thomas et al., 2004). The vertical grey areas are the glacial events.

by Sr derived from diagenetic fluids.

4.3.3 Sampling strategy

The focus of this study is the analysis of carbonates which, it is hoped, represent a primary seawater signal. In order to test this, three different Dalradian formations were sampled. These are located on the island of Islay and on the Tayvallich peninsula (Fig. 4.7). Firstly, the Lossit Limestone (or Islay limestone) formation was sampled on Islay. This formation underlies the Port Askaig Formation, and it is divided into two members: the Persabus member at the top of the formation and the Kiells limestone member at its base (Arnaud and Fairchild, 2011). The Persabus member consists of interbedded dolostones, quartzites, slates, and mixed litholigies, whereas the Kiells Limestone member consists of 70 m of pure limestone,

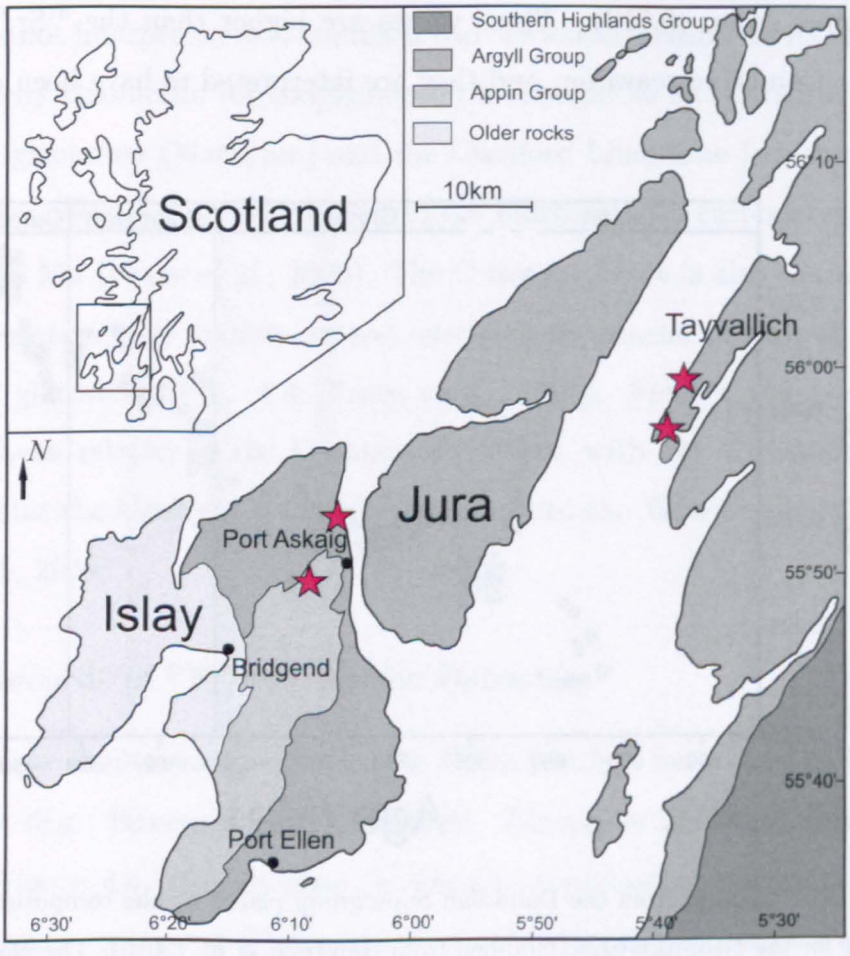

Figure 4.7: Simplified Geological map of Islay and the Tayvallich peninsula. Modified after Tanner (1998). The red stars are the sampling localities.

locally oolitic (Fig. 4.8). Secondly, the Bonahaven Formation was also sampled on Islay. This formation underlies the Jura Quartzite Formation and consists of mixed dolomitic-siliciclastic lithologies, which are divided into four members (1 to 4; Spencer and Spencer, 1972; Fairchild, 1985; Hambrey et al., 1991). The samples analysed in this study come from the top of member 1 (Fairchild, 1977; Fairchild, 1980). Finally, samples of the Tayvallich Limestone were collected from the Tayvallich Peninsula. The Tayvallich Limestone is part of the Argyll group and the Tayvallich Subgroup (Prave et al., 2009). This formation underlies the Tayvallich volcanic rocks that are dated at 601 Ma; this age can be interpreted as minimum age for the Tayvallich limestone.

In the literature, these three formations have been studied in terms of their carbon and Sr isotopic composition. The Lossit carbonates are characterised by a $\delta^{13}C$ negative excursion with $\delta^{13}C$ = -6‰ and $^{87}Sr/^{86}Sr$ in the range 0.7067-0.7072 (Fig.

Figure 4.8: Field photos in the Dalradian Supergroup. (a) Outcrop photo of sample I1 on Islay, (b) Outcrop photo of the disrupted beds (sample I24 and I24R), (c) Outcrop photos of the oolitic limestone I27 in the Islay Formation and (d) Outcrop photos of the oolitic limestone I28 in the Islay Formation.

4.6). These limestones are thought to record the primary seawater signal, because they have low Mn/Sr ratios and high Sr concentrations. The chemostratigraphy of the Bonahaven Formation includes a negative C isotope excursion ($\delta^{13}C$ = -8‰), which has been interpreted as a cap carbonate feature (Brasier and Shields, 2000). However, this excursion could also be explained by early diagenesis as this anomaly relates to the pyritic and ferroan dolomite lithologies of member 3 (Fairchild and Kennedy, 2007). The Tayvallich formation is characterised by a wide range of $\delta^{13}C$ values, from -2‰ to +8‰. The $^{87}Sr/^{86}Sr$ of the Tayvallich Limestone lies between 0.7082 and 0.7089, which is slightly high compared with the Sr seawater curve for the later part of the Ediacaran (Fig. 4.6).

4.4 The Anti-Atlas Margin, Morocco

The Precambrian to Early Cambrian section of Morocco consists of a nearly 3 km thick succession of platform carbonates and siliciclastic sedimentary rocks on Pan-African age basement. The Morocco sequence is divided into two Groups (the older Taroudant and the younger Tata Groups) that encompass Neoproterozoic and early Cambrian sediments (Fig. 4.9).

4.4.1 Taroudant group

This Group is divided into two formations: the Adoudounian Formation at the base and the Lie de Vin at the top (Fig 4.9). The Adoudounian formation is further divided into two members called Serie de Base (or Tabnia member) and Calcaires Inferieurs (or Tifnout member). The Serie de Base member made up of peritidal carbonates, evaporites, mudcracked siltstones and fluvial sandstones (Maloof et al., 2005). The upper part of the Serie de Base member is characterised by the presence of discoid structures that resemble taxa of the Ediacaran fauna (Houzay, 1979). The Calcaire Inferieur member reflects the beginning of the thermal subsidence regime and consists of peritidal dolostones (Maloof et al., 2005). The Lie de Vin Formation is characterised by cyclic alternation of burgundy-coloured argillite and biohermal carbonates (Monninger, 1979; Latham and Riding, 1990; Geyer and Landing, 1995).

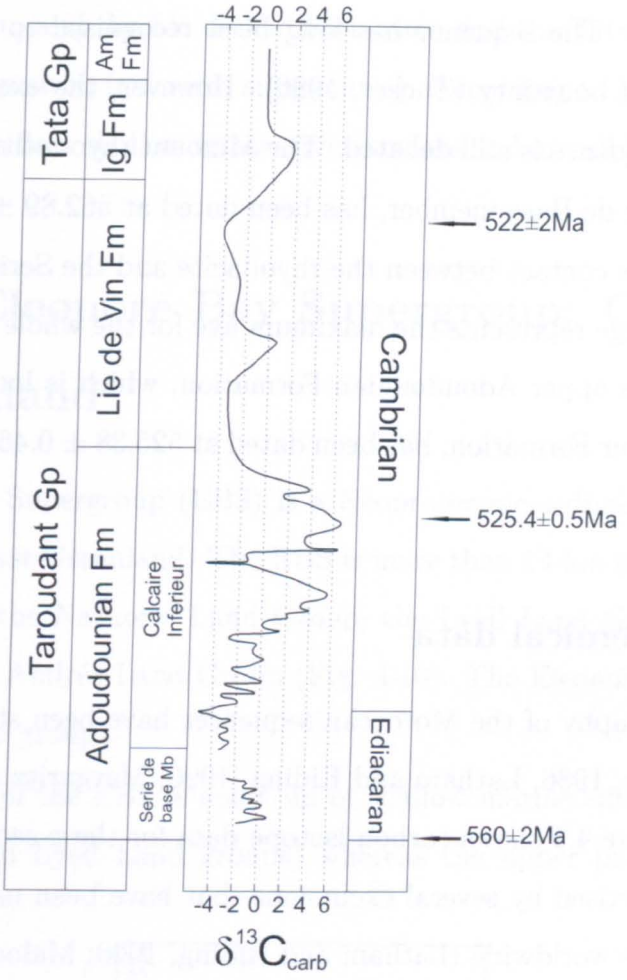

Figure 4.9: Carbon isotopic curve for the Morocco sequence. Modified after Maloof et al. (2005). Abbreviations: Ig Fm, Igoudine Formation; Am Fm, Amouslek Formation.

In the Tiout section, the Lie de Vin formation records deeper water conditions (Maloof et al., 2005).

4.4.2 Tata Group

The second group of Moroccan sedimentation is named the Tata Group and is divided into three Formations, the Ingoudine Formation, the Amouslek Formation and the Issafene Formation (Geyer and Landing, 1995). The Tata group reflects a transition to more energetic shallow marine conditions compared with the Lie de Vin formation (Destombes et al., 1985). The Ingoudine Formation contains the oldest known skeletal fossils from Morocco (Choubert and Hupe, 1953; Choubert et al., 1975; Boudda et al., 1979), which clearly indicate an early Cambrian age

for the Tata group. The sequence has long been recognised to straddle the Precambrian/Cambrian boundary (Tucker, 1986). However, the exact location of the boundary in the sequence is still debated. The Minount rhyodacite, which is located just below the Serie de Base member, has been dated at 562.89 ± 0.49 Ma (Maloof et al., 2005). As the contact between the rhyodacite and the Serie de Base member is discordant, this age represents the maximum age for the whole succession. Meanwhile, ash from the upper Adoudounian Formation, which is located at the top of the Calcaire Inferieur Formation, has been dated at 525.38 ± 0.46 Ma (Maloof et al., 2005).

4.4.3 Geochemical data

The chemostratigraphy of the Moroccan sequences have been studied by a number of authors (Tucker, 1986; Latham and Riding, 1990; Margaritz et al., 1991; Maloof et al., 2005). Figure 4.9 shows carbon isotope data for these sequences. The record of $\delta^{13}C$ is characterised by several excursions that have been used to correlate this sequence to others worldwide (Latham and Riding, 1990; Maloof et al., 2005). The $\delta^{13}C$ excursions occur on different timescales. The general pattern of the $\delta^{13}C$ curve is punctuated by a series of relatively short excursions (Fig. 4.9), that may reflect the release of carbon from isotopically depleted reservoirs (such as methane hydrate or organic carbon) and associated nutrient recycling and organic carbon burial (Maloof et al., 2005). The carbon isotope variations have also been used in attempts to locate the Precambrian/Cambrian boundary (Tucker, 1986; Latham and Riding, 1990). This is still under debate, but the latest radiometric ages indicate that the Precambrian/Cambrian boundary is located at the base of Calcaire Inferieur Formation (Maloof et al., 2005).

4.4.4 Sampling strategy

The aim of studying the Morocco section was to determine the seawater Cr isotopic composition at the beginning of the Cambrian. Samples from three different Formations have been analysed: the Taroudant Group, which lies in the Calcaire

Inferieur formation, and the Lie de Vin Formation and the Tata group, which lie in the Ingoudine Formation (calcaires superieures). According to Maloof et al. (2005), these samples all reflect shallow water environments and are all from the Cambrian.

4.5 The Eleonore Bay Supergroup: Central East Greenland

The Eleonore Bay Supergroup (EBS) is a Neoproterzoic sedimentary sequence located in Central East Greenland. The EBS is more than 14 km thick and is divided into four Groups, the Nathorst Land Group, the Lyell Land Group, the Ymer Ø Group and the the Andrée Land Group (Fig. 4.10). The Eleonore Bay Supergroup underlies the Tillite group.

The lower part of the EBS is made up of shallow marine siliciclastic sediments (Nathorst Land and Lyell Land groups) whereas the upper part is composed of

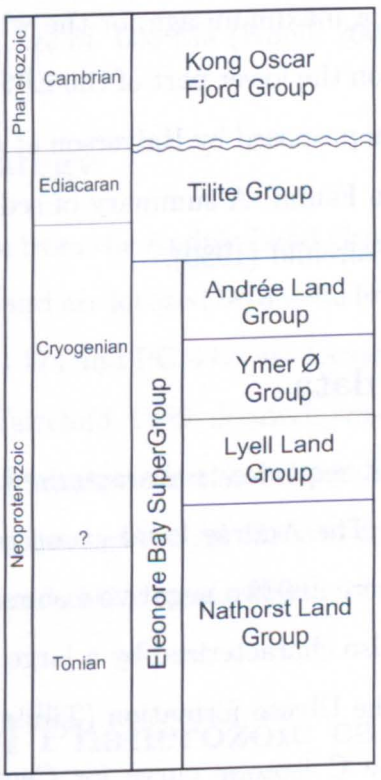

Figure 4.10: Simplified chronostratigraphy and lithostratigraphy of the Eleonore Bay Supergroup. Modified after Sønderholm et al. (2008).

carbonate platform deposits (Ymer Ø and Andrée Land groups; Sønderholm and Tirsgaard, 1993). The Tillite group, which is overlying the Andrée Land group, is divided into five formations and underlies the Cambrian-Ordovician Kong Oscar Fjord Group. The sedimentation of the Eleonore Bay Supergroup and the Tillite Group is divided into 4 sequences: (1) rapidly subsiding siliciclastic shelf, (2) stable siliciclastic shelf, (3) carbonate platform and (4) glacigenic deposits (Sønderholm et al., 2008). The interval studied here is located at the top of the carbonate platform, below the lower of the two glacial formations. The East Greenland section is closely correlated with the sedimentary basin of NE Svalbard (Knoll et al., 1986; Fairchild and Hambrey, 1995).

4.5.1 Age constraints

The age of the Eleonore Bay Supergroup and the glacigenic deposits of the Tillite group has been widely debated. Detrital zircons from the Nathorst Land Group suggest a maximum age for the EBS of 987 ± 18 Ma (Dhuime et al., 2007). This age has been interpreted as a maximum age for the whole sequence. There are no radiometric age constraints on the lower part of the EBS. A minimum age of 575 Ma for the Tillite group has been proposed by Halverson et al. (2004), based on the non-appearance of the Ediacaran Fauna. A summary of sedimentological interpretation is given in Herrington and Fairchild (1989).

4.5.2 Geochemical data

The Central East Greenland sequence is characterised by large variations in $\delta^{13}C$ values (Knoll et al., 1986). The Andrée Land group sediments have average $\delta^{13}C$ values of +5‰, although there are two negative excursions in the lower part of the section. The $\delta^{13}C$ curve is also characterized by a large negative C isotope anomaly just prior to deposition of the Ulvesø formation (Tillite Group) (Knoll et al., 1986; Fairchild et al., 2000). The C isotope curve for Central East Greenland is also characterised by very positive $\delta^{13}C$ values, of up to +10‰. These extremely high values are typical of the Neoproterozoic period and several mechanisms, such as a

strongly stratified ocean, have been proposed to explain their origin. The Sr isotopic composition of the Andrée Land Group is characterised by relatively unradiogenic $^{87}Sr/^{86}Sr$ ratios of around 0.7063 (Fairchild et al., 2000). This is consistent with the seawater Sr isotope curve for the Neoproterozoic (Halverson et al., 2010). The most unradiogenic values are found just below the glacial deposit, and are interpreted to reflect the seawater $^{87}Sr/^{86}Sr$ ratio for the Neoproterozoic (Halverson et al., 2010; Shields, pers comm.). The chemostratigraphy of the Eleonore Bay basin and the associated Svalbard deposits has led to a debate on the age of the Ulvesø glacial deposit. Fairchild et al. (2000) suggest that the Ulvesø Formation is related to the Port Askaig Formation and to the first Cryogenian glaciation. However, Halverson et al. (2004) interpreted the $\delta^{13}C$ curve in the equivalent Svalbard section in terms of a "Marinoan" signal (Halverson et al., 2004). More recently (e.g. Halverson et al., 2007), the Ulvesø glacial deposit has been correlated to the first Cryogenian glaciation, on the basis of Sr isotope chemostratigraphy. This observation is assumed to be the case in this study. The Storeelv Formation is therefore likely to be related to the second Cryogenian glaciation, and the cap carbonates associated with this formation therefore have an age of 635 Ma (Knoll, 2000).

4.5.3 Sampling strategy

The samples studied all come from the Andrée Land Group at the top of the Eleonore Bay Supergroup (Fig. 4.10) and are located below the first glacial deposit. The three samples studied (PG128, PG 174 and PG 440) are located at the top of Andrée Land Group (see Herrington and Fairchild, 1989; Sønderholm et al., 2008). This formation is characterized by an overall transgression and the sedimentation setting is located on the inner to mid ramp environment in specific settings such as lagoon and pisoid shoals (Frederiksen, 2000; Sønderholm et al., 2008).

4.6 Modern and Phanerozoic carbonates

During the course of this study, four modern carbonates have been analysed. These samples are all modern ooids and they are from the Bahamas Bank (B08, NPCOScim

and NPCOSunc) and Yucatan (C48). Five oolitic limestones from the Phanerozoic have also been studied in order to compare the chemical signal recorded in the Neoproterozoic carbonates. C17 is a middle Jurassic oolite from the Cotswolds. C171 is a oolitic limestone from the Caswell Bay oolite. C443 is a Cretaceous oolitic limestone from Spain and, finally, C514 is an Ordovician oolitic limestone. These samples were provided by Professor Ian Fairchild from the University of Birmingham.

Chapter 5

Chemical composition of carbonate samples

This chapter presents detailed geochemical information on the carbonates analysed in this study, and aims to assess whether they retain a primary chemistry, and can therefore be used for Cr isotopic studies. Rare earth elements (REEs), carbon and oxygen isotopes and strontium (Sr) isotopes, are used to identify processes that may have altered the primary signal, such as detrital and hydrothermal contamination. Those samples considered to be free of secondary alteration will then be interpreted in terms of their palaeo-depositional environment, and the chemistry of the seawater from which the carbonates precipitated. This chapter will also compare the data obtained in this study with other geochemical data published on the same successions.

5.1 Introduction

5.1.1 Chemical behaviour of the REEs

The REEs consist of 15 elements from lanthanum (La) to lutetium (Lu). As the atomic number increases, an electron is added to the inner 4f electron shell. Efficient shielding of these electrons by outermost orbitals prevents the large changes in chemical activity usually associated with varying electron configuration, leading to similar

chemical behaviour. Most of the REEs have one oxidation state (3+) but Cerium (Ce) and Europium (Eu) can exist in 4+ and 2+ oxidation states, respectively. Yttrium is commonly associated with the REEs, because its in 3+ oxidation state it has an ionic radius close to that of Dy and Ho. For this reason Y usually behaves in the same way as the REEs in the natural environment, and is plotted between Dy and Ho in REE diagrams. Rare earth elements are usually normalised to chondrite or shale concentrations, to produce a so-called "REE pattern" which can be divided into three subgroups: the heavy rare earth elements (HREEs), from gadolinium to lutetium, the light rare earth elements (LREEs), from lanthanum to europium, and the middle rare earth elements (MREEs), from samarium to holmium. Differences in the behaviour of neighbouring rare earth elements can be quantified as follows (e.g. Lawrence et al., 2006; Webb and Kamber, 2000):

$$\frac{La}{La^*} = \frac{La}{(Pr \times (Pr \times Nd)^2} \tag{5.1}$$

$$\frac{Ce}{Ce^*} = \frac{Ce}{(Pr \times (Pr/Nd)} \tag{5.2}$$

$$\frac{Eu}{Eu^*} = \frac{Eu}{(Sm^2 \times Tb)^{1/3}} \tag{5.3}$$

$$\frac{Gd}{Gd^*} = \frac{Gd}{(Tb^2 \times Sm)^{1/3}} \tag{5.4}$$

where La, Pr, Nd, Ce, Eu, Sm, Tb and Gd represent the mass concentration of the element normalised to shale concentration. The so-called "anomalies" are (i) negative, where REE/REE* is less than 1, (ii) positive if REE/REE* is greater than 1 and (iii) non-existent anomaly if REE/REE* is equal to 1. The Ce anomaly can be calculated in different ways (e.g. Lawrence et al., 2006) but in this study it is calculated with respect to Pr and Nd rather than La because some samples have

a positive La anomaly. The uncertainty on the Ce anomaly is about ± 0.05. In contrast to other elements, the Y anomaly is given by the mass ratio of Y (C_Y; where C is the mass concentration) and Ho (C_{Ho}):

$$\frac{Y}{Ho} = \frac{C_Y}{C_{Ho}} \tag{5.5}$$

REE-Y data have been widely obtained for natural samples affected by both high and low temperature processes (e.g. McLennan, 1989; McDonough and Frey, 1989). Over the past 25 years, the behaviour of the REEs in the ocean has been investigated (e.g. Dubinin, 2004), and it is now known that their distribution can be described in terms of their source, and their chemical behaviour (soluble, insoluble, oxidised, reduced, particle-reactive).

5.1.2 Sources of REEs in the ocean

River runoff is the dominant source of REEs to the ocean (Dubinin, 2004). The riverine input consists of both suspended and dissolved REEs. Secondary sources include aeolian dust and hydrothermal inputs from mid-ocean ridge systems. There is still a lot of debate about the source and residence time of the REE in the ocean and other sources such as aeolian dust has been proposed to resolve the variation in the oceanic residence time of Nd (Bertram and Elderfield, 1993). It is important to note that the sources of REE are likely to vary through time. During the Neoproterozoic the hydrothermal inputs from mid-ocean ridge was probably more important than in the modern system. The riverine input is characterised by highly variable REE patterns, which are strongly influenced by the lithological composition in the drainage area (e.g. Dupre et al., 1996; Rachold et al., 1996). The REE pattern in river water is also strongly influenced by the chemical properties of the river water; for example river waters exhibit a negative Ce anomaly if pH is high (Elderfield et al., 1990; Goldstein and Jacobsen, 1988; Sholkovitz, 1993). Marine hydrothermal fluids are enriched in the MREEs relative to the LREEs and HREEs (Fig. 5.1). High-temperature (>350°C) hydrothermal fluids are strongly enriched in Eu relative to Sm or Tb, with $Eu/Eu^* = 8$ to 62 (Fig. 5.1; Bau, 1991, Bau and

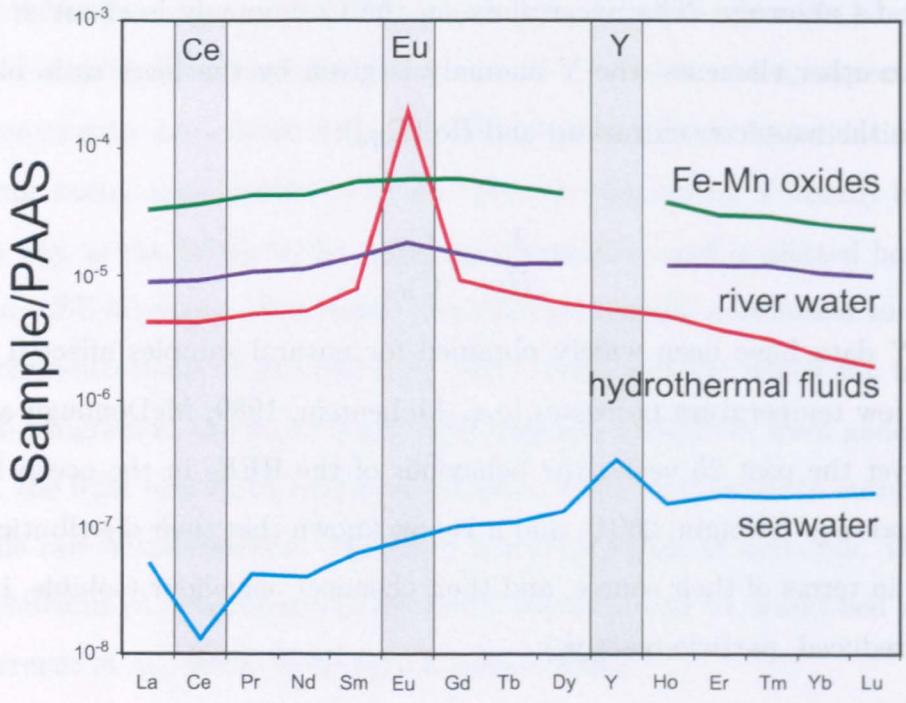

Figure 5.1: Typical REE patterns for modern shallow seawater (blue), high-temperature hydrothermal fluids (red), river water (purple) and Fe-Mn oxides (green). REE concentrations are reported normalised to PAAS (see text for details). Data are from Zhang and Nozaki (1998), James et al. (1995), Gutjahr et al. (2007) and Dupre et al. (1996). The grey bars highlight any Ce, Eu and Y anomalies.

Dulski, 1996; James et al., 1995) because at high temperatures and low pH, Eu is dominantly found in the soluble Eu(II) form.

5.1.3 Behaviour of the REEs in oxic seawater

As described in section 5.1.2, the REE budget of the ocean is strongly influenced by the riverine input. Suspended particles settle out on the continental shelves, so only the dissolved REEs are transferred to the open ocean (Bertram and Elderfield, 1993; Sholkovitz, 1993). Concentrations of the REEs in oxic seawater vary from 2 to 50 pM (Zhang and Nozaki, 1998). Concentrations generally increase with depth, but in detail their distribution is strongly dependent on their ability to form complexes and/or to stay in solution. The REE pattern of modern seawater is characterised by a strong negative Ce anomaly and a positive Y anomaly (Figs. 5.1 and 5.2). The LREEs are generally depleted relative to the MREEs and HREEs. The typical

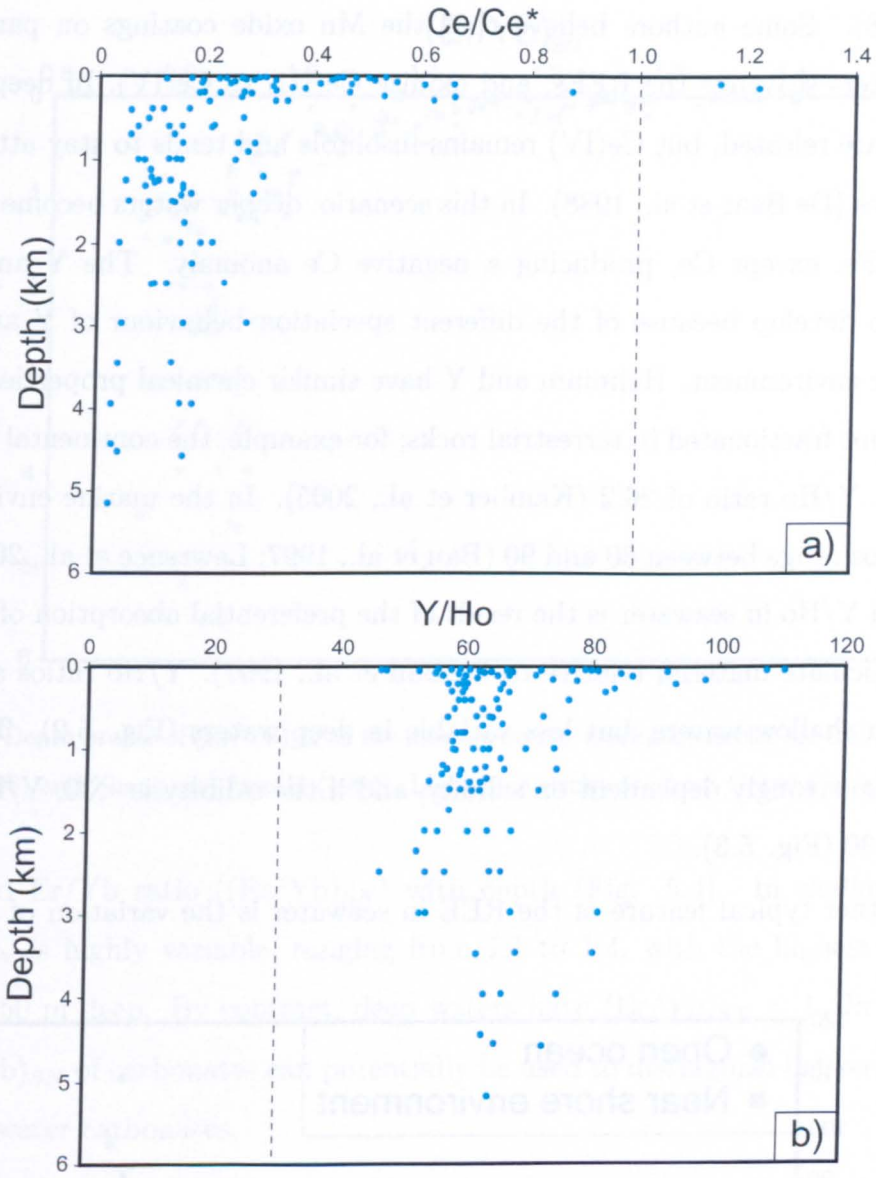

Figure 5.2: Depth profiles of (a) the Ce anomaly and (b) Y/Ho for open ocean seawater. Data are from Zhang and Nozaki (1996) and Zhang and Nozaki (1998). The dashed vertical lines show the continental crust value.

seawater pattern is also characterised by positive La and Gd anomalies (1.17 and 1.14, respectively).

The negative Ce anomaly is believed to develop both in surface seawater and in estuaries. In shallow waters, under oxic conditions, Ce(III) is oxidised to Ce(IV), which is insoluble and is absorbed rapidly onto particles leaving the remaining water depleted in Ce relative to its neighbours (La, Pr and Nd). The particles therefore become enriched in Ce and acquire a positive Ce anomaly ($Ce/Ce^* > 1.1$) (De Baar

et al., 1988). Some authors believe that the Mn oxide coatings on particles in surface waters scavenge the REEs, and oxidise Ce(III) to Ce(IV). In deep waters, the REEs are released, but Ce(IV) remains insoluble and tends to stay attached to the particles (De Baar et al., 1988). In this scenario, deeper waters become enriched in the REEs, except Ce, producing a negative Ce anomaly. The Y anomaly is believed to develop because of the different speciation behaviour of Y and Ho in the marine environment. Holmium and Y have similar chemical properties and are generally not fractionated in terrestrial rocks; for example, the continental crust has a constant Y/Ho ratio of 26.2 (Kamber et al., 2005). In the marine environment, Y/Ho ratios range between 60 and 90 (Bau et al., 1997; Lawrence et al., 2006). The increase in Y/Ho in seawater is the result of the preferential absorption of the REE on to particulate material relative to Y (Bau et al., 1997). Y/Ho ratios are highly variable in shallow waters, but less variable in deep waters (Fig. 5.2). The Y/Ho ratio is also strongly dependent on salinity, and if the salinity is <30, Y/Ho can be as low as 30 (Fig. 5.3).

The other typical feature of the REE in seawater is the variation of the shale-

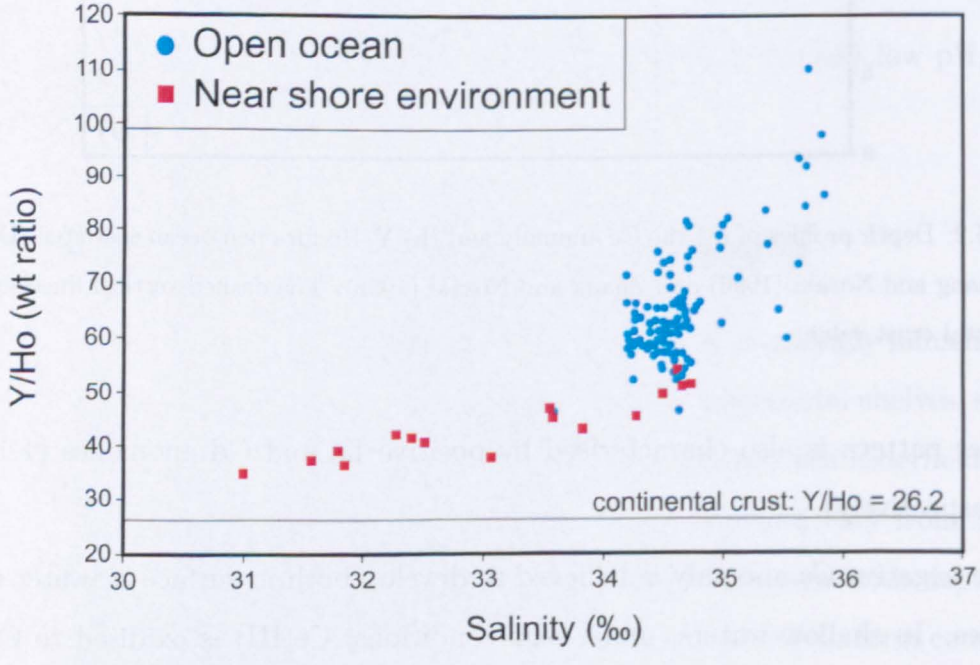

Figure 5.3: Y/Ho ratio of seawater versus salinity. Blue circles are open ocean seawater (Zhang and Nozaki, 1996; Zhang and Nozaki, 1998). Red squares are from near shore environments (Nozaki and Zhang, 1995).

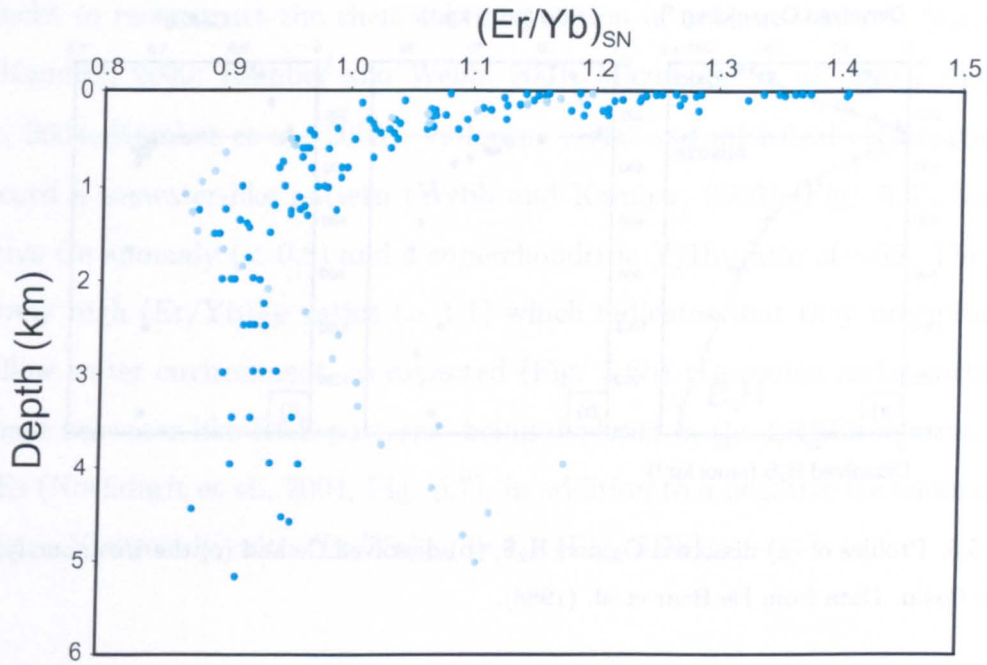

Figure 5.4: Depth profile of $(Er/Yb)_{SN}$ in the modern ocean. Dark blue circles are from Zhang and Nozaki (1996) and Zhang and Nozaki (1998). Light blue circles are from German et al. (1991a).

normalised Er/Yb ratio ($(Er/Yb)_{SN}$) with depth (Fig. 5.4). In shallow waters, $(Er/Yb)_{SN}$ is highly variable, ranging from 1.1 to 1.4, with the highest values in waters < 50 m deep. By contrast, deep waters have $(Er/Yb)_{SN} < 1$. In this way, the $(Er/Yb)_{SN}$ of carbonates can potentially be used to distinguish between shallow and deep water carbonates.

5.1.4 Behaviour of the REEs in anoxic seawater

Some parts of the ocean have restricted circulation and may have permanently anoxic intermediate and deep waters. This is the case in the Black Sea, the Cariaco Basin and the Saanich Inlet, for example (De Baar et al., 1988; German et al., 1991b; Bau et al., 1997). Seawater profiles of the REEs in these regimes are very different compared to a fully oxic regime (Fig. 5.5). Shallow waters are characterised by low Ce concentrations and negative Ce anomalies, and particles are characterised by high Ce concentrations and positive Ce anomalies. At the oxic/anoxic (or euxinic) boundary, the dissolved Ce concentration increases and the negative Ce anomaly disappears, leaving the seawater with a slight positive Ce anomaly (De Baar et al.,

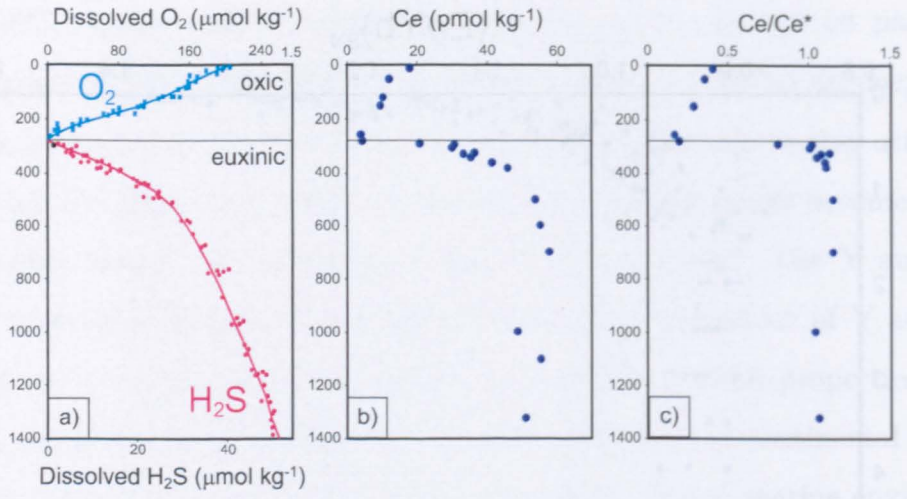

Figure 5.5: Profiles of (a) dissolved O_2 and H_2S, (b) dissolved Ce and (c) the Ce anomaly, in the Cariaco Basin. Data from De Baar et al. (1988).

1988). These features are associated with Mn cycling (De Baar et al., 1988).

5.1.5 REEs in the carbonate record

Carbonate rocks are believed to record the REE pattern of the seawater from which they precipitated because the REEs are not significantly fractionated during precipitation or diagenesis (e.g. Banner et al., 1988). Thus, the presence or absence of a Ce anomaly in carbonates has been used to reconstruct redox conditions in ancient seawater (Webb and Kamber, 2000; Kamber and Webb, 2001), and the Y/Ho ratio has been used to determine whether the carbonate was deposited in a distal versus near-shore environment (e.g. Frimmel, 2009; Frimmel, 2010). In this case, it is important to note that the partition coefficient (D_Y/D_{Ho}) between the Y/Ho ratio of a solution and a carbonate is 0.6-0.77 (Qu et al., 2009), i.e. the Y/Ho ratio recorded in carbonates is fractionated relative to seawater. The different behavior of Y and Ho can be explained by the difference in the complexing of Y by carbonates relative to the REEs (Liu and Byrne, 1998). The REE pattern of carbonates is thought to be largely controlled by the source of the REEs (e.g. Frimmel, 2009). For example, carbonates collected from close to Hawaii have an unusual bell-shaped REE pattern that is close to the REE pattern of the rocks located in the drainage area (Strekopytov and Dubinin, 1996). Several studies have attempted to use carbon-

ate rocks to reconstruct the chemical composition of ancient seawater (e.g. Webb and Kamber, 2000; Kamber and Webb, 2001; Mazumdar et al., 2003; Nothdurft et al., 2004; Kamber et al., 2005). Holocene reefal and microbial carbonates seem to record a seawater-like pattern (Webb and Kamber, 2000) (Fig. 5.6), having a negative Ce anomaly (< 0.8) and a superchondritic Y/Ho ratio of $\sim$50. They have relatively high $(Er/Yb)_{SN}$ ratios (> 1.1) which indicates that they precipitated in a shallow water environment, as expected (Fig. 5.6b). Devonian reefal carbonates also have seawater-like REE patterns, being depleted in the LREEs relative to the HREEs (Nothdurft et al., 2004; Fig. 5.7), in addition to a negative Ce anomaly and a positive Y anomaly, with $(Er/Yb)_{SN} = 1.1$ (Fig. 5.7b).

5.2 Methods

In this study, the carbonates were analysed for major and trace element concentrations and C and O isotopes. Selected samples were also analysed for radiogenic Sr isotopic compositions. The analytical methods are fully described in the Appendices, and only a brief description of the dissolution method is given here. Major and trace elements concentrations were determined on a weak acid (0.5M HCl) leach of the carbonates, to avoid the dissolution of any contaminant detrital material. Measurements of trace element concentrations were made at the Open University by ICP-MS (Agilent 7500), using 6 synthetic standard solutions to produce a calibration line.

C and O isotopes were determined using standard techniques at the Open University, and the carbon and oxygen isotopic compositions are reported relative to "Vienna Pee Dee Belemnite" (VPDB) using the standard notations of $\delta^{13}C$ and $\delta^{18}O$.

Sr isotopes analyses were performed by TIMS (ThermoFisher Scientific Triton) at the Open University. The chemical separation of Sr from the matrix was accomplished using Sr spec resin (Deniel and Pin, 2001).

The external reproducibility of the REE concentrations is $\sim$3 %, based on replicate analysis of the dolomite standard reference material JDo-1. After weak acid leaching of the carbonate samples, a small amount of residue always remained, indicative of a small detrital component. The residue was weighed to calculate the

total mass of material dissolved. As the amount of residue is small, the weighting error is relatively large (~5 %) and contributes to the uncertainty on the absolute concentrations of the samples. Nevertheless, it does not contribute any additional uncertainty to the REE patterns or element/element ratios.

REE-Y concentrations are normalised to the Post Archaean Australian Shale (PAAS) values of Taylor and McLennan (1985). The REE-Y patterns include all of the lanthanides from La to Lu, and Y is located between Dy and Ho. REE anomalies are also normalised to shale (SN), and have a precision of ~5 %. The relative

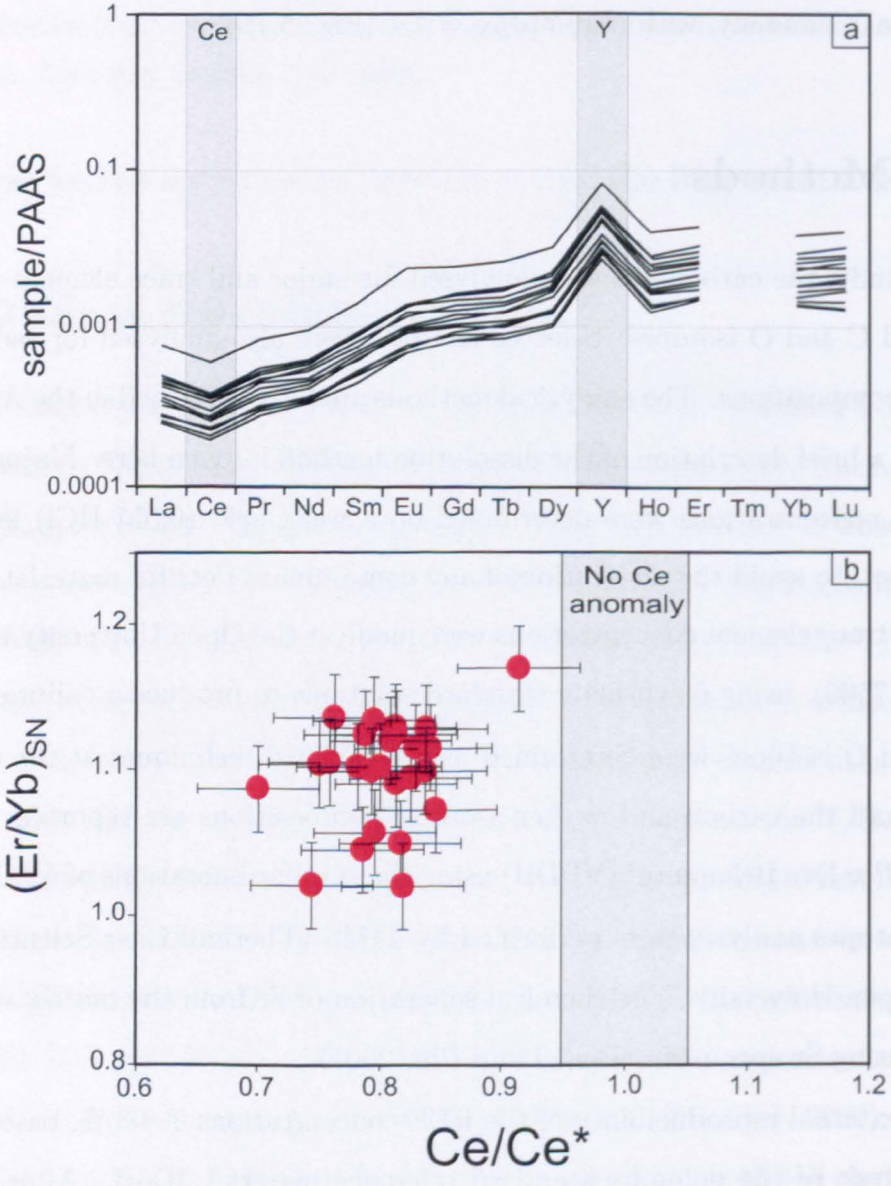

Figure 5.6: (a) Shale normalised REE-Y patterns and (b) $(Er/Yb)_{SN}$ versus Ce/Ce* for Holocene reefal microbialites. Data are from Webb and Kamber (2000).

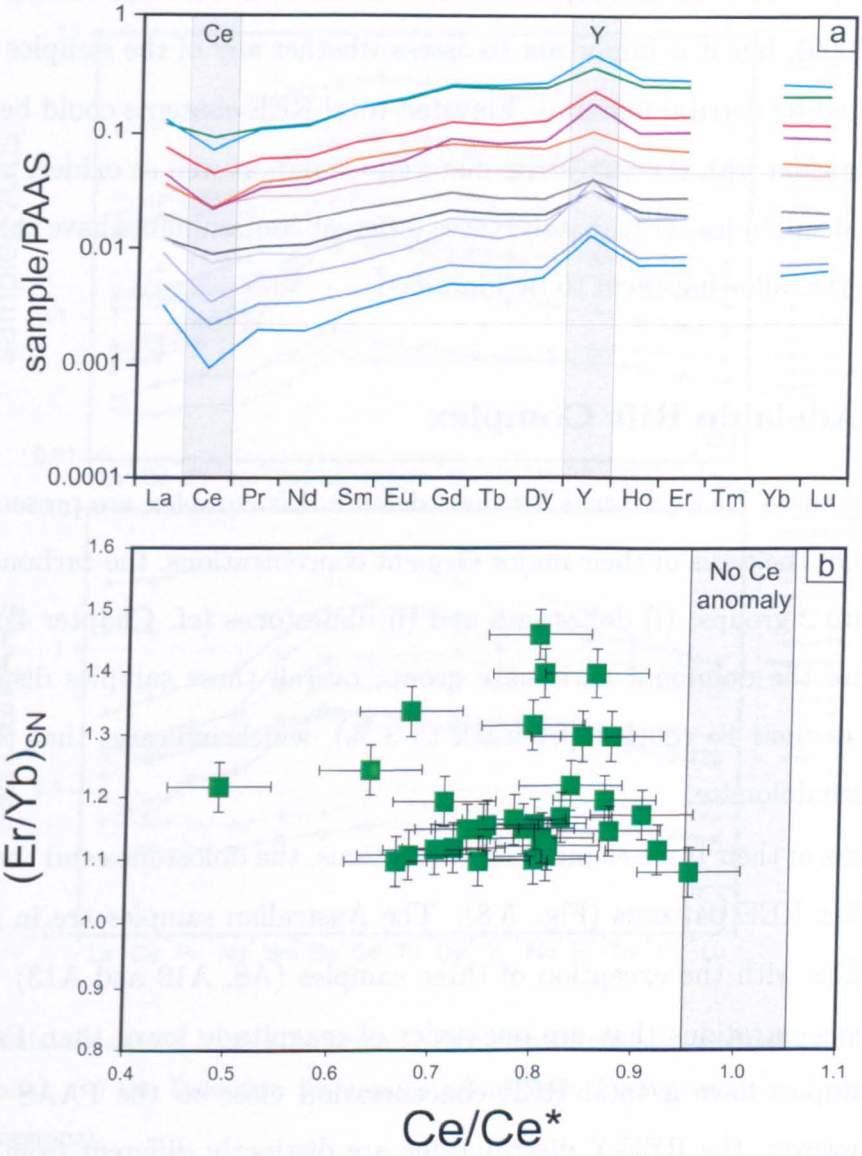

Figure 5.7: (a) Shale normalised REE-Y patterns and (b) $(Er/Yb)_{SN}$ versus Ce/Ce* for late Devonian reefal carbonates. Data are from Nothdurft et al. (2004).

enrichment or depletion of the MREEs to the HREEs is given by the $(Tb/Yb)_{SN}$ ratio. The $(Pr/Sm)_{SN}$ ratio is used to compare the LREEs with the MREEs and the $(Pr/Yb)_{SN}$ ratio is used to compare the LREEs with the HREEs.

5.3 Results

Trace element concentrations are reported in Appendix C. Overall, the REE concentrations of the carbonates vary by two orders of magnitude. This is in line with

other studies of carbonates (e.g. Webb and Kamber, 2000, Nothdurft et al., 2004, Frimmel, 2009), but it is important to assess whether any of the samples have been contaminated by detrital material. Elevated total REE contents could be the result of contamination with the terrestrial material (shale), as well as oxides, phosphates, silicates and sulphides. Fortunately, these different contaminants have characteristic REE patterns, allowing them to be identified.

5.3.1 Adelaide Rift Complex

Shale-normalised REE patterns for the Adelaide Rift complex are presented in Figure 5.8a. On the basis of their major element concentrations, the carbonates can be divided into 2 groups: (i) dolostones and (ii) limestones (cf. Chapter 4). Dolomitic samples are the dominant carbonate group; overall these samples display a large variation in their Fe content (from 0.2 to 3 %), which indicates that they are not simply pure dolomite.

In terms of their trace element concentrations, the dolostones and the limestones have similar REE patterns (Fig. 5.8). The Australian samples are in general rich in the REEs with the exception of three samples (A8, A10 and A13), which have REE-Y concentrations that are one order of magnitude lower than PAAS values. A few samples have a total REE concentration close to the PAAS values (Fig. 5.8a). However, the REE-Y distributions are distinctly different from PAAS, and they are very variable. Overall, the Australian samples display a marked MREE enrichment ($(Tb/Yb)_{SN}$ = 1.2 to 2.6) associated with a strong depletion in the LREEs ($(Pr/Sm)_{SN}$ = 0.19 to 0.82). Some samples have a positive Eu anomaly (Eu/Eu^{*} = 2.43) that is interpreted to be a primary signal. Moreover, the Australian samples have a small Y anomaly (Y/Ho = 23 to 29).

5.3.2 Dalradian Supergroup

The carbonate samples from Scotland are divided into three groups: (i) the Islay Formation, (ii) the Bonahaven Formation and (iii) the Tayvallich Limestone (Chapter 3).

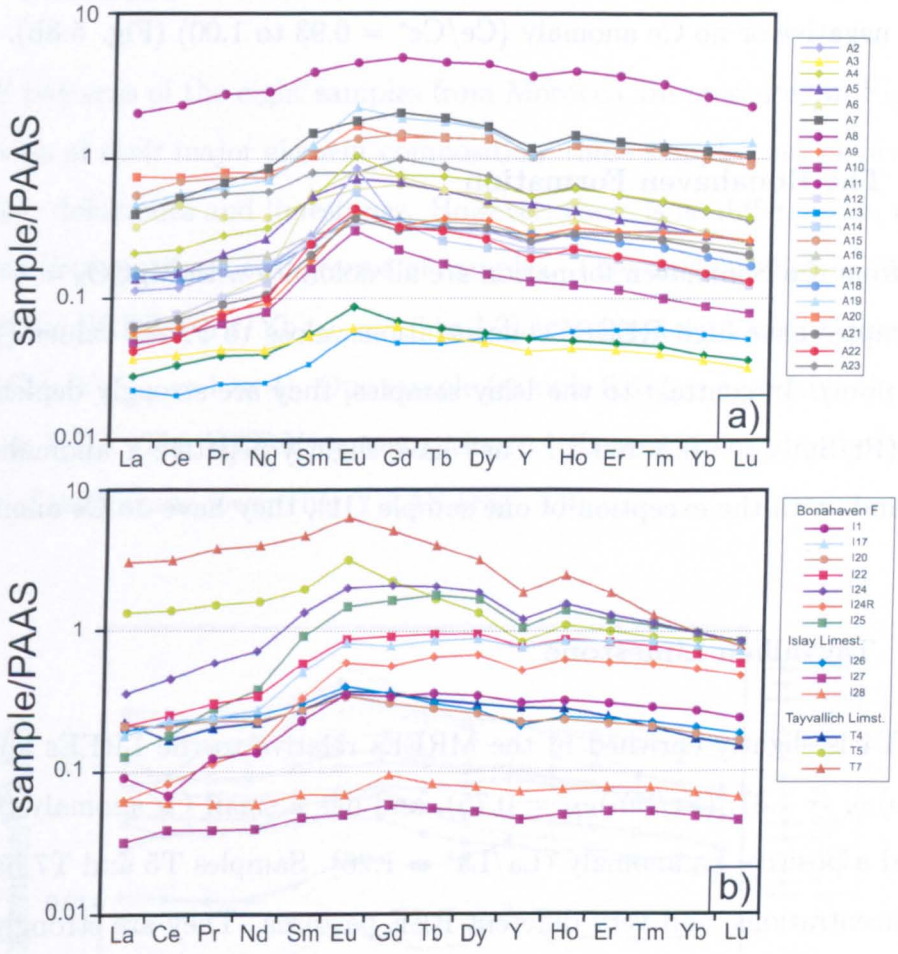

Figure 5.8: Shale normalised REE-Y patterns of carbonates from (a) the Adelaide rift complex (South Australia), (b) the Dalradian Supergroup (Bonahaven Formation, Islay Limestone and Tayvallich Limestone).

5.3.2.1 Islay limestone

All of the Islay Limestone samples are limestone with $CaCO_3$ concentrations of between 98 and 100 %. Two of these samples are oolitic limestones (I27 and I28) and the third sample is an impure limestone (I26) (Chapter 4). I27 and I28 have a relatively flat REE-Y pattern, with a slight depletion in the LREEs ($(Pr/Sm)_{SN}$ = 0.8). They also have a positive Gd anomaly (Gd/Gd^* = 1.2). Their total REE-Y concentration is one order of magnitude lower than PAAS (Fig. 5.8b). I26 has a slightly higher total REE-Y concentration, and a slight LREE depletion associated with a small MREE enrichment ($(Pr/Sm)_{SN}$ = 0.79 and $(Tb/Yb)_{SN}$ = 1.48). The

Islay limestone samples do not have a positive Y anomaly (Y/Ho = 23 to 26), and a slightly negative or no Ce anomaly ($Ce/Ce^* = 0.93$ to 1.00) (Fig. 5.8b).

5.3.2.2 The Bonahaven Formation

Samples from the Bonahaven formation are all dolomite with $MgCO_3 = \sim$ 30-42 %. These samples have high REE-Y concentrations, close to PAAS values ($\sum$REE = 22 to 54 ppm). In contrast to the Islay samples, they are strongly depleted in the LREEs ($(Pr/Sm)_{SN} = 0.3$ to 0.5). They have slightly negative Y anomalies (Y/Ho = ~23) and, with the exception of one sample (I1), they have no Ce anomaly.

5.3.2.3 Tayvallich Limestone

Sample T4 is slightly enriched in the MREEs relative to the LREEs and HREEs ($(Tb/Yb)_{SN} = 1.87$; $(Pr/Sm)_{SN} = 0.75$), and has a small Ce anomaly ($Ce/Ce^* = 0.88$) and a positive La anomaly ($La/La^* = 1.26$). Samples T5 and T7 have higher REE concentrations, and very different REE patterns. They are strongly enriched in the MREEs, and they have positive Eu anomalies and negative Y anomalies (Fig. 5.8).

5.3.3 Eleonore Bay Supergroup

REE patterns for the three samples from Greenland are shown in Figure 5.9a. All of these samples are limestones, and they have relatively flat REE patterns with no Ce anomaly ($Ce/Ce^* = \sim 1$), and only a small Y (Y/Ho = 27 to 33) and Gd anomalies ($Gd/Gd^* = 1.1$ to 1.2). They are slightly depleted in the LREEs relative to the MREEs and HREEs ($(Pr/Sm)_{SN} = 0.6$ to 0.8 and $(Pr/Yb)_{SN} = 0.3$ to 1.0). The total REE concentrations in these samples are one to two orders of magnitude lower than PAAS. Sample PG128 has the lowest REE concentration ($\sum$REE = 2.3 ppm) as well as a small positive Y anomaly (Y/Ho = 33) and a small positive Ce anomaly ($Ce/Ce^* = 1.08$).

5.3.4 Morocco

The REE patterns of the eight samples from Morocco are presented in Figure 5.9a. On the basis of their major element composition, these samples can be divided into two groups: dolostones and limestones. However, there is no difference in the REE-Y patterns between these two groups of samples. They are enriched in the LREEs relative to the HREEs ($(Pr/Yb)_{SN} = 1.3$ to 3.2) associated with an enrichment of the MREEs ($(Tb/Yb)_{SN} = 1$ to 4). One sample (sample 6.6) has a positive Eu anomaly ($Eu/Eu^* = 1.71$). The REE-Y concentrations of these samples are approximately one order of magnitude lower than PAAS (Fig. 5.9).

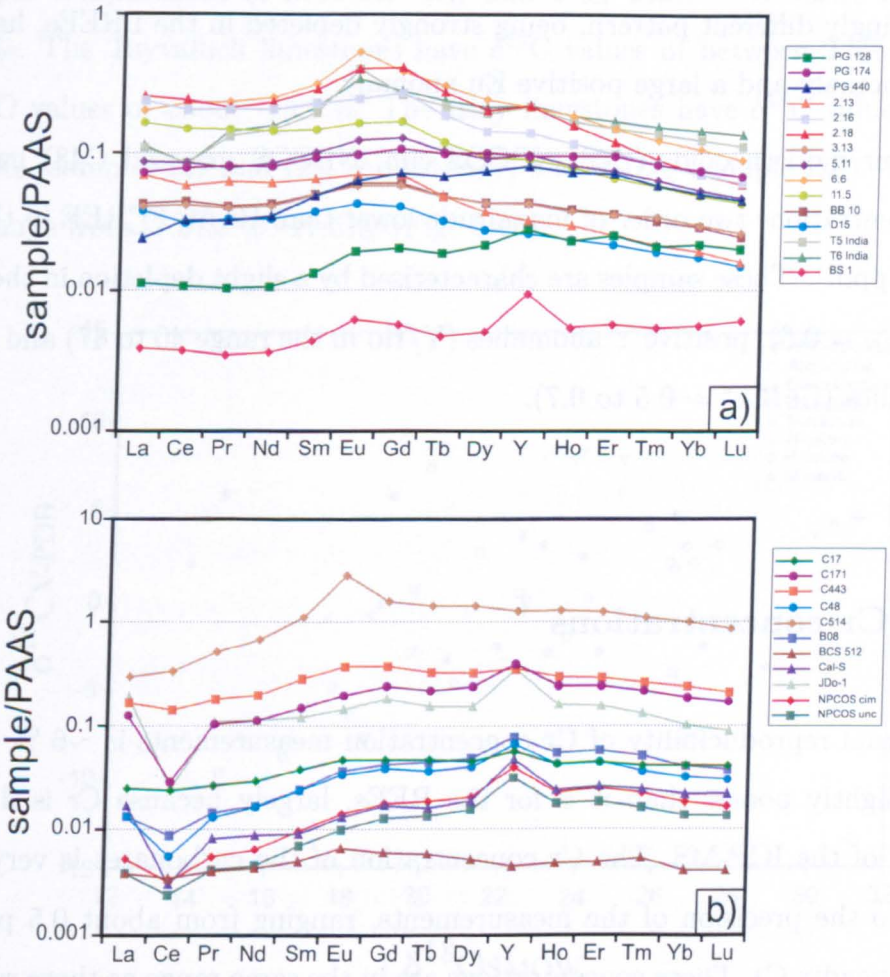

Figure 5.9: Shale normalised REE-Y patterns of carbonates from (a) Greenland (PG128, PG174 and PG440), Morocco, India (T5 and T6) and California (BS1), and (b) the modern-day (B08, NPCOS cim, NPCOS unc, C48) and the Phanerozoic.

5.3.5 Modern and Phanerozoic samples

The REE patterns of the eight samples from the Phanerozoic are shown in Figure 5.9b. The samples consist of both dolostones (JDo-1 and BCS CRM 512) and limestones (Cal-S, BCS CRM 513 C514, C443, C17 and C171). They have a large range in total REE concentrations, from two orders of magnitude less than PAAS to concentrations close to PAAS. However, none of the samples have PAAS REE patterns. Rather, they tend to be depleted in the LREEs relative to the MREEs and HREEs ($(Pr/Sm)_{SN}$ = 0.7 to 0.9, $(Pr/Yb)_{SN}$ = 0.5 to 0.9), they have strong positive Y (Y/Ho = 32 to 60) and negative Ce anomalies (Ce/Ce^* = 0.2 to 0.7), and they have small positive La and Gd anomalies. The exception is sample C514, which has a strikingly different pattern, being strongly depleted in the LREEs, having no Y or Ce anomaly and a large positive Eu anomaly.

The four modern ooids (B08, NPCOS cim, NPCOS unc and C48) have total REE concentrations two order of magnitude lower than PAAS ($\sum$REE in the range of 1 to 2.5 ppm). These samples are characterised by a slight depletion in the LREEs ($(Pr/Sm)_{SN}$ = 0.6), positive Y anomalies (Y/Ho in the range 40 to 47) and negative Ce anomalies (Ce/Ce^* = 0.5 to 0.7).

5.3.6 Cr concentrations

The external reproducibility of Cr concentration measurements is ~6 % (2 r.s.d.). This is slightly poorer than it is for the REEs, largely because Cr is difficult to wash out of the ICP-MS. The Cr concentration of the carbonates is very variable relative to the precision of the measurements, ranging from about 0.5 ppm to 20 ppm (Appendix C). These concentrations are in the same range as those reported in other studies (e.g. Aizawa, 2008). The Cr concentration of the carbonates is closely correlated with Th (R^2 = 0.81). However, there is no correlation between Cr and C and O isotopes.

5.3.7 C and O isotopes

The carbonates have very variable $\delta^{13}C$ and $\delta^{18}O$, as shown in Figure 5.10. Dolomitic samples from Australia have $\delta^{13}C$ values that range from -10‰ to +9‰, and $\delta^{18}O$ values that range from -12 to -2‰ (Fig. 5.10). The calcite samples from Australia have $\delta^{13}C$ values that range from -4‰ to +6‰ and $\delta^{18}O$ values that range from -15‰ to -4‰. There is no correlation between $\delta^{13}C$ and $\delta^{18}O$ in these samples (Fig. 5.10).

The oolitic limestones from the Eleonore Bay Supergroup have $\delta^{13}C$ values that range from +7.9 to +8.3‰, and $\delta^{18}O$ values that range from -6.9 to -5.7‰ (Fig. 5.10). The dolostones from the Bonahaven formation (Dalradian Supergroup) have C isotopic compositions of between -4‰ and 0‰, while $\delta^{18}O$ varies from -12‰ and -8‰. The Tayvallich limestones have $\delta^{13}C$ values of between 2.5‰ and 6‰, and $\delta^{18}O$ values of about -15.6‰. The Islay limestones have $\delta^{13}C$ values of 3.6‰ and 3.1‰ (samples I27 and I28, respectively) and -0.5‰ (sample I26). Their $\delta^{18}O$ values range from -7.6‰ to -11.6‰ (Fig. 5.10).

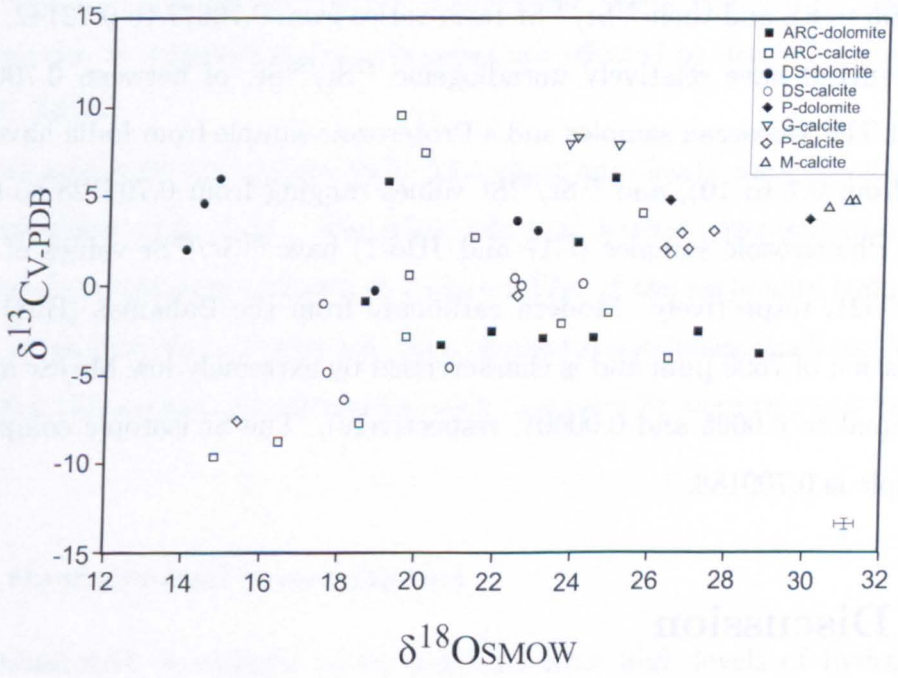

Figure 5.10: Carbon isotopic composition versus oxygen isotopic composition of the carbonate samples. ARC: Adelaide Rift Complex, DS: Dalradian Supergroup, G: Greenland, P: Phanerozoic and M: Modern. Error bars are smaller than the size of the data point.

The two dolomitic samples from the Phanerozoic have $\delta^{13}C$ values of 4.75‰ and 3.6‰, and $\delta^{18}O$ values of -4.3‰ and -1.1‰ respectively (Fig. 5.10).The three calcite standards JLs-1, Cal-s and BCS-CRM 513, have $\delta^{13}C$ = 2.0, 2.9, -0.6‰ and $\delta^{18}O$ = -4.1, -4.1 and -7.6‰, respectively (Fig. 5.10). The Phanerozoic samples, C17, C171, C443 and C514, have $\delta^{13}C$ values of 1.8, 3.0, 2.0 and -7.67‰ and $\delta^{18}O$ values of -4.3, -3.3, -3.9 and -15.1‰, respectively (Fig. 5.10). Finally, the modern ooids have $\delta^{13}C$ values close to + 4.5‰ and $\delta^{18}O$ values of between -0.4 and 0.3‰ (Fig. 5.10).

5.3.8 Mn/Sr and Sr isotopes

Sr isotope data and mass Mn/Sr ratios are presented in Appendix C. Overall, most of the carbonates have low Rb/Sr ratios (0.00004 to 0.006) and Mn/Sr ratios are usually less than 1.5 (although they can be as high as 54).

The four samples from South Australia have relatively high Mn/Sr (from 0.3 to 54), and relatively radiogenic $^{87}Sr/^{86}Sr$ ratios of between 0.70896 and 0.71868. The four samples from the Dalradian Supergroup have a wide range in Mn/Sr ratios (from 0.006 to 6), and their $^{87}Sr/^{86}Sr$ ratio varies from 0.70677 to 0.72142. Samples from Greenland have relatively unradiogenic $^{87}Sr/^{86}Sr$, of between 0.706937 and 0.7076941.The Moroccan samples and a Proterozoic sample from India have variable Mn/Sr (from 0.7 to 10), and $^{87}Sr/^{86}Sr$ values ranging from 0.707128 to 0.710643. The two Phanerozoic samples (C17 and JDo-1) have $^{87}Sr/^{86}Sr$ values of 0.707588 and 0.707521, respectively. Modern carbonate from the Bahamas (B08) has a Sr concentration of 7600 ppm and is characterised by extremely low Mn/Sr and Rb/Sr ratios (equal to 0.0005 and 0.00001, respectively). The Sr isotopic composition of this sample is 0.709188.

5.4 Discussion

As described above, modern seawater REE patterns are characterised by depletion in the LREEs relative to the MREEs and HREEs and by the presence of negative Ce anomaly and a positive Y anomaly (Fig. 5.1; e.g. Zhang and Nozaki, 1998). The

carbonates analysed in this and other studies (e.g. Frimmel, 2009) do not perfectly conform to the modern seawater pattern. This may be because carbonate REE patterns can be affected by contamination with detrital material and/or hydrothermal fluids, or by post-depositional processes, such as diagenesis, which overprint their original seawater signal (Frimmel, 2009). In order to interpret the REE patterns recorded in the Neoproterozoic samples, the potential influence of such processes needs to be critically assessed.

5.4.1 Contamination and post depositional alteration

5.4.1.1 Detrital contamination

The total REE concentration of the carbonate samples ranges from 2 ppm to 150 ppm. In order to assess whether the carbonates are affected by detrital contaminants, concentrations of Zr, Th and Al were determined. These elements are strongly enriched in detrital phases such as those that compose PAAS (Taylor and McLennan, 1985), whereas their concentration in seawater is very low (e.g. McKelvey and Orians, 1998). A positive correlation between the REEs and Zr, Th and Al concentrations can be expected if the carbonates are affected by detrital contamination (Frimmel, 2009).

The samples with the highest REE concentrations clearly have elevated Zr and Th concentrations (Fig. 5.11). The likely effect of detrital contamination on REE pattern of the carbonates is shown in Figure 5.12a. If the carbonate comprises >2 % PAAS (equivalent to > 4 ppm Zr), then elemental anomalies (such as Ce and Y) are lost. For this reason, all carbonates with > 4 ppm Zr were rejected for further analysis.

5.4.1.2 Hydrothermal contamination

The Neoproterozoic is thought to be a period with high levels of hydrothermal activity due to the breaking up of Rhodinia and the opening of ocean basins (Powell et al., 1994). Positive Eu anomalies are usually interpreted to reflect contamination by hydrothermal fluids; the effect of contamination by hydrothermal fluids on the

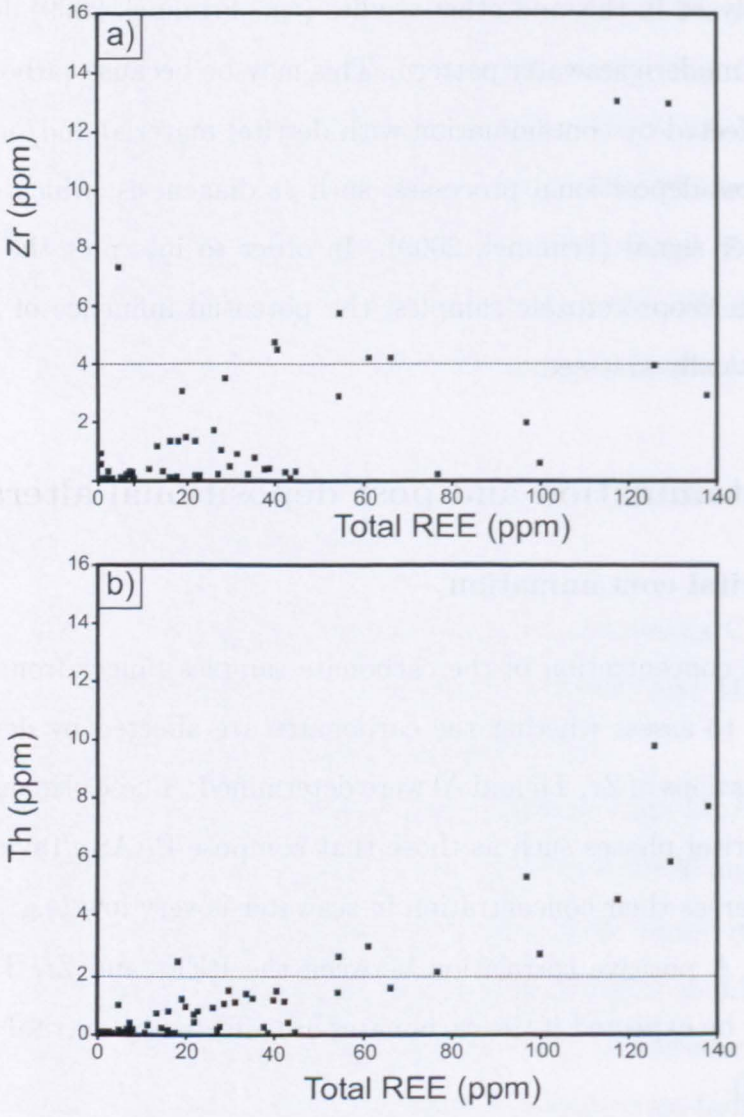

Figure 5.11: Total REE concentration versus (a) Zr and (b) Th for all carbonates analysed in this study. Error bars are smaller than the size of the data point. Dotted line indicates the cut-off between "contaminated" and "uncontaminated" samples.

REE pattern is shown in Figure 5.12b. In this case, the hydrothermal fluid is assumed to have a composition equivalent to the anomalous Phanerozoic limestone sample C514. Figure 5.12b shows that carbonates rapidly acquire a positive Eu anomaly if it is affected by hydrothermal contamination. However, care needs to be taken because the Eu anomaly is strongly dependent on the redox state of Eu (Eu^{3+} or Eu^{2+}), which is strongly dependent on temperature (Bau, 1991). This means that diffuse hydrothermal fluids with temperatures of less than 100°C may not have a positive Eu anomaly (Bau, 1991). Moreover, it has been argued that

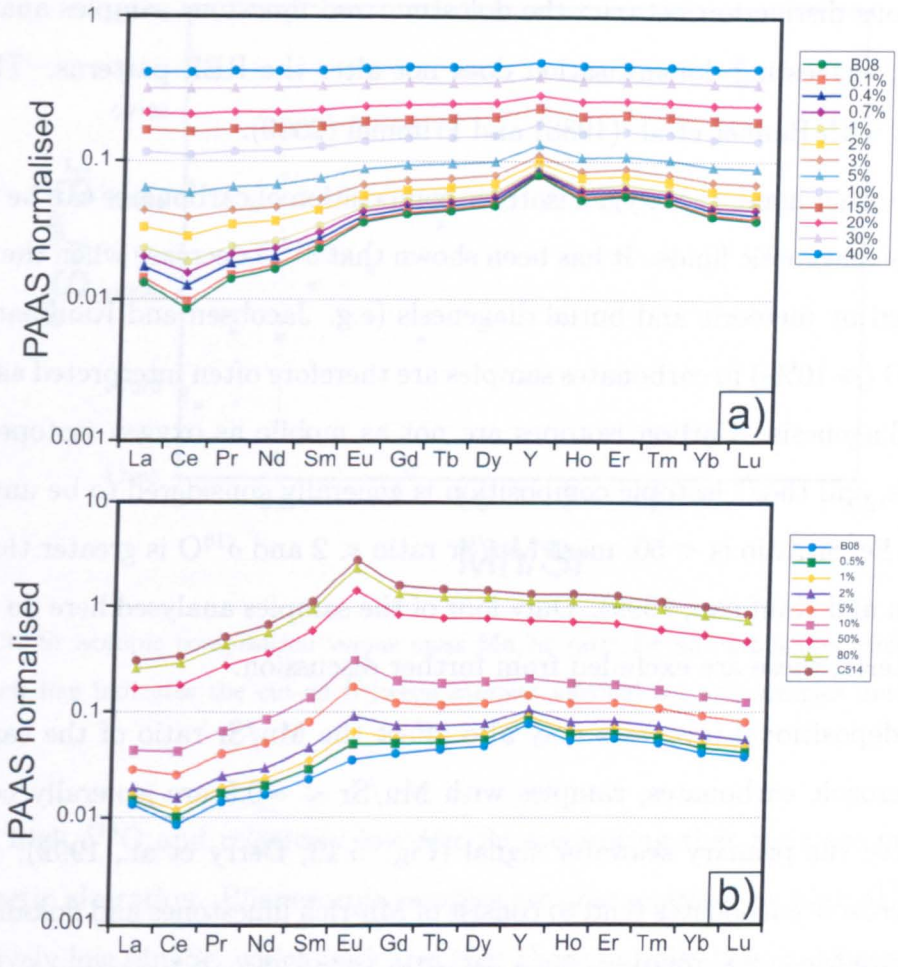

Figure 5.12: Modelled effects on shale-normalised REE patterns of (a) contamination of sample B08 by a shale (PAAS); (b) contamination of sample B08 by a hydrothermal fluid (sample C514).

hydrothermal fluids are not a source of REE in the ocean but rather a sink and that a lack of Eu anomaly in seawater does not necessarily imply no contribution from hydrothermal fluids (Olivarez and Owen, 1991). However, six samples analysed in this study have positive Eu anomalies, and there is no correlation between the Eu anomaly and total REE or Zr concentrations. These six samples were not subject to further analysis.

5.4.1.3 Post-depositional alteration: dolomitisation and diagenesis

Diagenesis and dolomitisation affect the chemical signature of carbonates in different ways. In general, REE concentrations and REE patterns are not strongly affected by diagenesis or dolomitisation (e.g. Banner et al., 1988). In this connection, there

is no obvious distinction between the dolostone and limestone samples analysed in this study, suggesting dolomitisation does not alter the REE patterns. This is in agreement with Banner et al. (1988) and Frimmel (2009).

On the other hand, the oxygen isotopic composition of carbonates can be strongly affected by diagenetic fluids. It has been shown that $\delta^{18}O$ decrease when the samples are affected by meteoric and burial diagenesis (e.g. Jacobsen and Kaufman, 1999). Light $\delta^{18}O$ (<-10‰) in carbonates samples are therefore often interpreted as affected by such diagenesis. Carbon isotopes are not as mobile as oxygen isotopes during diagenesis, and the C isotopic composition is generally considered to be unaltered if the mass Fe/Sr ratio is < 50, mass Mn/Sr ratio < 2 and $\delta^{18}O$ is greater than -10‰ (Jacobsen and Kaufman, 1999). Only four of the samples analysed here do not meet these criteria; these are excluded from further discussion.

Post-depositional processes may also affect the Mn/Sr ratio of the carbonates. In Phanerozoic carbonates, samples with Mn/Sr < ~0.5 are generally considered to preserve the primary seawater signal (Fig. 5.13; Derry et al., 1992). However, Neoproterozoic carbonates tend to consist of Mn-rich limestones and dolomites (Herrington and Fairchild, 1989), so a cut-off value of Mn/Sr = 0.5 may not be appropriate. The carbonates analysed in this study have highly variable Mn/Sr, which may indicate that they have been affected by diagenesis and/or dolomitisation processes. However, there is no obvious relationship between Mn/Sr and O isotopes. Samples from Greenland and Islay have highest Sr (2000 ppm) and low Mn/Sr (0.006-0.06), and heavy $\delta^{13}C$ and $\delta^{18}O$ values, and are therefore most likely to preserve a primary seawater signature for Sr isotopes. Similarly, the Phanerozoic and modern samples have Mn/Sr <0.5, and can be considered to record primary Sr isotope signals.

In summary, Australian carbonates have a large range $\delta^{18}O$ values, and it seems likely that a small number have been strongly influenced by diagenesis and/or dolomitisation. Samples from Greenland also have variable $\delta^{18}O$, in line with other data published for this succession (Prave et al., 2009). However, samples I27 and I28 have $\delta^{18}O$ and $\delta^{13}C$ values that are not consistent with alteration by diagenetic fluids. These two samples also have low Mn/Sr, indicating that they should preserve a primary Sr isotope signature. The Greenland samples analysed have $\delta^{13}C$

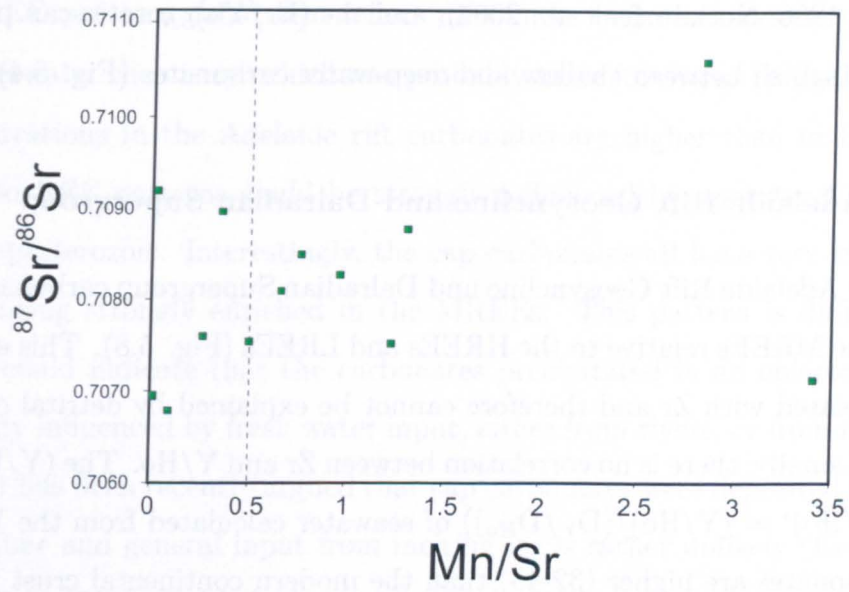

Figure 5.13: Sr isotopic composition versus mass Mn/Sr ratio for all carbonates with Mn/Sr < 3.5. Dashed line indicates the cut-off between samples affected by, and samples unaffected by, diagenesis.

= +8‰, high $\delta^{18}O$ and relatively low Mn/Sr, suggesting that they are unaffected by diagenetic alteration. Phanerozoic samples are characterised by high $\delta^{18}O$ values and relatively low Mn/Sr, which indicates that these samples have not been affected by diagenetic fluids. The modern samples have relatively high $\delta^{13}C$ (up to +4‰), and $\delta^{18}O$ values that accord with those of modern seawater (Kasting et al., 2006). In general, the ooids and oolitic limestones seem to be less affected by secondary alteration processes, and are likely to be the best samples to assess the chemical evolution of shallow seawater.

5.4.2 Environmental setting

Although some of the carbonate samples are clearly affected by contamination or secondary alteration processes (and are ruled out of further discussion), most of the remaining samples nevertheless have REE patterns that differ from that of modern seawater. As discussed in Section 1.3, REE patterns in carbonates may also record information about the environmental setting of carbonate precipitation, in terms of proximity to freshwater influences and redox conditions. For example, the Y/Ho ratio can be used to differentiate between marine and non-marine precipitates (Bau

and Dulski, 1996; Nothdurft et al., 2004), and the $(Er/Yb)_{SN}$ ratio can potentially help to distinguish between shallow and deep-water carbonates (Fig. 5.4).

5.4.2.1 Adelaide Rift Geosyncline and Dalradian Supergroup

Most of the Adelaide Rift Geosyncline and Dalradian Supergroup carbonates are enriched in the MREEs relative to the HREEs and LREEs (Fig. 5.8). This enrichment is not correlated with Zr and therefore cannot be explained by detrital contamination. Additionally, there is no correlation between Zr and Y/Ho. The $(Y/Ho)^*$ ratios (where $(Y/Ho)^* = (Y/Ho)/(D_Y/D_{Ho})$) of seawater calculated from the Y/Ho ratio of the carbonates are higher (32-43) than the modern continental crust value (Fig. 5.14). However, these values are still lower than the Y/Ho ratio of modern seawater (60-90, Lawrence et al., 2006). These low values could be explained by deposition in a near shore environment (i.e. with a salinity <30). Moreover, these samples have $(Er/Yb)_{SN} > 1.1$, which suggests that they have been deposited in shallow water (Fig. 5.4).

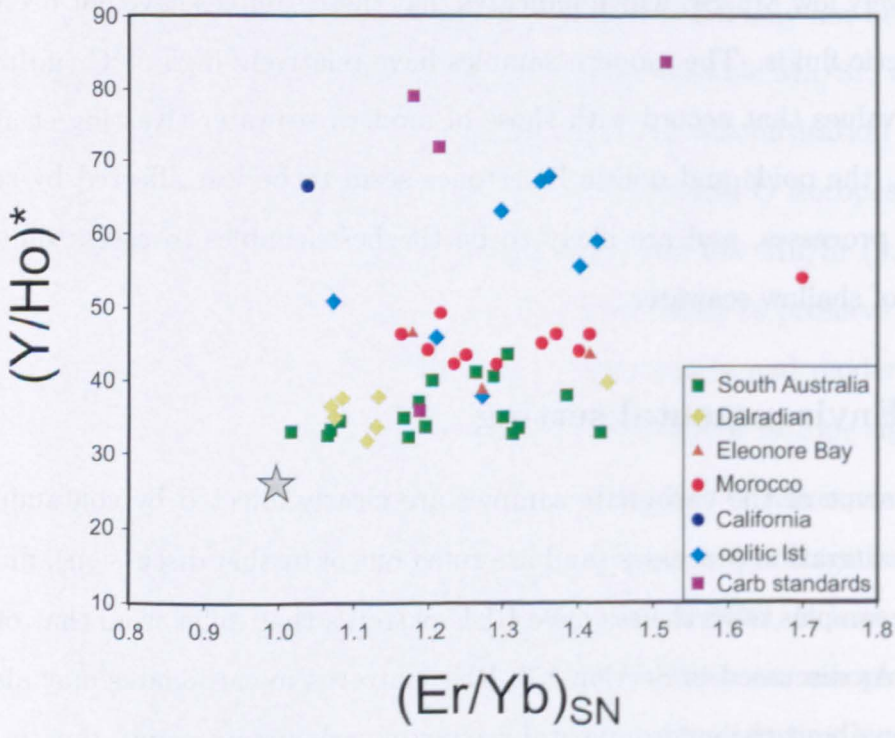

Figure 5.14: $(Y/Ho)^*$ versus $(Er/Yb)_{SN}$ for all carbonates considered to be unaffected by post depositional alteration. The grey star is the continental crust value Kamber et al. (2005).

The REE patterns could also reflect differences between modern and Neoproterozoic seawater chemistry, which was probably more iron-rich. In this connection, Fe concentrations in the Adelaide rift carbonates are higher than in Phanerozoic samples, so REE patterns could be strongly influenced by seawater Fe chemistry in the Neoproterozoic. Interestingly, the cap carbonates all have very similar REE patterns, being strongly enriched in the MREEs. This pattern is difficult to explain and could indicate that the carbonates precipitated in an environment that was strongly influenced by fresh water input, either from rivers, or from melting ice. However, it has been recently argued that cap carbonates were deposited over a long period of time and general input from melting ice is rather unlikely (Kennedy and Christie-Blick, 2011). If this is the case, then the REE patterns recorded in the cap carbonates genuinely reflects that of the ocean at that time. This would mean that the sources of the REEs and/or REE cycling with Fe oxides were different from the modern ocean.

The C and O isotopic composition of the Australian samples are comparable with previously published data (Calver, 2000; McKirdy et al., 2001). It has been argued that the O isotopic composition of carbonate rocks from the Nuccaleena formation are affected by diagenesis (Calver, 2000), and indeed some of the samples analysed in this study have low $\delta^{18}O$ values, and high Mn/Sr values, that support this idea. Overall, it is important to note that it is difficult to use the C chemostratigraphy in a global context, because these samples may be near shore with a significant local influence from freshwater, which may also perturb the C isotopic data. It makes it more complicated to interpret the REE pattern of these samples with respect to redox condition in seawater during the time of deposition.

5.4.2.2 Moroccan samples

Most of the samples from Morocco are strongly enriched in the MREEs relative to the HREEs and they are also slightly depleted in the LREEs relative to the MREEs. The $(Y/Ho)^*$ ratio ranges from 40 to 50 which is slightly lower than the open ocean value (60-90), suggesting that these samples have been deposited in shallow, near shore environment. This is in agreement with the $(Er/Yb)_{SN}$ ratio recorded in these

samples ($(Er/Yb)_{SN} > 1.2$). Similarly, the C isotopic composition of the carbonates is likely to be influenced by nearshore processes, as well as open seawater. The $^{87}Sr/^{86}Sr$ ratios are similar to the Sr isotopic composition of the seawater curve at the beginning of the Cambrian (Fig. 5.15), as might be expected for a well-mixed element such as Sr.

5.4.2.3 Oolitic limestones

The oolitic limestones are divided into three groups, on the basis of their age: modern, Phanerozoic and Neoproterozoic samples. The modern carbonates have REE patterns similar to seawater pattern (Fig. 5.16), i.e. they are characterised by a negative Ce anomaly and a positive Y anomaly. These modern samples are clearly recording the REE pattern of the ambient seawater and are not contaminated by detrital material or hydrothermal fluids. It is important to note that Y/Ho ratio of these modern samples (39-47) is lower than the open ocean value because Y/Ho is fractionated during carbonate precipitation. However, the $(Y/Ho)^*$ value (56-68) is consistent with a marine setting for these samples. The $(Er/Yb)_{SN}$ ratios recorded

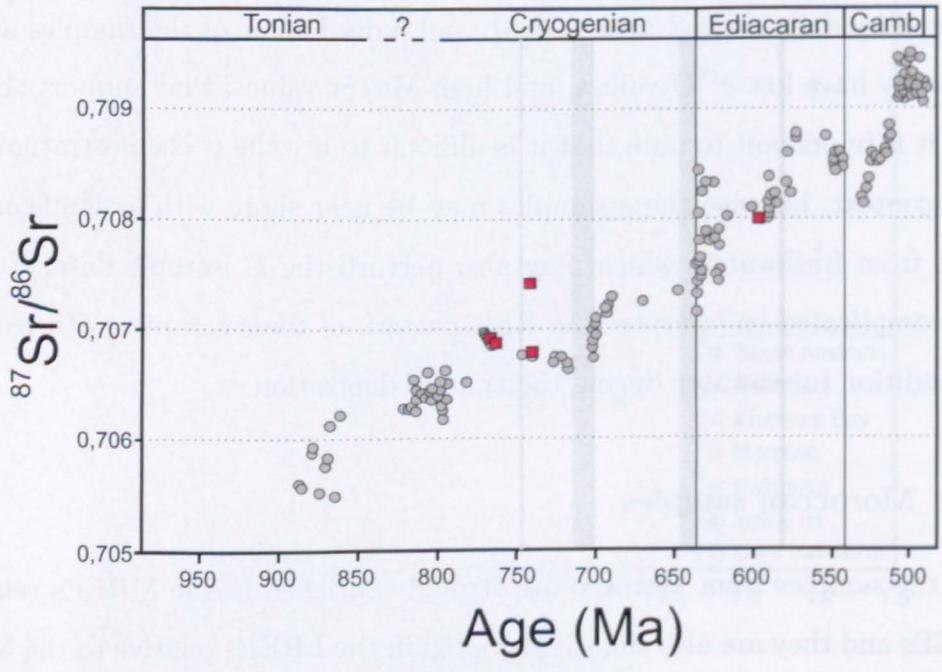

Figure 5.15: Sr isotope curve for the Neoproterozoic seawater, modified after Halverson et al. (2010). Red squares indicate carbonate samples analysed in this study. The age of the analysed samples are described in Chapter 4.

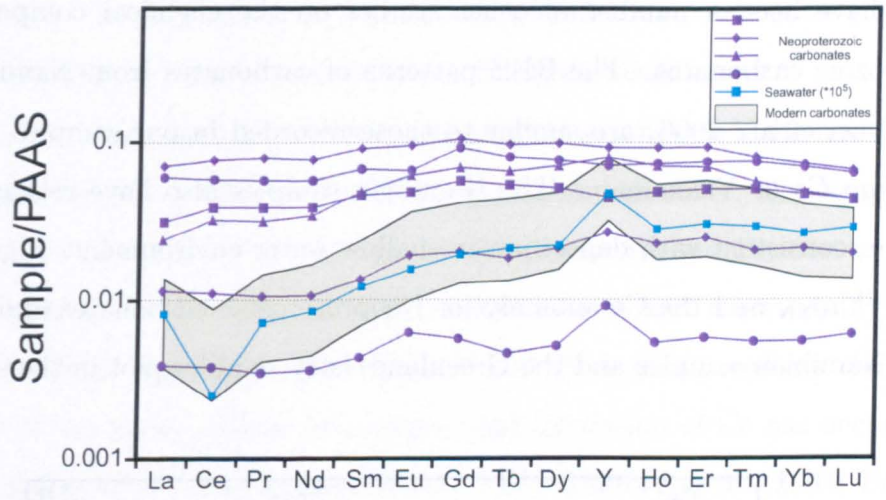

Figure 5.16: Shale normalised REE pattern for oolitic limestones and modern shallow seawater. Seawater data from Zhang and Nozaki (1998). The green area represents the modern carbonates analysed in this study.

in the modern ooids are between 1.36 and 1.43 and are consistent with a shallow water environment. Therefore the ooids and oolitic limestones are suitable for assessing variations in the chemical composition of shallow seawater.

The Phanerozoic oolitic limestones have variable REE patterns. C17 and C443 are characterised by weak Ce and Y anomalies and have $(Y/Ho)^*$ and $(Er/Yb)_{SN}$ ratios consistent with deposition in a shallow water environment. C171 is characterised by large Ce and Y anomalies and is interpreted to record an open marine setting.

Oolitic limestones from the Cryogenian period in the Neoproterozoic have relatively flat REE patterns. A lacustrine setting is very unlikely based on field observations (Herrington and Fairchild, 1989; Sawaki et al., 2010) and Sr isotope data (Fairchild et al., 2000; Sawaki et al., 2010; this study). The pattern observed for these samples is relatively similar to modern seawater, except for the Ce and Y anomalies. The REE patterns are however less depleted in the LREEs relative to modern ooids. The $(Y/Ho)^*$ ratio of these samples is in the range 40 to 50, consistent with a shallow water environment (Fig. 5.3). $(Er/Yb)_{SN}$ ratios (> 1.2) are also consistent with a shallow water setting. Thus, these samples are interpreted to record the chemical composition of shallow Cryogenian seawater.

There have been a number of other studies on the chemical composition of Neoproterozoic carbonates. The REE patterns of carbonates from Namibia (Fig. 5.17; Frimmel et al., 2006) are similar to those recorded in our samples and they also have no Ce or Y anomaly. The Namibian samples also have relatively high $(Er/Yb)_{SN}$, consistent with deposition in shallow water environment. Figure 5.17b shows $(Er/Yb)_{SN}$ and the Ce anomaly for Neoproterozoic carbonates and interestingly the Namibian samples and the Greenland/Islay samples plot in the same part

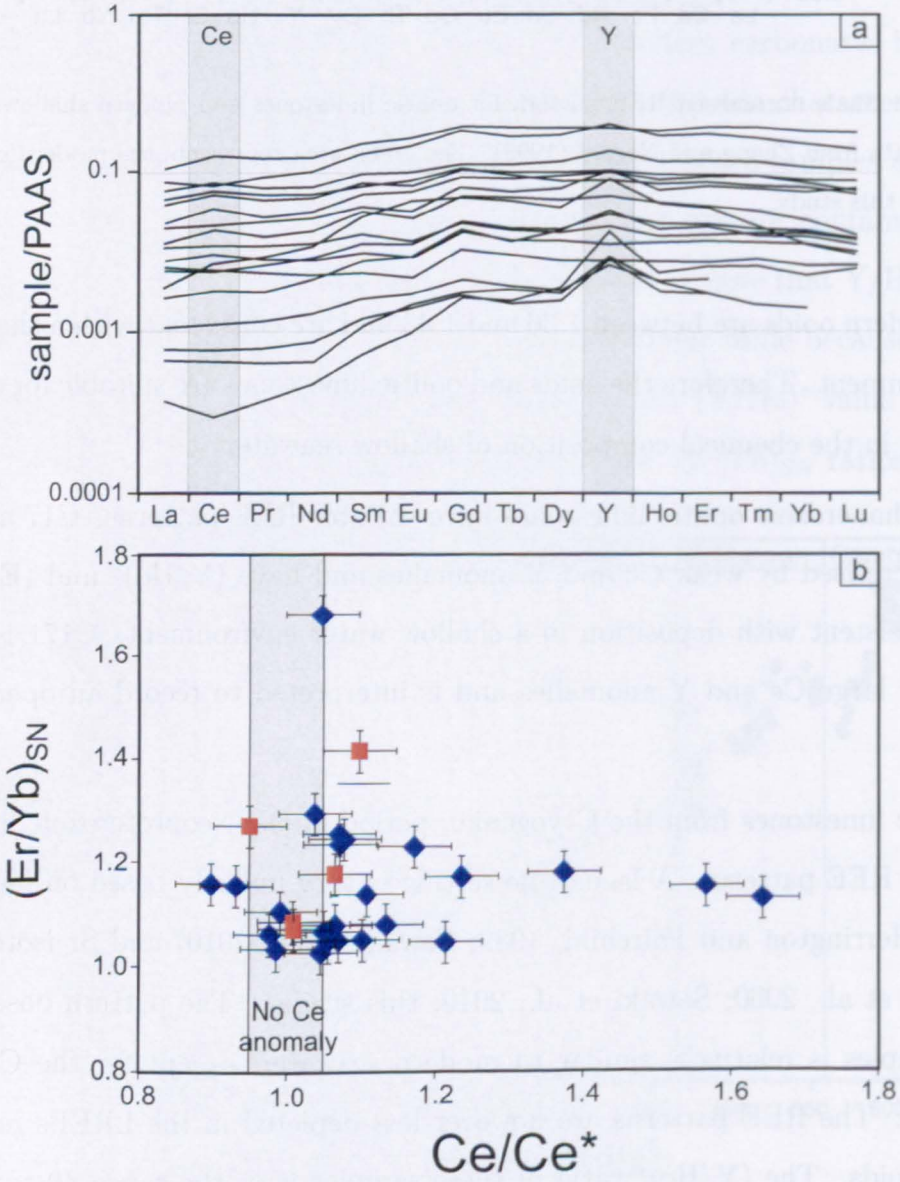

Figure 5.17: (a) Shale normalised REE-Y patterns and (b) $(Er/Yb)_{SN}$ versus Ce/Ce*, for Neoproterozoic carbonates (Frimmel, 2009). Brown squares are Neoproterozoic oolitic limestones analysed in this study.

of the graph. This suggests that the chemical signal of the carbonates (i.e. the lack of a Ce anomaly) is a global feature of the Neoproterozoic ocean.

The oolitic limestones have seawater-like REE patterns and Y/Ho and $(Er/Yb)_{SN}$ ratios characteristic of shallow water environment. However, the Neoproterozoic oolitic limestones have no Ce anomaly, whereas modern and Phanerozoic samples have a negative Ce anomaly. As Ce^{4+} is less soluble and more readily absorbed onto particulates than Ce^{3+}, the extent of the Ce anomaly reflects the oxygenation state of the water. There is evidence that oxydation of Ce has occurred since the Paleoproterozoic (Kamber and Webb, 2001; Kamber et al., 2004; Bolhar and Van Kranendonk, 2007). Cerium oxidation is however more sensitive to pH than it is to Eh, and is favoured in alkaline solutions (Elderfield and Sholkovitz, 1987). In general, Ce anomalies are absent in low pH solutions (< 6.5) and/or hydrothermal precipitates. Overall, the Neoproterozoic carbonates lack a negative Ce anomaly. Moreover, the Ce anomaly is not correlated with any tracers of detrital contamination and is therefore considered to be a primary signal. Frimmel (2009) proposed that flat REE patterns in Neoproterozoic carbonates were produced by contamination with colloids in a nearshore environment. Colloids have strong positive Ce anomalies and a negative Y anomaly. Mixing between colloids and seawater like pattern could therefore produce a flat REE pattern. As high levels of colloids are usually found in the presence of high levels of Fe, some correlation between the REEs and Fe may be expected if colloids are affecting the REEs (Frimmel, 2009). There is no relationship between Fe and the REEs in our samples (Fig. 5.18), so it seems unlikely that colloid contamination has affected their REE patterns. Moreover, the samples from Greenland and Scotland have Fe concentrations similar to that of modern ooids. Thus, samples from the Islay Formation and the Andree Land Group are interpreted to record shallow Cryogenian seawater.

5.4.3 Implications for redox conditions

The general lack of a Ce anomaly in our Neoproterozoic samples is in agreement with other previously published data (e.g. Komiya et al., 2008; Frimmel, 2009). This is therefore considered to be a global feature of the Neoproterozoic oceans.

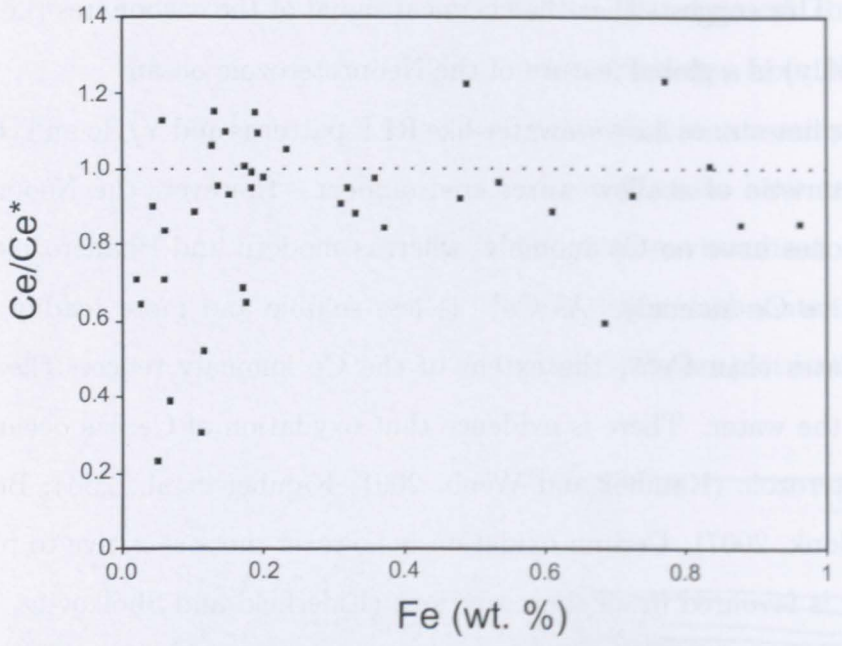

Figure 5.18: Ce/Ce* versus Fe concentration for all carbonates analysed in this study. The horizontal dashed line represents no Ce anomaly.

The lack of a Ce anomaly could indicate that (i) seawater was more acidic (pH < 6.5), or (ii) seawater was less oxygenated at that time. However, seawater cannot have been significantly more acidic in the Neoproterozoic than it is today, because calcium carbonate only precipitates at a pH of greater than 7.42 at the levels of total dissolved inorganic carbon (DIC) found in modern oceans (Krumbein and Garrels, 1952). By increasing the DIC, it is possible to just precipitate calcium carbonate at a pH of 6.7 ($\omega_{CaCO_3} > 1$), but this requires a -log pCO_2 of 0.99, which is too high for the Neoproterozoic (Kasemann et al., 2010). Moreover, the Ca and B isotopic composition of Neoproterozoic carbonates suggest that pH was relatively similar to the modern day value (Kasemann et al., 2010). The Islay limestones and the Andre Land samples have no Ce anomaly, and their REE pattern is similar to chemical precipitates from the Palaeo-Proterozoic, where seawater is interpreted to be anoxic (Webb and Kamber, 2000). Therefore the chemistry of the carbonates seems to indicate that the Neoproterozoic shallow ocean was not oxidised as extensively as modern seawater. Negative Ce anomalies can either be produced via direct oxidation of Ce(III) by O_2 or by Fe-Mn oxides. The lack of Ce anomaly in our samples is interpreted to reflect low O_2 conditions; under these conditions, Mn(IV) and Fe(III)

would also be unstable, preventing oxidation of Ce(III) by Mn or Fe oxides.

The REE patterns for the samples from Australia and Scotland (except the Islay limestone) seem to be strongly influenced by freshwater inputs and the carbonates therefore record information about the chemistry of near shore (proximal) seawater. Elements such as Sr and Cr, that have a longer residence time, will nevertheless be unaffected by local inputs. Therefore, those samples that are unaffected by contamination or secondary alteration should record the seawater composition at the time of deposition.

5.4.4 Cr concentration of carbonates

As rivers are the most important source of Cr to the oceans, it may be expected that the Cr concentration of sediments is correlated with tracers of detrital material, such as Zr. A key finding of this study is the Cr concentration of carbonates that are unaffected by detrital input (i.e. carbonates with low Zr concentration), is not zero. Indeed, as shown in Figure 5.19, samples with Zr concentrations of close to zero have Cr concentrations of up to 8 ppm. Moreover, O and C isotope data suggest that these samples are unaffected by diagenesis.

It has been shown that the partition coefficient of Cr in carbonates (as chromate) is strongly dependent on the Cr concentration in the solution (Tang et al., 2007). Assuming a concentration of 2 ppm in carbonates (section 3.6) and a seawater concentration of 5 nM (e.g. Connelly et al., 2006), the partition coefficient of Cr in carbonates is about 8000. This indicates that at low concentration carbonate precipitation could potentially be a sink of Cr in natural seawater. However, this partition coefficient can potentially vary with Cr concentration and redox conditions. It is also important to note that the change in ionic radius and in the aqueous behaviour between Cr(III) and Cr(VI) can influence the incorporation of Cr in the carbonate lattice (Garcia-Sanchez and Alvarez-Ayuso, 2002; Tang et al., 2007). There are a number of reasons why the concentration of Cr in carbonates is variable. Cr(VI) is believed to be incorporated into carbonates (Tang et al., 2007), but it is not clear if Cr(VI) is incorporated into the carbonate lattice in preference to Cr(III). So, the low Cr concentration in some of our samples could reflect changes in

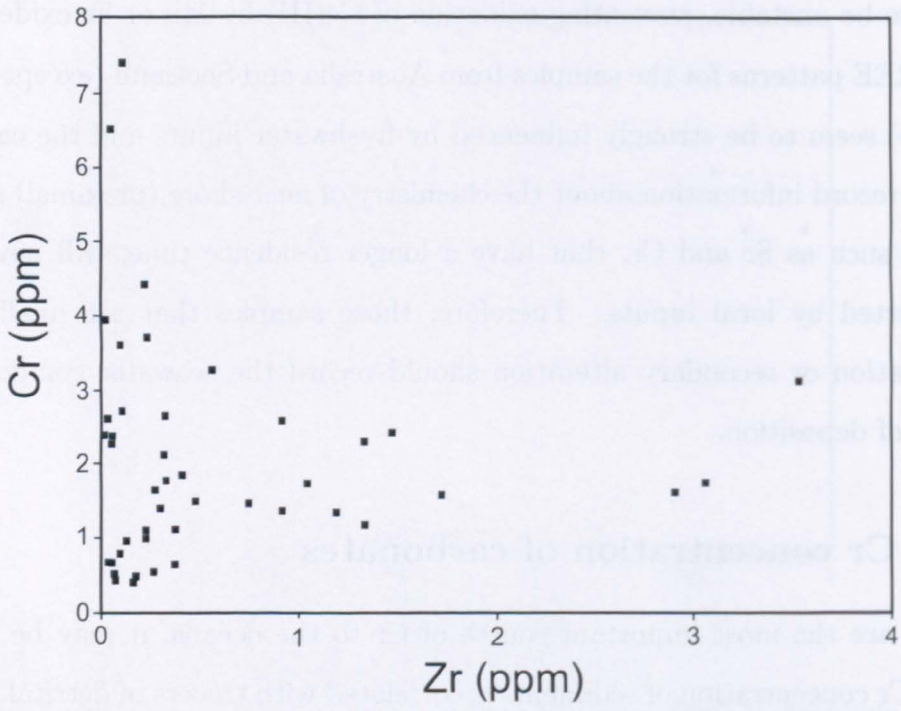

Figure 5.19: Cr versus Zr for all carbonate samples with < 4 ppm Zr. These are interpreted to be free of detrital contamination.

the Cr(III)/Cr(VI) ratio in seawater. On the other hand, if Cr is reduced to Cr(III) and removed from solution and Cr(VI) is the dominant species incorporated into carbonate, then the Cr concentration of the carbonates will directly reflect the Cr concentration of seawater.

5.5 Conclusions

The REE concentrations, C and O isotopes and Sr isotopes have been determined for modern, Phanerozoic and Neoproterozoic samples. These data suggest that few of our samples are affected by contamination and/or post depositional alteration. However, using empirical values (Zr < 4 ppm, Mn/Sr < 0.5, $\delta^{18}O$ > -10‰ and $Eu/Eu^* < 1.5$) the samples have been screened for such contaminations and the non-contaminated samples can therefore be used to assess the redox condition at the time of deposition. Modern and Phanerozoic samples are characterised by seawater like patterns and reflect oxidised conditions. The majority of the Neoproterozoic samples are characterised by bell shape patterns and are interpreted to be strongly influenced

by local input. Oolitic limestones from Islay and Greenland are characterised by REE patterns close to modern seawater, although they lack elemental anomalies which has been interpreted to reflect both a shallow water environment (consistent with high $(Er/Yb)_{SN}$ ratios) and low O_2 concentrations during the Cryogenian.

Chapter 6

Cr isotopic composition of marine carbonates

6.1 Introduction

Dissolved Cr concentrations in modern seawater are relatively low and range from 2 to 10 nM (Jeandel and Minster, 1987). In oxic seawater, chromium exists mainly as Cr(VI), which is consistent with thermodynamic calculations (Elderfield, 1970). However, significant amounts of Cr(III) have also been found; the percentage of Cr(III) is usually <5% (e.g. Mugo and Orians, 1993), although some authors have found much higher quantities, sometimes accounting for over 90% of the total dissolved Cr (Sander et al., 2003; Connelly et al., 2006). Cr in the continental crust occurs mainly as Cr(III) and is believed to be oxidised to Cr(VI) during oxidative weathering (Frei et al., 2009). Cr(VI) is much more soluble than Cr(III) (Pettine, 2000). Chromium in river waters and ground waters is predominantly in the form Cr(VI) (~90%) (Cranston and Murray, 1978; Izbicki et al., 2008), although significant quantities of Cr(III) in river water have also been reported (e.g. Pankow et al., 1977). Considered together, these data suggest that the proportion of Cr(III) to Cr(VI) varies as Cr cycles in the natural environment, depending on the environmental conditions and redox conditions. As reduction reactions fractionate Cr isotopes (Ellis et al., 2002, Zink et al., 2010), Cr isotopes may be useful for understanding the reactions that occur in the Cr cycle, such as weathering and reduction/oxidation

reactions in seawater.

Although there are no reports on the Cr isotopic composition of river waters, ground waters appear to have higher δ^{53}Cr values (δ^{53}Cr up to +5.9‰, Izbicki et al., 2008) than the continental crust (δ^{53}Cr = -0.12 ± 0.10‰; Schoenberg et al., 2008). As weathering of Cr(III) from primary minerals, and oxidation of Cr(III) to Cr(VI) do not seem to be accompanied by significant isotope fractionation (Ellis et al., 2004; Zink et al., 2010), it is thought that these high δ^{53}Cr values are caused by partial reduction of Cr(VI) on mineral surfaces, with retention of lighter isotopes in Cr(III) in the solid phase (Izbicki et al., 2008). However, it is also possible that the reduction of Cr(VI) to Cr(III) occurs in the riverine system (Pettine, 2000) and this reduction could also fractionate Cr isotopes.

Until recently, the Cr isotope composition of modern-day, oxic seawater was unknown, but was considered likely to be enriched in ^{53}Cr relative to the continental crust, similar to groundwaters (Izbicki et al., 2008; Frei et al., 2009). Data generated as part of this thesis (see Chapter 3) confirm that the δ^{53}Cr value of seawater is greater than that of the continental crust; the δ^{53}Cr value of total dissolved Cr is between 0.45 and 1.55‰.

6.1.1 Evolution of seawater oxygenation in the Neoproterozoic

The putative evolution of atmospheric oxygen in the Neoproterozoic is shown in Figure 6.1 (Holland, 2006). The variations in atmospheric O_2 are likely to be associated with changes in the redox conditions of the oceans. Previous studies of the Mo concentration of Neoproterozoic shales, Fe speciation and S isotopes, indicate that the Ediacaran ocean was stratified, with coeval oxic, euxinic, and ferruginous zones (Fike et al., 2006; Li et al., 2010). There is strong evidence that the deep waters were reduced during the Ediacaran (Canfield et al., 2008), but they are thought to have become oxic by the end of the Neoproterozoic (Canfield et al., 2007). Although most models of the Neoproterozoic ocean assume that shallow waters were oxic (Canfield et al., 2008; Li et al., 2010), there is only slim evidence for this based on carbon

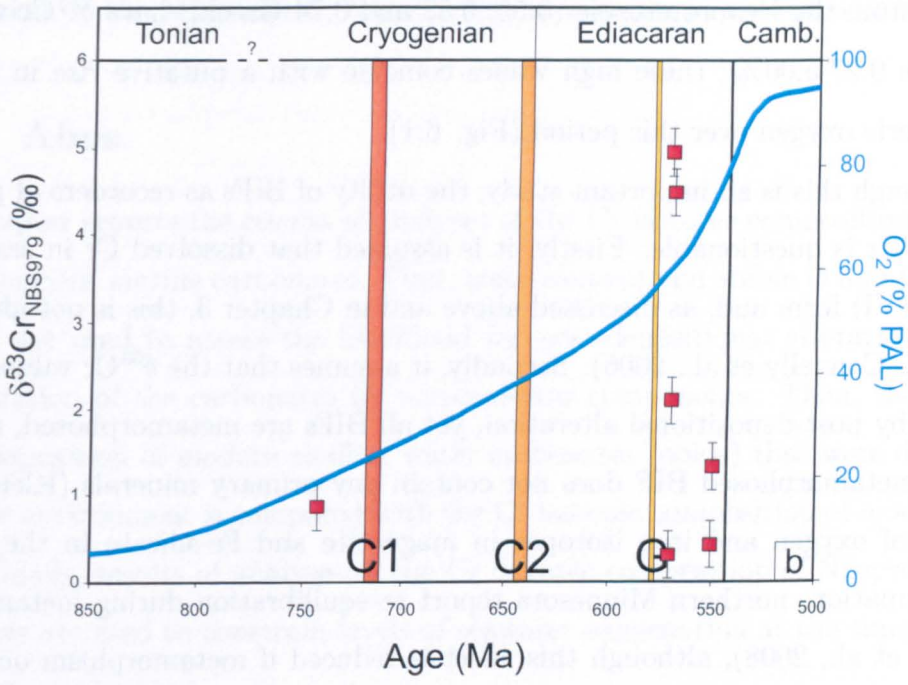

Figure 6.1: Cr isotopic composition of Neoproterozoic BIFs with Eu/Eu* < 1.5. Data from Frei et al. (2009). The blue line shows the putative evolution of atmospheric O_2, after Holland (2006). The verticals bars represent the main Neoproterozoic glaciations.

isotope studies (Des Marais et al., 1992) and, in general, very little is known about the level of oxygenation in shallow seawater in the Neoproterozoic (e.g. Li et al., 2010).

6.1.2 Cr isotopes as recorders of past ocean oxygenation?

It has been suggested that Cr isotopes in Fe-rich chemical precipitates can provide important information for palaeo-redox state of the seawater (Dossing et al., 2011) and, in this connection, recent work on Precambrian banded iron formations (BIFs) suggests that the Cr isotopic composition of seawater may have varied in the past, because of changes in atmospheric oxygenation (Frei et al., 2009). BIFs with high δ^{53}Cr are interpreted in terms of oxidative weathering, whereas low (continental crust-like) δ^{53}Cr values are interpreted in terms of low levels of atmospheric oxygen. Thus, high δ^{53}Cr in ~2.8 to 2.6 Ga-old BIFs suggest that Cr(VI) accumulated in ocean surface waters before the Great Oxidation Event, and low δ^{53}Cr values in ~1.88 Ga-old BIFs suggest that atmospheric oxygen levels declined at that time.

Samples from the Neoproterozoic (0.55, 0.57 and 0.74 Ga-old) have δ^{53}Cr values in the range 0.27-5.00‰; these high values coincide with a putative rise in levels of atmospheric oxygen over this period (Fig. 6.1).

Although this is an important study, the utility of BIFs as recorders of past seawater δ^{53}Cr is questionable. Firstly, it is assumed that dissolved Cr in seawater is in its Cr(VI) form and, as discussed above and in Chapter 3, this is not always the case (e.g. Connelly et al., 2006). Secondly, it assumes that the δ^{53}Cr values are unaffected by post-depositional alteration, yet all BIFs are metamorphosed, and even weakly metamorphosed BIF does not contain any primary minerals (Klein, 2005). Studies of oxygen and iron isotopes in magnetite and Fe-silicate in the Biwabik Iron Formation, northern Minnesota report re-equilibration during metamorphism (Hyslop et al., 2008), although this effect is reduced if metamorphism occurs in a closed system. The absence of any studies on the effects of metamorphism on Cr, and on Cr isotopes in particular, makes it difficult to assess whether this assumption is valid. Thirdly, it is assumed that all of the Cr in BIF is derived from seawater. However, most of the BIFs have high Eu anomalies (>1.5), indicative of hydrothermal inputs, and would have been excluded from further discussion in this study (see Chapter 4). Fourthly, BIFs contain a variety of different Fe-rich minerals, Fe-oxides, carbonates and chert. According to Frei et al. (2009), only Fe(III) bearing phases are able to record the former presence of Cr(VI), so the presence of Cr in other phases is problematic. Finally, seawater δ^{53}Cr is only recorded in Fe-rich sediments if the overlying water column contains Fe^{2+}, which acts as the reductant (Frei et al., 2009). This means that seawater δ^{53}Cr can only be reconstructed in this way if the oceans are ferruginous, which has not been the case for large parts of the Earth's history (Canfield et al., 2008).

6.1.3 Cr isotopic composition of carbonates

The Cr in uncontaminated carbonates can be considered to be derived from seawater (Chapter 4). Moreover, the carbonates are likely to have precipitated in shallow marine waters (see Chapter 4), which should be in equilibrium with the atmosphere. Thus, analyses of the Cr isotopic composition of carbonates should provide new

information on the oxygenation state of shallow seawater in ancient oceans.

6.1.4 Aims

This Chapter reports the results of analyses of the Cr isotopic composition of modern and ancient marine carbonates. First, trace element and stable O and C isotope analyses are used to assess the likelihood for post-depositional alteration and/or contamination of the carbonates by non-seawater components. Then, the Cr isotopic composition of modern shallow water carbonates (ooids) that were deposited in an oxic environment is compared with the Cr isotopic composition of modern seawater. Finally, results of analyses of the Cr isotopic composition of Neoproterozoic carbonates are used to constrain levels of seawater oxygenation at the time of their deposition.

6.2 Results

6.2.1 Modern and Phanerozoic carbonates

The Cr isotopic composition of the modern and Phanerozoic carbonates are reported in Table 6.1, together with other relevant element and isotope data. The modern carbonates all have positive δ^{53}Cr values, and are therefore isotopically heavy compared to the continental crust and mantle (-0.12‰; Schoenberg et al., 2008). The three Bahamas ooids (B08, NPCOScim and NPCOSunc) have similar δ^{53}Cr values, 0.65 ± 0.02‰. The sample from Yucatan (C48) has a slightly higher value (δ^{53}Cr = 0.765‰). The Cr isotopic composition of the modern ooids is not correlated with Cr concentration (Fig. 6.2a), Ce/Ce* (Fig 6.2b) or δ^{18}O (Fig. 6.2f).

The Phanerozoic carbonates have δ^{53}Cr values ranging from -0.22 to 1.994‰. The four oolitic limestones (C17, C171, C443 and C514) have δ^{53}Cr values that range from -0.22‰ to 1.939‰. The carbonate standards (the calcites Cal-s, JLs-1 and BCS CRM 513, and the dolomites JDo-1 and BCS CRM 512) have δ^{53}Cr values that range from 0.737 to 1.994‰. With the exception of sample C514, the Phanerozoic carbonates all have higher δ^{53}Cr than the continental crust and mantle

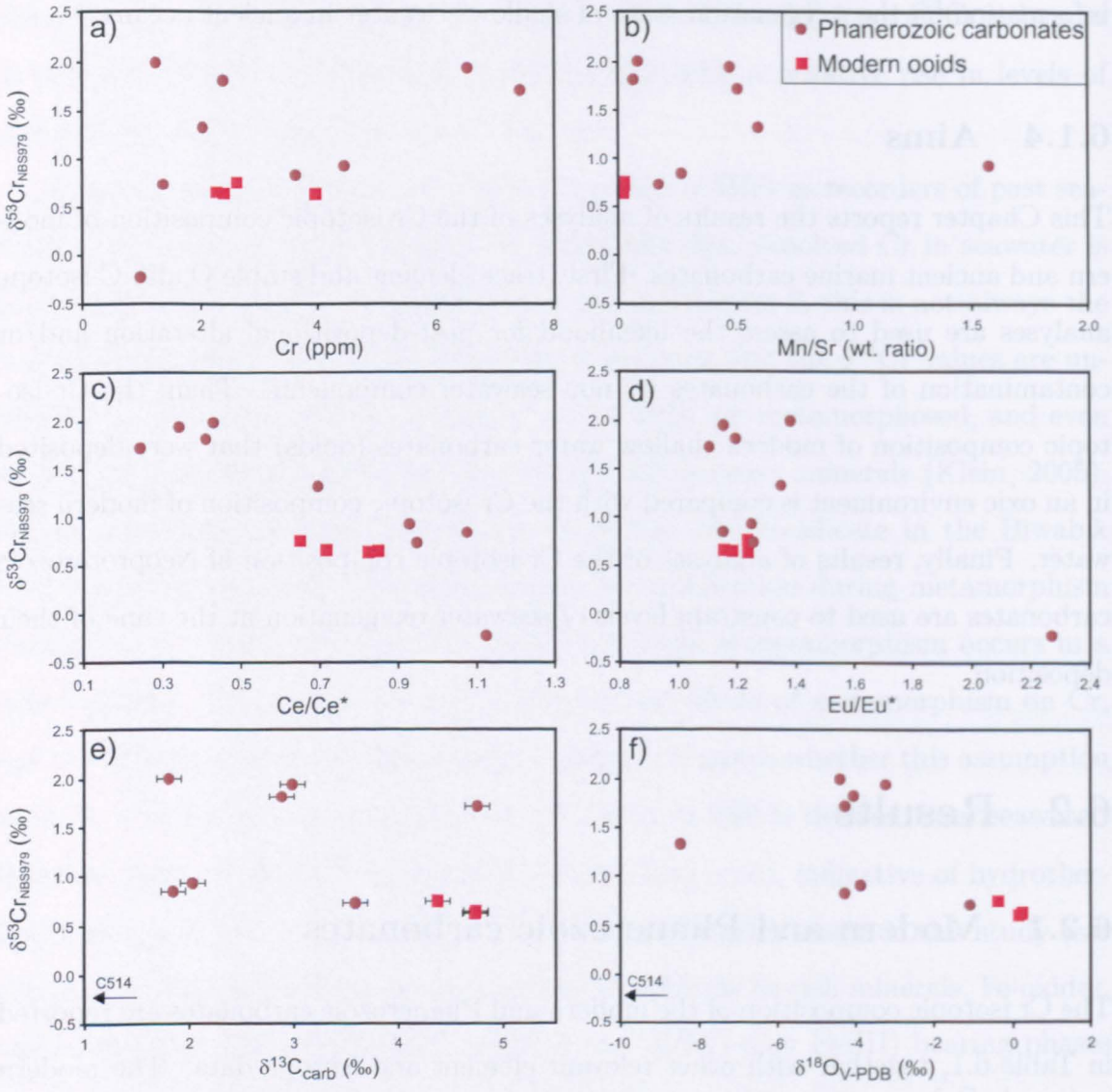

Figure 6.2: δ^{53}Cr versus (a) Cr concentration, (b) Mn/Sr ratio, (c) Ce anomaly, (d) Eu anomaly, (e) $\delta^{13}C_{carb}$ and (f) δ^{18}O, for Phanerozoic carbonates and modern ooids. The errors bars are only shown where larger than the size of the symbols. Sample C514 has exceptionally low δ^{13}C and low δ^{18}O and its position is indicated by the black arrow.

values. Although δ^{53}Cr does not correlate with the Cr concentration, Mn/Sr ratio, Eu anomaly, $\delta^{13}C_{carb}$ and δ^{18}O in Phanerozoic carbonates (Fig. 6.2), there is a strong negative correlation ($r^2 = 0.88$) between δ^{53}Cr and the Ce anomaly (Fig. 6.2c).

Table 6.1: Cr concentration and Cr isotopic composition of oolitic limestones and Phanerozoic carbonates, together with other key geochemical data. Samples shown in bold are considered to have been affected either by post-depositional alteration or contamination (see text for details).

Sample	Cr (ppm)	δ^{53}Cr (‰)	Mn/Sr	Ce/Ce*	Eu/Eu*	$\delta^{13}C_{carb}$ (‰)	δ^{18}O (‰)
Modern ooids							
C48	2.6	0.765	0.00	0.65	1.24	4.4	-0.4
NPCOS cim	2.4	0.651	0.00	0.85	1.19	4.7	0.3
NPCOS unc	2.3	0.663	0.00	0.72	1.16	4.7	0.3
B08	4.0	0.640	0.00	0.82	1.24	4.7	0.1
Phanerozoic oolitic limestones							
C17	3.6	0.848	0.27	1.07	1.15	1.8	-4.3
C171	6.5	1.939	0.47	0.34	1.15	3.0	-3.3
C443	4.4	0.931	1.58	0.93	1.25	2.0	-3.9
C514	**1.0**	**-0.224**	**15.79**	**1.12**	**2.27**	**-7.7**	**-15.1**
Carbonate standards							
BCS-CRM 512	0.8	0.737	0.17	0.95	1.25	3.6	-1.1
Cal-S	2.5	1.819	0.06	0.41	1.20	2.9	-4.1
JDo-1	7.2	1.719	0.51	0.24	1.11	4.8	-4.3
BCS-CRM 513	4.0	1.329	0.59	0.69	1.35	-0.7	-8.5
JLs-1	1.1	1.994	n.d.	n.d.	n.d.	1.8	-4.4

6.2.2 Neoproterozoic carbonates from South Australia

The South Australia carbonates have lower δ^{53}Cr than the modern and Phanerozoic carbonates, ranging from -0.529‰ to +0.107‰ (Table 6.2). The majority of the samples have a δ^{53}Cr comparable to the continental crust and mantle value, but four samples (A16, A18, A19 and A21) have resolvably higher δ^{53}Cr, between 0.073‰ and 0.107‰. Two samples (A6 and A13) have relatively low δ^{53}Cr (-0.529‰ and -0.408‰, respectively).

The Cr concentration of the samples from South Australia varies widely, between 0.9 and 22 ppm, but there is no correlation between the Cr concentration and δ^{53}Cr (Fig. 6.3a). Furthermore, there is no correlation between δ^{53}Cr and the Ce anomaly, the Eu anomaly, Mn/Sr ratio, $\delta^{13}C_{carb}$ and δ^{18}O (Fig. 6.3).

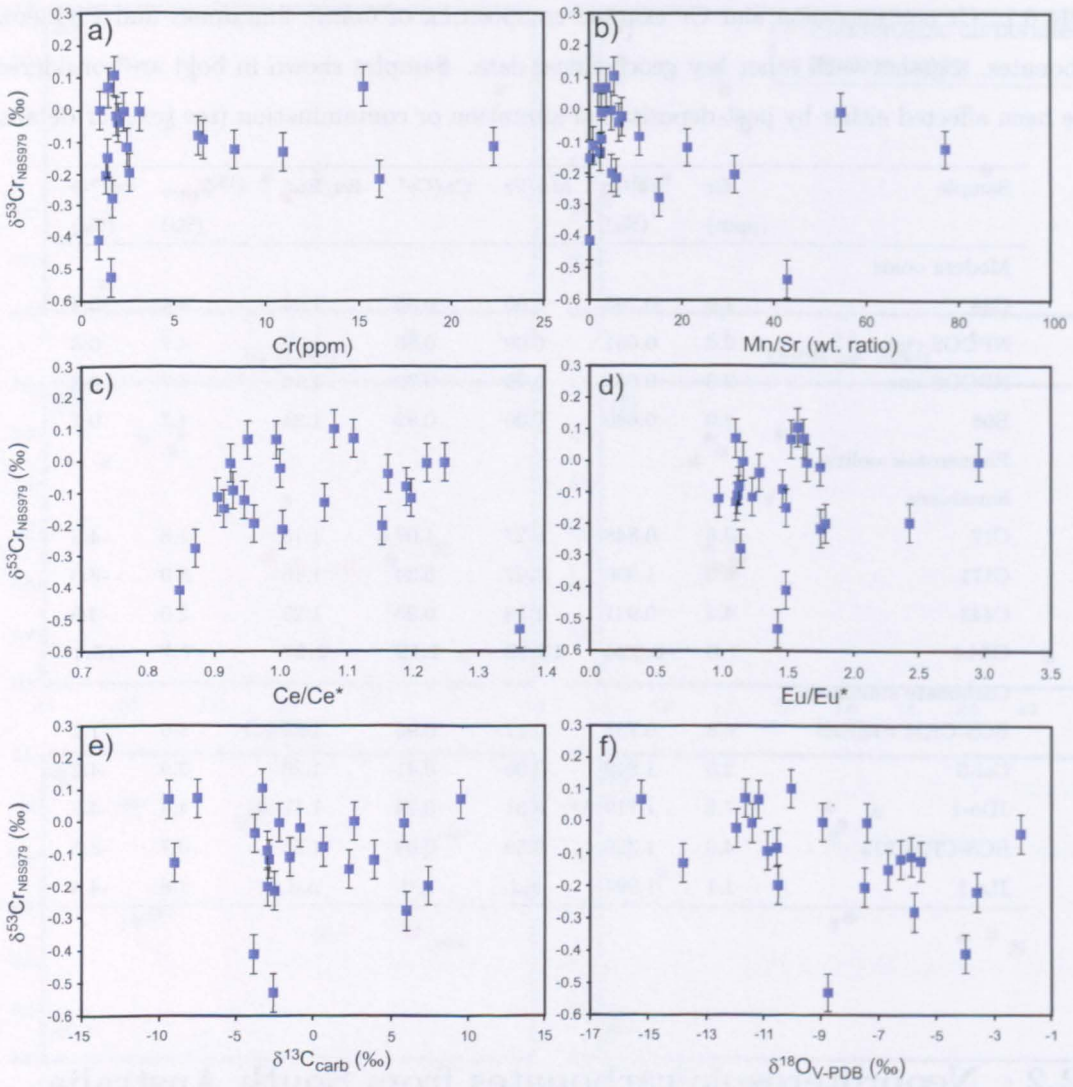

Figure 6.3: δ^{53}Cr versus (a) Cr concentration, (b) Mn/Sr ratio, (c) Ce anomaly, (d) Eu anomaly, (e) $\delta^{13}C_{carb}$ and (f) δ^{18}O, for carbonate samples from South Australia.

6.2.3 Neoproterozoic carbonates from the Dalradian succession

The Cr isotopic composition of carbonates from the Dalradian succession of Scotland and Ireland is reported in Table 6.3. The samples collected on Islay (Chapter 3) are characterised by a large range of δ^{53}Cr, from -0.852‰ to +0.859‰. Five samples (I17, I20, I22, I24 and I25) have δ^{53}Cr values close to the continental crust value, whereas four samples (I24R, I26, I27 and I28) have higher δ^{53}Cr, ranging from +0.148‰ to +0.859‰. The δ^{53}Cr value of one sample (I1) is lower than the conti-

Table 6.2: Cr concentration and Cr isotopic composition of carbonates from South Australia, together with other key geochemical data. Samples shown in bold are considered to have been affected either by post-depositional alteration or contamination (see text for details).

Sample	Cr (ppm)	δ^{53}Cr (‰)	Mn/Sr	Ce/Ce*	Eu/Eu*	$\delta^{13}C_{carb}$ (‰)	δ^{18}O (‰)
South Australia							
A2	**3.1**	**-0.002**	**2.73**	**0.92**	**2.95**	**5.8**	**-11.4**
A3	**1.7**	**-0.276**	**15.05**	**0.87**	**1.14**	**6.0**	**-5.7**
A4	**16.1**	**-0.214**	**6.10**	**1.00**	**1.75**	**-2.5**	**-3.6**
A5	**2.0**	**-0.036**	**6.45**	**1.16**	**1.28**	**-3.8**	**-2.0**
A6	**1.6**	**-0.529**	**42.90**	**1.36**	**1.42**	**-2.5**	**-8.8**
A7	**6.3**	**-0.078**	**10.81**	**1.19**	**1.13**	**0.6**	**-10.5**
A8	1.4	-0.148	0.36	0.91	1.49	2.4	-6.7
A9	**1.9**	**-0.018**	**7.07**	**1.00**	**1.75**	**-0.9**	**-11.9**
A10	**1.4**	**-0.201**	**31.45**	**1.15**	**1.79**	**-3.0**	**-7.5**
A11	22.2	-0.109	0.86	0.90	1.12	-1.6	-5.9
A12	**2.4**	**-0.113**	**21.35**	**1.20**	**1.23**	**-2.9**	**-6.2**
A13	0.9	-0.408	0.01	0.85	1.49	-3.9	-4.0
A14	**2.6**	**-0.195**	**4.96**	**0.96**	**2.43**	**7.4**	**-10.5**
A15	**11.0**	**-0.127**	**2.43**	**1.07**	**1.11**	**-9.0**	**-13.8**
A16	**1.5**	**0.073**	**3.68**	**0.95**	**1.10**	**-9.4**	**-15.2**
A17	**1.0**	**0.002**	**4.86**	**1.25**	**1.16**	**2.6**	**-8.9**
A18	**1.5**	**0.073**	**2.06**	**0.99**	**1.53**	**9.5**	**-11.1**
A19	**15.3**	**0.075**	**2.06**	**1.11**	**1.62**	**-7.5**	**-11.6**
A20	**6.6**	**-0.088**	**2.60**	**0.93**	**1.46**	**-3.0**	**-10.8**
A21	**1.8**	**0.107**	**5.51**	**1.08**	**1.58**	**-3.3**	**-10.0**
A22	**2.3**	**-0.003**	**54.63**	**1.22**	**1.65**	**-2.2**	**-7.4**
A23	**8.3**	**-0.119**	**77.23**	**0.94**	**0.98**	**3.9**	**-5.5**

nental crust value, at -0.852‰. This is the lightest isotopic composition measured in any sample analysed to date. The two samples from Tayvallich have δ^{53}Cr similar to the continental crust value. There is no evidence of correlation between δ^{53}Cr and the Ce anomaly, the Eu anomaly, the Mn/Sr ratio, $\delta^{13}C_{carb}$ and δ^{18}O (Fig. 6.4).

6.2.4 Carbonates from the Eleonore Bay Supergroup and the Morocco succession

Carbonates from the Eleonore Bay Supergroup have relatively high δ^{53}Cr, ranging from +0.781‰ to +1.004‰ (Table 6.3). The Cr isotopic composition of the Moroccan samples is more variable, ranging from -0.236‰ to +0.110‰. The carbonate

sample from India (T6) has a δ^{53}Cr value close to that of the continental crust, whereas the sample from California has high δ^{53}Cr (+0.966‰), close to the values measured in modern ooids and some of the carbonates from the Dalradian and Eleonore Bay successions.

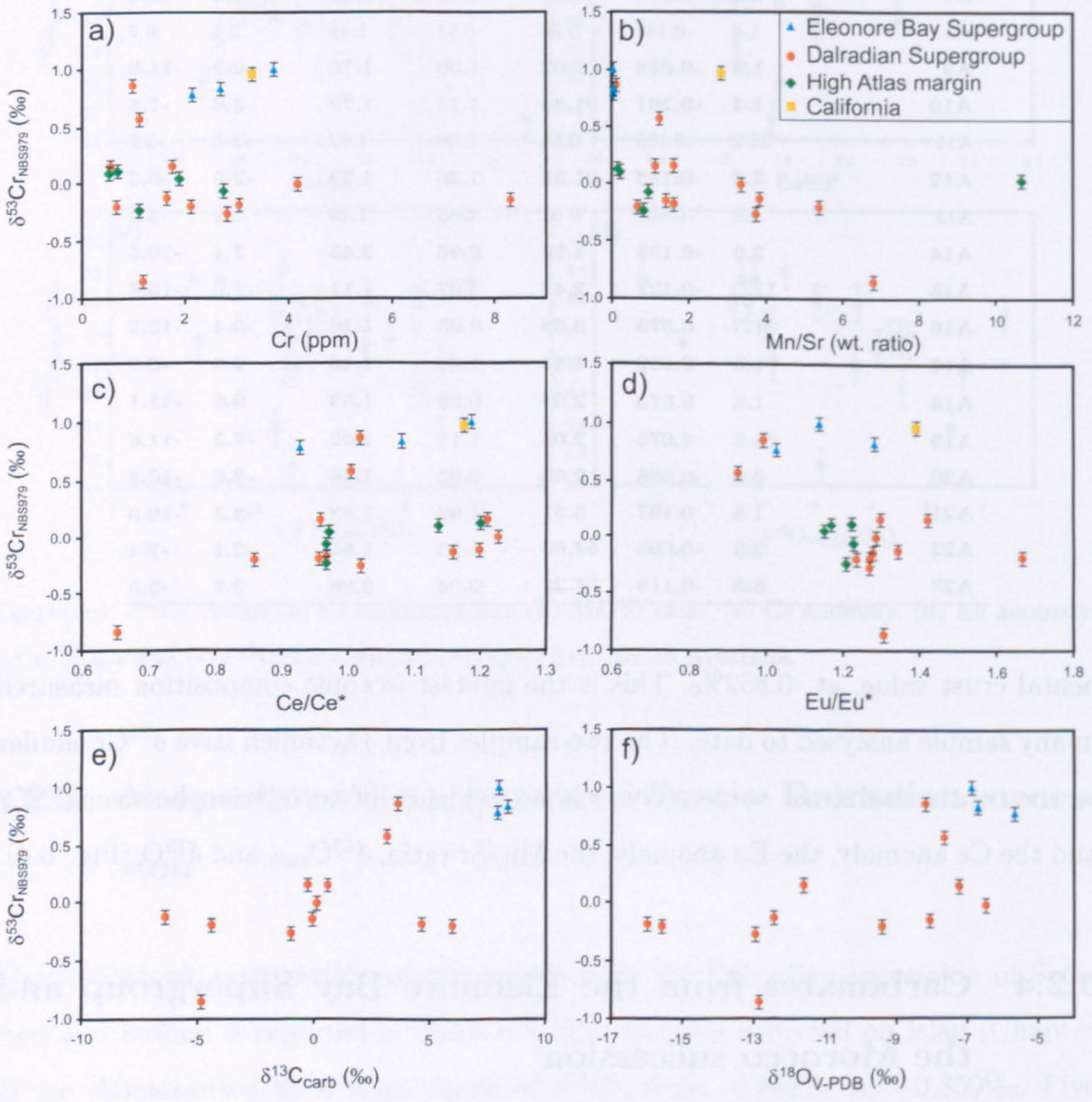

Figure 6.4: δ^{53}Cr versus (a) Cr concentration, (b) Mn/Sr ratio, (c) Ce anomaly, (d) Eu anomaly, (e) $\delta^{13}C_{carb}$ and (f) δ^{18}O, for carbonates from the Eleonore Bay Supergroup, Morocco and the Dalradian Supergroup of Scotland and Ireland.

Table 6.3: Cr concentration and Cr isotopic composition of carbonates from the Dalradian Supergroup, the Eleonore Bay Supergroup, Morocco, India and California, together with other key geochemical data. Samples shown in bold are considered to have been affected either by post-depositional alteration or contamination (see text for details). n.d. = not determined.

Sample	Cr (ppm)	δ^{53}Cr (‰)	Mn/Sr	Ce/Ce*	Eu/Eu*	$\delta^{13}C_{carb}$ (‰)	δ^{18}O (‰)
Dalradian Supergroup							
I1	**1.2**	**-0.852**	**6.81**	**.65**	**1.31**	**-4.8**	**-12.9**
I17	**1.6**	**-0.126**	**3.85**	**1.20**	**1.34**	**-6.4**	**-12.4**
I20	2.1	-0.200	5.40	0.86	1.24	-4.4	-9.4
I22	**2.8**	**-0.268**	**3.77**	**1.02**	**1.27**	**-1.0**	**-13.0**
I24	8.3	-0.145	1.41	1.16	1.28	-0.1	-8.1
I24R	1.7	0.148	1.63	1.21	1.43	0.6	-7.2
I25	4.2	-0.009	3.34	1.23	1.29	0.1	-6.5
I26	**0.5**	**0.151**	**1.11**	**0.96**	**1.30**	**-0.3**	**-11.6**
I27	1.0	0.859	0.10	1.02	0.99	3.6	-8.2
I28	1.1	0.571	1.23	1.00	0.93	3.1	-7.6
T4	**0.6**	**-0.203**	**0.67**	**0.96**	**1.27**	**6.0**	**-15.6**
T5	**3.0**	**-0.183**	**1.61**	**0.97**	**1.67**	**4.6**	**-16.0**
T7	**4.8**	**n.d.**	**19.92**	**0.93**	**1.43**	**2.1**	**-15.9**
Eleonore Bay Supergroup							
PG128	2.7	0.834	0.01	1.08	1.28	8.3	-6.7
PG174	2.1	0.781	0.02	0.93	1.03	7.9	-5.7
PG440	3.7	1.004	0.01	1.19	1.14	7.9	-6.9
Morocco							
2.16	**1.9**	**0.048**	**10.71**	**0.97**	**1.15**	**n.d.**	**n.d.**
3.13	0.5	0.102	0.21	1.14	1.17	n.d.	n.d.
11.5	1.1	-0.236	0.77	0.97	1.21	n.d.	n.d.
BB10	0.7	0.110	0.17	1.20	1.23	n.d.	n.d.
D15	2.7	-0.059	0.97	0.97	1.23	n.d.	n.d.
BS1 (California)	3.3	0.966	2.85	1.18	1.39	n.d.	n.d.
T6 (India)	**0.5**	**-0.177**	**3.41**	**0.72**	**1.54**	**n.d.**	**n.d.**

6.3 Discussion

6.3.1 Do the carbonates record seawater δ^{53}Cr?

As described in Chapter 4, the trace element concentration and oxygen, carbon and strontium isotopic composition of a number of the carbonates indicates that they may have been affected by post-depositional processes, or contamination by non-seawater sources. The likely effects of these processes on the Cr isotopic composition

of the carbonates are discussed below.

6.3.1.1 Diagenesis

The oxygen isotopic composition of carbonates can be strongly affected by diagenesis, with $\delta^{18}O$ values decreasing as a result of exchange with diagenetic fluids (see Chapter 4). The relationship between $\delta^{53}Cr$ and $\delta^{18}O$ for all or the carbonates analysed in this study is shown in Figure 6.5. Although the samples are from a wide range of settings, there is no obvious correlation between $\delta^{53}Cr$ and $\delta^{18}O$ (see also

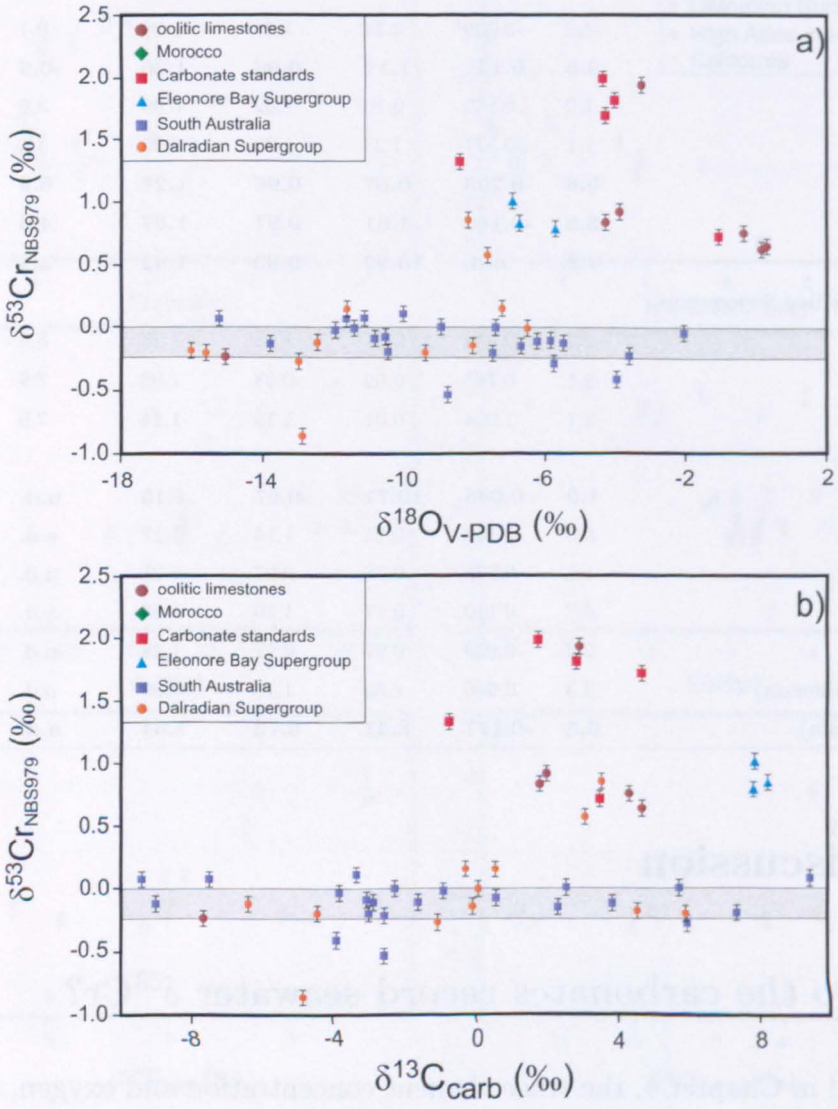

Figure 6.5: $\delta^{53}Cr$ versus (a) $\delta^{18}O$ and (b) $\delta^{13}C_{carb}$ for all of the carbonates samples. The grey shaded area represents the range in $\delta^{53}Cr$ measured for the bulk silicate Earth (Schoenberg et al., 2008).

Figures 6.2e, 6.3e and 6.4e). However, all of the samples with $\delta^{18}O$ < -10‰, i.e. those that are most likely to have been affected by diagenesis, have $\delta^{53}Cr$ close to the continental crust value. For this reason, carbonates with $\delta^{18}O$ values of < -10‰ are not considered to reliably record the $\delta^{53}Cr$ value of ancient seawater. Similarly, diagenesis results in a decrease in $\delta^{13}C$ values (Jacobsen and Kaufman, 1999), and samples with $\delta^{18}O$ values of < -3‰ have $\delta^{53}Cr$ values that are close to that of continental crust (Fig. 6.5b). The carbonate Mn/Sr ratio may also be used to assess whether carbonates have been affected by diagenesis, as carbonate Mn/Sr increases during diagenesis (e.g. Jacobsen and Kaufman, 1999). Figure 6.6 indicates that samples with high Mn/Sr have $\delta^{53}Cr$ values close to that of continental crust. For this reason, only carbonates with Mn/Sr of less than 3 can be considered to preserve seawater signals.

Thus, these data indicate that diagenesis shifts carbonate $\delta^{53}Cr$ towards the continental crust value. Nevertheless, the majority of the carbonates appear to be minimally affected by diagenesis, and are likely to record the Cr isotope signature of the seawater from which they precipitated.

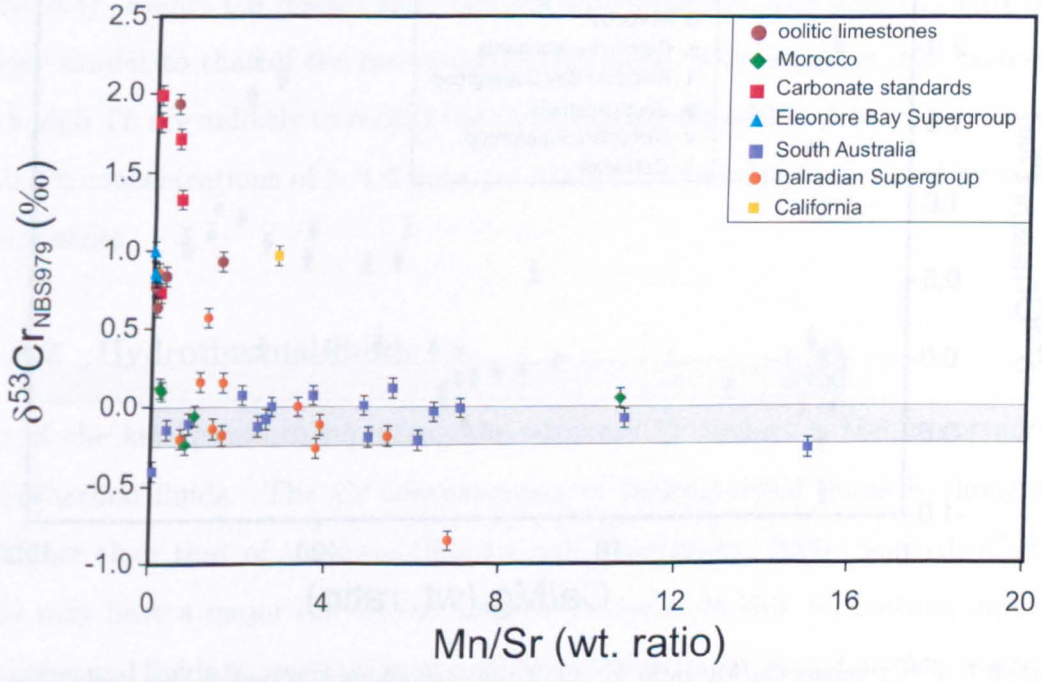

Figure 6.6: $\delta^{53}Cr$ versus Mn/Sr for all carbonates of the analysed in this study. The grey shaded area represents the range in $\delta^{53}Cr$ measured for the bulk silicate Earth (Schoenberg et al., 2008).

6.3.1.2 Dolomitisation

A number of the Neoproterozoic carbonates analysed in this study are dolomite, so the impact of dolomitisation on the Cr isotopic composition needs to be assessed. Figure 6.7 shows that there is no clear relationship between Ca/Mg and δ^{53}Cr, and both dolomites and calcites can have δ^{53}Cr values higher than continental crust. Nevertheless, Figure 6.7 does suggest that dolomites are more likely to have δ^{53}Cr close to the continental crust, and are thus less likely to record primary seawater δ^{53}Cr.

6.3.1.3 Subaerial weathering

The majority of carbonates analysed in this study have been sampled in the field and have been therefore subject to subaerial weathering. In order to assess the effects of oxidative weathering on δ^{53}Cr, drill-core samples (A22) recovered from the Nuccaleena formation (South Australia) can be compared with outcrop samples. Two of the outcrop samples (A10 and A12) appear to be relatively fresh in hand specimen,

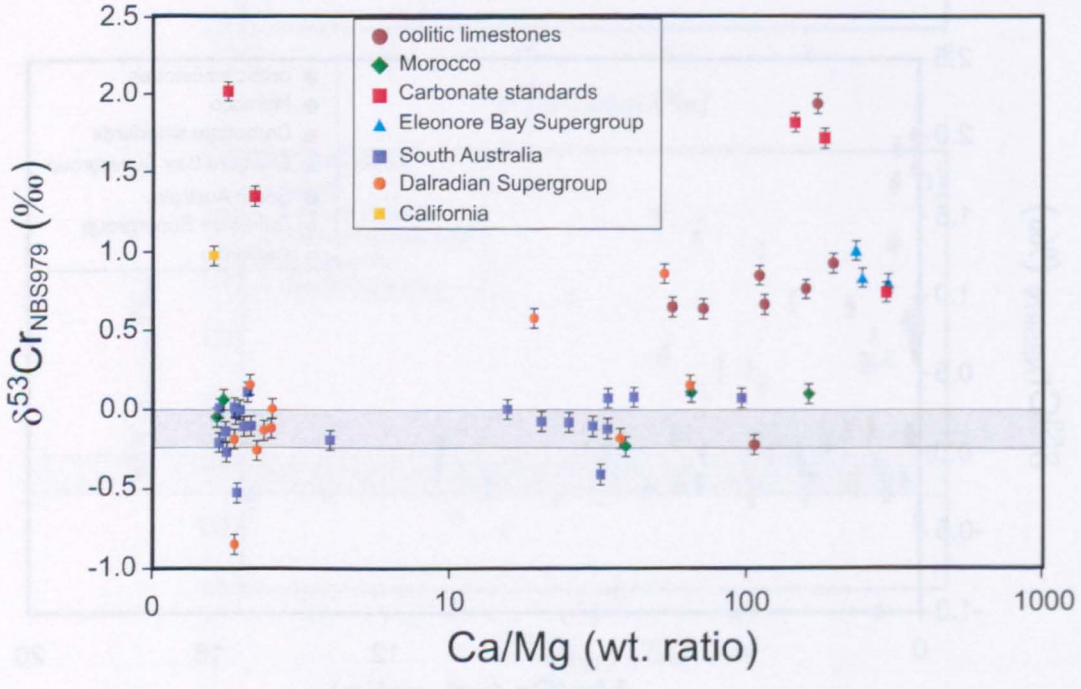

Figure 6.7: δ^{53}Cr versus Ca/Mg ratio for all of the carbonates analysed in this study. The grey shaded area represents the range in δ^{53}Cr measured for the bulk silicate Earth (Schoenberg et al., 2008).

whereas a third sample (A6) appears red in hand specimen, and is considered to be oxidised. The drill core sample has slightly higher δ^{53}Cr (-0.003‰) compared to the two relatively fresh outcrop samples (-0.201 to -0.113‰), but all samples are within the range determined for the Nuccaleena formation (-0.201 to -0.003‰). However, the obviously weathered sample has lower δ^{53}Cr, -0.529‰. This suggests that Cr isotopes are fractionated during oxidative weathering, with preferential retention of the lighter isotopes in the weathered residue. This is consistent with high δ^{53}Cr measured in groundwaters (Izbicki et al., 2008) and seawater (this study). For this reason, only samples that did not show any evidence for subaerial weathering in hand specimen were analysed in this study.

6.3.2 Sources of contamination

6.3.2.1 Detrital material

Some of the carbonates analysed in this study show evidence for contamination with detrital material (Chapter 4). The effects of this on the Cr isotopic composition of the carbonates can be assessed by comparing δ^{53}Cr with Cr and Th concentration (Fig. 6.8). Figure 6.8 reveals that samples with high Th (and high Cr) have δ^{53}Cr values similar to that of the continental crust value. This suggests that carbonates with high Th are unlikely to record the Cr isotopic composition of seawater. Samples with Th concentrations of > 1.5 ppm are considered to be contaminated by detrital components.

6.3.2.2 Hydrothermal fluids

One of the key questions regarding the seawater Cr budget is the importance of hydrothermal fluids. The Cr concentration of hydrothermal fluids is thought to be higher than that of seawater (Sander and Koschinsky, 2000), so hydrothermal fluids may have a major role in the modern Cr cycle. In this connection, inputs of hydrothermal fluids to seawater may have been higher in the past than they are today (e.g. Canfield, 2004). The size of the Eu anomaly in carbonates makes it possible to assess the influence of hydrothermal inputs. Some of the carbonates analysed in this

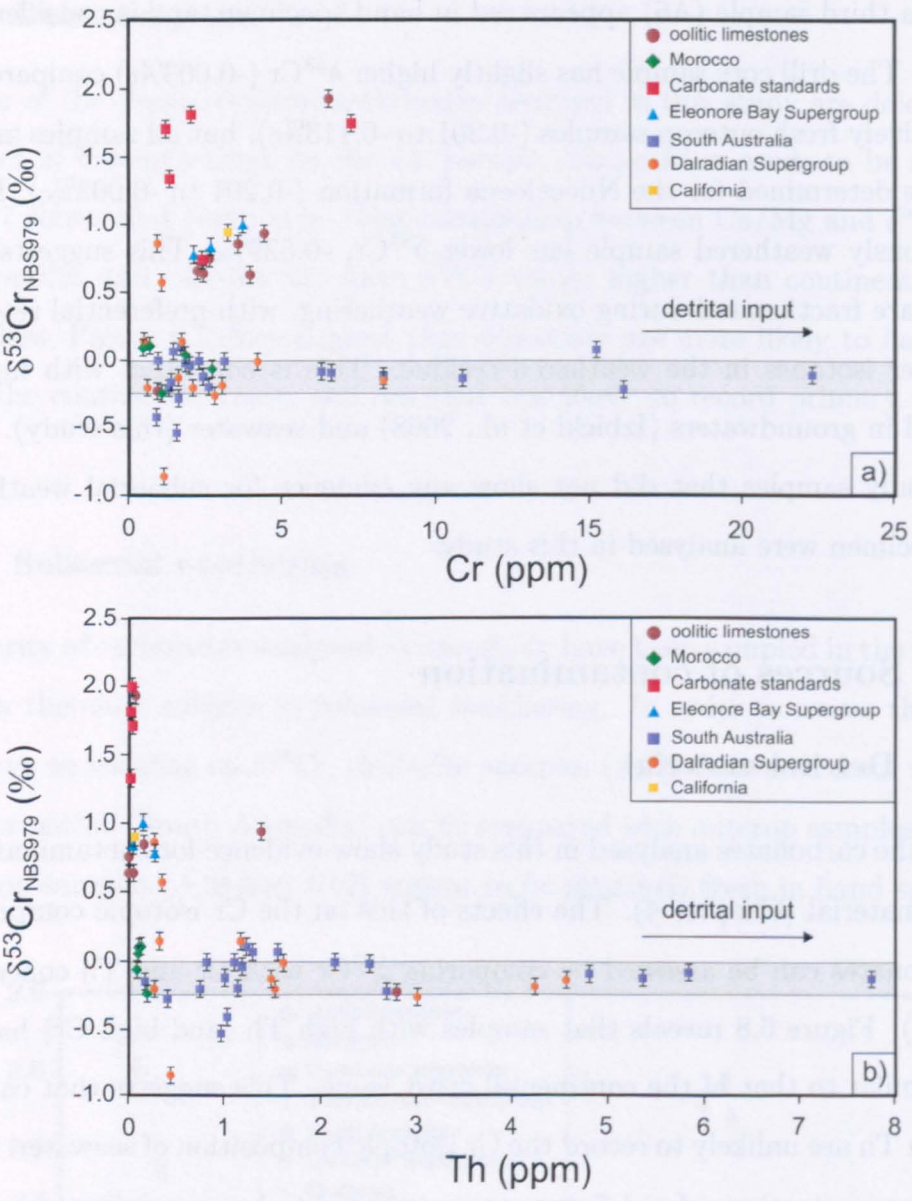

Figure 6.8: δ^{53}Cr versus (a) Cr and (b) Th concentration for all of the carbonates analysed in this study. The grey shaded area represents the range in δ^{53}Cr measured for the bulk silicate Earth (Schoenberg et al., 2008).

study have a relatively large positive Eu anomaly (>1.5), and these are thought to have been contaminated by hydrothermal fluids. The effect of hydrothermal input on δ^{53}Cr is assessed by comparing δ^{53}Cr with the Eu anomaly in Figure 6.9. Samples with a Eu anomaly of >1.5 all have the same δ^{53}Cr value as bulk silicate Earth. Thus, only samples with Eu/Eu* <1.5 are considered to record the Cr isotopic composition of seawater. It is however important to note that the lack of Eu anomaly does not necessarily indicate the absence of any hydrothermal inputs, because diffuse (low

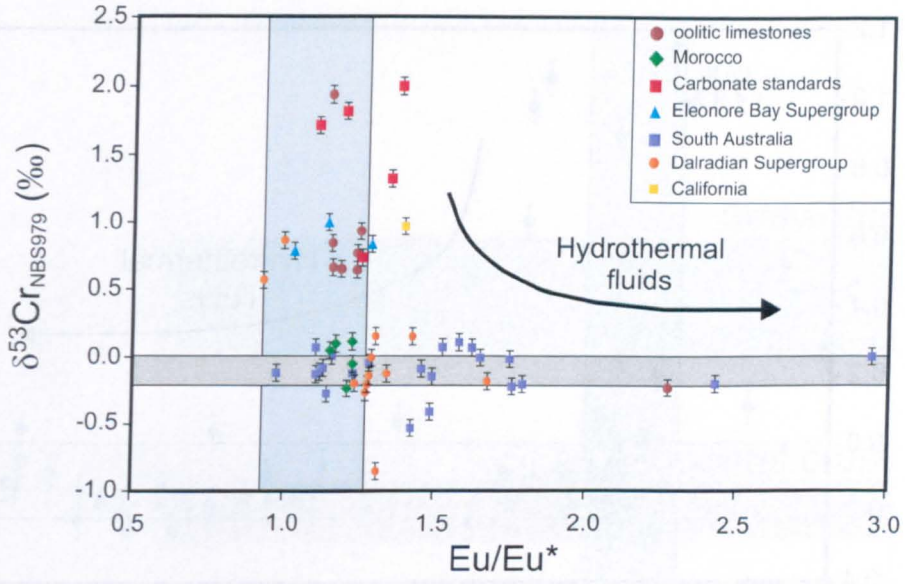

Figure 6.9: δ^{53}Cr versus Eu/Eu* for all of the carbonates analysed in this study. The grey shaded area represents the range in δ^{53}Cr measured for the bulk silicate Earth (Schoenberg et al., 2008), and the blue shaded area represents the range of Eu/Eu* found in modern seawater.

temperature) hydrothermal fluids do not have a positive Eu anomaly (Olivarez and Owen, 1991), yet they may contain significantly higher Cr than seawater (up to ~50 nM; Sander and Koschinsky, 2000).

Figure 6.9 implies that the δ^{53}Cr value of hydrothermal fluids is the same as the crust/mantle value, meaning that Cr is not fractionated by high temperature processes occurring in hydrothermal systems. BIFs also seem to show the same relationship between δ^{53}Cr and the Eu anomaly (Fig. 6.10). Thus, many of the BIF samples analysed by Frei et al. (2009) are likely to contain a hydrothermal component.

6.3.3 Relationship between δ^{53}Cr and redox conditions

6.3.3.1 Cr isotopic composition of modern carbonates deposited under oxic conditions

The four modern carbonate samples all have positive δ^{53}Cr values (0.640 to 0.765‰). None of these samples have experienced significant alteration, and their δ^{53}Cr values are within the range of modern seawater (Chapter 3). One of the aims of this study

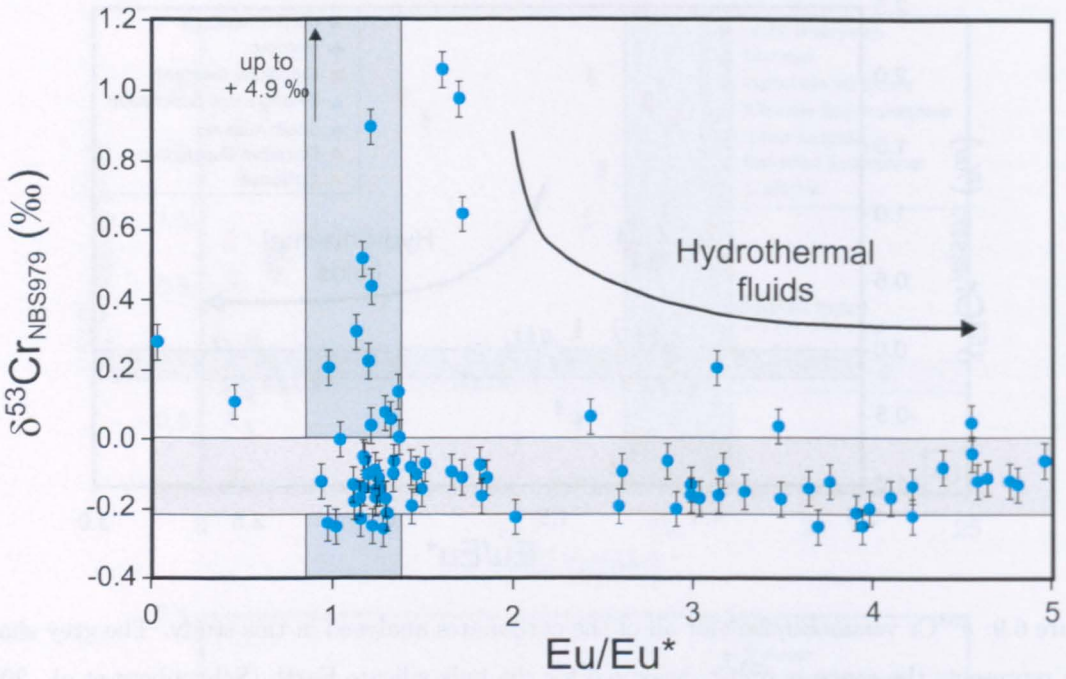

Figure 6.10: δ^{53}Cr versus Eu/Eu* for Precambrian BIFs (Frei et al., 2009). The grey shaded area represents the range in δ^{53}Cr measured for the bulk silicate Earth (Schoenberg et al., 2008), and the blue shaded area represents the range of Eu/Eu* found in modern seawater.

is to assess whether the Cr isotopic composition of modern seawater is recorded by modern carbonates, because Cr isotopes could be fractionated from seawater values during carbonate precipitation. However, initial indications are that this fractionation is negligible. Crucially, analyses of the Cr isotopic composition of seawater (Chapter 3) indicate that δ^{53}Cr values of total Cr ($\delta^{53}Cr_{TOT}$) vary from $+0.55 \pm 0.75$‰ in the open ocean, and are ~1.55‰ in coastal seawater. Although no conjugate samples of seawater and marine carbonates were collected in this study, the δ^{53}Cr values of the modern ooids (Table 6.1) are within the range of modern seawater (Fig. 6.11). Thus, these initial data suggest that the carbonate record could be used to reconstruct the Cr isotopic composition of the past ocean. Nevertheless, more work needs to be done to confirm this, including laboratory studies of Cr isotope behaviour during the precipitation of carbonate.

The Cr isotopic composition of modern seawater is determined by the balance between riverine, hydrothermal, dust, groundwater and benthic input fluxes (Table 6.4):

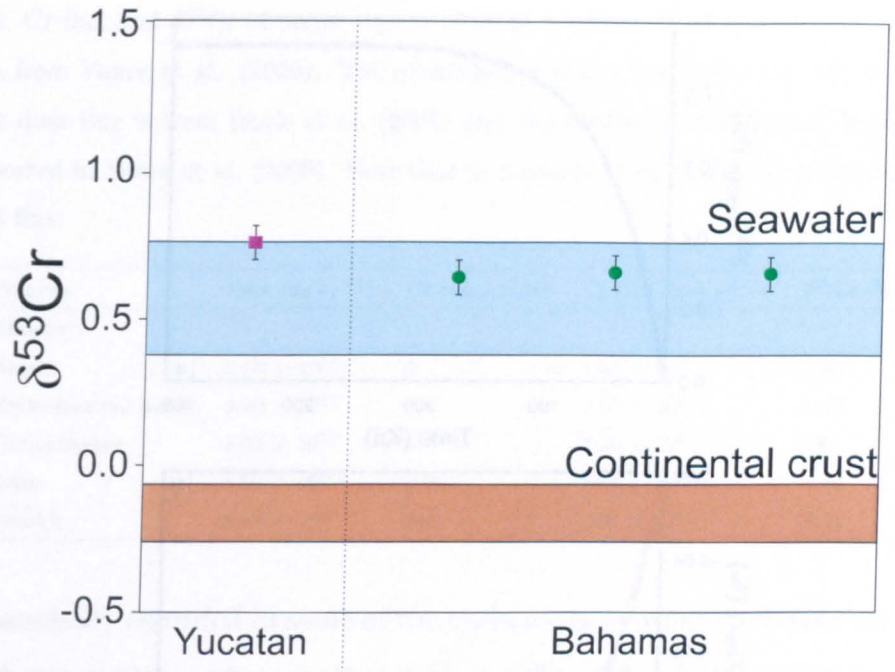

Figure 6.11: Cr isotopic composition of four modern ooids from Yucatan (purple square) and the Bahamas Bank (green circles). The blue area shows the range of δ^{53}Cr values for total Cr ($\delta^{53}Cr_{TOT}$) measured in the Argentine Basin seawater samples. Seawater samples from Southampton Water have $\delta^{53}Cr_{TOT} = +1.55‰$. The brown area shows the continental crust value form Schoenberg et al. (2008).

$$\delta^{53}Cr = \frac{f_R \times \delta^{53}Cr_{rivers} + f_H \times \delta^{53}Cr_{hydro} + f_D \times \delta^{53}Cr_{dust} + f_B \times \delta^{53}Cr_{benthic}}{f_R + f_H + f_D + f_B} \quad (6.1)$$

where f_R, f_H, f_D and f_B are the rivers, the hydrothemal, the dust and the bethic fluxes respectively. The evolution of seawater δ^{53}Cr is shown in Figure 6.12a; this model assumes that the Cr concentration of seawater is 5 nM, and the δ^{53}Cr value of the output flux is the same as seawater (i.e. Cr isotopes are not fractionated as Cr is removed from seawater). Over time, the Cr isotopic composition of seawater evolves from δ^{53}Cr equal to the continental crust value, to a value that is close to that of the riverine input (Fig. 6.12a). According to this model, the residence time of Cr in seawater is 45,000 years, which is close to that estimated by Broecker and Peng (1982) and Whitfield and Turner (1987) (10,000 - 40,000 yrs).

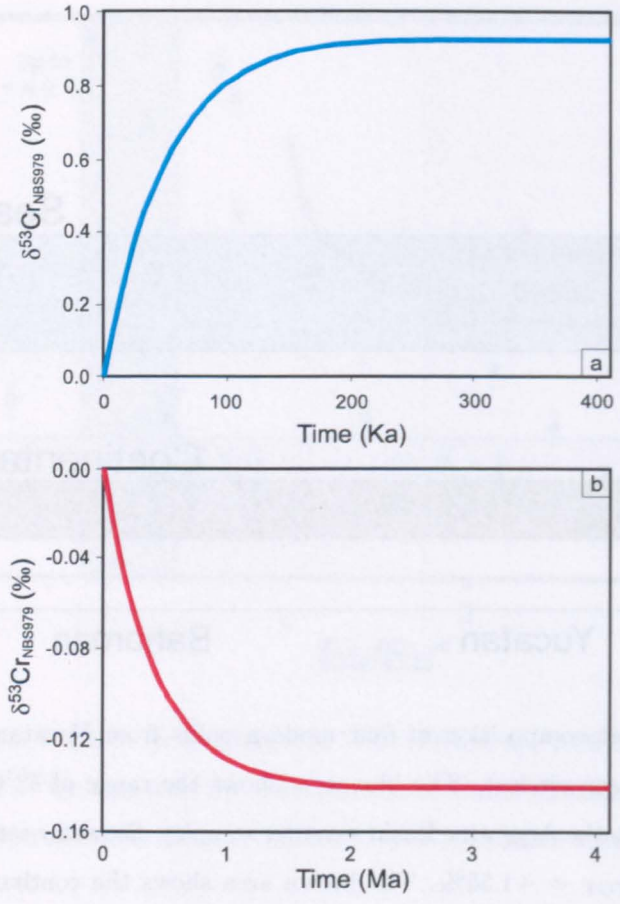

Figure 6.12: Models of the evolution of seawater δ^{53}Cr in (a) the modern ocean, and (b) during a glacial period. See text for details.

6.3.3.2 Cr isotopic composition of Phanerozoic carbonates

The Phanerozoic carbonates have δ^{53}Cr in the range 0.737 to 1.994‰; i.e. most samples have higher δ^{53}Cr than the modern ooids and the seawater samples analysed in this study (Chapter 3). The generally higher δ^{53}Cr values may indicate that the Phanerozoic carbonates were deposited in deeper waters; note that deeper waters tend to have higher δ^{53}Cr (see Chapter 3). It is also possible that the difference in δ^{53}Cr is due to a change in the operation of the seawater Cr cycle during the Phanerozoic, for example, a change in the balance between the different input fluxes. Importantly, the level of oxygen in the atmosphere during the Phanerozoic is believed to have been high (although highly variable; Holland, 2006), so oxidative weathering was always present. Interestingly, the Cr isotopic composition of the Phanerozoic carbonates is negatively correlated with the Ce anomaly (Fig. 6.2c). The large

Table 6.4: Cr flux and δ^{53}Cr of major inputs of Cr to seawater. The riverine and hydrothermal fluxes are from Vance et al. (2009). The groundwater flux is assumed to be 8% of the riverine flux. The dust flux is from Boyle et al. (2005) and the benthic flux is derived from benthic Sr fluxes reported in Vance et al. (2009). Note that in a steady state model the input flux equal the Cr output flux.

Sources	Flux (kg yr^{-1})	Cr conc. (nM)	Cr flux (mol yr^{-1})	δ^{53}Cr (‰)
Inputs				
Rivers	2.40×10^{16}	5	1.20×10^{8}	0.95
Hydrothermal fluids	3.00×10^{12}	50	1.50×10^{5}	-0.15
Groundwater	1.92×10^{15}	5	9.59×10^{6}	1.91
Dust	4.50×10^{11}	1930	8.65×10^{5}	-0.13
Benthic	3.40×10^{9}	38.5	9.59×10^{6}	-0.13

negative anomaly recorded in some of the carbonates is usually interpreted to reflect long-lived oxic systems, where cycling of Mn and Fe oxides drives oxidation of Ce(III) to Ce(IV), producing Ce depleted seawater over time. This suggests that high δ^{53}Cr values correspond to sustained oxic conditions in shallow seawater.

6.3.3.3 Cr isotopic composition of Neoproterozoic carbonates

The δ^{53}Cr values of the Neoproterozoic carbonates analysed in this study range from -0.8 to +0.9‰. However, some of these samples are clearly affected by post-depositional alteration and/or contamination (Tables 6.2 and 6.3). Samples considered to be "pristine" have δ^{53}Cr values from -0.2 to +1.0‰. Although the oolitic limestones from Eleonore Bay and Islay have high δ^{53}Cr (+0.571 to 1.004‰), the majority of the Neoproterozoic carbonates have δ^{53}Cr values close to the continental crust value. The carbonates deposited in a shallow marine environment (i.e. oolitic limestones) have high δ^{53}Cr, similar to modern ooids. This suggests that oxidative weathering was supplying Cr(VI) to the oceans at this time and the surface oceans were oxygenated. This is in agreement with data from BIFs in the Neoproterozoic that recorded positive δ^{53}Cr values (Fig. 6.1; Frei et al., 2009). Carbonates deposited in deeper seawater (such as the Nuccaleena formation, Dyson, 1992) tend to have lower δ^{53}Cr values, suggesting that the Neoproterozoic ocean was stratified in terms of Cr isotopes. It has been postulated that the deep Neoproterozoic ocean was ferruginous (Li et al., 2010) and, in this connection, it should be noted that

the Fe concentration of the Neoproterozoic carbonates is greater than it is in the modern carbonates (Appendix C). A Fe(II) rich ocean will have a strong influence on the Cr budget in the ocean. The Cr in hydrothermal fluids precipitates almost instantaneously with Fe oxides in the modern oxidised ocean (Jeandel and Minster, 1984). However, in a ferruginous ocean, the Cr is likely to remain in the dissolved phase, increasing the Cr concentration in deep water. As hydrothermal fluids are likely to be characterised by mantle δ^{53}Cr values, the δ^{53}Cr value of ferruginous seawater is likely to be lower than it is today.

Secondly, the variation in the δ^{53}Cr values of the Neoproterozoic carbonates could be due to changes in the level of seawater oxygenation at this time. The evolution of atmospheric oxygen, the Cr isotopic composition and Ce anomaly of carbonates, are shown in Figure 6.13. Most of the carbonates do not have a strong negative Ce anomaly, suggesting that most of the carbonates were deposited in environments with low oxygen. The δ^{53}Cr values of the Neoproterozoic are generally close to the continental crust value, but there is a notable shift to high δ^{53}Cr values, at least in oolitic limestones, just prior to the first Cryogenian glaciation (C1). These heavy isotopic compositions are similar to the δ^{53}Cr value recorded in BIFs for the same period (Fig. 6.13). This suggests that at the beginning of the Cryogenian there was enough oxygen in the atmosphere to produce Cr(VI) and allow Cr isotopes to be fractionated by oxidative weathering. However, throughout the remainder of the Neoproterozoic, carbonates have δ^{53}Cr values that are close to those of the continental crust. This may suggest that oxygen concentrations decreased after the first Cryogenian glaciation, although Frei et al. (2009) report high δ^{53}Cr values for BIFs deposited after the Gaskiers glaciation.

Shifts in the δ^{53}Cr value of the carbonates could also be due to a change in the operation of the Cr cycle. During glacial periods, the riverine input to the oceans is likely to be strongly reduced. The effect of this on the Cr isotope composition of the oceans is explored in Fig. 6.12b. In this case, deep waters are considered to be ferruginous and the input/output fluxes of Cr are given in Table 6.5. In this glacial ocean, the residence time of Cr (400,000 yrs) is approximately an order of magnitude higher than it is today, because input fluxes of Cr to the ocean were reduced.

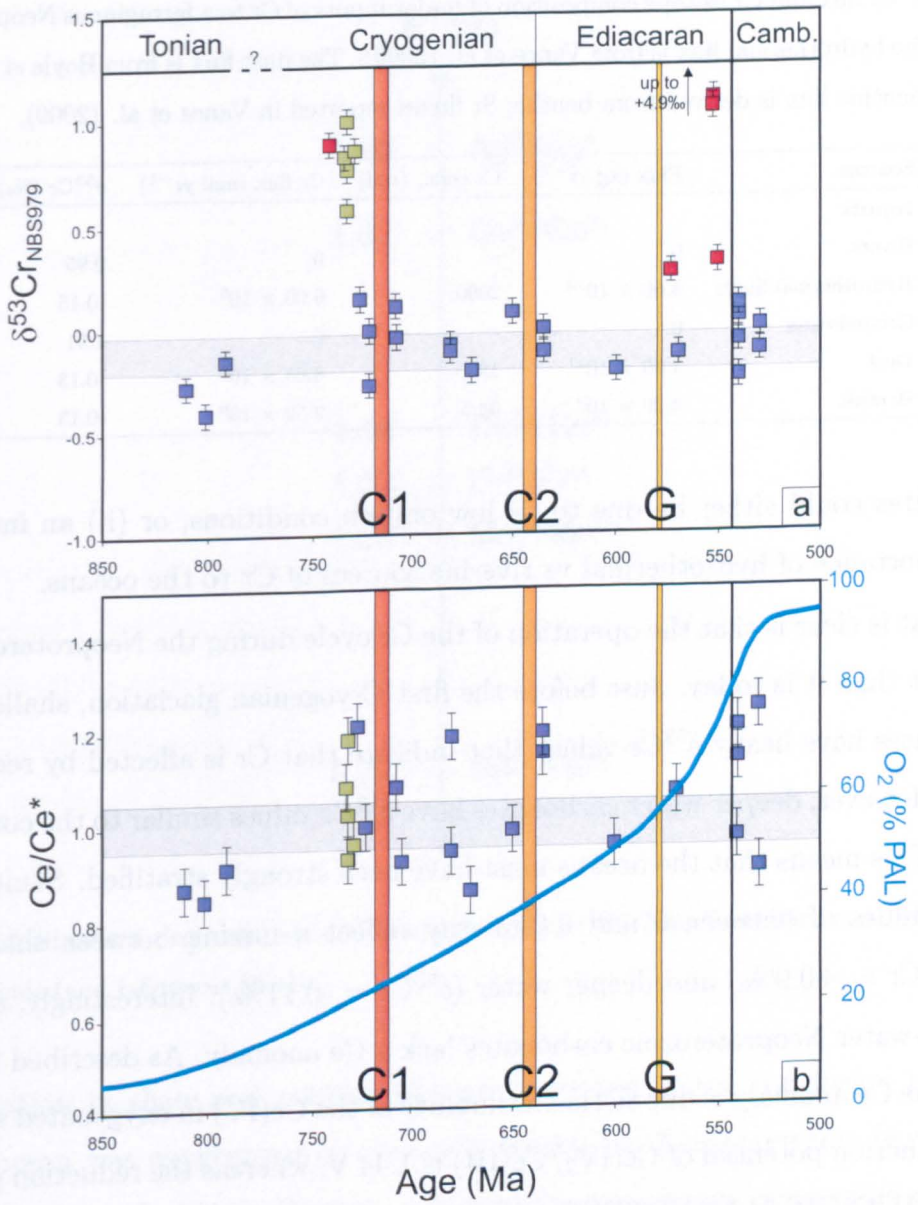

Figure 6.13: Variation of (a) the Cr isotopic composition and (b) the Ce anomaly of carbonates through the Neoproterozoic. The verticals bars represent the main Neoproterozoic glaciations; the horizontal bars in (a) and (b) represent the Cr isotope composition of bulk silicate Earth and no Ce anomaly respectively. The green squares are the oolitic limestones form Greenland and Islay, the purple squares are Neoproterozoic carbonates analysed in the study and red squares are Neoproterozoic BIFs with $Eu/Eu^* < 1.5$ (Frei et al., 2009). The blue line shows the putative evolution of atmospheric O_2, after Holland (2006).

The increased importance of the hydrothermal flux, relative to the riverine flux, shifts the Cr isotope composition of seawater towards the continental crust value (about -0.14‰). Thus, the light isotopic composition of most of the Neoproterozoic

Table 6.5: Cr flux and Cr isotope composition of major inputs of Cr to a ferruginous Neoproterozoic ocean. The hydrothermal flux is from Vance et al. (2009). The dust flux is from Boyle et al. (2008) and the benthic flux is derived from benthic Sr fluxes reported in Vance et al. (2009).

Sources	Flux (kg yr^{-1})	Cr conc. (nM)	Cr flux (mol yr^{-1})	$\delta^{53}Cr$ (‰)
Inputs				
Rivers	0	-	0	0.95
Hydrothermal fluids	3.00×10^{12}	2000	6.00×10^{6}	-0.15
Groundwater	0	-	0	1.91
Dust	4.50×10^{11}	1930	8.65×10^{5}	-0.13
Benthic	3.40×10^{9}	38.5	9.59×10^{6}	-0.13

carbonates could either be due to (i) low oxygen conditions, or (ii) an increase in the importance of hydrothermal vs riverine sources of Cr to the oceans.

What is clear is that the operation of the Cr cycle during the Neoproterozoic was different than it is today. Just before the first Cryogenian glaciation, shallow-water carbonates have heavy $\delta^{53}Cr$ values that indicate that Cr is affected by redox reactions. However, deeper water carbonates have $\delta^{53}Cr$ values similar to the continental crust. This means that the oceans must have been strongly stratified. Samples with $\delta^{53}Cr$ values of between 0 and 0.2‰ may reflect a mixing between shallow water ($\delta^{53}Cr$ = +0.9‰) and deeper water ($\delta^{53}Cr$ = -0.11‰). Interestingly, all of the shallow-water Neoproterozoic carbonates lack a Ce anomaly. As described in Chapter 4, the Ce anomaly is due to the insolubility of the Ce(IV) in oxygenated seawater. The reduction potential of Ce(IV)/Ce(III) is 1.44 V, whereas the reduction potential of Cr(VI)/Cr(III) is 1.33 V (Fig. 6.14). This means that Cr is oxidised before Ce. Thus, during the Cryogenian, the redox conditions in the atmosphere-ocean system were high enough to produce Cr(VI), but not high enough to produce Ce(IV).

6.3.3.4 Implications for the O_2 concentration of the atmosphere during the Neoproterozoic

There is a general consensus that the deep ocean was anoxic and ferruginous until the end of the Neoproterozoic (Canfield et al., 2008). Some areas of the continental shelf might have been euxinic, although global euxinia is thought not to be a feature of the Neoproterozoic ocean (Li et al., 2010). On the other hand, studies of Mo

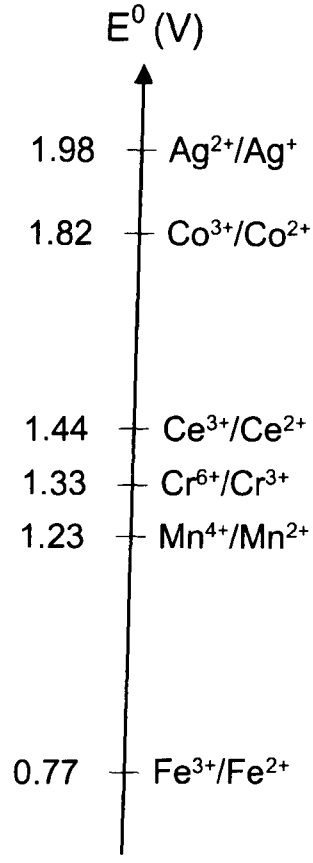

Figure 6.14: Standard electrode potentials for selected elements. Data from Bard et al. (1985) and WebElements (and references therein).

concentration in shale and sulphur isotopes have led to the conclusion that the surface ocean was oxygenated or even oxic during the Neoproterozoic (e.g. Scott et al., 2008, Li et al., 2010). However, all of the Neoproterozoic carbonates analysed in this study lack a Ce anomaly, which suggests that shallow waters must have been poorly oxygenated. Crucially, the Cr isotopic composition of the carbonates indicates that the level of oxygen in the atmosphere was high enough to produce Cr(VI), so the shallow waters could not have been anoxic. If speculation that shallow waters were ferruginous during the Tonian period is correct (Johnston et al., 2010), this means that levels of atmospheric oxygen must have risen between the Tonian and the Cryogenian. This observation is in agreement with the Canfield model which suggests oxygentaed shallow waters during the Neoproterozoic (Canfield et al., 2008). Changes in the oxygenation of seawater during the Neoproterozoic can be modelled as follows. At the start of the Tonian period, both shallow and deep

waters are assumed to be anoxic and ferruginous (Johnston et al., 2010). Then, the oxygen concentration of the shallow oceans is assumed to increase as the O_2 concentration in the atmosphere increases through the Neoproterozoic (Fig. 6.13). The parameters that control the level of seawater oxygenation, and the depth of oxygen penetration from the atmosphere into seawater, can be expressed in terms of an advection-diffusion-reaction model:

$$\frac{\partial C}{\partial t} = 0 = K\frac{\partial^2 C}{\partial z^2} - w\frac{\partial C}{\partial z} + J \tag{6.2}$$

where C is oxygen concentration, z is depth (positive upward), K is the vertical turbulent diffusivity, w is the vertical velocity (positive upward) and J is the oxygen production rate (negative for consumption). The vertical turbulent diffusivity term K (m s^{-1}) and the vertical velocity term w (m^2 s^{-1}) are assumed to be 1.3 x 10^{-4} and 2.3 x 10^{-7} respectively (Craig, 1969). The equation 6.2 can be solved using an explicit finite difference method (see Fletcher, 1991). In this model, surface waters are assumed to be in equilibrium with atmospheric O_2, and deep waters have a constant dissolved Fe concentration. Oxygen is consumed as O_2 is reduced and Fe^{2+} is oxidised; this reaction is assumed to be instantaneous and stoichiometric. Although the supply of Fe to deep waters has almost certainly varied during the course of the Neoproterozoic, it is likely to have remained constant in the early stages of oxygenation.

In the first case (Fig. 6.15a), deep waters (>100 m) are assumed to have a constant Fe concentration of 150 μmol l^{-1}, while the level of atmospheric O_2 is in the range 10 - 250 μmol l^{-1}. At steady state, the model shows that if atmospheric O_2 is low (10 μmol l^{-1}), only the uppermost 5 m of the water column is oxygenated; below this depth, the water column remains anoxic and ferruginous. However, as atmospheric O_2 increases, the depth of oxygen penetration increases, reaching 60 m for an O_2 concentration of 250 μmol l^{-1} (i.e. 100% PAL).

In the second case (Fig. 6.15b), the level of atmospheric O_2 remains constant (25 μmol l^{-1}; or 10% PAL), while the concentration of dissolved Fe in the deep water varies from 50 to 250 μmol l^{-1}. The depth of the anoxic-oxic boundary shifts as

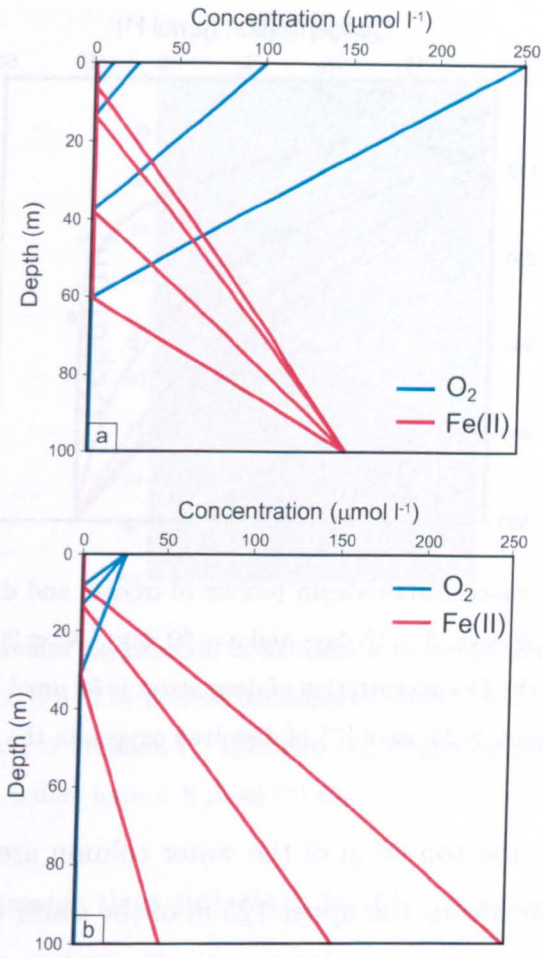

Figure 6.15: Variation in concentrations of oxygen and dissolved Fe with depth in the oceans (a) as a function of the level of atmospheric O_2 and (b) as a function of the concentration of dissolved Fe in deep (>100 m) waters. Note that the models have been run to steady-state.

a function of the dissolved Fe concentration of deep water: if the Fe concentration is 250 μmol l^{-1}, then the boundary is at 8 m water depth, whereas if the Fe concentration is 50 μmol l^{-1}, the boundary occurs at ~30 m water depth. Thus, the higher the concentration of dissolved Fe in the deep waters, the thinner the surface oxygenated layer. The evolution of seawater oxygenation is considered in Figure 6.16. In this case, the Fe concentration of deep waters (>500 m) is 50 μmol l^{-1} and the oxygen concentration of seawater in equilibrium with the atmosphere is 25 μmol l^{-1}. In this scenario, the model reaches steady state after about 20 days; note that this time scale is a function of the ratio of diffusion to advection, rather than the kinetics of Fe oxidation. The model shows that after 1 day, the top 40 m of the water column are oxygenated and, below this depth, the Fe concentration increases

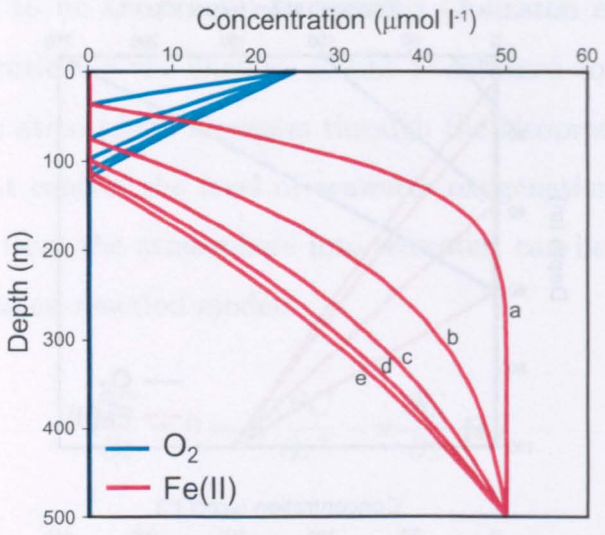

Figure 6.16: Evolution of concentration-depth profiles of oxygen and dissolved Fe in seawater. a = 1 day, b = 5 days, c = 10 days, d = 15 days and e = 20 days. After 20 days, the profiles reach a steady-state. In this run, the Fe concentration of deep water is 50 μmol l^{-1}, and the concentration of oxygen in surface seawater is 25 μmol l^{-1} of dissolved oxygen in the surface water.

rapidly. After 5 days, the top 80 m of the water column are oxygenated. After 20 days, steady state is attained: the upper 125 m of the water column are oxygenated and, below this depth, the Fe concentration increases slowly to the deep water value at 500 m.

The models reveal that if the level of oxygen in the atmosphere is low, oxygen only penetrates a few metres into the surface of the oceans. Additionally, the presence of O_2 in seawater does not necessarily indicate fully oxic conditions in the water column (Fig. 6.17). For example, if the deep ocean is ferruginous, with a dissolved Fe concentration of 100 μmol l^{-1}, and the atmospheric O_2 concentration is 25 % PAL, then oxygen penetrates ~35 m into the water column. However, the concentration of oxygen in seawater is very low, between 1 and 65 μmol l^{-1}, which means that the surface layer is suboxic to dysoxic (Chapter 1). If the atmospheric oxygen concentration is 40 % PAL, then only the uppermost 5 m of the water column is fully oxic. The oxic layer depth increases to ~30 m for atmospheric O_2 concentrations of 75% PAL.

Thus, the model demonstrates that although surface waters can be weakly oxygenated at low levels of atmospheric O_2, they can only be fully oxic if the level

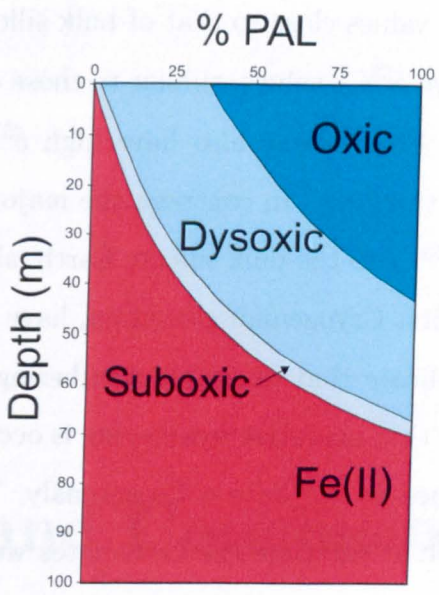

Figure 6.17: Profiles of seawater oxygenation in an ocean with ferruginous deep water as a function of the level of atmospheric O_2. The present atmospheric level (PAL) of oxygen is equal to 250 μmol l^{-1}. Oxic waters have $>$ 90 μmol l^{-1} dissolved O_2, dysoxic waters have between 9 and 90 μmol l^{-1} O_2, and suboxic waters have $<$ 9 μmol l^{-1} O_2.

of atmospheric O_2 is greater than 40% PAL. In this connection, the positive δ^{53}Cr values recorded by some of the Neoproterozoic carbonates analysed in this study indicates that levels of atmospheric O_2 were high enough for oxidative weathering on the continents, but the lack of a Ce anomaly indicates that surface seawater must have been only weakly oxygenated, i.e dysoxic or suboxic. This new result suggests that shallow waters were still not fully oxidised at the start of the Cryogenian, and that the oxygen concentration in the atmosphere was unlikely to have been higher than 30-40% of the PAL at that time.

6.4 Conclusions

Analyses of trace element concentrations and the oxygen, carbon and Cr isotopic composition of modern, Phanerozoic and Neoproterozoic carbonates suggests that some have been affected by post-depositional alteration or contamination, whereas others have not and can be expected to record the δ^{53}Cr composition of ancient seawater. Samples that show evidence for post-depositional alteration or contami-

nation tend to have δ^{53}Cr values close to that of bulk silicate earth.

Modern ooids have positive δ^{53}Cr values, similar to those of modern seawater. Carbonates deposited in the Phanerozoic also have high δ^{53}Cr, consistent with oxic conditions in seawater at this time. In contrast, the majority of the Neoproterozoic carbonates have similar δ^{53}Cr to the bulk silicate Earth, although some samples, deposited just prior to the first Cryogenian glaciation, have positive δ^{53}Cr. Low δ^{53}Cr values are thought to indicate that oxidative weathering of Cr is absent, whereas high δ^{53}Cr values suggest that oxidative weathering is occurring. However, the samples with high δ^{53}Cr values do not have a Ce anomaly. This suggests that surface waters were not fully oxic at the time the carbonates were deposited; rather, they were suboxic or dysoxic.

Chapter 7

Summary and Conclusions

The oxygen concentration of the atmosphere is believed to have increased during the Neoproterozoic, and this is thought to have resulted in changes in redox conditions in the Neoproterozoic oceans. Models developed to explain the redox conditions in the ocean during this Era generally agree that deep waters were ferruginous (Chapter 1). However, little is known about the redox conditions in shallow waters. The aim of this study is to better understand redox conditions in shallow seawater during the Neoproterozoic, by analysis of the REE concentration and Cr isotopic composition of carbonates. Cr is a redox sensitive element and its isotopes are fractionated during redox reactions. For this reason, Cr isotopes should be an effective tracer of redox conditions in the both modern and ancient oceans.

The concentration of Cr in carbonates is relatively low (<3 ppm), so measurement of Cr isotopes in carbonates was not possible using pre-existing techniques. Therefore, a new methodology has been developed for Cr isotopic analysis in low concentration samples using double-spike MC-ICP-MS techniques. These techniques have been used to determine the Cr isotopic composition of modern, Phanerozoic and Neoproterozoic carbonates, as well as the Cr isotopic composition of modern seawater, for the first time.

This chapter summarizes the key results of this work, and discusses the wider implications for the potential of Cr isotopes as a tracer of past seawater oxygenation.

7.1 Cr isotopic measurement of low concentration natural samples

A new method has been developed that allows the separation of small quantities of Cr (>250 ng) from carbonate samples using a one step column procedure. This allows precise analysis of Cr isotope ratios by MC-ICP-MS (Thermo-Fisher Neptune) using an Aridus 2 introduction system. The method uses a ^{50}Cr-^{54}Cr double spike that allows correction of mass fractionation during Cr separation and mass spectrometric analysis. The long-term reproducibility of δ^{53}Cr for a spiked NBS979 reference material is ± 0.031‰ (2 s.d., n = 147). The external reproducibility of δ^{53}Cr has been determined by multiple measurements of the JDo-1 dolomite standard reference material and is equal to ± 0.059‰ (2 s.d., n = 10). This new technique has been applied to the measurement of Cr isotopes in low-level terrestrial carbonates.

In order to measure the Cr isotopic composition of seawater samples, Cr is first preconcentrated by co-precipitation with Fe hydroxide. In order to effectively separate the Cr fraction from the Fe, a column separation procedure using an anion exchange resin was developed. Replicate analysis of a seawater samples from Southampton Water indicate that the external reproducibility of this technique is ± 0.036‰ (2 s.d., n = 4)

7.2 Cr isotopic composition of seawater

The chromium concentration and Cr isotopic composition of seawater has been determined for samples collected from (i) the Argentine Basin, and (ii) Southampton Water. The Cr concentrations are found to be higher in the open ocean (5.8-6.5 nM) than in coastal seawater (1.8 nM). In the Argentine Basin, the total Cr concentrations show little variation with depth, whereas Cr(III) is slightly depleted in shallow water. This may indicate that Cr(III) is consumed by biological activity. Surprisingly, Cr(III) is found to be the dominant species in both the open ocean and coastal seawater. The reason for the presence of unexpected Cr(III) could be

an artefact from the Fe co-precipitation procedure, or differences in the kinetics of oxidation and reduction reactions in the water column. In the case of Southampton Water, the presence of high levels of Cr(III) concentration could be due to the increased influence of riverine inputs and/or anthropogenic Cr.

The Cr isotopic composition of seawater from the Argentine Basin samples range from -0.116 to +0.793‰. Interestingly, the δ^{53}Cr value of total Cr is higher than that of the continental crust (-0.12 ± 0.11‰, Schoenberg et al., 2008). As rivers are the most important source of Cr to the oceans (Jeandel and Minster, 1987), this implies that rivers have high δ^{53}Cr. This is consistent with analyses of oxic groundwaters (Izbicki et al., 2008). The δ^{53}Cr value of Cr(III) in the sample collected from closest to the sea surface in the Argentine Basin is -0.116‰, which is close to the continental crust value. This suggests that dust is an important source of Cr(III) in the surface ocean.

The Cr isotopic composition of the Southampton Water samples ranges from 1.543 to 1.748‰. These δ^{53}Cr values are all heavier than the continental crust value. In this case, differences in the δ^{53}Cr value of Cr(III) and total Cr cannot be explained by reduction of Cr(VI) to Cr(III), as the δ^{53}Cr value of Cr(III) is higher than the δ^{53}Cr value of total Cr. This may indicate that the Cr isotopic composition of Southampton Water is influenced by input of Cr(III) from rivers, or from input of anthropogenic Cr.

7.3 Cr isotopic composition of carbonates

Modern ooids from the Bahamas Bank and from Yucatan have δ^{53}Cr values ranging from 0.55 to 0.73‰. These δ^{53}Cr values are within the range of seawater, as determined for the first time as part of this study. Although analysis of paired seawater and carbonate samples was not possible, the similarity between the δ^{53}Cr values of the modern ooids and seawater implies that fractionation of Cr isotopes between seawater and carbonates is minimal, and carbonates can be used to reconstruct the Cr isotopic composition of ancient seawater.

Samples of Phanerozoic marine carbonates have been screened for potential post-

depositional alteration and/or the presence of contaminants, and all of the 'pristine' samples are characterised have heavy δ^{53}Cr values that range from 0.74-1.99‰. This is consistent with oxidative weathering on the continents at this time.

Samples of Neoproterozoic carbonates have been collected from four different locations. These have also been screened for post-depositional alteration (i.e. diagenesis and dolomitisation) and for contamination (i.e. detrital and hydrothermal phases). Samples contaminated by detrital inputs (characterised by high Th concentrations) have δ^{53}Cr values close to the continental crust, whereas samples contaminated by hydrothermal fluids (characterised by a strong positive Eu anomaly) have δ^{53}Cr close to the mantle value (-0.15 $\pm$ 0.11‰). The majority of the unaltered and uncontaminated carbonates have δ^{53}Cr values similar to that of the continental crust. However, shallow water oolitic limestones from Islay and Greenland deposited just before the first Cryogenian glaciation (~730 Ma) are characterised by positive δ^{53}Cr values (up to 1.0‰). These data suggest that the Neoproterozoic oceans were strongly stratified with respect to Cr isotopes, with a shallow surface layer with high δ^{53}Cr and a deeper layer with δ^{53}Cr close to that of the continental crust. The δ^{53}Cr value of the surface layer suggests that oxidative weathering on the continents was occurring at this time. The low δ^{53}Cr value of the deeper layer indicates input of hydrothermal Cr.

Interestingly, the six oolitic limestones that have high δ^{53}Cr do not have a Ce anomaly. This suggests that there was enough oxygen in the atmosphere during the Cryogenian to produce Cr(VI), but not enough oxygen in the water column to produce Ce(IV). To this end, a model for seawater oxygenation has been developed. This indicates that shallow waters always contain oxygen even when levels of atmospheric O_2 are very low (<20% PAL), but this layer is not fully oxic (i.e. concentrations of dissolved O_2 are less than 90 μmol l^{-1}) unless atmospheric O_2 is greater than 40-50% PAL. Thus, considered together, the Cr isotope and REE data indicate that just prior to the first Cryogenian glaciation, surface waters were either dysoxic or suboxic, but not anoxic.

7.4 Implications for the Cr cycle

Several aspects of the Cr cycle have been investigated during the course of this study, and direct or indirect estimates of the Cr isotopic composition of the different sources of Cr to the ocean have been made. This information is summarised in Figure 7.1. The Cr isotopic composition of the hydrothermal flux is likely to be close to the mantle value. The δ^{53}Cr value of the dust input to the ocean is considered to be close to the continental crust value, on the basis of analysis of the δ^{53}Cr value of Cr(III) in the surface ocean . Open ocean seawater has δ^{53}Cr up to 0.706‰, but the δ^{53}Cr of coastal seawater appears to be higher (up to 1.549‰). The seawater Cr isotopic composition is characterised by positive δ^{53}Cr values. Box modelling indicates that the Cr isotopic composition of the oceans is controlled by the δ^{53}Cr value of the riverine input.

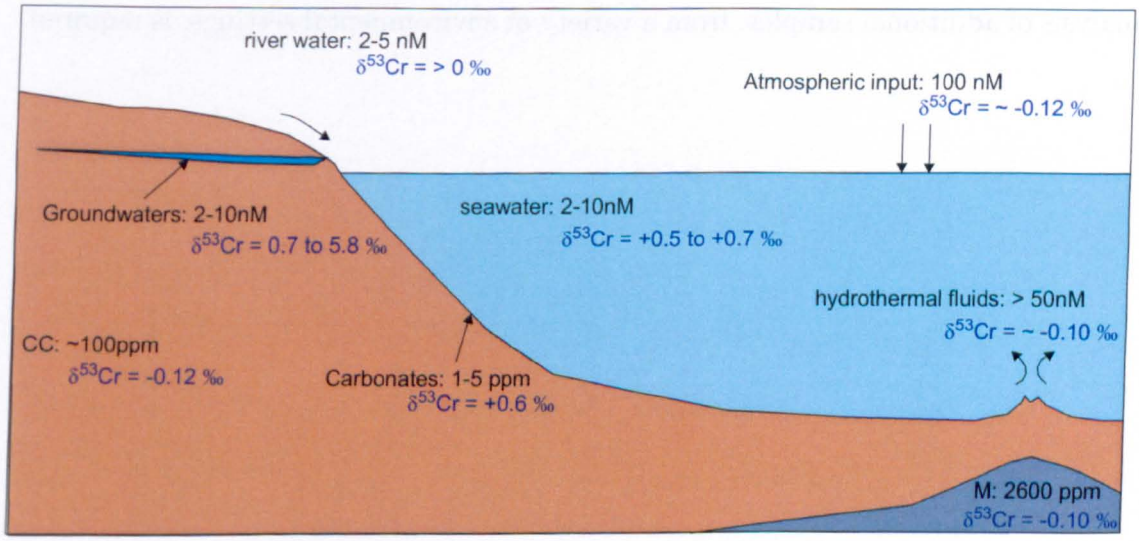

Figure 7.1: Chromium concentration and chromium isotopic composition of inputs to the modern oceans. CC is the continental crust, M is the mantle. Data are from Cranston and Murray (1980), Sander and Koschinsky (2000), Ellis et al. (2004),Schoenberg et al. (2008) and Izbicki et al. (2008) and this study. Note that only a fraction of the Cr in dust is likely to dissolve (e.g. Kieber et al., 2002).

7.5 Future work

This study has provided new insights as to the behaviour of Cr isotopes in the natural environment, and the utility of Cr isotopes as tracers of past seawater oxygenation. Aspects of this work nevertheless require additional study.

- Although this study suggests that there is limited fractionation between seawater and carbonates, it is important to properly test this by analysis of paired natural seawater and carbonate samples, and experimental studies.
- It has been postulated that the Cr budget in the ocean is strongly influenced by the riverine input and therefore studies of Cr isotopic composition of river waters is imperative to fully constrain the Cr cycle. More work on the effects of chemical weathering on Cr isotopes is also required.
- In order to provide additional constraints on redox conditions in the Neoproterozoic oceans, it would be helpful to study other redox sensitive isotope systems. For example, $\delta^{238}U$ has been showed to correlate with dissolved oxygen concentrations in modern oceans (Andersen et al., 2010).
- Finally, it is clear that the $\delta^{53}Cr$ value of seawater is variable. For this reason, analysis of additional samples, from a variety of environmental settings, is required.

Appendix A

Field localities

This appendix presents field data including sample locations and the name of the formations samples in the Adelaide rift complex (Table A.1) and in the Dalradian Supergroup (Table A.2).

Table A.1: Sample localities and formation names for the Adelaide Geosyncline Complex samples (South Australia)

Sample number	Latitude	Longitude	Formation names
A1	34° 51.332' S	138° 48.584' E	Woolshed flat Formation
A2	34° 51.363' S	138° 44.158' E	Dolomite MonteCute
A3	34° 51.561' S	138° 44.577' E	Catambul Dolomite
A4	34° 57.649' S	138° 39.109' E	Beaumont Dolomite
A5	35° 01.502' S	138° 34.376' E	Sturtian Cap Carbonate
A6	n.d.	n.d.	Nuccaleena formation
A7	35° 04.328' S	138° 30.688' E	Brighton Limestone
A8	34° 04.389' S	138° 41.787' E	Upper skillogallee Dolomite
A9	34° 02.582' S	138° 42.223' E	Auburn Dolomite
A10	32° 25.053' S	137° 58.265' E	Nuccalena Formation
A11	32° 00.392' S	138° 20.774' E	Mernmerna Formation
A12	n.d.	n.d.	Nuccalena Formation
A13	30° 36.493' S	138° 23.700' E	Skillogalee Limestone
A14	30° 31.181' S	138° 22.838' E	Balcanoona Dolomite
A15	30° 31.917' S	138° 37.830' E	Wonoka Formation
A16	30° 32.240' S	138° 37.420' E	
A17	31° 05.297' S	138° 49.213' E	Wirrapowie Limestone
A18	31° 28.894' S	138° 39.712' E	Etina Formation
A19	31° 48.932' S	138° 22.319' E	Wonoka Formation
A20	32° 10.352' S	139° 56.217' E	Umberalana Formation
A21	32° 10.402' S	139° 56.329' E	Pualco Cap carbonate
A22	31° 37.406' S	137° 33.307' E	Nuccaleena formation
A23	31° 37.479' S	137° 34.033' E	Brighton Formation (equivalent)

Table A.2: Sample localities and formation names for the Dalradian Supergroup samples

Sample number	Latitude	Longitude	Formation names
I1	55° 51.482' N	006° 06.486' W	Unit 5. Member 1
I17	55° 52.873' N	006° 07.141' W	Member 3
I20	55° 52.984' N	006° 07.244' W	Member 4
I22	55° 48.597' N	006° 07.398' W	Great Breaccia
I24	n.d.	n.d.	Disrupted beds
I24R	n.d.	n.d.	Disrupted beds
I25	55° 48.452' N	006° 07.771' W	Disrupted beds
I26	55° 48.404' N	006° 07.674' W	Islay Limestone
I27	55° 48.321' N	006° 07.404' W	Islay Limestone
I28	n.d.	n.d.	Islay Limestone
T4	55° 57.450' N	005° 42.247' W	Tayvallich Limestone
T5	55° 57.455' N	005° 42.243' W	Tayvallich Limestone
T7	55° 57.456' N	005° 42.286' W	Tayvallich Limestone

Appendix B

Analytical methods

This appendix outlines the methods used in this study for sample preparation and the chemical preparation for major and trace element analysis, carbon and oxygen isotopes analysis and Sr isotopes measurements. Details of the samples and their localities can be found in Chapter 3 and Appendix A.

B.1 Sample preparation

The whole rock samples were screened for post deposition alteration and weathered surfaces were removed with a diamond tipped saw. The samples were crushed by hand to avoid metal contamination from the jaw crusher and then grounded by hand in a ceramic pestle and mortar. Large samples were grounded in an agate ball mill. The ball mill was cleaned using quartz powder and a small amount of sample was used to pre-contaminate the ball mill prior to grinding.

B.2 Laboratory reagents and cleaning procedure

All of the acids used in this study were subject to a two steps purification procedure. Quartz distilled (QD) acid was produced by sub-boiling analytical grade acid in a quartz still. Teflon distilled (TD) acids were produced by a further thermal distillation of the QD grade acid in a Teflon still. Hydrochloric acid was thermally distilled in a "cupola" system. All the water utilised in this study was purified through a

Millipore filtration system (MQ) to a resistivity of > 18.2 MΩ.

The dissolution procedure was accomplished in pre-cleaned PFA centrifuge tubes and these tubes were cleaned as follows:

- Rinsed three times with MQ H_2O
- 50% TD HNO_3 and heated on a hotplate at 110°C overnight.
- Rinsed three times with MQ H_2O
- 50% TD HNO_3 and heated on a hotplate at 110°C overnight.
- Rinsed three times with MQ H_2O
- Dried in clean hood.

Teflon vessels were used for major and trace element analysis and Cr isotopes measurements and were cleaned as follows:

- Any previous marker pen was removed with acetone and the beakers and lid were boiled in a large beaker of 33% QD HNO_3 for at least 24 hours.
- Rinsed three times with MQ H_2O
- Add 4 ml of QD HNO_3, seal and heated on a hotplate at 130°C overnight.
- Discard the acid. Rinsed three times with MQ H_2O
- Add 4 ml of TD HNO_3, seal and heated on a hotplate at 130°C overnight.
- Discard the acid. Rinsed three times with MQ H_2O
- Left to dry in clean hood.

Plastic bottles were cleaned with weak acid (10% TD HNO_3) and leached at room temperature for at least 48 hours. The bottles were then rinsed with MQ H_2O and left to dry in a clean hood.

B.3 Major and trace elements analysis

B.3.1 Rock dissolution procedure

Rock powders (~30 mg) were leached in a PFA centrifuge tube using 8 ml of 0.5M HCl at room temperature. The leaching procedure lasted for about 24 hours. The

samples were centrifuged for 10 min at 4000 rpm. The supernatant was transferred to a cleaned PFA Savillex beaker. The residue was rinsed with 4 ml of MQ H_2O, centrifuged and the supernatant was added to the acid. The samples were dried down slowly at 110°C on a hotplate. The residue was transferred to a weighed PFA Savillex beaker and dried down. The beaker + sample was then weighed and the mass of residue was determined. The samples were dissolved in 3% TD HNO_3 and diluted by ~100 000 fold for major elements analysis and by ~2000 fold for trace element analysis.

B.3.2 Inductively coupled plasma mass spectrometry (ICP MS)

Major and trace element concentrations were determined by ICP-MS (Agilent 7500a) at the Open University. The instrument is fitted with a standard quartz spray chamber and a Babington nebuliser for major element analysis and a PFA nebuliser for trace element analysis. Analyses were standardised against at least five synthetic solutions that were measured at the beginning of each analytical run. Synthetic solutions were made in the clean lab using ultra pure multi elemental standard solutions. For major analysis, six standards were analysed: 3% HNO_3 (blank), 1 ppb, 50 ppb, 250 ppb, 1 ppm and 4 ppm. The solutions contained Na, Mg, Al, Ca, Si, Mn, Fe, Ti, K and Sr. The Sr concentration in the five standard solutions described above were 1 ppb, 2 ppb, 5 ppb, 10 ppb and 50 ppb respectively. For trace element analysis, standard solutions were made in order to match sample matrices. Two batches of standards were prepared; one for calcite samples (Ca marix) and one for dolomitic samples (Ca-Mg matrix). In each case, seven standards were prepared with concentration of 10 ppt, 50 ppt, 100 ppt, 200 ppt, 500 ppt, 1 ppb and 2 ppb. Additionally, an extra standard solution was prepared with only the elements of the matrix (Ca or Ca-Mg), to make sure that the concentrations of the trace elements was neglible in the Ca and Mg standard solutions. For the dolomitic matrix, the standards were prepared with 65 ppm Mg and 110 ppm Ca whereas for the calcite matrix, standards were prepared with 200 ppm Ca. One of the standard solutions

was analysed as an "unknown" sample every 7-8 samples together with another real sample in order to monitor instrumental drift during the run.

Carbonate standards are not well characterised, particularly for trace elements. In this study, we decided to use JDo-1 to assess both the accuracy and the precision of the utilised method. Data for JDo-1 are presented in Table B.1 with the accepted values. Overall, there is a good agreement between the data obtained in this study and the published values. Detection limits are usually < 10 ppt in solution for heavy elements (atomic masses > 85) and are slightly higher for lighter elements ($\sim$50 ppt in solution). The total reproducibility was assessed by multiple measurements of JDo-1 standards, and the 2 rsd is equal or better than 3% for the REE. For other elements, the reproducibility is slightly worse and for example the reproducibility for the Cr concentration is about 5%.

B.4 Carbon and oxygen isotopes analysis

Carbon and oxygen isotopic composition were determined by Continuous flow isotope ratio mass spectrometer (CFIRMS) at the Open University. The mass spectrometer was equipped with a robotic sampling arm as an introduction system (Thermoquest GasBench II).

The vessel used in this study was cleaned in an ultra sonic bath in MQ H_2O. The samples were initially dried in an oven overnight. About 400 μg of each sample was introduce into a sample vessel and sealed. The GasBench II then automatically flushed the samples with helium using the flushing needle to inject helium and displace the air contained above the samples. Helium is the carrier gas for the CFIRMS; it is inert and reacts with neither the sample nor the mass spectrometer. After the flushing process was complete, acid (phosphoric acid) was added to the calcium carbonate. For calcite samples, the dissolution procedure was done at 70°C whereas for dolomitic samples the temperature was fixed at 90°C. The samples were then introduced in the mass spectrometer where both oxygen and carbon isotopic composition were measured. Every 6 samples an "in house" standard was analysed associated with an international standard (NIST 19) in order to monitor

instrumental drift during the run. The carbon and oxygen isotopic compositions are reported relative to "Vienna Pee Dee Belemnite" (VPDB) using the standard notations of $\delta^{13}C$ and $\delta^{18}O$. The external reproducibility for carbon and oxygen isotopic composition ($\delta^{13}C$ and $\delta^{18}O$) was determined by multiple measurement of NIST 19 standard and is $\pm$ 0.15 ‰. The data obtained in this study are reported in Tables 5-1, 5-2 and 5-3.

B.5 Sr isotopes analysis

B.5.1 Sample preparation and chemical procedure

20 samples were analysed for Sr isotopic composition. Between 40 and 60 mg of sample powder was weighed. Samples were leached with 0.5 M HCl for about 24 hours at room temperature. Samples were then centrifuged and the acid was pipette out and placed in a clean Savillex beaker. The residue was rinsed with 4 ml of MQ H_2O and the supernatant was added to the acid. The samples were dried down slowly on the hotplate at 110°C. Sr was separated from the sample matrix using Eichrom Sr spec resin, following a modified method, based on Deniel and Pin (2001). Each batch of resin was pre-cleaned by repeating the following procedure described below 5 times:

- 250 ml 6 M HCL
- 250 ml MQ H_2O
- 250 ml 3M HNO_3
- 250 ml MQ H_2O

150 μl of resin was loaded into a pre-cleaned and fritted 1ml pipette tip. The resin and columns were then cleaned with ~1.5 ml of 6 M HCl and 3 ml of MQ H_2O. The resin was pre-conditioned with 1.5 ml of 2 M HNO_3. The samples were loaded in 1 ml of 2 M HNO_3 and washed with an additional 0.4 ml of the same acid. The column was washed with 1 ml of 7 M HNO_3 and 0.2 ml of 2M HNO_3. The Sr cut was then collected in 1 ml 0.05M HNO_3. The collected fraction was dried down slowly

on the hotplate at 110°C. At this point the samples were ready to be loaded on the Re filament. Total procedure blank is negligible (~20 pg) relative to the amount of Sr processed through the column (~500 ng). The total yield was close to 90 %.

B.5.2 Thermal ionization mass spectrometry (TIMS)

Sr isotopes were analysed at the Open University using a ThermoFisher Triton TIMS. The samples were loaded onto a degassed Re filament following the procedure described by Charlier et al. (2006). The filaments were fixed on the source magazine and introduced into the machine. Sample filaments were heated to ~1460°C and Sr beam was tuned to get a stable signal of ~8 V of ^{88}Sr. Strontium isotopes were corrected for instrumental mass fractionation using the exponential mass fractionation law and an $^{86}Sr/^{88}Sr$ ratio of 0.1194. In this study, each measurement consists of collecting 240 ratios in 24 blocks of 10 ratios, with each ratio representing 8.384 seconds of beam integration. A baseline is collected and the amplifiers are rotated before each block. An internal precision of ~10 ppm (2s.e.) was obtained and the external reproducibility of Sr measurement was assessed by multiple analysis of a standard (NIST 987) and is equal to ~15 ppm (2s.d., n = 5). The NIST 987 $^{86}Sr/^{88}Sr$ ratio measured in this study is 0.710224 ± 0.000011. The Sr data is reported in Table C.11.

Table B.1: Major and trace elements concentration for JDo-1 dolomite standard analysed in this study together with literature values (in house OU (Watson (XRF)) and Aizawa, 2008)

	JDo-1	2 s.d.	Watson (XRF)	Aizawa (2008)
%				
NaO	0.016	0.001	0.009	
MgO	18.9	0.6	18.4	
Al_2O_3	0.05	0.001	0.013	
SiO_2	0.02	0.001	0.2	
K_2O	0.05	0.001	0.002	
CaO	35.6	1.3	34.12	
TiO_2	0	0.001	n.d.	
MnO	0.01	0.001	0.006	
Fe_2O_3	0.01	0.003	0.02	
Sr (ppm)	119	6	119	
ppb				
Li	444	21	400	n.d.
Sc	89	4.5	200	130
Ti	1177	92	n.d.	n.d.
V	3336	48	n.d.	n.d.
Cr	7424	232	7000	7600
Co	85	6.9	200	14000
Ni	2028	146	2900	n.d.
Cu	1663	139	1400	n.d.
Zn	28188	698	34400	31000
Rb	54	8.4	n.d.	90
Y	9340	114	n.d.	n.d.
Zr	111	23	n.d.	n.d.
Nb	4	0.9	n.d.	n.d.
Mo	80	34	n.d.	n.d.
Cs	6	1.1	n.d.	n.d.
Ba	4992	224	n.d.	n.d.
La	7359	101	7900	7000
Ce	1946	37	3000	2300
Pr	973	13	n.d.	n.d.
Nd	3907	72	4800	n.d.
Sm	675	18	790	730
Eu	157	1.6	180	160
Gd	854	13	n.d.	n.d.
Tb	118	3.4	130	130
Dy	719	14	n.d.	n.d.
Ho	159	2.9	n.d.	n.d.
Er	443	6	n.d.	n.d.
Tm	54	0.4	n.d.	n.d.
Yb	289	8.9	310	320
Lu	39	1.7	50	n.d.
Hf	3	0.8	n.d.	13
Th	42	1	50	42
U	769	35	880	900

Appendix C

Data tables

This appendix presents the data collected for the carbonate samples, described in Chapter 4 and 5 of this thesis.

Table C.1, C.2 and C.3 presents major and trace element concentrations for the Adelaide rift complex samples (South Australia). Table C.4 and C.5 reports major and trace element concentrations for the Dalradian Supergroup samples. Table C.6 presents major and trace element concentrations for the Morrocan samples and Table C.7 reports concentrations for the Eleonore Bay Supergroup samples. Table C.8 reports the major and trace concentrtions for Indian and Californian samples. Table C.9 reports major and trace element concentrations for the modern ooids and Phanerozoic oolitic limestones analysed in this study. Finally, table C.10 reports the concentrations in the carbonate standards. The major element concentrations are presented as weight % oxides. The Sr concentration are reported in ppm and the trace element data are given in ppb. Major and trace element data were colletced by ICP-MS. The external reproducibility has been determined by multiple measurement of the JDo-1 carbonate standard and the data is reported in Appendix A.

Table C.11 reports the $^{87}Sr/^{86}Sr$ for the selected samples analysed in this study and presented in Chapter 4. Sr isotopic data were analysed by TIMS at the Open University.

Table C.1: Major and trace elements concentration for the Adelaide rift complex samples

%	A2	A3	A4	A5	A6	A7	A8	A9	A10	A11
NaO	0.11	0.03	0.12	0.09	0.10	0.23	0.03	0.04	0.04	0.19
MgO	19.19	20.91	18.84	19.37	18.70	2.74	22.08	18.75	20.01	1.86
Al_2O_3	2.81	0.12	4.93	0.44	0.52	2.28	0.09	0.30	0.17	6.34
SiO_2	0.98	0.00	1.47	0.05	0.07	0.44	0.00	0.08	0.04	1.91
K_2O	1.65	0.02	0.67	0.19	0.25	0.66	0.01	0.13	0.07	1.32
CaO	27.07	31.34	26.69	31.21	30.51	46.87	32.86	30.97	31.96	47.42
CaO	27.61	32.17	27.61	31.97	31.34	48.20	33.77	31.75	32.56	47.34
TiO_2	0.04	0.00	0.05	0.00	0.00	0.01	0.00	0.00	0.00	0.01
MnO	0.12	0.11	0.38	0.28	0.70	0.58	0.03	0.48	0.39	0.20
FeO	1.24	0.43	4.51	1.55	1.91	1.29	0.13	4.43	0.69	3.50
ppm										
Sr	339	57	481	334	126	418	648	526	97	1841
ppb										
Sc	1751	214	9697	2408	4059	8448	233	2147	1051	11943
V	4070	1192	40417	5395	3366	7557	6575	2829	2143	36192
Cr	3138	1663	16144	1998	1593	6297	1415	1891	1351	22287
Co	713	680	6291	1387	12132	3344	0	841	2118	5148
Ni	174	0	8723	4913	7189	7223	0	948	527	24506
Cu	1342	1703	7295	1781	1763	3118	971	478	20408	49317
Zn	43324	12348	51387	18530	25095	12181	6511	12675	13293	57260
Rb	29692	795	24697	2222	2597	6479	736	1538	359	9418
Y	6644	1159	14499	12661	8830	31335	1428	7358	3539	100429
Zr	3530	269	5764	4772	1721	12949	295	1329	1189	8771
Nb	197	9	11	22	28	49	3	11	5	51
Cs	1508	24	1927	56	125	201	79	30	24	237
Ba	61740	10897	177126	41008	25651	175922	19513	12938	1288705	266907
La	4382	1418	8016	5267	2217	15227	1083	2213	1868	79361
Ce	9562	3148	17851	11730	5909	41043	2709	4950	4326	186632
Pr	1343	391	2504	1830	923	5992	348	711	596	24608
Nd	5576	1481	10827	8985	4908	28790	1376	3104	2738	97956
Sm	1530	301	2946	2937	3078	8322	317	1046	902	21678
Eu	912	67	1128	756	877	1968	95	445	324	4986
Gd	1500	293	3544	3161	3431	9564	320	1516	1023	23202
Tb	238	41	577	445	465	1443	48	284	137	3550
Dy	1418	231	3269	2287	2215	7733	270	1680	692	20408
Ho	287	44	609	412	359	1416	51	315	124	3993
Er	827	124	1578	1062	856	3661	141	858	326	10585
Tm	125	17	206	138	108	489	19	121	42	1332
Yb	804	103	1227	803	651	3103	115	792	251	7602
Lu	112	14	163	111	87	449	16	112	34	987
Hf	115	8	172	69	50	519	10	45	24	343
Ta	31	0	15	0	1	26	0	3	0	93
Pb	85926	1422	17713	6832	3811	19249	1074	829	1048	53110
Th	1104	400	2688	1183	960	5837	169	2504	741	16807
U	301	27	466	1412	475	1419	97	241	270	32212

Table C.2: Major and trace elements concentration for the Adelaide rift complex samples

%	A12	A13	A14	A15	A16	A17	A18	A19	A20	A21
NaO	0.05	0.08	0.03	0.20	0.09	0.03	0.04	0.08	0.03	0.02
MgO	18.72	1.96	11.33	1.64	0.62	3.83	1.76	1.41	2.37	17.14
Al_2O_3	0.51	1.07	0.14	3.69	0.54	0.08	0.37	2.44	2.66	0.14
SiO_2	0.05	0.22	0.04	0.47	0.14	0.01	0.11	0.51	0.55	0.03
K_2O	0.17	0.05	0.07	0.46	0.17	0.05	0.13	0.45	1.64	0.08
CaO	33.76	54.04	37.56	47.18	50.79	50.37	50.64	49.45	50.25	30.29
CaO	33.97	53.66	37.70	47.41	50.16	49.81	50.59	49.15	50.19	30.44
TiO_2	0.00	0.00	0.00	0.01	0.09	0.00	0.00	0.01	0.10	0.00
MnO	0.23	0.00	0.50	0.41	0.36	0.18	0.10	0.15	0.29	0.30
FeO	0.41	0.08	4.31	2.13	0.40	0.99	0.61	1.49	3.22	4.53
ppm										
Sr	83	2087	783	1316	756	280	380	570	874	424
ppb										
Sc	1727	1317	1475	5581	1827	306	696	7343	3179	2167
V	6294	2066	5219	6877	1730	1173	841	7885	7811	1444
Cr	2432	936	2597	10913	1478	1003	1509	15255	6591	1755
Co	2911	17	216	1976	463	14	221	4376	2175	4891
Ni	1682	128	278	3521	118	0	67	7784	2540	3788
Cu	3048	3723	1010	440	461	80	3474	38877	1233	1693
Zn	14409	5144	19035	16494	3077	1879	4586	28131	18206	32586
Rb	1182	227	629	3866	863	254	606	4178	29169	442
Y	6045	1446	5871	27922	7534	10966	7797	28273	27804	6820
Zr	1470	7319	912	2920	742	223	474	3973	2811	3065
Nb	14	8	4	23	5	1	7	28	164	3
Cs	22	19	31	142	35	21	24	161	2973	12
Ba	122044	107128	9847	176046	25007	3898	17163	8846533	61017	3488
La	2460	869	5816	20668	6016	12189	5465	17335	28289	2427
Ce	6126	1663	12245	54093	13225	36204	10480	43268	58357	5664
Pr	896	223	1508	6446	1683	3307	1356	5460	6973	802
Nd	4320	866	5974	26491	6748	12868	5601	23564	26761	3619
Sm	1442	195	1236	6187	1536	2714	1350	6757	5802	1124
Eu	365	63	610	1442	358	650	441	2418	1810	400
Gd	1561	231	1388	6897	1717	3031	1650	8737	6440	1420
Tb	237	38	196	1084	272	451	249	1366	1071	242
Dy	1265	252	1077	6291	1570	2527	1408	7368	6332	1466
Ho	226	59	205	1229	307	473	270	1341	1212	286
Er	560	175	535	3344	835	1213	716	3622	3354	784
Tm	69	26	69	457	114	150	93	511	480	108
Yb	399	160	411	2817	707	839	560	3516	3107	648
Lu	54	23	56	381	96	105	74	551	433	87
Hf	31	239	31	112	33	13	19	162	135	73
Ta	0	9	0	27	2	4	0	21	104	0
Pb	1306	464	6698	5254	2623	4267	4430	25600	26959	57427
Th	1009	1031	1142	7752	1284	2149	1554	9749	4797	1224
U	503	4098	193	3211	297	780	530	1362	334	327

Table C.3: Major and trace elements concentration for the Adelaide rift complex samples

%	A22	A23
NaO	0.05	0.17
MgO	19.93	18.21
Al_2O_3	0.22	0.95
SiO_2	0.03	0.35
K_2O	0.10	0.27
CaO	32.04	31.53
CaO	32.35	31.77
TiO_2	0.00	0.00
MnO	0.66	0.87
FeO	1.34	3.60
ppm		
Sr	94	88
ppb		
Sc	1189	6352
V	3654	19765
Cr	2301	8321
Co	2075	1659
Ni	822	1264
Cu	4862	4953
Zn	20726	27147
Rb	1086	2702
Y	5283	14517
Zr	1332	1978
Nb	8	10
Cs	59	78
Ba	1506194	65925
La	1654	15838
Ce	4232	39128
Pr	681	4889
Nd	3478	19362
Sm	1361	4334
Eu	470	852
Gd	1524	4548
Tb	235	668
Dy	1257	3520
Ho	226	627
Er	578	1556
Tm	74	199
Yb	433	1170
Lu	58	155
Hf	29	76
Ta	0	11
Pb	1509	22852
Th	807	5355
U	390	379

Table C.4: Major and trace elements concentration for the Dalradian Supergroup samples

%	I1	I17	I20	I22	I24	I24R	I25
NaO	0.04	0.04	0.03	0.06	0.13	0.05	0.04
MgO	19.74	15.65	20.30	16.07	13.05	17.53	13.89
Al_2O_3	0.33	0.87	0.14	0.91	10.06	0.15	2.41
SiO_2	0.01	0.24	0.11	0.20	3.10	0.05	0.27
K_2O	0.09	0.54	0.10	0.51	5.96	0.04	1.12
CaO	31.45	33.07	32.23	30.20	26.11	31.24	29.56
CaO	31.79	33.19	32.41	30.40	26.60	31.31	30.15
TiO_2	0.00	0.01	0.00	0.02	0.09	0.00	0.01
MnO	0.19	0.22	0.13	0.26	0.23	0.26	0.55
FeO	0.88	3.64	1.39	8.89	9.50	6.95	11.06
ppm							
Sr	220	434	185	524	1255	1248	1266
ppb							
Sc	1325	1415	1233	4076	10813	3963	5555
V	4013	3755	3599	3742	27713	2660	6233
Cr	1174	1631	2099	2809	8319	1747	4191
Co	4220	1623	388	5732	7045	4344	4807
Ni	1167	2095	520	7362	14507	3586	6242
Cu	790	1682	3068	5594	16299	1088	10660
Zn	137259	19201	24856	30614	51768	22592	22802
Rb	409	2431	465	4850	59171	287	5051
Y	8281	20378	6028	20212	32490	13687	28132
Zr	1334	2906	4515	4250	13086	1040	4258
Nb	3	34	13	16	40	10	1
Cs	6	5	8	67	3322	27	34
Ba	263211	34027	7493	27574	1250662	10629	64057
La	3517	6786	7974	8152	13569	2358	4905
Ce	5391	18223	16635	19738	35929	6522	14539
Pr	1100	2140	2040	2676	5194	1007	2438
Nd	4631	9256	7642	11470	24495	5019	12750
Sm	1284	2777	1502	3182	7460	1812	5066
Eu	377	864	365	928	2136	629	1579
Gd	1578	3591	1423	4202	9627	2581	7479
Tb	274	648	215	724	1568	494	1351
Dy	1618	4035	1205	4433	8636	3090	7743
Ho	313	833	230	862	1513	611	1364
Er	863	2384	628	2345	3705	1674	3429
Tm	117	342	86	318	465	234	449
Yb	753	2191	523	1927	2721	1481	2725
Lu	101	304	71	251	356	202	358
Hf	36	79	123	119	407	28	143
Ta	4	9	7	12	43	8	18
Pb	23515	3470	2958	16886	12806	7385	11878
Th	434	1490	1520	3006	4560	325	1613
U	1535	4130	1417	248	768	68	295

Table C.5: Major and trace elements concentration for the Dalradian Supergroup samples

%	I26	I27	I28	T4	T5	T7
NaO	0.01	0.01	0.02	0.01	0.07	0.24
MgO	1.01	1.28	3.32	0.24	1.60	9.95
Al_2O_3	0.12	0.05	0.06	0.61	6.40	34.07
SiO_2	0.05	0.03	0.05	0.11	0.69	4.75
K_2O	0.10	0.06	0.05	0.09	0.78	15.00
CaO	55.42	57.08	53.54	59.23	50.55	8.99
CaO	55.54	56.53	53.33	59.09	50.69	9.75
TiO_2	0.00	0.00	0.00	0.00	0.04	0.90
MnO	0.10	0.03	0.22	0.12	0.27	0.43
FeO	0.93	0.22	1.07	0.78	6.44	27.35
ppm						
Sr	728	2089	1367	1438	1283	168
ppb						
Sc	1452	158	180	381	3909	8117
V	438	472	588	1299	9865	36866
Cr	547	972	1116	645	3047	4817
Co	35	-2	443	490	4313	19614
Ni	0	0	0	0	2946	8181
Cu	1394	233	218	3767	5029	35029
Zn	11469	2171	1710	19868	56641	364525
Rb	339	118	66	251	3830	105087
Y	5667	1250	1957	7620	21772	49566
Zr	265	126	373	372	2791	10640
Nb	2	1	0	41	115	1417
Cs	5	7	4	15	100	976
Ba	4881	2892	5960	9642	95405	1699971
La	7550	1216	2352	8382	50796	114879
Ce	17271	3101	4752	13231	109151	247324
Pr	2128	344	521	1788	13486	33000
Nd	8431	1332	1991	7409	53773	134059
Sm	1694	263	385	1504	10819	25661
Eu	428	53	74	394	3350	6768
Gd	1663	273	438	1695	10212	23561
Tb	234	42	63	247	1298	3035
Dy	1279	246	365	1407	6234	14516
Ho	240	49	74	273	1088	2391
Er	661	149	219	702	2814	5172
Tm	92	21	31	84	368	527
Yb	578	137	200	482	2428	2701
Lu	80	19	28	66	366	331
Hf	8	2	7	16	105	294
Ta	0	0	0	8	38	811
Pb	28049	739	572	6537	2760	5836
Th	1173	271	344	266	4244	10761
U	185	171	121	682	354	540

Table C.6: Major and trace elements concentration for the Moroccan samples

%	2.13	2.16	2.18	3.13	5,11	6,6	11,5	BB10	D15
NaO	0.07	0.06	0.13	0.07	0.07	0.03	0.11	0.04	0.08
MgO	0.59	22.39	20.86	0.43	0.51	0.45	1.36	0.89	19.23
Al_2O_3	0.04	0.05	0.05	0.05	0.03	0.10	0.30	0.00	0.06
SiO_2	0.14	0.04	0.04	0.04	0	0	0	0	0
K_2O	0.04	0.04	0.09	0.10	0	0	0	0	0
CaO	58.53	32.32	33.42	59.55	50.94	46.68	44.98	48.90	26.61
CaO	56.23	31.91	32.69	56.90	48.93	44.99	43.09	46.57	25.86
TiO_2	0.00	0.00	0.00	0.00	0.01	0.00	0.02	0.00	0.01
MnO	0.02	0.08	0.11	0.02	0.08	0.08	0.04	0.01	0.02
FeO	0.20	0.46	0.63	0.25	0.24	0.30	0.24	0.17	0.18
ppm									
Sr	201	60	78	628	455	508	393	538	145
ppb									
Sc	208	291	356	120	259	592	855	111	194
V	420	1484	1589	385	575	551	1754	367	2801
Cr	454	1869	1791	507	795	666	1098	676	2728
Co	17	1453	3646	74	56	102	287	46	314
Ni	-250	1058	742	0	15	165	154	0	314
Cu	1893	1117	46900	533	730	406	2206	271	1771
Zn	505	6938	6411	5030	12950	3552	16700	3379	8024
Rb	84	110	83	49	158	278	114	45	87
Y	871	3776	5895	1161	2612	5680	2455	1171	702
Zr	67	410	327	62	95	48	223	28	102
Nb	4	3	3	1	2	1	8	1	4
Cs	8	12	10	6	230	21	9	6	4
Ba	4468	8441	5949	3909	4371	6912	3415	3210	9009
La	2623	9111	9904	1575	3296	7712	6366	1658	1466
Ce	4638	16280	19220	3377	6850	18440	11950	3629	2511
Pr	544	1846	1882	353	699	2072	1297	364	292
Nd	2059	7065	7827	1401	2843	8508	4847	1457	1131
Sm	357	1258	1592	277	559	1776	809	277	208
Eu	75	264	438	62	134	581	178	65	47
Gd	322	1272	1916	270	598	1811	782	282	191
Tb	37	143	209	37	80	234	91	37	25
Dy	175	670	948	203	430	1120	437	204	129
Ho	29	116	155	37	80	184	78	38	24
Er	72	282	339	101	208	422	188	103	62
Tm	9	34	37	14	26	51	23	13	8
Yb	55	197	197	83	150	298	137	82	50
Lu	7	26	25	11	20	38	19	11	6
Hf	5	6	11	3	4	4	7	1	4
Ta	6	1	3	-2	0	0	4	0	0
Pb	2921	1071	1771	2143	10610	3414	6936	681	1800
Th	64	102	108	102	170	446	199	124	87
U	188	167	100	207	58	144	239	152	123

Table C.7: Major and trace elements concentration for the Eleonore Bay Supergroup samples

%	PG128	PG174	PG440
NaO	0.02	0.01	0.02
MgO	0.28	0.23	0.30
Al_2O_3	0.04	0.06	0.02
SiO_2	0.04	0.07	0.03
K_2O	0.11	0.11	0.09
CaO	58.52	58.07	58.49
CaO	57.92	57.27	57.14
TiO_2	0.00	0.00	0.00
MnO	0.00	0.01	0.00
FeO	0.16	0.24	0.19
ppm			
Sr	2932	1930	3494
ppb			
Sc	86	472	191
V	533	706	688
Cr	2667	2129	3712
Co	32	79	55
Ni	344	720	566
Cu	0	110	52
Zn	128	1075	318
Rb	43	157	75
Y	745	2534	2195
Zr	322	319	234
Nb	2	1	0
Cs	8	102	5
Ba	14404	12963	21358
La	439	2761	935
Ce	884	6259	2602
Pr	93	716	284
Nd	363	2689	1177
Sm	76	514	275
Eu	21	105	68
Gd	95	500	333
Tb	14	76	52
Dy	101	470	343
Ho	23	93	72
Er	73	269	202
Tm	9	34	24
Yb	61	209	141
Lu	9	29	19
Hf	6	7	5
Ta	0	0	0
Pb	0	684	188
Th	46	274	152
U	102	141	128

Table C.8: Major and trace elements concentration for the Californian and Indian samples

%	BS1	T5 India	T6 India
NaO	0.06	0.03	0.05
MgO	20.65	0.23	0.36
Al_2O_3	0.00	0.06	0.10
SiO_2	0	0.01	0
K_2O	0	0	0
CaO	27.99	41.14	40.89
CaO	27.14	39.25	38.94
TiO_2	0.00	0.00	0.01
MnO	0.02	0.07	0.08
FeO	0.07	0.22	0.23
ppm			
Sr	49	219	180
ppb			
Sc	21	2015	2084
V	1342	315	326
Cr	3295	420	473
Co	229	245	239
Ni	1910	840	588
Cu	3445	407	434
Zn	10650	11360	13930
Rb	39	463	450
Y	251	5811	5889
Zr	563	163	175
Nb	20	2	4
Cs	10	57	64
Ba	4555	2119000	892100
La	149	4243	4327
Ce	301	6676	6619
Pr	31	1179	1255
Nd	123	4967	5348
Sm	24	1097	1185
Eu	7	440	369
Gd	27	1215	1307
Tb	4	167	182
Dy	24	895	990
Ho	5	168	181
Er	17	431	479
Tm	2	56	63
Yb	16	350	407
Lu	3	48	58
Hf	4	10	7
Ta	0	3	3
Pb	1251	1607	5788
Th	8	730	835
U	172	23	18

Table C.9: Major and trace elements concentration for modern ooids (B08, NPCOScim, NPCOSunc and C48) and Phanerozoic oolitic limstones

%	B08	NPCOScim	NPCOSunc	C48	C17	C171	C443	C514
NaO	0.57	0.92	0.73	0.36	0.06	0.03	0.04	0.01
MgO	0.91	1.23	0.63	0.44	0.61	0.38	0.37	0.63
Al_2O_3	0.04	0.02	0.09	0.05	0.10	0.07	0.08	0.14
SiO_2	0.00	0	0	0.03	0.04	0.02	0.05	0.04
K_2O	0.06	0	0	0.09	0.04	0.04	0.13	0.09
CaO	54.59	58.30	61.43	58.85	56.93	56.28	60.20	56.65
CaO	53.28	58.79	61.87	57.34	56.60	55.65	59.99	55.93
TiO_2	0.00	0.00	0.00	0.00	0.00	0.00	0.00	0.00
MnO	0.00	0.00	0.00	0.00	0.02	0.01	0.04	1.15
FeO	0.08	0.03	0.03	0.15	0.26	0.14	0.48	1.13
ppm								
Sr	7645	8141	9232	8544	444	164	200	562
ppmb								
Sc	41	0	0	33	242	265	1001	5514
V	845	556	688	541	5172	2130	13983	1669
Cr	3950	2390	2276	2629	3618	6536	4428	979
Co	0	0	0	6	185	69	3648	2042
Ni	0	0	0	301	540	387	2676	989
Cu	80	106	52	292	601	512	214	3058
Zn	356	1988	2358	161	1346	7038	2264	16805
Rb	91	78	70	59	100	45	241	193
Y	2124	1082	854	1804	1538	10854	9690	35335
Zr	18	54	50	27	95	47	219	596
Nb	4	0	0	1	5	2	2	1
Cs	5	3	3	1	6	3	14	25
Ba	8845	5257	4577	8481	2146	1813	26204	23437
La	514	202	144	512	953	4827	6497	11589
Ce	702	257	187	444	1876	2263	11296	26970
Pr	128	48	36	117	233	907	1625	4618
Nd	568	220	153	558	982	3868	6843	23337
Sm	133	54	39	132	212	830	1611	6326
Eu	39	15	11	37	51	212	409	3034
Gd	195	82	60	180	220	1137	1747	7414
Tb	34	14	10	28	36	170	256	1124
Dy	228	97	73	189	218	1132	1517	6774
Ho	54	23	18	43	43	244	298	1314
Er	164	72	54	133	130	706	843	3643
Tm	21	9	7	15	17	90	108	464
Yb	116	52	40	92	120	539	688	2835
Lu	16	7	6	13	18	74	91	376
Hf	1	24	22	3	3	2	7	19
Ta	0	0	0	0	4	0	7	17
Pb	102	0	0	8	410	6613	3843	10193
Th	41	8	10	9	163	70	1390	2791
U	3885	2025	2287	2959	475	420	562	65

Table C.10: Major and trace elements concentration for carbonate standards

%	BCS-CRM 512	BCS-CRM 513	Cal-s	JDo-1
NaO	0.14	0.24	0.02	0.02
MgO	21.08	0.22	0.37	18.90
Al_2O_3	0.03	0.03	0.03	0.05
SiO_2	0.03	0.11	0.02	0.02
K_2O	0.02	0.16	0.05	0.05
CaO	32.29	53.38	57.76	35.56
CaO	32.33	54.25	57.69	36.05
TiO_2	0.00	0.00	0.00	0.00
MnO	0.00	0.01	0.00	0.01
FeO	0.06	0.09	0.09	0.06
ppm				
Sr	195	125	235	119
ppb				
Sc	25	0	23	89
V	1295	862	1176	3336
Cr	1371	2046	2399	7424
Co	0	0	0	0
Ni	0	0	0	941
Cu	36	170	104	1663
Zn	2738	4789	4719	27004
Rb	67	46	49	54
Y	120	1664	1308	9340
Zr	915	53	14	111
Nb	2	0	6	4
Cs	37	10	4	6
Ba	1696	44881	762	4992
La	148	673	650	7359
Ce	275	670	242	1946
Pr	36	132	73	973
Nd	144	565	298	3907
Sm	27	107	51	675
Eu	7	32	14	157
Gd	28	158	80	854
Tb	5	22	12	118
Dy	24	148	89	719
Ho	5	33	24	159
Er	14	101	74	443
Tm	2	14	10	54
Yb	12	83	62	289
Lu	2	12	10	39
Hf	2	20	0	3
Ta	0	1	0	0
Pb	155	2152	64	0
Th	21	2	19	42
U	397	151	809	769

Table C.11: Sr isotopic composition for the samples analysed in this study. The external error is 15 ppm and is presented in Appendix B.

sample name	$^{87}Sr/^{86}Sr$	2 s.e.
A5	0.714730	0.000004
A8	0.708973	0.000004
A10	0.714825	0.000008
A22	0.718691	0.000008
I1	0.721433	0.000004
I27	0.707527	0.000004
I28	0.706786	0.000004
T4	0.708101	0.000004
PG128	0.706949	0.000004
PG440	0.706953	0.000004
B08	0.709200	0.000004
JDo-1	0.707533	0.000004
C17	0.707600	0.000004
2.16	0.708037	0.000004
5.11	0.708763	0.000004
11.5	0.708495	0.000004
BS1	0.710655	0.000004
D15	0.708264	0.000004
T6 India	0.707140	0.000006

Appendix D

PHREECQ calculation parameters

This appendix reports the parameters and major anions and cations concentrations used in the modelling done with PHREECQ and presented in Chapter 3 of this thesis.

Table D.1: physical parameters and average concentrations (ppm) of major cations and anions in seawater. The concentrations are reported in ppm.

temperature (°C)	25
pH	8.22
density (g cm^{-3})	1.023
Ca	412.3
Mg	1291.8
Na	10768
K	399.1
Fe	0.002
Mn	0.0002
Si	4.28
Cl	19353
Alkalinity (as HCO_3)	141.682

Bibliography

Accornero, M., Marini, L., and Lelli, M. (2010). Prediction of the thermodynamic properties of metal-chromate aqueous complexes to high temperatures and pressures and implications for the speciation of hexavalent chromium in some natural waters. *Applied Geochemistry*, 25(2):242–260.

Achterberg, E. P. and Van Den Berg, C. M. G. (1997). Chemical speciation of chromium and nickel in the western Mediterranean. *Deep Sea Research Part II: Topical Studies in Oceanography*, 44(3-4):693–720.

Adesodun, J. K. and Mbagwu, J. S. C. (2008). Distribution of heavy metals and hydrocarbon contents in an alfisol contaminated with waste-lubricating oil amended with organic wastes. *Bioresource Technology*, 99(8):3195–3204.

Aizawa, S. (2008). Determination of trace elements in carbonate reference samples by instrumental neutron activation analysis. *Journal of Radioanalytical and Nuclear Chemistry*, 278(2):349–352.

Albarede, F. and Beard, B. (2004). Analytical methods for non-traditional isotopes. In Johnson, C. M., Beard, B. L., and Albarede, F., editors, *Geochemistry of Non-Traditional Stable Isotopes*, volume 55 of *Reviews in Mineralogy and Geochemistry*, pages 113–152, Washington. Mineralogical Soc America.

Albarede, F., Telouk, P., Blichert-Toft, J., Boyet, M., Agranier, A., and Nelson, B. (2004). Precise and accurate isotopic measurements using multiple-collector ICPMS. *Geochimica Et Cosmochimica Acta*, 68(12):2725–2744.

Algeo, T. J. and Lyons, T. W. (2006). Mo-Total Organic Carbon covariation in

modern anoxic marine environments: Implications for analysis of paleoredox and paleohydrographic conditions. *Paleoceanography*, 21(1):21.

Amthor, J. E., Grotzinger, J. P., Schroder, S., Bowring, S. A., Ramezani, J., Martin, M. W., and Matter, A. (2003). Extinction of cloudina and namacalathus at the Precambrian-Cambrian boundary in Oman. *Geology*, 31(5):431–434.

Anbar, A. D., Roe, J. E., Barling, J., and Nealson, K. H. (2000). Nonbiological fractionation of iron isotopes. *Science*, 288(5463):126–128.

Andersen, M. B., Stirling, C. H., Zimmermann, B., and Halliday, A. N. (2010). Precise determination of the open ocean $^{234}U/^{238}U$ composition. *Geochemistry Geophysics Geosystems*, 11.

Anderton, R. (1985). Sedimentation and tectonics in the Scottish Dalradian. *Scottish Journal of Geology*, 21:407–426.

Arnaud, E. and Eyles, C. H. (2006). Neoproterozoic environmental change recorded in the Port Askaig Formation, Scotland: Climatic vs tectonic controls. *Sedimentary Geology*, 183(1-2):99–124.

Arnaud, E. and Fairchild, I. J. (2011). The Port Askaig formation, Dalradian Supergroup, Scotland. In Arnaud, E., Halverson, G. P., and Shields-Zhou, G. A., editors, *The Geological Record of Neoproterozoic glaciations*, page In press. Geological Society of London.

Auger, Y., Bodineau, L., Leclercq, S., and Wartel, M. (1999). Some aspects of vanadium and chromium chemistry in the English Channel. *Continental Shelf Research*, 19(15-16):2003–2018.

Azmy, K., Veizer, J., Wenzel, B., Bassett, M. G., and Copper, P. (1999). Silurian strontium isotope stratigraphy. *Geological Society of America Bulletin*, 111(4):475–483.

Ball, J. W. and Bassett, R. L. (2000). Ion exchange separation of chromium from natural water matrix for stable isotope mass spectrometric analysis. *Chemical Geology*, 168(1-2):123–134.

Ball, J. W. and Izbicki, J. A. (2004). Occurrence of hexavalent chromium in ground water in the Western Mojave Desert, California. *Applied Geochemistry*, 19(7):1123–1135.

Ball, J. W. and Nordstrom, D. K. (1998). Critical evaluation and selection of standard state thermodynamic properties for chromium metal and its aqueous ions, hydrolysis species, oxides, and hydroxides. *Journal of Chemical and Engineering Data*, 43(6):895–918.

Banner, J. L., Hanson, G. N., and Meyers, W. J. (1988). Rare-earth element and Nd isotopic variations in regionally extensive dolomites from the Burlington-Keokuk formation (Mississippian) - implications for REE mobility during carbonate diagenesis. *Journal of Sedimentary Petrology*, 58(3):415–432.

Bao, H. M., Fairchild, I. J., Wynn, P. M., and Spotl, C. (2009). Stretching the envelope of past surface environments: Neoproterozoic glacial lakes from Svalbard. *Science*, 323(5910):119–122.

Bao, H. M., Lyons, J. R., and Zhou, C. M. (2008). Triple oxygen isotope evidence for elevated CO_2 levels after a Neoproterozoic glaciation. *Nature*, 453(7194):504–506.

Bard, A. J., Parsons, R., and Jordan, J. (1985). *Standard potentials in aqueous solutions*. Marcel Dekker, New York.

Bartlett, R. and James, B. (1979). Behavior of chromium in soils .3. oxidation. *Journal of Environmental Quality*, 8(1):31–35.

Bau, M. (1991). Rare-earth element mobility during hydrothermal and metamorphic fluid-rock interaction and the significance of the oxidation state of europium. *Chemical Geology*, 93(3-4):219–230.

Bau, M. and Dulski, P. (1996). Distribution of yttrium and rare-earth elements in the Penge and Kuruman iron-formations, Transvaal Supergroup, South Africa. *Precambrian Research*, 79(1-2):37–55.

Bau, M., Muller, P., and Dulski, P. (1997). Yttrium and lanthanides in eastern Mediterranean seawater and their fractionation during redox-cycling. *Marine Chemistry*, 56(1-2):123–131.

Benson, B. B. and Krause, D. (1984). The concentration and isotopic fractionation of oxygen dissolved in fresh-water and seawater in equilibrium with the atmosphere. *Limnology and Oceanography*, 29(3):620–632.

Bermin, J., Vance, D., Archer, C., and Statham, P. J. (2006). The determination of the isotopic composition of Cu and Zn in seawater. *Chemical Geology*, 226(3-4):280–297.

Bertram, C. J. and Elderfield, H. (1993). The geochemical balance of the rare-earth elements and neodymium isotopes in the oceans. *Geochimica Et Cosmochimica Acta*, 57(9):1957–1986.

Birck, J. L. (2004). An overview of isotopic anomalies in extraterrestrial materials and their nucleosynthetic heritage. *Reviews in Mineralogy and Geochemistry*, 55(1):25–64.

Birck, J. L. and Allegre, C. J. (1984). Chromium isotopic anomalies in Allende refractory inclusions. *Geophysical Research Letters*, 11(10):943–946.

Birck, J. L. and Allegre, C. J. (1985). Evidence for the presence of ^{53}Mn in the early solar-system. *Geophysical Research Letters*, 12(11):745–748.

Birck, J. L. and Allegre, C. J. (1988). Manganese chromium isotope systematics and the development of the early solar-system. *Nature*, 331(6157):579–584.

Bolhar, R. and Van Kranendonk, M. J. (2007). A non-marine depositional setting for the northern Fortescue group, Pilbara craton, inferred from trace element geochemistry of stromatolitic carbonates. *Precambrian Research*, 155(3-4):229–250.

Bonnand, P., Parkinson, I., James, R., Fairchild, I., and Rogers, N. (2009). Redox state of the Neoproterozoic oceans: Insights from the REE and Cr isotopes. *Geochimica Et Cosmochimica Acta*, 73(13):A137–A137.

Bonnand, P., Parkinson, I. J., James, R. H., Karjalainen, A. M., and Fehr, M. A. (2011). Accurate and precise determination of stable Cr isotope compositions in carbonates by double spike MC-ICP-MS. *Journal of Analytical Atomic Spectrometry*, 26(3):528–535.

Boudda, A., Choubert, G., and Faure-Muret, A. (1979). Essai de stratigraphie de la couverture sedimentaire de l'anti-Atlas: Aboudounien-Cambrien inferieur. *Notes et memoires du service geologiaue du Maroc*, 261.

Boussemart, M., Vandenberg, C. M. G., and Ghaddaf, M. (1992). The determination of the chromium speciation in sea-water using catalytic cathodic stripping voltammetry. *Analytica Chimica Acta*, 262(1):103–115.

Boyle, E. A., Bergquist, B. A., Kayser, R., and Mahowald, N. (2005). Iron, manganese and lead at Hawaii Ocean time-series station ALOHA: Temporal variability and an intermediate water hydrothermal plume. *Geochimica Et Cosmochimica Acta*, 69(4):933–952.

Brasier, M. D. and Shields, G. (2000). Neoproterozoic chemostratigraphy and correlation of the Port Askaig glaciation, Dalradian Supergroup of Scotland. *Journal of the Geological Society*, 157:909–914.

Broecker, W. S. and Peng, T.-H. (1982). *Tracers in the Sea*. Eldigio Press, New York.

Calver, C. R. (2000). Isotope stratigraphy of the Ediacaran (Neoproterozoic III) of the Adelaide Rift Complex, Australia, and the overprint of water column stratification. *Precambrian Research*, 100:121–150.

Calver, C. R., Black, L. P., Everard, J. L., and Seymour, D. B. (2004). U-Pb zircon age constraints on late Neoproterozoic glaciation in Tasmania. *Geology*, 32(10):893–896.

Calver, C. R. and Walter, M. R. (2000). The late Neoproterozoic Grassy group of King Island, Tasmania: correlation and palaeogeographic significance. *Precambrian Research*, 100(1-3):299–312.

Campbell, J. A. and Yeats, P. A. (1981). Dissolved chromium in the northwest Atlantic-ocean. *Earth and Planetary Science Letters*, 53(3):427–433.

Canfield, D. E. (2004). The evolution of the Earth surface sulfur reservoir. *American Journal of Science*, 304(10):839–861.

Canfield, D. E., Poulton, S. W., Knoll, A. H., Narbonne, G. M., Ross, G., Goldberg, T., and Strauss, H. (2008). Ferruginous conditions dominated later Neoproterozoic deep-water chemistry. *Science*, 321(5891):949–952.

Canfield, D. E., Poulton, S. W., and Narbonne, G. M. (2007). Late-Neoproterozoic deep-ocean oxygenation and the rise of animal life. *Science*, 315(5808):92–95.

Canfield, D. E. and Teske, A. (1996). Late proterozoic rise in atmospheric oxygen concentration inferred from phylogenetic and sulphur-isotope studies. *Nature*, 382(6587):127–132.

Cawood, P. A., Nemchin, A. A., and Smith, M.and Loewy, S. (2003). Source of the Dalradian Supergroup constrained by U-Pb dating of detrital zircon and implications for the East Laurentian margin. *Journal of the geological Society*, 160:231–246.

Charlier, B. L., Ginibre, C., Morgan, D., Nowell, D., Pearson, D. G., Davidson, J. P., and Ottley, C. J. (2006). Methods for the microsampling and high-precision analysis of strontium and rubidium isotopes at single crystal scale for petrological and geochronological applications. *Chemical Geology*, 232(3-4):114–133.

Chester, R. and Murphy, K. (1988). Metals in the marine atmosphere. In Furness, R. and Rainbow, P., editors, *Heavy metals in the Marine Environment*, Florida. CRC Press.

Choubert, G., Boudda, A., and Faure-Muret, A. (1975). *Essai de stratigraphie de la couverture sedimentaire de l'anti-Atlas: Aboudounien-Cambrien inferieur: Agadir-Rabat.*

Choubert, G. and Hupe, P. (1953). Formations georgiennes a trilobites sur le pourtour de l'Anti-Atlas central. *Comptes Rendus Hebdomadaires Des Seances De L'Academie Des Sciences*, 237(19):1168–1171.

Compston, W., Crawford, A. R., and Bofinger, V. M. (1966). A radiometric estimate of the duration of sedimentation in the Adelaide Geosyncline, South Australia. *J. Geol. Soc. Australia*, 13:229–276.

Condon, D., Zhu, M. Y., Bowring, S., Wang, W., Yang, A. H., and Jin, Y. G. (2005). U-Pb ages from the Neoproterozoic Doushantuo Formation, China. *Science*, 308(5718):95–98.

Condon, D. J. and Prave, A. R. (2000). Two from Donegal: Neoproterozoic glacial episodes on the northeast margin of Laurentia. *Geology*, 28(10):951–954.

Connelly, D. P., Statham, P. J., and Knap, A. H. (2006). Seasonal changes in speciation of dissolved chromium in the surface Sargasso Sea. *Deep-Sea Research Part I-Oceanographic Research Papers*, 53(12):1975–1988.

Cooper, J. A., Jenkins, R. J. F., Compston, W., and Williams, I. S. (1992). Ion-probe zircon dating of a mid-early Cambrian tuff in South Australia. *Journal of the Geological Society*, 149(2):185–192.

Craig, H. (1969). Abyssal carbon and radiocarbon in the pacific. *Journal Geophys. Res.*, 74:5491–5506.

Cranston, R. E. (1983). Chromium in Cascadia Basin, Northeast Pacific-Ocean. *Marine Chemistry*, 13(2):109–125.

Cranston, R. E. and Murray, J. W. (1978). Determination of chromium species in natural-waters. *Analytica Chimica Acta*, 99(2):275–282.

Cranston, R. E. and Murray, J. W. (1980). Chromium species in the Columbia river and estuary. *Limnology and Oceanography*, 25(6):1104–1112.

Croudace, I. W. and Cundy, A. B. (1995). Heavy-metal and hydrocarbon pollution in recent sediments from southampton water, southern England - a geochemical and isotopic study. *Environmental Science Technology*, 29(5):1288–1296.

Cundy, A. B., Croudace, I. W., Cearreta, A., and Irabien, M. J. (2003). Reconstructing historical trends in metal input in heavily-disturbed, contaminated estuaries: studies from Bilbao, Southampton Water and Sicily. *Applied Geochemistry*, 18(2):311–325.

Cutter, G. A. (1992). Kinetic controls on metalloid speciation in seawater. *Marine Chemistry*, 40(1-2):65–80.

Danielson, A., Moller, P., and Dulski, P. (1992). The europium anomalies in banded iron formations and the thermal history of the oceanic-crust. *Chemical Geology*, 97(1-2):89–100.

De Baar, H. J. W., German, C. R., Elderfield, H., and Vangaans, P. (1988). Rare-earth element distributions in anoxic waters of the Cariaco Trench. *Geochimica Et Cosmochimica Acta*, 52(5):1203–1219.

De Laeter, J. R., Bohlke, J. K., De Bievre, P., Hidaka, H., Peiser, H. S., Rosman, K. J. R., and Taylor, P. D. P. (2003). Atomic weights of the elements: Review 2000. *Pure and Applied Chemistry*, 75(6):683–800.

Dempster, T. J., Rogers, G., Tanner, P. W. G., Bluck, B. J., Muir, R. J., Redwood, S. D., Ireland, T. R., and Paterson, B. A. (2002). Timing of deposition, orogenesis and glaciation within the Dalradian rocks of Scotland: constraints from U-Pb zircon ages. *Journal of the Geological Society*, 159:83–94.

Deniel, C. and Pin, C. (2001). Single-stage method for the simultaneous isolation of lead and strontium from silicate samples for isotopic measurements. *Analytica Chimica Acta*, 426(1):95–103.

Derry, L. A. (2010). A burial diagenesis origin for the Ediacaran Shuram-Wonoka carbon isotope anomaly. *Earth and Planetary Science Letters*, 294(1-2):152–162.

Derry, L. A. and Jacobsen, S. B. (1990). The chemical evolution of Precambrian seawater - evidence from REEs in banded iron formations. *Geochimica Et Cosmochimica Acta*, 54(11):2965–2977.

Derry, L. A., Kaufman, A. J., and Jacobsen, S. B. (1992). Sedimentary cycling and environmental-change in the late Proterozoic - evidence from stable and radiogenic isotopes. *Geochimica Et Cosmochimica Acta*, 56(3):1317–1329.

Des Marais, D. J., Strauss, H., E., S. R., and M., H. J. (1992). Carbon isotope evidence for the stepwise oxidation of the Proterozoic environment. *Nature*, 359(6):605–609.

Destombes, J., Hollard, H., and Willefert, S. (1985). Lower Paleozoic rocks of Morocco. In C., H., editor, *Lower Paleozoic of North-Western and west central Africa*, volume 4, pages 91–336, New York. JohnWiley & Sons.

Detmers, J., Bruchert, V., Habicht, K. S., and Kuever, J. (2001). Diversity of sulfur isotope fractionations by sulfate-reducing prokaryotes. *Applied and Environmental Microbiology*, 67(2):888–894.

Dhuime, B., Bosch, D., Bruguier, O., Caby, R., and Pourtales, S. (2007). Age, provenance and post-deposition metamorphic overprint of detrital zircons from the Nathorst Land group (NE Greenland) - A LA-ICP-MS and SIMS study. *Precambrian Research*, 155(1-2):24–46.

Dicks, B. and Levell, D. (1989). Refinery-effluent discharges into Milford Haven and Southampton Water. In Dicks, B., editor, *Ecological impacts of the oil industry*, pages 287–316, Chichester. Inst. Petroleum/Wiley.

Dodson, M. H. (1963). A theoretical study of use of internal standards for precise isotopic analysis by surface ionization technique .1. general first-order algebraic solutions. *Journal of Scientific Instruments*, 40(6):289.

Dolamore-Frank, J. A. (1984). The analysis, occurence and chemical speciation of zinc and chromium in natural waters. *PhD thesis, University of Southampton, UK.*

Dossing, L. N., Dideriksen, K., Stipp, S. L. S., and Frei, R. (2011). Reduction of hexavalent chromium by ferrous iron: a process of chromium isotope fractionation and its relevance to natural environments. *Chemical Geology, in press.*

Duan, Y., Anbar, A. D., Arnold, G. L., Lyons, T. W., Gordon, G. W., and Kendall, B. (2010). Molybdenum isotope evidence for mild environmental oxygenation before the Great Oxidation Event. *Geochimica Et Cosmochimica Acta*, 74(23):6655–6668.

Dubinin, A. V. (2004). Geochemistry of rare earth elements in the ocean. *Lithology and Mineral Resources*, 39(4):289–307.

Dupre, B., Gaillardet, J., Rousseau, D., and Allegre, C. J. (1996). Major and trace elements of river-borne material: The Congo Basin. *Geochimica Et Cosmochimica Acta*, 60(8):1301–1321.

Dyson, I. A. (1992). Stratigraphic nomenclature and sequence stratigraphy of the lower Wilpena Group, Adelaide Geosyncline: the Sandison Supergroup. *South Australian Geol. Survey Quart. Geol. Notes*, 122:2–13.

Elderfield, H. (1970). Chronium speciation in sea water. *Earth and Planetary Science Letters*, 9(1):10.

Elderfield, H. (1988). The oceanic chemistry of the rare-earth elements. *Philosophical Transactions of the Royal Society of London Series a-Mathematical Physical and Engineering Sciences*, 325(1583):105–126.

Elderfield, H., Kastner, M., and Martin, J. B. (1990). Composition and sources of fluids in sediments of the Peru subduction zone. *Journal Geophys. Res.*, 85:8811–8828.

Elderfield, H. and Sholkovitz, E. R. (1987). Rare-earth elements in the pore waters of reducing nearshore sediments. *Earth and Planetary Science Letters*, 82(3-4):280–288.

Ellis, A. S., Johnson, T. M., and Bullen, T. D. (2002). Chromium isotopes and the fate of hexavalent chromium in the environment. *Science*, 295(5562):2060–2062.

Ellis, A. S., Johnson, T. M., and Bullen, T. D. (2004). Using chromium stable isotope ratios to quantify Cr(VI) reduction: Lack of sorption effects. *Environmental Science & Technology*, 38(13):3604–3607.

Eyles, C. H. and Eyles, N. (1983). Glaciomarine model for upper precambrian diamictites of the Port-Askaig Formation, Scotland. *Geology*, 11(12):692–696.

Eyles, N. and Januszczak, N. (2004). 'Zipper-rift': a tectonic model for Neoproterozoic glaciations during the breakup of Rodinia after 750 Ma. *Earth-Science Reviews*, 65(1-2):1–73.

Fairchild, I. J. (1977). Phengite spherules from Dalradian Bonahaven formation, Islay, Scotland - glauconitized microfossils. *Geological Magazine*, 114(5):355.

Fairchild, I. J. (1980). Sedimentation and origin of a late Precambrian dolomite from Scotland. *Journal of Sedimentary Petrology*, 50(2):423–446.

Fairchild, I. J. (1985). Glaciomarine model for upper Precambrian diamictites of the Port Askaig formation, Scotland - comment. *Geology*, 13(1):89–89.

Fairchild, I. J. (1993). Balmy shores and icy wastes: the paradox of carbonates associated with glacial deposits in Neoproterozoic times. In Wright, V. P., editor, *Sedimentology Review*, volume 1, pages 1–16. Blackwell Scientific Publications.

Fairchild, I. J. and Hambrey, M. J. (1995). Vendian basin evolution in East Greenland and NE Svalbard. *Precambrian Research*, 73(1-4):217–233.

Fairchild, I. J. and Kennedy, M. J. (2007). Neoproterozoic glaciation in the earth system. *Journal of the Geological Society*, 164:895–921.

Fairchild, I. J., Spiro, B., Herrington, P. M., and Song, T. (2000). Controls on Sr and C isotope compositions of Neoproterozoic Sr-rich limestones of E. Greenland and N. China. In Grotzinger, J. P. and James, N. P., editors, *Carbonate Sedimentition and Diagenesis in the Evolving Precambrian World*, volume 67, pages 297–313. SEPM Special Publications.

Fanning, C. M., Ludwig, K. R., Forbes, B. G., and Preiss, W. V. (1986). Single and multiple grain U-Pb zircon anlyses for the early Adelaidean Rook Tuff, Willouran Ranges, South Australia. *8th Australian Geological Convention, Adelaide. Geol. Soc. Australia Abstr.*, 15:71–72.

Fike, D. A., Grotzinger, J. P., Pratt, L. M., and E., S. R. (2006). Oxidation of the Ediacaran Ocean. *Nature*, 444(7):744–747.

Fletcher, C. A. J. (1991). *Computational techniques for fluids dynamics.* Spinger, Berlin.

Frederiksen, K. S. (2000). Evolution of a late Proterozoic carbonate ramp (Ymer ø and Andree Land Groups, Eleonore Bay Supergroup, East Greenland. *Polarforschung*, 68:125–130.

Frei, R., Gaucher, C., Poulton, S. W., and Canfield, D. E. (2009). Fluctuations in Precambrian atmospheric oxygenation recorded by chromium isotopes. *Nature*, 461(7261):250–U125.

Frimmel, H. E. (2009). Trace element distribution in Neoproterozoic carbonates as palaeoenvironmental indicator. *Chemical Geology*, 258(3-4):338–353.

Frimmel, H. E. (2010). On the reliability of stable carbon isotopes for Neoproterozoic chemostratigraphic correlation. *Precambrian Research*, 182(4):239–253.

Frimmel, H. E., Tack, L., Basel, M. S., Nutman, A. P., and Boven, A. (2006). Provenance and chemostratigraphy of the Neoproterozoic West Congolian Group in the Democratic Republic of Congo. *Journal of African Earth Sciences*, 46(3):221–239.

Gaberell, M., Chin, Y. P., Hug, S. J., and Sulzberger, B. (2003). Role of dissolved organic matter composition on the photoreduction of Cr(VI) to Cr(III) in the presence of iron. *Environmental Science & Technology*, 37(19):4403–4409.

Galer, S. J. G. (1999). Optimal double and triple spiking for high precision lead isotopic measurement. *Chemical Geology*, 157(3-4):255–274.

Garcia-Sanchez, A. and Alvarez-Ayuso, E. (2002). Sorption of Zn, Cd and Cr on calcite. application to purification of industrial wastewaters. *Minerals Engineering*, 15(7):539–547.

German, C. R., Campbell, A. C., and Edmond, J. M. (1991a). Hydrothermal scavenging at the mid-atlantic ridge - modification of trace-element dissolved fluxes. *Earth and Planetary Science Letters*, 107(1):101–114.

German, C. R., Holliday, B. P., and Elderfield, H. (1991b). Redox cycling of rare-earth elements in the suboxic zone of the Black-Sea. *Geochimica Et Cosmochimica Acta*, 55(12):3553–3558.

Geyer, G. and Landing, E. (1995). The Cambrian of the Moroccan Atlas regions. In *Morocco: The lower-middle Cambrian standard of Western Gondwana.*, volume 28, pages 7–46, Würtzburg. Beringeria.

Ghaddaf, M. A. (1990). Dissolved chromium speciation in estuarine and sea water and trace metal speciation in sediments, eolian dust and surface water particulate from N.E. Atlantic. *PhD thesis, University of Liverpool, UK.*

Goldstein, S. J. and Jacobsen, S. B. (1988). Rare-earth elements in river waters. *Earth and Planetary Science Letters*, 89(1):35–47.

Golimowski, J., Valenta, P., and Nurnberg, H. W. (1985). Trace determination of chromium in various water types by absorption differential pulse voltammetry. *Fresenius Zeitschrift Fur Analytische Chemie*, 322(3):315–322.

Gotz, A. and Heumann, K. G. (1988). Chromium trace determination in inorganic, organic and aqueous samples with isotope-dilution mass-spectrometry. *Fresenius Zeitschrift Fur Analytische Chemie*, 331(2):123–128.

Grimaud, D. and Michard, G. (1974). Concentration du chrome dans deux profils de l'ocean Pacifique. *Marine Chemistry*, 2(3):229–237.

Gutjahr, M., Frank, M., Stirling, C. H., Klemm, V., van de Flierdt, T., and Halliday, A. N. (2007). Reliable extraction of a deepwater trace metal isotope signal from

Fe-Mn oxyhydroxide coatings of marine sediments. *Chemical Geology*, 242:351–370.

Halicz, L., Yang, L., Teplyakov, N., Burg, A., Sturgeon, R., and Kolodny, Y. (2008). High precision determination of chromium isotope ratios in geological samples by MC-ICP-MS. *Journal of Analytical Atomic Spectrometry*, 23(12):1622–1627.

Halliday, A. N., Graham, C. M., Aftalion, M., and Dymoke, P. (1989). The depositional age of the Dalradian Supergroup - U-Pb and Sm-Nd isotopic studies of the Tayvallich volcanics, Scotland. *Journal of the Geological Society*, 146:3–6.

Halverson, G. P., Dudas, F. O., Maloof, A. C., and Bowring, S. A. (2007). Evolution of the $^{87}Sr/^{86}Sr$ composition of Neoproterozoic seawater. *Palaeogeography Palaeoclimatology Palaeoecology*, 256(3-4):103–129.

Halverson, G. P., Hoffman, P. F., Schrag, D. P., and Kaufman, A. J. (2002). A major perturbation of the carbon cycle before the Ghaub glaciation (Neoproterozoic) in Namibia: Prelude to Snowball Earth? *Geochemistry Geophysics Geosystems*, 3.

Halverson, G. P., Hoffman, P. F., Schrag, D. P., Maloof, A. C., and Rice, A. H. N. (2005). Toward a Neoproterozoic composite carbon-isotope record. *Geological Society of America Bulletin*, 117(9-10):1181–1207.

Halverson, G. P., Maloof, A. C., and Hoffman, P. F. (2004). The Marinoan glaciation (Neoproterozoic) in northeast Svalbard. *Basin Research*, 16(3):297–324.

Halverson, G. P., Wade, B. P., Hurtgen, M. T., and Barovich, K. M. (2010). Neoproterozoic chemostratigraphy. *Precambrian Research*, 182(4):337–350.

Hambrey, M. J., Fairchild, I., Glover, B. W., Stewart, A., Treagus, J. E., and Winchester, J. A. (1991). The late Precambrian geology of the scottish highlands and islands. *Geologists Association Guide*, 44.

Harris, N., Haselock, P. J., Kennedy, M. J., and Mendum, J. R. (1994). The Dalradian Supergroup in Scotland, Shetland and Ireland. In Gibbons, W. and Harris, A. L., editors, *A revised correlation of Precambrian Rock in the British Isles.*, volume 22 of *Specil Reports*, pages 33–53, London. Geological Society of London.

Hayes, J. M., Strauss, H., and Kaufman, A. J. (1999). The abundance of ^{13}C in marine organic matter and isotopic fractionation in the global biogeochemical cycle of carbon during the past 800 Ma. *Chemical Geology*, 161(1-3):103–125.

Hein, J. R., Koschinsky, A., Halbach, P., Manheim, F. T., Bau, M., Kang, J.-K., and Lubick, N. (1997). Iron and manganese oxide mineralization in the Pacific. In Nicholson, K. J., Hein, J., Bu'hn, B., and Dasgupta, S., editors, *Manganese Mineralization: Geochemistry and Mineralogy of Terrestrial and Marine Deposits*, volume 119 of *Reviews in Mineralogy & Geochemistry*, pages 123–138, London. Special Publication, GEological Society of London.

Henderson, P. (1982). *Inorganic Geochemistry*. Pergamon Press, Oxford.

Herrington, P. and Fairchild, I. (1989). Carbonate shelf and slope facies evolution prior to Vendian glaciation, central East Greenland. In *The Caledonide Geology of Scandinavia*, pages 263–273. Gayer, R. A.

Heywood, K. J. and King, B. A. (2002). Water masses and baroclinic transports in the South Atlantic and Southern oceans. *Journal of Marine Research*, 60(5):639–676.

Higgins, J. A. and Schrag, D. P. (2003). Aftermath of a snowball Earth. *Geochemistry Geophysics Geosystems*, 4.

Hoffman, P. F., Kaufman, A. J., Halverson, G. P., and Schrag, D. P. (1998). A Neoproterozoic snowball Earth. *Science*, 281(5381):1342–1346.

Hoffman, P. F. and Schrag, D. P. (2002). The snowball Earth hypothesis: testing the limits of global change. *Terra Nova*, 14(3):129–155.

Hoffmann, K. H., Condon, D. J., Bowring, S. A., and Crowley, J. L. (2004). U-Pb zircon date from the Neoproterozoic Ghaub Formation, Namibia: Constraints on Marinoan glaciation. *Geology*, 32(9):817–820.

Holland, H. D. (2006). The oxygenation of the atmosphere and oceans. *Philosophical Transactions of the Royal Society B: Biological Sciences*, 361(1470):903–915.

Houzay, J.-P. (1979). Empreintes attribuables a des meduses dans la serie de base de l'Adoudounien (Precambrien terminal de l'Anti-Atlas, Maroc). *Geologie Meditarraneenne*, 3:379–384.

Hurtgen, M. T., Arthur, M. A., and Halverson, G. P. (2005). Neoproterozoic sulfur isotopes, the evolution of microbial sulfur species, and the burial efficiency of sulfide as sedimentary pyrite. *Geology*, 33(1):41–44.

Hyslop, E. V., Valley, J. W., Johnson, C. M., and Beard, B. L. (2008). The effects of metamorphism on O and Fe isotopes compositions in the Biwabik iron formation, northern Minnesota. *Contributions to Mineralogy and Petrology*, 155(3):313–328.

Isshiki, K., Sohrin, Y., Karatani, H., and Nakayama, E. (1989). Preconcentration of chromium(III) and chromium(VI) in sea-water by complexation with quinolin-8-ol and adsorption on macroporous resin. *Analytica Chimica Acta*, 224(1):55–64.

Izbicki, J. A., Ball, J. W., Bullen, T. D., and Sutley, S. J. (2008). Chromium, chromium isotopes and selected trace elements, western Mojave desert, USA. *Applied Geochemistry*, 23(5):1325–1352.

Jacobsen, S. B. and Kaufman, A. J. (1999). The Sr, C and O isotopic evolution of Neoproterozoic seawater. *Chemical Geology*, 161(1-3):37–57.

Jaffres, J. B. D., Shields, G. A., and Wallmann, K. (2007). The oxygen isotope evolution of seawater: A critical review of a long-standing controversy and an improved geological water cycle model for the past 3.4 billion years. *Earth-Science Reviews*, 83(1-2):83–122.

James, R. H., Elderfield, H., and Palmer, M. R. (1995). The chemistry of hydrothermal fluids from the Broken Spur site, 29-degrees-N mid-atlantic ridge. *Geochimica Et Cosmochimica Acta*, 59(4):651–659.

Jeandel, C. and Minster, J. F. (1984). Isotope-dilution measurement of inorganic chromium(III) and total chromium in seawater. *Marine Chemistry*, 14(4):347–364.

Jeandel, C. and Minster, J. F. (1987). Chromium behavior in the ocean: Global versus regional processes. *Global Biogeochem. Cycles*, 1(2):131–154.

Jenkins, R., Cooper, J., and Compston, W. (2002). Age and biostratigraphy of early Cambrian tuffs from SE Australia and southern China. *Journal of the Geological Society*, 159(6):645–658.

Jiang, G. Q., Kaufman, A. J., Christie-Blick, N., Zhang, S. H., and Wu, H. C. (2007). Carbon isotope variability across the Ediacaran Yangtze platform in South China: Implications for a large surface-to-deep ocean delta ^{13}C gradient. *Earth and Planetary Science Letters*, 261:303–320.

Johnson, T. M. and Bullen, T. D. (2004). Mass-dependent fractionation of selenium and chromium isotopes in low-temperature environments. In Johnson, C. M., Beard, B. L., and Albarede, F., editors, *Geochemistry of Non-Traditional Stable Isotopes*, volume 55 of *Reviews in Mineralogy & Geochemistry*, pages 289–317, Washington. Mineralogical Soc America.

Johnston, D. T., Poulton, S. W., Dehler, C., Porter, S., Husson, J., Canfield, D. E., and Knoll, A. H. (2010). An emerging picture of Neoproterozoic ocean chemistry: Insights from the Chuar Group, Grand Canyon, USA. *Earth and Planetary Science Letters*, 290(1-2):64–73.

Jones, C. E. and Jenkyns, H. C. (2001). Seawater strontium isotopes, oceanic anoxic events, and seafloor hydrothermal activity in the Jurassic and Cretaceous. *American Journal of Science*, 301(2):112–149.

Kaczynski, S. E. and Kieber, R. J. (1994). Hydrophobic c_{18} bound organic-complexes of chromium and their potential impact on the geochemistry of chromium in natural-waters. *Environmental Science and Technology*, 28(5):799–804.

Kamber, B. S., Bolhar, R., and Webb, G. E. (2004). Geochemistry of late Archaean stromatolites from Zimbabwe: evidence for microbial life in restricted epicontinental seas. *Precambrian Research*, 132(4):379–399.

Kamber, B. S., Greig, A., and Collerson, K. D. (2005). A new estimate for the composition of weathered young upper continental crust from alluvial sediments, Queensland, Australia. *Geochimica et Cosmochimica Acta*, 69:1041–1058.

Kamber, B. S. and Webb, G. E. (2001). The geochemistry of late Archaean microbial carbonate: Implications for ocean chemistry and continental erosion history. *Geochimica Et Cosmochimica Acta*, 65(15):2509–2525.

Kasemann, S. A., Hawkesworth, C. J., Prave, A. R., Fallick, A. E., and Pearson, P. N. (2005). Boron and calcium isotope composition in Neoproterozoic carbonate rocks from Namibia: evidence for extreme environmental change. *Earth and Planetary Science Letters*, 231(1-2):73–86.

Kasemann, S. A., Prave, A. R., Fallick, A. E., Hawkesworth, C. J., and Hoffmann, K. H. (2010). Neoproterozoic ice ages, boron isotopes, and ocean acidification: Implications for a snowball Earth. *Geology*, 38(9):775–778.

Kasting, J. F., Howard, M. T., Wallmann, K., Veizer, J., Shields, G., and Jaffres, J. (2006). Paleoclimates, ocean depth, and the oxygen isotopic composition of seawater. *Earth and Planetary Science Letters*, 252(1-2):82–93.

Kaufman, A. J., Knoll, A. H., and Narbonne, G. M. (1997). Isotopes, ice ages, and terminal Proterozoic Earth history. *Proceedings of the National Academy of Sciences of the United States of America*, 94(13):6600–6605.

Kemp, A. I. S., Hawkesworth, C. J., Heinrich, D. H., and Karl, K. T. (2003). Granitic perspectives on the generation and secular evolution of the continental crust. In *Treatise on Geochemistry*, pages 349–410, Oxford. Pergamon.

Kendall, B., Creaser, R. A., and Selby, D. (2006). Re-Os geochronology of postglacial black shales in Australia: Constraints on the timing of "Sturtian" glaciation. *Geology*, 34(9):729–732.

Kennedy, M. J. (1996). Stratigraphy, sedimentology, and isotopic geochemistry of Australian Neoproterozoic postglacial cap dolostones: Deglaciation, delta ^{13}C excursions, and carbonate precipitation. *Journal of Sedimentary Research*, 66(6):1050–1064.

Kennedy, M. J. and Christie-Blick, N. (2011). Condensation origin for Neoproterozoic cap carbonates during deglaciation. *Geology*, 39(4):319–322.

Kennedy, M. J., Christie-Blick, N., and Prave, A. R. (2001). Carbon isotopic composition of Neoproterozoic glacial carbonates as a test of paleoceanographic models for snowball Earth phenomena. *Geology*, 29(12):1135–1138.

Keto, L. S. and Jacobsen, S. B. (1988). Nd isotopic variations of Phanerozoic paleoceans. *Earth and Planetary Science Letters*, 90(4):395–410.

Kieber, R. J., Willey, J. D., and Zvalaren, S. D. (2002). Chromium speciation in rainwater: Temporal variability and atmospheric deposition. *Environmental Science and Technology*, 36(24):5321–5327.

Kimbrough, D. E., Cohen, Y., Winer, A. M., Creelman, L., and Mabuni, C. (1999). A critical assessment of chromium in the environment. *Critical Reviews in Environmental Science and Technology*, 29(1):1–46.

Kirschvink, J. (1992). Late Proterozoic low-latitude glaciation. In Schopf, J. W., editor, *The Proterozoic Biosphere*, pages 51–52. Cambridge University Press, Cambridge.

Kleber, R. J. and Helz, G. R. (1992). Indirect photoreduction of aqueous chromium(VI). *Environmental Science & Technology*, 26:307–312.

Klein, C. (2005). Some Precambrian banded iron formations (BIFs) from around the world: their age, geologic setting, mineralogy, metamorphism, geochemistry and origin. *American Mineralogist*, 90(10):1473–1499.

Knauth, L. P. and Kennedy, M. J. (2009). The late Precambrian greening of the Earth. *Nature*, 460(7256):728–732.

Knoll, A. H. (2000). Learning to tell Neoproterozoic time. *Precambrian Research*, 100(1-3):3–20.

Knoll, A. H. (2003). Vestiges of a beginning? Paleontological and geochemical constraints on early animal evolution. *Annales de Palaeontologie*, 89(4):205–221.

Knoll, A. H., Hayes, J. M., Kaufman, A. J., Swett, K., and Lambert, I. B. (1986). Secular variation in carbon isotope ratios from upper Proterozoic successions of Svalbard and East Greenland. *Nature*, 321(6073):832–838.

Komiya, T., Hirata, T., Kitajima, K., Yamamoto, S., Shibuya, T., Sawaki, Y., Ishikawa, T., Shu, D., Li, Y., and Han, J. (2008). Evolution of the composition of seawater through geologic time, and its influence on the evolution of life. *Gondwana Research*, 14(1-2):159–174.

Krumbein, W. C. and Garrels, R. M. (1952). Origin and classification of chemical sediments in terms of ph and oxidation-reduction potentials. *Journal of Geology*, 60(1):1–33.

Latham, A. and Riding, R. (1990). Fossil evidence for the location of the Precambrian Cambrian boundary in Morocco. *Nature*, 344(6268):752–754.

Lawrence, M. G., Jupiter, S. D., and Kamber, B. S. (2006). Aquatic geochemistry of the rare earth elements and yttrium in the Pioneer River catchment, Australia. *Marine and Freshwater Research*, 57(7):725–736.

Li, C., Love, G. D., Lyons, T. W., Fike, D. A., Sessions, A. L., and Chu, X. L. (2010). A stratified redox model for the Ediacaran Ocean. *Science*, 328(5974):80–83.

Li, S. X., Zheng, F. Y., Hong, H. S., Deng, N. S., and Lin, L. X. (2009). Influence of marine phytoplankton, transition metals and sunlight on the species distribution of chromium in surface seawater. *Marine Environmental Research*, 67(4-5):199–206.

Li, Y. J. and Xue, H. B. (2001). Determination of Cr(III) and Cr(VI) species in natural waters by catalytic cathodic stripping voltammetry. *Analytica Chimica Acta*, 448(1-2):121–134.

Liu, X. W. and Byrne, R. H. (1998). Comprehensive investigation of yttrium and rare earth element complexation by carbonate ions using ICP mass spectrometry. *Journal of Solution Chemistry*, 27(9):803–815.

Lovley, D. R. (1993). Dissimilatory metal reduction. *Annual Review of Microbiology*, 47:263–290.

Ludwig, K. R. (1986). Constraints on time-efficient data-taking strategies for single-collector, isotope-ratio mass spectrometers. *US Geological Survey Bulletin*, 1622:219–221.

Lugmair, G. W. and Shukolyukov, A. (1998). Early solar system timescales according to ^{53}Mn-^{53}Cr systematics. *Geochimica Et Cosmochimica Acta*, 62(16):2863–2886.

Lyons, T. W. and Severmann, S. (2006). A critical look at iron paleoredox proxies: New insights from modern euxinic marine basins. *Geochimica Et Cosmochimica Acta*, 70(23):5698–5722.

Macdonald, F. A., Schmitz, M. D., Crowley, J. L., Roots, C. F., Jones, D. S., Maloof, A. C., Strauss, J. V., Cohen, P. A., Johnston, D. T., and Schrag, D. P. (2010). Calibrating the Cryogenian. *Science*, 327(5970):1241–1243.

Mahan, K. H., Wernicke, B. P., and Jercinovic, M. J. (2010). Th-U-total Pb geochronology of authigenic monazite in the Adelaide rift complex, South Australia, and implications for the age of the type Sturtian and Marinoan glacial deposits. *Earth and Planetary Science Letters*, 289(1-2):76–86.

Maloof, A. C., Schrag, D. P., Crowley, J. L., and Bowring, S. A. (2005). An expanded record of early Cambrian carbon cycling from the Anti-Atlas margin, Morocco. *Canadian Journal of Earth Sciences*, 42(12):2195–2216.

Margaritz, M., Kirschvink, J., Latham, A., Zhuralev, A., and Rosanev, A. (1991). Precambrian/Cambrian boundary problem: Carbon isotope correlations for Vendian and Tommotian time between Siberia and Morocco. *Geology*, 19:847–850.

Mazumdar, A., Tanaka, K., Takahashi, T., and Kawabe, I. (2003). Characteristics of rare earth element abundances in shallow marine continental platform carbonates of late Neoproterozoic successions from India. *Geochemical Journal*, 37(2):277–289.

McCay, G. A., Prave, A. R., Alsop, G. I., and Fallick, A. E. (2006). Glacial trinity: Neoproterozoic Earth history within the British-Irish Caledonides. *Geology*, 34(11):909–912.

McDonough, W. F. and Frey, F. A. (1989). Rare earth elements in upper mantle rocks. *Reviews in Mineralogy and Geochemistry*, 21(1):100–145.

McDonough, W. F. and Sun, S. S. (1995). The composition of the Earth. *Chemical Geology*, 120(3-4):223–253.

McKelvey, B. A. and Orians, K. J. (1998). The determination of dissolved zirconium and hafnium from seawater using isotope dilution inductively coupled plasma mass spectrometry. *Marine Chemistry*, 60(3-4):245–255.

McKirdy, D. M., Burgess, J. M., Lemon, N. M., Yu, X. K., Cooper, A. M., Gostin, V. A., Jenkins, R. J. F., and Both, R. A. (2001). A chemostratigraphic overview of the late Cryogenian interglacial sequence in the Adelaide fold-thrust belt, South Australia. *Precambrian Research*, 106(1-2):149–186.

McLennan, S. M. (1989). Rare earth elements in sedimentary rocks; influence of provenance and sedimentary processes. *Reviews in Mineralogy and Geochemistry*, 21(1):169–200.

McLennan, S. M. (2001). Relationships between the trace element composition of sedimentary rocks and upper continental crust. *Geochemistry Geophysics Geosystems*, 2.

Monninger, W. (1979). The section of Tiout (Precambrian/Cambrian boundary beds, Anti-Atlas, Morocco): An environmental model. *Arb. Palaont. Inst.*, 1:289–302.

Morse, J. W. and Luther, G. W. (1999). Chemical influences on trace metal sulfide interactions in anoxic sediments. *Geochimica et Cosmochimica Acta*, 63:3373–3378.

Muehlenbachs, K. (1998). The oxygen isotopic composition of the oceans, sediments and the seafloor. *Chemical Geology*, 145(3-4):263–273.

Mugo, R. K. and Orians, K. J. (1993). Seagoing method for the determination of chromium(III) and total chromium in sea-water by electron-capture detection gas-chromatography. *Analytica Chimica Acta*, 271(1):1–9.

Murray, J. W., Spell, B., and B., P. (1983). The contrasting geochemistry of manganese and chromium in the eastern tropical Pacific. In Wong, C. S., Boyle, E. A., and Bruland, K. W., editors, *Trace Metals in Seawater*, Reviews in Mineralogy & Geochemistry, pages 447–465. Plenum Press.

Nagy, R. M., Porter, S. M., Dehler, C. M., and Shen, Y. (2009). Biotic turnover driven by eutrophication before the Sturtian low-latitude glaciation. *Nature Geoscience*, 2(6):414–417.

Nakayama, E., Kuwamoto, T., Tokoro, H., and Fujinaga, T. (1981). Chemical speciation of chromium in sea-water .3. the determination of chromium species. *Analytica Chimica Acta*, 131(NOV):247–254.

Noble, S. R., Hyslop, E. K., and Highton, A. J. (1996). High-precision U-Pb monazite geochronology of the c.806 Ma grampian shear zone and the implications for the evolution of the central highlands of Scotland. *Journal of the Geological Society*, 153:511–514.

Nothdurft, L. D., Webb, G. E., and Kamber, B. S. (2004). Rare earth element geochemistry of late Devonian reefal carbonates, canning basin, Western Australia: Confirmation of a seawater REE proxy in ancient limestones. *Geochimica Et Cosmochimica Acta*, 68(2):263–283.

Nowell, G. M., Pearson, D. G., Ottley, C. J., Schwieters, J., and Dowall, D. (2003). *Long-term performance characteristics of a plasma ionisation multi-collector mass spectrometer (PIMMS): The ThermoFinnigan Neptune.* Plasma Source Mass Spectrometry: Applications and Emerging Technologies. Royal Soc Chemistry, Cambridge.

Nozaki, Y. and Zhang, J. (1995). The rare earth elements and yttrium in the coastal/offshore mixing zone of Tokyo Bay waters and the Kuroshio. In Sakai, H.

and Nozaki, Y., editors, *Biogeochemical Processes and Ocean Flux in the western Pacific*, pages 171–174, Washington. Terra.

Nozaki, Y., Zhang, J., and Amakawa, H. (1997). The fractionation between Y and Ho in the marine environment. *Earth and Planetary Science Letters*, 148(1-2):329–340.

Olivarez, A. M. and Owen, R. M. (1991). The europium anomaly of seawater: implications for fluvial versus hydrothermal REE inputs to the oceans. *Chemical Geology*, 92(4):317–328.

Palme, H., O'Neill, H. S. C., Heinrich, D. H., and Karl, K. T. (2007). Cosmochemical estimates of mantle composition. In *Treatise on Geochemistry*, pages 1–38. Pergamon, Oxford.

Palmer, M. R. and Edmond, J. M. (1992). The strontium isotope budget of the modern ocean. *Earth and Planetary Science Letters*, 109(1-2):37–46.

Pankow, J. F., Leta, D. P., Lin, J. W., Ohl, S. E., Shum, W. P., and Janauer, G. E. (1977). Analysis for chromium traces in aquatic ecosystem .2. study of Cr(III) and Cr(VI) in Susquehanna river basin of New-York and Pennsylvania. *Science of the Total Environment*, 7(1):17–26.

Pettine, M. (2000). Redox processes of chromium in sea water. In Gianguzza, A., Pelizzetti, E., and Sammartano, S., editors, *Chemical Processes in Marine Environments*, Environmental Science, pages 281–296. Springer.

Pettine, M., Mastroianni, D., Camusso, M., Guzzi, L., and Martinotti, W. (1997). Distribution of As, Cr and V species in the Po-Adriatic mixing area, (Italy). *Marine Chemistry*, 58(3-4):335–349.

Pichat, S., Douchet, C., and Albarede, F. (2003). Zinc isotope variations in deep-sea carbonates from the eastern equatorial Pacific over the last 175 ka. *Earth and Planetary Science Letters*, 210(1-2):167–178.

Planavsky, N., Bekker, A., Rouxel, O. J., Kamber, B., Hofmann, A., Knudsen, A., and Lyons, T. W. (2010). Rare earth element and yttrium compositions of Archean and Paleoproterozoic Fe formations revisited: New perspectives on the significance and mechanisms of deposition. *Geochimica Et Cosmochimica Acta*, 74(22):6387–6405.

Powell, C. M., Preiss, W. V., Gatehouse, C. G., Krapez, B., and Li, Z. X. (1994). South Australian record of a Rodinian epicontinental basin and its mid-Neoproterozoic breakup (similar-to-700 Ma) to form the palaeo-Pacific ocean. *Tectonophysics*, 237(3-4):113–140.

Prave, A. R., Fallick, A. E., Thomas, C. W., and Graham, C. M. (2009). A composite C-isotope profile for the Neoproterozoic Dalradian Supergroup of Scotland and Ireland. *Journal of the Geological Society*, 166:845–857.

Preiss, W. V. (1982). Supergroup classification in the Adelaide Geosyncline. *Trans. Roy. Soc. South Australia*, 106:81–83.

Preiss, W. V. (1987). The Adelaide Geosyncline -late Proterozoic stratigraphy, sedimentation, paleontology and tectonics. *South Australia Geol. survey Bull.*, 53.

Preiss, W. V. (2000). The Adelaide Geosyncline of South Australia and its significance in Neoproterozoic continental reconstruction. *Precambrian Research*, 100(1-3):21–63.

Preiss, W. V., Belperio, A. P., M., C. W., and R., R. L. (1993). Neoproterozoic. In Drexel, J. F., Preiss, W. V., and J., P. A., editors, *The Geology of South Australia*, volume 54 of *South Australian Geol. Survey Bull.*, pages 170–203, Washington. Mineralogical Soc America.

Puls, R. W., Paul, C. J., and Powell, R. M. (1999). The application of in situ permeable reactive (zero-valent iron) barrier technology for the remediation of chromate contaminated groundwater: a field test. *Applied Geochemistry*, 14(8):989–1000.

Qu, C. L., Liu, G., and Zhao, Y. F. (2009). Experimental study on the fractionation of yttrium from holmium during the coprecipitation with calcium carbonates in seawater solutions. *Geochemical Journal*, 43(6):403–414.

Quinby-Hunt, M. S., Wilde, P., Orth, C. J., and Berry, W. B. N. (1997). Elemental geochemistry of black shales - statistical comparison of low calcic shales with other shales. *U.S. Geological Survey*.

Rachold, V., Alabyan, A., Hubberten, H. W., Korotaev, V. N., and Zaitsev, A. A. (1996). Sediment transport to the Laptev Sea - hydrology and geochemistry of the Lena River. *Polar Research*, 15(2):183–196.

Rai, D., Eary, L. E., and Zachara, J. M. (1989). Environmental chemistry of chromium. *Science of the Total Environment*, 86(1-2):15–23.

Rai, D., Sass, B. M., and Moore, D. A. (1987). Chromium(III) hydrolysis constants and solubility of chromium(III) hydroxide. *Inorganic Chemistry*, 26(3):345–349.

Raymont, J. E. G. (1972). Some aspects of pollution in Southampton Water. *Proceedings of the Royal Society of London Series B-Biological Sciences*, 180(1061):451.

Richard, F. C. and Bourg, A. C. M. (1991). Aqueous geochemistry of chromium - a review. *Water Research*, 25(7):807–816.

Rooney, A. D., Chew, D. M., and Selby, D. (2011). Re-Os geochronology of the Neoproterozoic-Cambrian Dalradian Supergroup of Scotland and Ireland: Implications for Neoproterozoic stratigraphy, glaciations and Re-Os systematics. *Precambrian Research*, 185(3-4):202–214.

Rouxel, O. J., Bekker, A., and Edwards, K. J. (2005). Iron isotope constraints on the Archean and Paleoproterozoic ocean redox state. *Science*, 307:1088–1091.

Rudge, J. F., Reynolds, B. C., and Bourdon, B. (2009). The double spike toolbox. *Chemical Geology*, 265(3-4):420–431.

Rudnick, R. L., Gao, S., Heinrich, D. H., and Karl, K. T. (2003). Composition of the continental crust. In *Treatise on Geochemistry*, pages 1–64. Pergamon, Oxford.

Sander, S. and Koschinsky, A. (2000). Onboard-ship redox speciation of chromium in diffuse hydrothermal fluids from the North Fiji Basin. *Marine Chemistry*, 71(1-2):83–102.

Sander, S., Koschinsky, A., and Halbach, P. (2003). Redox speciation of chromium in the oceanic water column of the Lesser Antilles and offshore Otago Peninsula, New Zealand. *Marine and Freshwater Research*, 54(6):745–754.

Sawaki, Y., Kawai, T., Shibuya, T., Tahata, M., Omori, S., Komiya, T., Yoshida, N., Hirata, T., Ohno, T., Windley, B. F., and Maruyama, S. (2010). $^{87}Sr/^{86}Sr$ chemostratigraphy of Neoproterozoic Dalradian carbonates below the Port Askaig glaciogenic formation, Scotland. *Precambrian Research*, 179(1-4):150–161.

Schoenberg, R., Zink, S., Staubwasser, M., and von Blanckenburg, F. (2008). The stable Cr isotope inventory of solid Earth reservoirs determined by double spike MC-ICP-MS. *Chemical Geology*, 249(3-4):294–306.

Schrag, D. P., Berner, R. A., Hoffman, P. F., and Halverson, G. P. (2002). On the initiation of a snowball Earth. *Geochemistry Geophysics Geosystems*, 3.

Schrag, D. P. and Hoffman, P. F. (2001). Geophysics - life, geology and snowball Earth. *Nature*, 409(6818):306–306.

Schroder, S. and Grotzinger, J. P. (2007). Evidence for anoxia at the Ediacaran-Cambrian boundary: the record of redox-sensitive trace elements and rare earth elements in Oman. *Journal of the Geological Society*, 164:175–187.

Scott, C., Lyons, T. W., Bekker, A., Shen, Y., Poulton, S. W., Chu, X., and Anbar, A. D. (2008). Tracing the stepwise oxygenation of the Proterozoic ocean. *Nature*, 452(7186):456–U5.

Sherrell, R. M. and Boyle, E. A. (1988). Zinc, chromium, vanadium and iron in the Mediterranean-Sea. *Deep-Sea Research Part a-Oceanographic Research Papers*, 35(8):1319–1334.

Thirlwall, M. F. and Anczkiewicz, R. (2004). Multidynamic isotope ratio analysis using MC-ICP-MS and the causes of secular drift in Hf, Nd and Pb isotope ratios. *International Journal of Mass Spectrometry*, 235(1):59–81.

Thomas, C. W., Graham, C. M., Ellam, R. M., and Fallick, A. E. (2004). $^{87}Sr/^{87}Sr$ chemostratigraphy of Neoproterozoic Dalradian limestones of Scotland and Ireland: constraints on depositional ages and time scales. *Journal of the Geological Society*, 161:229–242.

Thomson, J. (1871). On the occurence of pebbles and boulders of granite in schistose rocks in Isaly, Scotland. *Rep. Annu. Meet. Br. Assoc. Adv. Sci.*, 40:88.

Tribovillard, N., Algeo, T. J., Lyons, T., and Riboulleau, A. (2006). Trace metals as paleoredox and paleoproductivity proxies: An update. *Chemical Geology*, 232(1-2):12–32.

Trinquier, A., Birck, J. L., and Allegre, C. J. (2007). Widespread ^{54}Cr heterogeneity in the inner solar system. *Astrophysical Journal*, 655(2):1179–1185.

Trinquier, A., Birck, J. L., and Allegre, C. J. (2008a). High-precision analysis of chromium isotopes in terrestrial and meteorite samples by thermal ionization mass spectrometry. *Journal of Analytical Atomic Spectrometry*, 23(12):1565–1574.

Trinquier, A., Birck, J. L., Allegre, C. J., Gopel, C., and Ulfbeck, D. (2008b). ^{53}mn-^{53}Cr systematics of the early solar system revisited. *Geochimica Et Cosmochimica Acta*, 72(20):5146–5163.

Tucker, M. E. (1986). Carbon isotope excursions in Precambrian Cambrian boundary beds, Morocco. *Nature*, 319(6048):48–50.

Tyson, R. V. and Pearson, T. H. (1991). Modern and ancient continental shelf anoxia: an overview. *Geological Society, London, Special Publications*, 58(1):1–24.

Vance, D., Teagle, D. A. H., and Foster, G. L. (2009). Variable Quaternary chemical weathering fluxes and imbalances in marine geochemical budgets. *Nature*, 458(7237):493–496.

Veizer, J., Ala, D., Azmy, K., Bruckschen, P., Buhl, D., Bruhn, F., Carden, G. A. F., Diener, A., Ebneth, S., Godderis, Y., Jasper, T., Korte, C., Pawellek, F., Podlaha, O. G., and Strauss, H. (1999). $^{87}Sr/^{86}Sr$, delta ^{13}C and delta ^{18}O evolution of Phanerozoic seawater. *Chemical Geology*, 161:59–88.

Voegelin, A. R., Nagler, T. F., Beukes, N. J., and Lacassie, J. P. (2010). Molybdenum isotopes in late Archean carbonate rocks: Implications for early Earth oxygenation. *Precambrian Research*, 182(1-2):70–82.

Walter, M. R., Veevers, J. J., Calver, C. R., Gorjan, P., and Hill, A. C. (2000). Dating the 840-544 Ma Neoproterozoic interval by isotopes of strontium, carbon, and sulfur in seawater, and some interpretative models. *Precambrian Research*, 100(1-3):371–433.

Webb, G. E. and Kamber, B. S. (2000). Rare earth elements in Holocene reefal microbialites: A new shallow seawater proxy. *Geochimica Et Cosmochimica Acta*, 64(9):1557–1565.

Weyer, S. and Schwieters, J. (2003). High precision Fe isotope measurements with high mass resolution MC-ICP-MS. *International Journal of Mass Spectrometry*, 226(3):355–368.

Whitfield, M. and Turner, D. R. (1987). The role of particle in regulating the composition of seawater. In Stumm, W., editor, *Aquatic surface chemistry.*, pages 457–493. John Wiley and Sons, New York.

Williams, G. E. (2000). Geological constraints on the Precambrian history of Earth's rotation and the moon's orbit. *Reviews of Geophysics*, 38(1):37–59.

Williams, G. E. (2008). Proterozoic (pre-Ediacaran) glaciation and the high obliquity, low-latitude ice, strong seasonality (HOLIST) hypothesis: Principles and tests. *Earth-Science Reviews*, 87(3-4):61–93.

Wingate, M. T. D., Campbell, I. H., Compston, W., and Gibson, G. M. (1998). Ion microprobe U-Pb ages for Neoproterozoic basaltic magmatism in south-central

Australia and implications for the breakup of Rodinia. *Precambrian Research*, 87(3-4):135–159.

Winter, M. (2001). Webelements, the periodic table on the www, http://www.webelements.com.

Wombacher, F. and Rehkamper, M. (2003). Investigation of the mass discrimination of multiple collector ICP-MS using neodymium isotopes and the generalised power law. *Journal of Analytical Atomic Spectrometry*, 18(11):1371–1375.

Wright, J., Schrader, H., and Holser, W. T. (1987). Paleoredox variations in ancient oceans recorded by rare-earth elements in fossil apatite. *Geochimica Et Cosmochimica Acta*, 51(3):631–644.

Zhang, J. and Nozaki, Y. (1996). Rare earth elements and yttrium in seawater: ICP-MS determinations in the East Caroline, Coral Sea, and South Fiji basins of the western South Pacific Ocean. *Geochimica Et Cosmochimica Acta*, 60(23):4631–4644.

Zhang, J. and Nozaki, Y. (1998). Behavior of rare earth elements in seawater at the ocean margin: A study along the slopes of the Sagami and Nankai troughs near Japan. *Geochimica Et Cosmochimica Acta*, 62(8):1307–1317.

Zink, S., Schoenberg, R., and Staubwasser, M. (2010). Isotopic fractionation and reaction kinetics between Cr(III) and Cr(VI) in aqueous media. *Geochimica Et Cosmochimica Acta*, 74(20):5729–5745.